2005-13

Final Report

Retrofitting Shear Cracks in Reinforced Concrete Pier Caps Using Carbon Fiber Reinforced Polymers

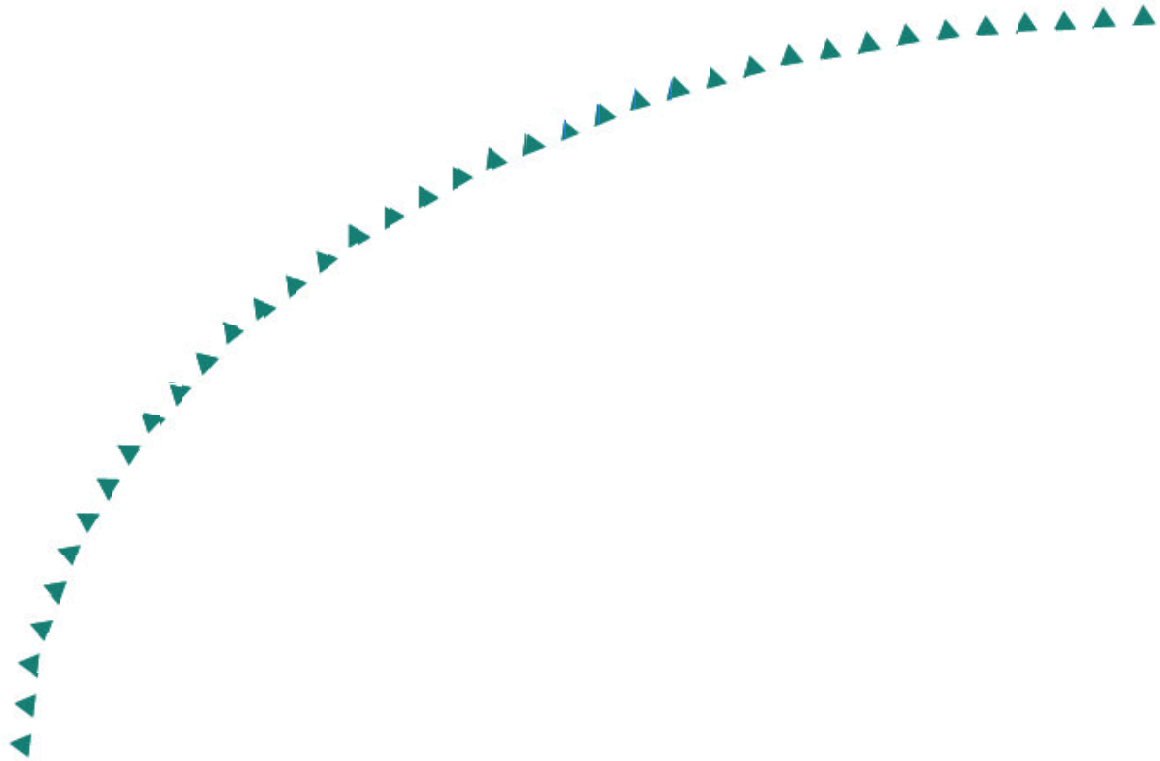

Research

Technical Report Documentation Page

1. Report No. MN/RC 2005-13	2.	3. Recipients Accession No.	
4. Title and Subtitle Retrofitting Shear Cracks in Reinforced Concrete Pier Caps Using Carbon Fiber Reinforced Polymers		5. Report Date April 2005 6.	
7. Author(s) Emily Milde, Carol Shield, Catherine French, Jon Wacker		8. Performing Organization Report No.	
9. Performing Organization Name and Address Department of Civil Engineering University of Minnesota 500 Pillsbury Dr SE Minneapolis, MN 55455		10. Project/Task/Work Unit No. 11. Contract (C) or Grant (G) No. (c) 74708 (wo) 157	
12. Sponsoring Organization Name and Address Minnesota Department of Transportation Research Services Section 395 John Ireland Boulevard Mail Stop 330 St. Paul, Minnesota 55155		13. Type of Report and Period Covered Final Report 14. Sponsoring Agency Code	
15. Supplementary Notes http://www.lrrb.org/PDF/200513.pdf			

16. Abstract (Limit: 200 words)

The Minnesota Department of Transportation (Mn/DOT) documented the appearance of excessive cracks in the reinforced concrete pier cap overhangs of State Highway Bridges 19855 and 19856. As a part of this study, the ultimate capacity of the pier cap overhangs was estimated by comparing predicted capacities calculated using standard design specifications to experimental results published in the worldwide literature. It was determined that the ultimate capacity of the pier cap overhangs was more than sufficient to assure that a cracked, but undeteriorated, pier cap is not prone to structural failure. An estimate of the initial cracking load of the pier cap overhangs was also created to determine what changes to pier cap design would be required to prevent future overhangs from cracking. It was determined that the depth of the overhangs would have to be increased by approximately 20% to prevent them from cracking. The changes to pier cap overhang design required to prevent cracking or meet recommendations to reduce crack widths may not be economically feasible. Therefore, other methods for controlling crack widths must were examined. An experimental study was conducted to investigate the use of externally bonded (EB) FRP sheets and near surface mounted (NSM) FRP tape for shear strengthening of reinforced concrete beams. This report describes the experimental program, presents the results of the study, and discusses the outcome of that investigation.

17. Document Analysis/Descriptors		18. Availability Statement	
Pier Caps Concrete Cracking	FRP Polymers	No restrictions. Document available from: National Technical Information Services, Springfield, Virginia 22161	
19. Security Class (this report) Unclassified	20. Security Class (this page) Unclassified	21. No. of Pages 238	22. Price

Retrofitting Shear Cracks in Reinforced Concrete Pier Caps Using Carbon Fiber Reinforced Polymers

Final Report

Prepared by:

Emily Milde

Jon Wacker

Carol Shield

Catherine French

Department of Civil Engineering
University of Minnesota

April 2005

Published by:

Minnesota Department of Transportation
Research Services Section
395 John Ireland Boulevard, MS 330
St. Paul, Minnesota 55155-1899

Acknowledgements

Sika Corp., Fyfe Co., MBT/Chemrex, and Hughes Brothers are recognized for donating materials used in this research.

Table of Contents

List of Tables

List of Figures

Executive Summary

The Minnesota Department of Transportation (Mn/DOT) documented the appearance of excessive cracks in the reinforced concrete pier cap overhangs of State Highway Bridges 19855 and 19856. The cracks are a combination of flexure and flexure/shear. The cracks are of sufficient width such that a motorist traveling under the bridge at freeway speed can identify them using the naked eye. These cracks are detrimental because they expose the steel reinforcing bars in the pier cap to corrosive elements. Corrosion may reduce the cross-sectional area of the steel reinforcing bars inhibiting their ability to carry the design load. Corrosion byproducts also occupy more volume than the original steel causing concrete spall. Together, these factors may reduce the load-carrying capacity of the overhangs and, if severe, could cause structural failure. Due to these negative effects caused by cracking, it would be desirable to prevent cracking from occurring in future overhang design, or at least limit the crack widths.

As a part of this study, the ultimate capacity of the pier cap overhangs was estimated by comparing predicted capacities calculated using standard design specifications to experimental results published in the worldwide literature. Pier cap overhangs are commonly deep beams having large depths in comparison to their shear spans. Deep beams have nonlinear stress distribution and behave differently than shallow beams. However deep beam provisions were not included in the design specifications when the pier cap overhangs were designed and therefore they were designed as shallow beams. Therefore, a more extensive study was required to assure that the shallow beam provisions used to design the overhangs sufficiently predicted ultimate capacity and to determine if current deep beam specification provide any better prediction. It was determined that the ultimate capacity of the pier cap overhangs was more than sufficient to assure that a cracked, but un-deteriorated, pier cap is not prone to structural failure. It was also determined that the strut and tie provision included in the current design specifications provided the best prediction of the ultimate capacity of a pier cap overhang.

An estimate of the initial cracking load of the pier cap overhangs was also created to determine what changes to pier cap design would be required to prevent future overhangs from cracking. Procedures for calculating the initial cracking load were developed from elementary beam mechanics and finite element analysis and calibrated using published experimental results to produce an acceptable estimation. It was determined that the depth of the overhangs would have to be increased by approximately 20% to prevent them from cracking. Design specification serviceability requirements were also examined. It was determine that the pier cap overhang design was acceptable for most requirements, but violated one pertaining to the horizontal spacing of the flexural tensile reinforcement. However, it is unlikely that the changes required to meet this provision would have eliminated the cracking problem. Recommendations for reducing crack widths in pier cap overhangs published in worldwide literature were also examined. It was determined that the amount of flexural tensile steel would have to be increased by approximately 30% and stirrup spacing decreased by approximately 15% to meet the recommendations.

The changes to pier cap overhang design required to prevent cracking or meet recommendations to reduce crack widths may not be economically feasible. Therefore, other methods for controlling crack widths must be examined. The use of fiber reinforced polymers (FRP) for retrofit of concrete structures has become popular in recent years due to its high strength to weight ratio and corrosion resistance. FRP has been widely studied and used for flexural strengthening and column wrapping, but its behavior in shear is not fully understood.

An experimental study has been conducted to investigate the use of externally bonded (EB) FRP sheets and near surface mounted (NSM) FRP tape for shear strengthening of reinforced concrete beams. This report describes the experimental program, presents the results of the study, and discusses the outcome of the investigation.

Eighteen small-scale bond tests were performed to study the behavior of EB FRP sheets and NSM FRP tape applied across a simulated concrete crack. Variables included strip width and spacing, fiber orientation, and unbonded region for the EB specimens, and fiber orientation, adhesive type, and vibrations during epoxy cure for the NSM specimens. The results of the EB tests showed that a fiber orientation of 90 degrees to the crack was stronger and stiffer than a fiber orientation of 45 degrees to the crack when tested in tension orthogonal to the crack. Using multiple smaller strips instead of one larger strip of the same total width was more effective. Unbonding a portion of the strip over the crack reduced the effectiveness of the strip. In general, the bond between the EB sheets and the concrete was inconsistent, and the specimens failed in the concrete-to-adhesive interface, with varying amounts of concrete substrate removed with the sheets. The specimens strengthened with NSM tape performed better overall than the specimens with EB sheets because inserting the fibers into a groove in the concrete provided greater confinement and seemed to enhance the bond. The results of the NSM tests also showed that a fiber orientation of 90 degrees to the crack was stronger and stiffer, but less ductile than a fiber orientation of 45 degrees to the crack when tested in tension orthogonal to the crack. The type of adhesive used had an influence on the effectiveness of the strip, but vibrations during cure of the adhesive did not have an effect. The specimen with the most effective configuration of EB FRP sheets was able to reach 30% of the strength of the FRP laminate. The specimen with the most effective configuration of NSM FRP was able to achieve 78% of the strength of the FRP laminate.

Tests were then conducted on two large-scale simply supported beam specimens. The beams were loaded at midspan with a concentrated load. They were fabricated with no internal shear reinforcement in one of the two shear spans. The other shear span had minimum internal shear reinforcement. The distance between stirrups was one-half the effective depth, the maximum allowable stirrup spacing. The application of a concentrated load at midspan simulated the behavior of a cantilevered bridge pier cap with flexure shear cracking. One beam specimen was initially loaded to produce shear cracking in the span without stirrups. Near surface mounted FRP tape was used to strengthen that span. The beam was loaded again to produce shear cracking on the side of the beam with stirrups. The shear cracks on that side of the beam were then repaired with FRP. After strengthening both spans for shear, the beam ultimately failed in flexure. The other beam was reinforced with FRP on the side without stirrups. It was loaded to failure with no additional FRP reinforcement on the side of the beam with minimum stirrups. The second beam also failed in flexure, so it was not possible to determine how much additional strength was provided by the NSM FRP. However, strain gages on the stirrups showed significant reductions in strain after FRP reinforcement was applied to the

beam. This indicated that the NSM FRP tape provided a considerable amount of additional shear strength when used to repair an existing shear crack.

Chapter 1 Introduction

1.1 Cracking in the Pier Caps of Bridges 19855/56

The Minnesota Department of Transportation (Mn/DOT) documented the appearance of excessive cracking in the reinforced concrete pier cap overhangs of Minnesota State Bridges 19855 and 19856 in 1995 and 1994, respectively. The cracking consists of flexure and flexure/shear cracks. The cracks can be seen with the naked eye by a motorist traveling under the bridge at highway speeds. These cracks are of concern because they expose the pier caps to deterioration problems and possibly structural failure. The following investigation was required to determine the extent to which these cracks jeopardize the structural integrity of the pier caps, the likely cause of the cracks, and possible measures that can be taken to reduce or eliminate cracking in future pier cap designs.

Cracking similar to that observed by Mn/DOT has been documented in reinforced concrete pier caps throughout the country (Ferguson, 1964; Yazdani and Mesidor, 1996; Young et. al., 2002). Fine cracking is common in reinforced concrete beams under service loads and although excessive cracking does not necessarily indicate that structural failure is imminent, it does present cause for examining the structural integrity of the member. One major reason for this is that excessive cracking exposes the steel reinforcing bars in the concrete to the possibility of corrosion. This is critical for pier caps because they are in highly corrosive environments. Corrosion causes the steel reinforcing bars to lose cross-sectional area and hence the ability to carry the design load. In addition, the corrosion by-products occupy more volume than the original steel. This increased volume can cause concrete spalling. These factors weaken the pier cap and, if severe, could initiate structural failure. Due to problems associated with excessive cracking, it would be ideal to design pier caps in the future so they will not crack or at least have reduced crack widths.

Several studies have been conducted to investigate the appearance of cracks in reinforced concrete pier cap overhangs (Ferguson, 1964; Yazdani and Mesidor, 1996; Young et. al., 2002). However there is still not an established reason for why pier cap overhangs have excessive cracking and what changes in design can be made to reduce cracking. In some cases, researchers have identified cracked pier cap overhangs and similar overhangs that have not cracked (Yazdani and Mesidor, 1996). One reason for this lack of understanding is that pier cap overhangs are usually deep beams with short shear spans. Behavior of pier cap overhangs is complicated including non-linear stress distributions throughout the depth (Ferguson, 1964; Yazdani and Mesidor, 1996). The specifications commonly used to design pier caps do not apply to deep beams and are not necessarily sufficient for assuring an acceptable design. Therefore, pier cap overhangs cannot be assessed by simply determining whether they meet code specifications, which are typically for ultimate strength, but rather a more in-depth investigation utilizing experimental results is required.

There were two primary objectives associated with this study. The first objective was to determine if the undeteriorated pier cap overhangs are prone to structural failure. This required the ultimate capacity of the pier cap overhangs to be estimated using design specifications which were calibrated with experimental results found in the literature. The design load, the largest load that could be applied to the pier cap overhang by vehicular traffic and the weight of the bridge superstructure, was also determined and compared to the estimated ultimate capacity to

determine if the overhangs are at risk of failure. The specification that provides the best estimate for the strength of the pier cap overhangs was also determined for future designs.

The second objective of this research was to determine reasons for the cracking problem and possible changes in future design to prevent it. This included estimating the cracking load for the pier cap and comparing it to the service load, the largest load likely to be applied to the overhangs, to determine whether it is economical to alter pier cap designs to prevent cracking. Cracking serviceability specifications from the design specifications and recommendations from the literature were also compared to determine what changes could be made to pier cap design to reduce cracking in the future.

1.2 Literature Review on Cracking of Pier Caps

Without the resources to perform experimental tests on pier cap specimens modeled after the Bridge 19855/56 pier cap overhangs, this investigation relied on the data of previously performed experiments for calibrating analytical models to approximate the cracking load and ultimate capacity of the pier cap overhangs. A literature review was performed to identify previous studies with experimental results pertinent to the current investigation. Despite the lack of highly relevant data, several studies have been performed specifically to determine the strength of pier caps with designs similar to the Mn/DOT pier cap. A brief description outlining the specimens tested, results, and conclusions of each of these studies is provided below. These results were used to create the experimental database used in this investigation. In addition, recommendations from these studies on how to reduce cracking were compiled to help determine methods for reducing crack widths in future pier caps designed by Mn/DOT.

Ferguson, P.- 1964

The first noted experimental study on pier cap overhangs, also referred to as bent cap overhangs, was performed by Ferguson (1964) at the University of Texas. The study consisted of the experimental testing of 36 pier cap overhang specimens. The test specimens were all 36 in. deep. Variables associated with the specimens included shear span, bar anchorage length, grade of steel reinforcement, amount of flexural reinforcement, amount of shear reinforcement, the presence of horizontal skin steel, and cap width. All specimens were tested to failure. The failure load and type of failure was reported for all specimens. Only qualitative data was provided on the appearance of cracks.

One key finding of the study was that vertical stirrups placed at standard spacing had little to no effect on the shear capacity of the overhangs. This is because the cracks in the overhang were at very steep angles and did not cross many stirrups. Ferguson suggested that placing horizontal skin steel in the pier caps could alleviate this problem. The horizontal bars would cross the cracks in more places providing greater shear strength along with reducing crack widths. The study also determined that bond failure would not occur if at least nine inches of reinforcing bar extended past the location of applied load in the overhang. The study found that crack widths were larger in caps designed using grade 60 reinforcing bars than in caps using intermediate grade reinforcement. Ferguson recommended that a service load stress limit of 24-26 ksi in the tensile flexural reinforcement be used to control crack widths.

Young et al.- 2002

This study performed by Young et al. (2002) at Texas A&M University consisted of the experimental testing of 16 pier cap overhang specimens. All specimens were 36 in. deep, 33 in.

wide and had a shear span of 54 in. The study investigated reinforcing details to reduce the widths of flexure and flexure-shear cracks in the specimens at loads similar to bridge service loads. Design alterations considered included varying the amount and spacing of tensile steel, the amount and spacing of horizontal skin steel, and the amount of transverse steel. The specimens were instrumented with strain gages on the longitudinal and transverse reinforcement. Each specimen was loaded in 40 kip increments with crack widths and propagation measured at every increment until the specimen failed. All of the specimens failed in shear.

The results reported by Young et. al. provide a very detailed description of crack propagation in the pier cap overhang specimens. The study found that the first flexural cracks appeared in the caps with stresses of 4- 7 ksi in the flexural tensile reinforcing steel. It was also determined that the stress in the flexural tensile steel was a primary factor affecting crack widths. The study recommends limiting this stress to 24-26 ksi. The horizontal distribution of this steel, within reasonable limits, was found to have little effect on crack widths. Contrary to the findings of Ferguson, the study also determined that increasing the amount of transverse steel was effective in reducing the widths of flexure-shear cracks.

The study recommends that pier cap overhangs be designed using the center of the column as the critical section instead of the column face. This will cause the pier cap to be overdesigned at the face of the column and accordingly reduce the stress levels in the steel at service loads. To limit the widths of flexure-shear cracks, the study suggests designing pier cap overhangs to have sufficient shear strength to develop flexural over strength at the column face as well as meet the shear demand.

Other Studies

Two other studies have been performed on the strength of pier caps. Yazdani and Mesidor (1996) performed a study that included the experimental testing of two pier cap specimens. The experimental data from this study is excluded from this research because of the small number of specimens and inconsistencies in reported results, however qualitative observations are included.

Ferguson and Liao (1966) studied the strength of pier caps between columns. The study found that the same cracking problem witnessed in overhangs occurred in the continuous spans of the pier caps. The study is not further referenced in this report because the current research dealt exclusively with the overhang portions of pier caps.

1.3 Background Information on the Bridges

Minnesota State Bridges 19855 and 19856 were designed in 1983 using the 1977 American Association of State Highway and Transportation Officials (AASHTO) Standard Design Specification (AASHTO, 1977). Each bridge carries one direction of Trunk Highway 52 over Trunk Highway 494. Both bridges consist of steel plate girders supported by a cast-in-place substructure. The bridge span of 346 ft. is split into two equal portions by a center pier which contains the pier cap overhangs being investigated. An elevation and plan view of Bridge 19855, which is nearly identical to 19856, is included as Figure 1-3. Each bridge consists of two through traffic lanes in addition to one merging lane which is part of a cloverleaf system facilitating traffic exchange between Highway 52 and Highway 494. The bridge was originally designed for an HS20 truck load according to the 1977 AASHTO specification.

The center piers consist of four cast-in-place columns on pile foundations. The cast-in-place pier cap spans the distance between the columns and overhang both at ends. An identical pier cap design was used for both bridges. The pier cap spans approximately 12.5 ft. between the faces of the columns and overhangs the exterior column face by approximately 7 ft. An elevation view of the pier cap is included as Figure 1-2. The pier cap is 5 ft. deep at the face of the columns and is 3.5 ft. thick. The pier cap overhang consists of 18 No. 9 reinforcing bars for longitudinal tensile reinforcement, and two No. 6 two-legged stirrups spaced at six inches along the length. The standard reinforcement detail cross-section of an overhang is included as Figure 1-3. The pier cap overhang supports the exterior bridge girder which applies a concentrated load to the pier cap at a distance of 4 ft. from the exterior face of the column.

Both bridges were constructed simultaneously in 1985. The pier caps were poured in February with daily temperatures ranging between 7 and 41 °F on days that concrete was poured. The 28-day compressive strength was determined experimentally to be 6490 psi and 4810 psi for the pier caps of Bridges 19855 and 19856 respectively. The first girders were placed on Bridge 19855 only eight days after the pier cap was poured. All other girders were placed after the pier caps had reached 28-day strengths. There were no recorded observations of cracking in the pier caps during construction, however only limited construction documentation is still available. The bridges did not open to traffic until 1992.

Official Mn/DOT bridge inspections noted the appearance of cracks in the pier cap overhang of Bridge 19856 in 1994 and in Bridge 19855 the following year. The exact description for Bridge 19855 was: “Both ends of cap have 100 lf of fine diagonal stress cracks.” A similar comment was made for Bridge 19856. Both bridges also had the appearance of concrete spall documented in 1996. Besides this, no other mention of these cracks was made in the inspection notes. Although inspection reports do not document cracking until 1994, other documentation obtained from the Mn/DOT Bridge Office indicate that the cracking was present and identified as a potential problem as early as 1992. Due to this disparity, it is unknown when the pier caps cracked and impossible to identify a specific cause. It is possible that the overhangs cracked under construction loads or immediately after being opened to vehicular traffic as was witnessed in other studies (Yazdani and Mesidor, 1996). There are also no other bridges with similar characteristics along Highway 52 for providing additional data on what possibly caused these overhangs to crack. A photo of a typical cracked overhang is included as Figure 1-4.

The load transmitted to the pier cap overhang by the exterior bridge girder due to the self-weight of the bridge superstructure and traffic on the bridge must be calculated for two distinct cases. The first case considers the largest load that could ever reasonably be placed on the pier cap. This is the design load which is factored to account for possible uncertainty in loading and to produce a margin of safety. The second case considers the largest load that has likely been placed on the pier cap overhang. This is the service load which is an unfactored load.

AASHTO specifications were used to calculate the design load. The design load was determined using service loads provided by the Mn/DOT Bridge Office in 2001. The Strength I load case controlled design producing a design load of 815.6 kips using the 1998 AASHTO Load and Resistance Factor Design (LRFD) specification. This was the largest reaction generated in the overhang due to the weight of the bridge superstructure and a distributed live lane load of 16.1 kpf along the bridge in the two 10 ft. traffic lane nearest the edge of the bridge. The original design load calculated with the 1977 AASHTO specification is similar in magnitude.

There is no prescribed procedure for calculating the service load. Therefore, a method for determining the service load was created for this study. The dead load was calculated by determining the portion of the weight of the bridge superstructure transferred to the pier cap overhang and found to be 404 kips. The live load was assumed to be dependent on the number and location of trucks traveling across the bridge. The live load was difficult to determine because it was impossible to examine every different traffic pattern that has crossed the bridge to determine which caused the largest live load. Therefore assumptions had to be made about traffic patterns.

The number of trucks distributed across the bridge has no significant effect on the load transmitted to the pier cap overhang. Only trucks in the exterior lane transfer a significant portion of load to the pier cap overhang. All trucks in the interior lanes transfer weight to the middle sections of the pier cap. Accordingly, only traffic in the exterior lane was considered when determining the service load applied to the overhang. It was also determined that only trucks located near the pier along the length of the bridge contributed significant load to the overhang. Therefore, a reasonable estimate of the service load on the overhang was achieved by only considering the loading of the exterior lane near the pier cap.

The traffic pattern used to determine the service load consisted of three 80 kip trucks centered over the pier. This was considered to be reasonable because several trucks often travel in a caravan across the bridge. Each truck was modeled as a 10 kip load spaced 14 ft. from two 35 kip loads separated by 28 ft. Two different movement cases were considered. The first case was the trucks traveling at 60 mph. The distance between trucks was estimated to be one second of time which is equivalent to 88’ between the back wheel of one truck and the front wheel of the following truck. The second case consisted of the trucks stopped on the bridge with 20 ft. spacing between them as defined above. This case is included because of the possibility of traffic being affected by entering and exiting traffic. For trucks traveling at 60 mph, the loads were multiplied by 1.3 to account for dynamic loading effects. Diagrams of the truck spacings for both cases and the standard truck dimensions and loads are included as Figure 1-5.

The trucks were placed on the bridge for both cases to maximize the load on the pier cap overhang. The trucks traveling at 60 mph produced a live load of 88.7 kips on the overhang and the stationary trucks produced a load of 136.0 kips. The service design load is the unfactored combination of the dead load and the maximum live load and was calculated to be 540 KIPS.

1.4 Ultimate Capacity of Pier Caps

There are several reasons why it is necessary to determine the ultimate capacity of the pier cap overhangs of Bridges 19855 and 19856. The appearance of excessive cracking is one reason. Although large cracks are not necessarily an indication that failure is imminent, they are often seen as a reason for checking the ultimate capacity to assure that there is no risk of failure. In typical situations, this would involve an engineer using the applicable design specifications to check the design calculations to assure the ultimate capacity of the overhangs is sufficient. However, the pier cap overhangs in Bridges 19855 and 19856 were designed using the 1977 AASHTO Standard Specification which required all beams to be designed using shallow beam design provisions (AASHTO, 1977). Current design specifications (AASHTO, 1998; ACI, 2002) require that beams with large depths with respect to their spans, such as the pier cap overhangs, be designed using special deep beam provisions. Therefore, it was necessary to perform further

investigation to assure that the ultimate strength predicted by the shallow beam provisions is in fact a conservative representation of the ultimate capacity of the overhangs.

A second reason for performing a more in-depth study into the ultimate capacity of pier cap overhangs is to determine which design specifications provide the best predictions of ultimate capacity. This would allow more accurate design of pier caps in future projects. Design provisions for the shear and flexural strength of reinforced concrete beams from AASHTO and American Concrete Institute (ACI) specifications were examined in this study to determine which is most accurate for deep beam overhangs based on the available test data in the literature. Both current specifications and specifications available when the bridges were designed were examined to determine if changes made to the specifications have affected the design of overhangs. The development length of the flexural reinforcement in the overhangs was checked with both specifications and found to be sufficient.

Significant changes to the design provisions for calculating ultimate capacity of reinforced concrete beams have been made since the bridges were constructed. One key change is that current design specifications (ACI, 2002; AASHTO, 1998) require special provisions be used for the design of deep beams whereas the design specifications available when the bridges were constructed (ACI, 1981; AASHTO, 1977) required that all beams be designed using shallow beam provisions. Shallow beam flexural design provisions from the AASHTO and ACI specifications are nearly identical and have not changed. The shallow beam shear provisions in ACI 318-81, ACI318-02 and, 1977 AASHTO standard specifications are identical, however the 1998 AASHTO LRFD specification uses a different procedure based on modified compression field theory. The current AASHTO LRFD (AASHTO, 1998) and ACI 318-02 (ACI, 2002) specifications require that deep beams be designed for flexure and shear using either a strut and tie based approach or another method that accounts for nonlinear stress distributions in deep beams. Both specifications have provisions based on the strut and tie model which differ slightly in details. By examining all of these provisions, it can be determined if they are practical for designing pier cap overhangs and whether current design provisions are more accurate for this application than the provisions used to design the bridge.

The following nomenclature is used throughout this report to differentiate ultimate capacities determined by applying design provisions and those improved by correlating the capacity predicted by the provision to experimental results. A predicted ultimate capacity is determined solely by applying a design provision. An estimated ultimate capacity is the predicted ultimate capacity multiplied by the corresponding correction factor determined from experimental results. Neither the predicted nor estimated ultimate capacities are reduced by a resistance factor.

A method was established to determine how well a provision predicts the ultimate capacity of a pier cap overhang. The provision was used to predict the ultimate capacity of the overhang specimens tested in previous studies (Ferguson, 1964; Young et al., 2002). The predicted capacity for a given specimen was then compared to its experimental capacity to determine how well the provision predicted the ultimate capacity. This was expressed numerically using a correction factor equal to the experimental capacity divided by the predicted capacity. A correction factor was calculated for each specimen tested. These correction factors were averaged and the standard deviation was calculated. The average correction factor was then multiplied by the ultimate capacity of the Bridge 19855 and 19856 pier cap overhang predicted

using the provision to determine an estimated ultimate capacity. This was repeated for each provision.

Each provision was only applied to experimental specimens which exhibited the failure type for which the provision predicts ultimate capacity. In other words, shear provisions were only applied to specimens that failed in shear and flexural provisions were only applied to specimens that failed in flexure. Both flexure and shear failures were used to create correction factors for provisions based on strut and tie models. The data bank used in this study consisted of six specimens that failed in flexure (Ferguson, 1964) and 14 specimens that failed in shear (Ferguson, 1964; Young et al., 2002). Specimens tested by Ferguson (1964) are indicated with identification labels starting with the letter F followed by the original identification label used by Ferguson. Specimens tested by Young et al. at Texas A&M University are indicated by an identification label starting with TAM followed by the original identification label.

1.4.1 Provisions Used to Estimate Ultimate Capacity

Each of the provisions used to estimate ultimate capacity is briefly described below. Calculations for the predicted ultimate capacity of the Bridge 19855/56 pier cap overhangs using each provision are included in Appendix A.

ACI318 (81 and 02), 1977 AASHTO, and 1998 AASHTO LRFD Shallow Beam Provision:

The shallow beam flexural provision is based on conventional beam theory. The applied moment is equilibrated by an internal force couple consisting of a compressive force from the concrete and a tensile force from the reinforcing steel (MacGregor, 1997). One primary assumption is that plane sections in the beam prior to bending remain plane during bending. Although this does not hold for deep beams due to their nonlinear stress distribution, Ferguson suggests that shallow beam provisions can be used to predict their ultimate capacity because pier cap overhangs display cracking patterns similar to shallow beams (1964). Shallow beam flexural design also assumes that the complex compressive stress distribution can be represented as an equivalent stress block of uniform distribution (ACI, 2002). Assumptions used to simplify design can be found in Section 10.2 of the ACI 318-02 specification (ACI, 2002).

Calculations were performed both accounting for and neglecting the reinforcing steel in the compression region of the cross section. There was no significant difference, less than 8%, in the calculated flexural strength. Therefore, the presented results were calculated by neglecting the compression steel, which is common in design.

ACI318-81, ACI318-02, and 1977 AASHTO Shallow Beam Shear Provision:

The shallow beam shear provisions in the ACI 318-81, ACI 318-02, and 1977 AASHTO specifications predict the shear strength of a reinforced concrete member based upon the load required to create a flexure-shear crack from the tip of a previously formed flexure crack (MacGregor, 1997). The stresses at the tip of the longitudinal crack due to shear and flexure are analyzed to determine the principal tensile stress. The principal tensile stress is compared to the cracking stress of concrete to find the maximum shear stress that can be applied without cracking the member (Collins and Mitchell, 1987). ACI 318-02 Eqn (11-5), which is used to predict the contribution of concrete to shear resistance, was created by calibrating this method with existing test data.

ACI Eqn (11.5) $$V_c = (1.9\sqrt{f'_c} + 2500\rho_w \frac{V_u d}{M_u})bd \le 3.5\sqrt{f'_c}bd \quad (1\text{-}1)$$

This equation is simplified by approximating the second by $0.1f'_c$. This simplified equation is included as Eqn (11-3) in the ACI 318-02 specification.

ACI Eqn (11-3) $$V_c = 2\sqrt{f'_c}bd \quad (1\text{-}2)$$

The code allows either of these equations to be used for predicting the shear strength resistance of concrete. Currently, there is controversy over which of these equations provides the most accurate prediction (MacGregor, 1997). Therefore, this research examines these equations separately to determine which is most accurate for deep pier cap overhangs.

The shear resistance provided by transverse reinforcement is assumed to be the yielding strength of all stirrups crossing a shear crack (MacGregor, 1997). The number of stirrups crossing a crack is determined by assuming that cracks form at 45 degree angles such that the number of stirrups crossing a crack is equal to the section's effective depth divided by the stirrup spacing. ACI 318-02 Eqn (11-15) is used to approximate this.

ACI Eqn (11-15) $$V_S = \frac{A_V f_y d}{s} \quad (1\text{-}3)$$

The total resistance to shear is the sum of the concrete and steel components.

1998 AASHTO LRFD Modified Compression Field Theory (MCFT) Shear Design:

The 1998 AASHTO MCFT provisions assume that reinforced concrete members carry shear using an imaginary truss mechanism. In this mechanism, the web of the member is assumed to be composed of concrete compression struts separated by diagonal shear cracks. Regions of the beam in flexural compression are also modeled as compression struts. The transverse and longitudinal reinforcement is assumed to be the tension members in the truss. The concrete contribution to shear resistance is computed by considering both compressive and tensile stresses to determine the principal stresses in the concrete struts and determine the amount of shear load they can withstand without failing (MacGregor, 1997; Collins and Mitchell, 1989).

The 1998 AASHTO specification also contains a simplified MCFT design provision which can be used for reinforced concrete with adequate reinforcement. This provision is identical to other shallow beam shear provisions provided that ACI 318-02 Eqn (11-3) is used. Due to this redundancy, the simplified method is excluded from this study.

ACI318-02 Strut and tie design:

Strut and tie design consists of modeling the pier cap overhang as a truss constructed of concrete compression struts and steel tensile ties. Currently, there is no prescribed method for modeling pier cap overhangs so the design of the model is left to the engineer's best judgment. An appropriate model depicts the actual paths which forces would follow through the overhang. Ferguson reported that the compression zone of a pier cap overhang is approximately a straight line from the point of applied load to the bottom corner of the cap (Ferguson, 1964). Ferguson also reported that stirrups had little effect on the strength of the pier cap overhang (Ferguson , 1964). Based on these findings, the most appropriate truss model consists of a single compressive strut and tension tie as illustrated in Figure 1-6. After creating a truss model, the geometry and material properties of the pier cap overhang are then used to determine the

capacities of the compressive strut and tensile tie. The maximum capacity of a tensile tie is the yield strength of the steel being modeled as the tie. The maximum capacity of a compression strut is the area of the strut, determined from geometry and the reinforcement detail, multiplied by the maximum allowable compressive stress. The nodal zones where multiple struts and ties meet in the truss must also be examined to assure that they do not experience a crushing failure. The ultimate capacity of the overhang is the largest load that can be applied before exceeding the capacity of a strut, tie or nodal zone. The mechanistic nature of the strut and tie procedure allows it to be used for predicting the failure of overhangs in both flexure and shear.

AASHTO LRFD 98 Strut and tie design:

AASHTO LRFD strut and tie design is very similar to ACI strut and tie design. The only key difference is that the method for calculating the maximum capacity of compression struts is altered to account for tensile stress applied perpendicular to the compressive struts.

1.4.2 Accuracy of Provisions to Predict Ultimate Capacity

A correction factor was used to measure how well a provision predicted the ultimate capacity of a pier cap overhang. A correction factor of 1 represents a perfect prediction. A correction factor larger than 1 represents a conservative design (experimental capacity larger than predicted) while a correction factor smaller than 1 represents an unconservative design (experimental capacity less than predicted). The standard deviation of the correction factors was used as a measure of how precise a provision was at predicting the ultimate capacity. Figures 1-7 through 1-11 show plots of the correction factors for each specimen calculated with a given provision. Table 1-1 shows the average correction factor and standard deviation for each provision.

The correction factors for all provisions were greater than 1 implying that all of the provisions produced conservative designs. The shallow beam flexural provision provided an accurate prediction of ultimate capacity with an average correction factor of 1.11. The provision was very precise with a standard deviation of 0.08. The shallow beam flexural design provision is accordingly an effective method for designing pier cap overhangs. The shallow beam shear provision was more conservative with an average correction factor of over 1.20. Whether Eq. (1-1) or (1-2) was used to calculate the shear resistance contribution of the concrete had little effect on the accuracy or precision of the provision. Equation (1-1) predicted failure with slightly greater accuracy having a correction factor of 1.23 compared to 1.27 for Eq. (1-2).

The provisions based on the strut and tie method were accurate in predicting the ultimate capacity of overhangs. The ACI 318-02 and 1998 AASHTO LRFD provisions both had average correction factors of 1.23 and standard deviation of 0.15. However, both strut and tie provisions a number of specimens with correction factors less than 1 representing an unconservative design. Therefore, appropriate resistance factor must be employed to assure that pier cap overhangs designed with these provisions are not unconservative. These results support the incorporation of strut and tie modeling into the design of pier cap overhangs. Many designers are hesitant to use strut and tie modeling because it can be a complex, time extensive process. However, in the case of pier cap overhangs with a shear span of less than the pier cap height, the design is extremely simple and requires little more effort than shallow beam provisions. This study alone does not warrant the replacement of separate shear and flexural design provisions with the strut and tie design provision. All experimental specimens and the Bridge 19855/56 overhangs were limited

by tie failure when applying the strut and tie design provision. It is unknown how the ultimate capacity prediction will be affected if the concrete strut in the model fails. This should be investigated before using strut and tie provisions for the design of pier cap overhangs.

The effect of the failure capacity value on the correction factor was examined and found to have no influence.

1.4.3 Comparison of Estimated Ultimate Capacity to Factored Design Load

The provisions were applied to the Bridge 19855/56 pier cap overhangs and the average correction factors calculated above were used to determine the estimated ultimate capacities of the overhangs. The lowest estimated ultimate capacity of the pier cap overhang was 1308 kips for Bridge 19855 and 1328 kips for Bridge 19856 using the shallow beam flexural provision. The difference in the compressive strengths of the concrete in the two bridges had an affect of less than five percent on the ultimate capacity estimates for all provisions. Due to this similarity, the remainder of the report will deal only with the capacity of Bridge 19855. Table 1-2 contains the predicted ultimate capacity, average correction factor, and estimated ultimate capacity of the Bridge 19855 overhang for each provision

The ultimate capacities estimated using the strut and tie models were similar to the shallow beam flexure estimate which is attributed to the overhangs being limited by the strength of the tie in the strut and tie model. The shallow beam shear and 1998 AASHTO MCFT predictions were also similar and approximately 300 kips larger. Therefore it is expected that the pier cap overhangs of Bridges 19855 and 19856 will fail in flexure, but could possibly fail in shear due to greater scatter in the shear failure data.

The estimated ultimate capacities are reduced by resistance factors to account for variation of material properties, construction tolerances, and inaccuracies in design equations (ACI, 2002) before being compared to the factored design load. This assures a sufficiently conservative design. The reduced ultimate capacity is equal to the estimated ultimate capacity multiplied by the appropriate resistance factor. The estimated ultimate capacity, appropriate resistance factor from the 1998 AASHTO LRFD or ACI 318-02 specification, and reduced ultimate capacity for each of the provisions are compiled in Table 1-3. The smallest reduced ultimate capacity is 1037 kips calculated from the strut and tie provision in the ACI 318-02 specification. This is 27% larger than the factored design load of 816 kips confirming that the design of the Bridge 19855/56 pier cap overhangs is conservative. It is concluded that the overhangs are not likely to fail in an undeteriorated condition.

1.5 Cracking

This study investigated detailing for limiting cracking in pier cap overhangs and eliminating cracking entirely. Although it would be ideal to prevent cracks from forming, this may prove to be uneconomical and therefore reducing crack widths is required to prevent deterioration due to corrosion.

The cracking load is the load which will initiate the first crack in the overhang. To prevent cracking, the service load must remain under this value. The cracking load was estimated using the same correction factor method as was used to estimate the ultimate capacity in the previous section. It would be ideal to use a similar method to estimate the loads required to cause further cracking or produce certain crack widths, however neither the experimental data nor

analytical methods exist for doing this. Due to this inability, a more qualitative position must be taken to examine detailing for reducing cracking. The design of the pier cap overhangs for Bridges 19855 and 19856 will be checked with serviceability provisions in the AASHTO specification for limiting cracking. This will determine if the overhangs were properly designed and if the serviceability provisions are adequate for controlling cracking in pier cap overhangs. Design suggestions for reducing pier cap cracking from the literature will then be examined to determine how the Bridge 19855/56 overhang design could be modified to possibly reduce cracking.

1.5.1 Prediction of Cracking Load

Unlike ultimate capacity, there are no provisions in the ACI or AASHTO specifications explicitly for predicting the flexural cracking load of a reinforced concrete member. Therefore, models were created in this study to predict the cracking load of a pier cap overhang. The initial crack in a pier cap overhang was assumed to be a flexure crack originating above the column. This is consistent with experimental tests (Young et al., 2002) and the cracking pattern of the overhangs of Bridges 19855 and 19856. For each model, the load required to cause the extreme tensile fibers of the overhang to reach the cracking stress of concrete was examined.

The first model, referred to as the "gross section" model, estimates the stress in the extreme tensile fibers using elementary mechanics. The overhang is assumed to be a homogenous, linear-elastic solid. The stress at cracking in the cap is related to the applied moment by:

$$s = \frac{M_{Crack}\, y}{I} \tag{1-4}$$

where M_{crack} is the applied moment that causes the overhang to crack, y is the distance from the extreme tension face to neutral axis, and I is the moment of inertia.

Since the cap is symmetric about the horizontal axis, the distance from the neutral axis to the extreme tension fibers is one half the height. The gross moment of inertia is used and calculated as follows.

$$I_g = \frac{1}{12} b h^3 \tag{1-5}$$

where b is the width of the overhang and h is the height of the overhang. The moment can be related to the applied load as:

$$M_{Crack} = P_{Crack}\, a \tag{1-6}$$

where P_{crack} is the load that causes the pier cap to crack and a is the shear span. The critical stress at which the overhang is predicted to crack is the modulus of rupture calculated as:

$$s = 7.5\sqrt{f'_c} \tag{1-7}$$

where f'_c is the compressive strength of concrete. Combining Eqns. (1-4) through (1-6) produces the following expression for the cracking load:

$$P_{Crack} = \frac{7.5\sqrt{f'_c}\, b h^2}{6a} \tag{1-8}$$

The main advantage of this provision is its simplicity. One disadvantage is that it does not account for any increase in cracking resistance due to the presence to reinforcing steel. It is

however unlikely that the reinforcing steel will have a large effect because little force is carried in the reinforcing steel prior to cracking (Macgregor, 1997).

The second model, referred to as the "transformed section" model, is identical to the simplified mechanics model except the longitudinal flexural reinforcing steel is transformed into an equivalent concrete area. The equivalent area of concrete is determined by multiplying the actual steel area by the ratio of the modulus of elasticity for steel to the modulus of elasticity for concrete. This results in a cross section similar to the one shown in Figure 1-12. This cross section is not symmetric about the horizontal axis. Accordingly the distance from the neutral axis to the extreme tensile fibers is not one half of the height. The distance is determined to be the following.

$$c_{tr} = \frac{\frac{bh^2}{2} + nA_s(h-d)}{bh + nA_s} \tag{1-9}$$

where n is the modular ratio, d is the distance from extreme compression fibers to centroid of tensile reinforcement, and A_s is the area of tensile longitudinal reinforcement. The transformed moment of inertia must also be calculated with the following equation.

$$I_{tr} = \frac{1}{12}bh^3 + bh(\frac{h}{2} - c_{tr}) + nA_s(h - d - c_{tr}) \tag{1-10}$$

The load required to crack the pier cap can be determined by combining Eqns. (1-4), (1-6), (1-7), (1-9) and (1-10).

$$P_{Crack} = \frac{7.5\sqrt{f'_c}\,I_{tr}}{ac_{tr}} \tag{1-11}$$

Although this model accounts for the presence of longitudinal flexural reinforcing steel possibly making it more accurate than the simplified mechanics model it is more computationally extensive due to the absence of horizontal symmetry.

The third model consisted of a finite element analysis of the pier cap overhang. Referred to as the "finite element" model, Abaqus CAE software was used to create a finite element model of the pier cap overhang. The load applied to the pier cap was increased in the model until the maximum principal stress in the extreme tensile fibers reached the modulus of rupture. Modeling was primarily performed in two dimensions, but was verified to accurately represent a three-dimensional model by creating both a two- and three-dimensional model for one of the experimentally tested specimens. A standard mesh size of 1 in. x 1in., approximately $1/100^{th}$ the overall dimensions, was used. The finite element model had an advantage over the other two models in that it accounted for the dimensions and specific loading of the pier cap overhang, not just a specific cross section and applied moment. Accordingly, separate models were created for the experimental test results and Bridge 19855/56 overhangs to account for any effects due to geometry or placement of loads on cracking load. The finite element model did not account for any contribution of reinforcing steel in increasing the cracking resistance of an overhang.

As was performed for ultimate strength, correction factors were calculated by applying these provisions to experimental test data from the literature. The database for this calibration consisted of 16 specimens. The correction factors were then used to estimate the cracking load of the pier cap overhangs of Bridges 19855/56.

Accuracy of Models for Predicting Cracking Load

A plot of the correction factors for each specimen calculated with a given model is included as Figure 1-13. The average correction factor and standard deviation for each provision are tabulated in Table 1-4. The predicted cracking load, applicable correction factor, and estimated cracking load for the pier caps associated with Bridges 19855/56 are tabulated in Table 1-5 and 1-6.

The transformed section model estimated the largest cracking load for the pier cap overhangs. The cracking load was 375 kips and 428 kips for Bridges 19855 and 19856, respectively. The finite element model estimated the smallest cracking loads of 329 and 382 kips for Bridges 19855 and 19856, respectively.

Sufficient information is not available to tell which of the models is most accurate at predicting the cracking load of a pier cap overhang. The provisions were calibrated using the experimental results of only one experiment and therefore the correction factors do not account for much variability in pier cap overhang design. It is noted that all three of the estimated cracking values are within 10 percent of each other creating a precise range. In practice, the gross section model may be the best method because it requires no extensive calculations or software programs and allows a good estimate of the cracking load to be calculated easily.

Comparison of Estimates for Cracking Loads to Service Loads

From comparison, it is seen that the estimated service load on Bridges 19855/56 of 540 kips is larger than the largest estimate for cracking load of the pier cap of 427 kips. The dead load of the bridge superstructure is 404 kips which is very close to the cracking load, supporting the hypothesis that the bridge cracked shortly after being opened to traffic. The fact that the service load is much larger than the cracking load also supports the cracks becoming excessive. Preventing cracking would require measures such as increasing the depth of the overhangs by 20%. This is likely uneconomical, in which case attention must shift to reducing cracking.

1.5.2 Methods for Reducing Cracking

Serviceability Provisions

Serviceability provisions are included in both the ACI and AASHTO provisions for reducing cracking in reinforced concrete members. Commonly these provisions place a limit on maximum spacing of steel reinforcing bars to control crack widths. Presented below is a summary of cracking serviceability provisions from the 1998 AASHTO LRFD specification and the 1977 AASHTO standard specification. ACI serviceability provisions are neglected in this section because they are intended for buildings which commonly require less stringent crack control than bridges. The Bridge 19855/56 overhangs were examined with each provision to determine if the design is acceptable. If it is not, the required changes were determined.

The bridge pier cap overhangs were designed according to the serviceability specifications of the 1977 AASHTO specification. The primary requirement on the longitudinal bar spacing is controlled by the following variation of the Gergely-Lutz equation.

$$z \le 0.6 f_y (d' A)^{1/3} \tag{1-12}$$

where z is the crack width parameter, f_y is the yield stress of the reinforcing steel, d' is the distance from extreme tensile fibers to centroid of tensile reinforcement, and A is the area of

concrete with the same centroid as the tension reinforcement divided by the number of tensile reinforcing bars.

The specification requires that the *z* value for structures in highly corrosive environments such as the overhangs be less than 130 k-in. The Bridge 19855/56 overhang design is unacceptable with a *z* value of 143k-in. Correcting this would require altering the design to include 24 longitudinal reinforcing bars in the tension zone instead of the current 18 longitudinal reinforcing bars. Cross-sectional reinforcing details for the as-built and required steel configurations are included as Figure 1-14. No change in the total amount of steel is required. The 1977 AASHTO specification also requires that beams with depths greater than two feet have longitudinal skin steel with an area at least ten percent of the primary longitudinal reinforcing steel area. The original design of the pier cap overhangs was acceptable with respect to this provision with skin steel equaling 15% of the longitudinal flexural steel.

The 1998 AASHTO LRFD specification uses the same requirement on longitudinal bar spacing as the 1977 AASHTO specification requiring the same alterations to the overhang design. The provision for spacing of skin steel however was changed to require that the following ratio of skin steel per foot depth be distributed throughout the region within one-half of the effective depth of the flexural tension reinforcement.

$$A_{sk} \geq 0.012(d - 30) \leq \frac{A_s}{4} \tag{1-13}$$

This provision requires that the maximum spacing of no. 6 diameter skin steel bars be 9.4 in. The spacing of these bars in the original design was 12 in. and should be reduced to 9 in. to meet this provision.

Recommendations from Literature

Ferguson (1964) and Young et. al. (2002) reported design recommendations for reducing cracking of pier cap overhangs. Both recommend that the stress due to service loads in the flexural tensile reinforcement be limited to 24 ksi at the face of the column. Applying this to the present design of Bridges 19855/56, the maximum allowable service load on the overhangs would be 420 kips. Young et al. suggests that a simple way to reduce these stresses at the column face would be to design the pier cap for the moment present at the center of the column rather than the face of the column (2002). This would require the amount of flexural tensile steel in the pier caps to be increased by 39% but allow a maximum service load of 578 kips. Young et al. also recommends that the shear resistance of the cap be designed not only for the estimated shear demand, but also to develop flexural over strength in the member to limit flexure-shear cracking. Adopting this would require that the spacing of stirrups in the overhangs of Bridges 19855/56 be reduced from 6 in. to 5 in.

Conclusions and Comparisons to Service Loads

From examination of the serviceability requirements and recommendations from the literature it may prove beneficial to increase the amount of flexural tensile steel in the pier cap overhangs to reduce stress levels, limiting crack widths. This would also increase the ultimate capacity of the overhangs in flexure. It is unknown how changes to pier cap design will affect the extent of cracking. The calculated service load of 540 kips creates a stress of 31.2 ksi in the flexural tensile reinforcement of the Bridge 19855/56 overhangs based on transformed sections. Reducing this stress to 24 ksi, as recommended in the literature, would require increasing the

amount of steel to 23.1 in^2. Designing the pier cap for the moment at the center of the column would result in the amount of longitudinal steel being increased to more than this. These measures should be considered and explored further to solve the cracking problem. The effectiveness or economic aspects of these changes is outside the scope of this research.

Chapter 2 FRP for Shear Strengthening Bridges

2.1 Introduction

In the United States, 61% of all bridges over 20 feet long are constructed from concrete (FHWA, 2003). Many of these are aging and deteriorating, and 18% are currently structurally deficient or functionally obsolete. These bridges may have fatigue, deterioration or corrosion problems due to aging, capacity problems due to an increase in loading, or clearance or geometry problems due to a change in standards or use. Replacement is often not an option due to economical reasons, and recent advances in strengthening techniques have made repair an attractive alternative.

Fiber reinforced polymers (FRP) have emerged in recent years as a popular new method for strengthening or retrofitting of reinforced concrete structures. Externally bonded (EB) FRP sheets and plates are available from several different manufacturers and have been widely used for applications including flexural strengthening of beams and slabs and wrapping of columns to improve strength and ductility. Several studies on shear strengthening of beams with FRP have also been undertaken, but this complex problem requires more investigation (Bousselham et al., 2004).

Several different types of FRP are available for use in strengthening applications. The most common are EB sheets and plates. Externally bonded FRP plates are pre-cured laminates that are attached to the structure with an appropriate adhesive. Externally bonded FRP sheets are attached to the structure using a manual lay-up procedure. A primer or putty may be required to fill cavities in the concrete. The fabric sheets are then cut to the desired size and shape and impregnated with a resin. The impregnated sheets are then affixed to the structure and pressed with a roller to eliminate air bubbles. The FRP forms to the shape of the structure as it cures. Near surface mounted (NSM) reinforcement is a recent development that has not been studied extensively. Round FRP rods have been studied by researchers for use as NSM reinforcement (De Lorenzis et al., 2000-2004, Valerio et al., 2003). Rectangular FRP tape is emerging as another alternative NSM reinforcement, but is not yet widely available. Near surface mounted FRP is installed by first cutting a groove in the surface of the concrete. The groove is then filled with an appropriate adhesive, and the NSM reinforcement is placed in the groove.

Externally bonded and near surface mounted FRP each have their own advantages and drawbacks. Externally bonded FRP sheets can easily form to the shape of the structural member. This makes them more suitable for curved, I-shaped, T-shaped or otherwise oddly shaped members. Although NSM FRP cannot usually form to the shape of a beam, it can be anchored into flanges or adjacent members. A disadvantage of the EB FRP is the possibility of premature debonding. The NSM FRP is much less sensitive to surface preparation than the EB FRP. NSM FRP also has more consistent quality because it is pre-cured and pultruded. It is also better protected after installation because it is embedded in the concrete.

The three fiber materials that are commonly used for FRP reinforcement are glass, carbon, and aramid. Table 1-1 lists typical properties of the three types of fibers and steel for comparison. Glass fibers are generally the least expensive, but they have low stiffness and sensitivity to alkaline conditions. Aramid fibers are stiffer than glass, have the lowest density and also resist abrasion very well, but can be sensitive to moisture and UV light. Carbon fibers

are the optimal choice for many structural applications due to their high strength, high stiffness, low density, and environmental resistance.

FRP offers several advantages over traditional retrofit techniques such as section enlargement, external post-tensioning and steel plate bonding. Section enlargement requires heavy machinery and a lot of labor for installation. It also increases the self-weight of the structure. External post-tensioning may not be possible for some shear applications. If a bridge deck is supported by the beam that requires shear strengthening, tendons may have to be installed through the bridge deck. Steel plate bonding is sensitive to corrosion, especially in marine environments and cold climates where salt is used on the roads throughout the winter. FRP is appealing for these applications because it is resistant to corrosion. It also has a high strength to density ratio in comparison to steel which makes installation faster and easier. The strength to density ratios of steel and a typical carbon fiber reinforced polymer (CFRP) sheet are shown in Table 1-2. Less heavy machinery and labor are required for installation, which can minimize traffic interruptions. Savings in labor, installation, and maintenance costs can offset the higher initial material costs making FRP a more cost-effective solution over the life cycle of the structure.

There are some disadvantages of FRP that must also be considered. FRP has a high initial material cost. It also has brittle behavior in comparison to steel. Because retrofitting with FRP is a fairly new procedure, there is a relative lack of experience in application of the materials, as well as a lack of understanding of some technical aspects, such as shear strengthening. As more research is completed, understanding of these complex problems will increase.

The objective of the research presented in this report was to expand on previous research that has been done to gain more understanding about one of the least understood applications of FRP: shear strengthening of beams. An initial investigation on the bond between FRP and concrete was conducted. Small-scale bond tests were used to investigate two different types of CFRP: externally bonded sheets and near surface mounted tape. Several other parameters were also examined to determine the most suitable FRP type and surface configuration for retrofit. Based on the results of the bond tests, large-scale beam tests were conducted. Beam tests were performed to study the behavior of FRP used for shear strengthening in a region that also had a large moment. This was equivalent to the loading conditions of a cantilevered structure near the support. This research was motivated by flexure-shear cracking of cantilevered bridge pier caps on MN Bridge 19855/56 in Minnesota.

2.2 Previous Research

Extensive research has been done on strengthening of structural members with FRP. This review has focused on a subset of those studies that relates directly to this investigation. The results that are included are from bond tests and tests on shear strengthening of beams using EB FRP and NSM FRP. Variables that have been addressed in these studies include strength and geometry of the concrete member, surface preparation, adhesive and fiber types, number of plies, wrapping scheme and anchorage conditions, bonded length, strip width and spacing, orientation of the fibers, and stirrup and FRP ratios.

2.2.1 Experimental Research Using EB FRP

Concrete strength was investigated as a variable in some bond tests. Chajes et al. (1996) conducted bond tests on single lap shear specimens, and discovered a trend of increased bond strength with increased concrete compressive strength. This is because the failure mode of the tests was generally through shearing of the concrete directly beneath the surface. Iketani et al. (1997) found that the failure modes were different between bond tests using normal and high strength concrete. The tests using normal-strength concrete failed by peeling of the sheets and breaking off of the concrete, while the tests with high-strength concrete all failed at higher loads by peeling of the sheets without breaking off concrete. The same correlation was found in bond tests conducted by Nakaba et al. (2001). From this information it can be reasoned that increasing the concrete strength will increase the bond strength of the FRP until the failure is no longer in the concrete.

Surface preparation is very important to the success of strengthening with EB FRP. Chajes et al. (1996) conducted bond tests using mechanical abrasion, grinding, and as-formed conditions as surface preparations. They recommended mechanical abrasion. Hutchinson (1999) found that specimens prepared with hydro-blasting performed better than specimens prepared by grinding with wire brush or sandpaper. Kachlakev et al. (1999) found that sandblasting was a very effective surface preparation.

Chajes et al (1996) also investigated different adhesives for bonding FRP to concrete, because the success of the strengthening scheme depends greatly on the adhesive. They found that an adhesive with sufficient strength and stiffness to transfer the stresses into the concrete was necessary. The adhesive should also be tough enough to resist brittle failure, but not have excessive elongation. The adhesive that performed best in their tests was Fusor 320/322, manufactured by the Lord Corp. It had a tensile modulus of 230 ksi and a 3% elongation at failure.

Many researchers investigated different fiber types for strengthening applications. Umezu et al. (1997) and Kamiharako et al. (1997) used carbon fiber sheets and aramid fiber sheets to strengthen beams in shear, but did not see a significant difference in strength between beams strengthened with the two types of sheets. Nakaba et al. (2001) conducted bond tests using aramid fiber sheets and two different types of carbon fiber sheets with different stiffnesses. They found that the carbon fiber sheets with the high stiffness had the highest strength. Chajes et al. (1995) strengthened beams in shear with glass, graphite, and aramid fiber sheets. The beams strengthened with carbon fiber sheets had the highest strength, but the beams strengthened with aramid fibers exhibited the best ductility because the sheets did not tear and continued to carry some load when the beam experienced shear failure. Araki et al. (1997) also found that aramid fiber sheets had better ductility than carbon fiber sheets. Funakawa et al. (1997) strengthened beams in shear and found that good ductility was achieved by combining one layer of carbon fibers with one layer of aramid fibers. It is important to consider that the failure mode has an impact on whether there is a significant difference in strength between one fiber type and another. When the failure was primarily in the concrete or adhesive, the fiber type was not as likely to play a significant role because the strength of the sheet was not fully utilized.

Maeda et al. (1997), Iketani et al. (1997), Ueda et al. (1999), Funakawa et al. (1997), Umezu (1997, and Ono (1997) conducted bond or beam tests with number of plies as a variable. The researchers all found that increasing the number of plies of FRP increased the ultimate

strength of the specimen, but not in a proportional way. Uji (1992), Miyauchi et al. (1997), and Hutchinson et al. (1999) conducted shear beam tests with number of plies as a variable and found no significant increase in shear strength of the specimen when additional plies were added. The failure mode is important in determining whether an increase in the number of plies results in a significant strength increase. Tests that failed by rupture of the fibers were more likely to see a significant advantage from adding additional plies than tests that failed in the concrete or adhesive. Because the increase in shear strength was not proportional to the amount of materials used for specimens that failed in the concrete or adhesive, it does not seem economical in most situations to use multiple plies.

Wrapping scheme was a variable in many tests. The three types of wrapping schemes are shown in Figure 2-1. Since a total wrap is not always possible on beams because of slabs or girders above, many researchers used a U-wrap instead. Uji (1992) conducted shear beam tests and found that a total wrap around all four sides of the beam had a great increase in strength over a two-side wrap. Taerwe et al. (1997) tested shear beams with a U wrap and a total wrap, and found that the total wrap was more effective. Al-Sulaimani et al. (1994) and Sato et al. (1996) tested beams in shear and found that a U-wrap was more effective than a two-side wrap. Although the U-wrap has shown to be more effective on average than the two-side wrap, researchers have had mixed results. Failure modes have been divided between rupture of the sheets and debonding of the sheets. It seems that using a U-wrap reduces the probability that the sheets will debond because there are only two free ends instead of four for the two-side wrap. The wrapping scheme also has an effect on other variables such as fiber type or number of plies. Because a U-wrap or total wrap is more likely to fail by rupture of the sheet, it can affect whether variables such as fiber type or number of plies have a significant effect.

Researchers have used various types of anchorage to try to utilize more of the strength of the sheets. Ueda et al. (1999) and Hutchinson et al. (1999) found an increase in bond strength when using anchor plates that were bolted to the concrete. Sato et al. (1997) conducted bond tests using an anchor plate and found that it more than doubled the bond strength in those tests. Sato et al. (1997) also strengthened beams in shear using FRP with four different anchoring methods. The anchoring methods are shown in Figure 2-2. The most effective anchorage scheme was a "closed" type in which a set of angles were bolted to the beam and bolted through the slab to a plate. Using this scheme more than doubled the shear strength of the beam. Anchor plates bolted to the beam with long bolts were also very effective. Anchor plates bolted to the beam with short bolts were less effective. Anchoring the sheets with nails shot into the concrete with a nail gun was the least effective method, but the easiest to implement. The nails and the short bolts failed by peeling off with the sheet. All of the anchoring methods used resulted in some increase in the ultimate strength over sheets that were not anchored.

Some researchers took bonded length of the sheet as a variable to try to identify the effective bond length. The effective bond length of a sheet is the length over which most of the load is transferred from the FRP into the concrete. As debonding occurs, the effective bond length shifts along the sheet. Taljsten (1997) tested four single ply CFRP plates with lengths of 100, 200, 300, and 400 mm. The ultimate load did not increase when the bonded length was greater than 300 mm. The strain distribution for the 400 mm specimen showed that the strain only reached approximately 180 mm from the end until the load reached 25 kN. At this point, the strain shifted toward the end of the sheet with the strain gradient unchanged. This demonstrated the debonding process. The loaded end of the sheet began to debond at 25 kN, and

the maximum strain occurred in the debonded region. As more of the strip debonded, the effective bond length, indicated by the strain gradient from the maximum to minimum strain, shifted toward the end of the sheet. Iketani et al. (1997) also conducted bond tests with strips 100, 200, 300, and 400 mm in length and found that strips longer than 100 mm did not have a significant increase in strength. Bizindavyi et al. (1999) conducted bond tests using single-ply and double-ply GFRP and CFRP laminates. The strain distribution showed that a single ply of GFRP had an effective bond length of 160 mm. A single ply of CFRP had an effective bond length of 80 mm. For double-ply GFRP and CFRP, the effective bond lengths were 260 mm and 220 mm, respectively. Chajes et al. (1996) conducted bond tests with CFRP plates having 100, 150, and 200 mm bond lengths, and found similar failure loads for all lengths. The strain profiles showed an effective bond length of 75 to 100 mm. The information from these tests indicated that the effective bond length is approximately 75 to 100 mm for a single layer of CFRP sheet tested in tension in the fiber direction. Modulus of elasticity, thickness and number of plies, and angle of the fibers with respect to the force could all have an impact on the effective bond length.

Strip width was taken as a variable in bond tests performed by Ueda et al. (1999). The failures occurred by debonding with some concrete torn out with the sheets. It was discovered that the concrete torn out was not proportional to the width of the strip, with relatively larger areas of concrete being torn out for the narrower strips. This phenomenon is shown in Figure 2-3.

Several researchers used fiber orientation as a variable when strengthening beams for shear. Shear cracks are assumed to form at an angle of 45 degrees to the beam, so fibers at a 45 degree angle to the beam are perpendicular to the crack, and fibers at a 90 degree angle to the beam are 45 degrees to the crack. Fiber orientations of 45 and 90 degrees to the beam are shown in Figure 2-4. Chajes et al. (1995) tested beams with a bi-directional fabric with horizontal and vertical fibers, and found that the horizontal and vertical fibers resisted the shear forces equally. Kage et al. (1997) tested beams with carbon fibers oriented horizontally, vertically, or both. They found that the most effective arrangement was one horizontal and one vertical layer. Uji (1992) found that the shear strength of the beam was 60% higher when fibers were oriented perpendicular to the crack rather than perpendicular to the beam. Hutchinson et al. (1999) strengthened I-beams in shear and also found that strips perpendicular to the crack increased the shear capacity of the beam more than strips perpendicular to the beam. They also found that adding sheets with horizontal fibers on top of sheets with fibers perpendicular to the crack could provide an even larger strength increase. Chaallal et al. (1998) found that strips perpendicular to the crack had higher strength and better ductility than strips perpendicular to the beam. Norris et al. (1997) found that orienting strips perpendicular to the crack resulted in a higher ultimate strength but less ductility.

Some researchers added longitudinal sheets for flexural strengthening in addition to shear strengthening. Malvar et al. (1995) tested beams that were strengthened with FRP for flexure or flexure and shear. The beams that were strengthened for flexure and shear performed better because they failed in flexure and were more ductile than the beams strengthened only for flexure. Alexander et al. (1996) tested beams in shear and found that adding longitudinal sheets did not contribute significantly to the ultimate shear capacity of the beam.

Prestress was a variable in beam tests conducted by Izumo et al. (1997). It was found that prestressing the sheets increased the shear capacity significantly.

Miyauchi et al. (1997) strengthened beams with different shear span to depth ratios and found that the effectiveness of the FRP increased as the shear span to depth ratio increased. Khalifa et al. (2002) also found that the FRP contribution to the shear strength of the beam was greater for a larger shear span to depth ratio. FRP becomes less effective in deeper beams because arch action in the concrete takes over.

Some researchers added longitudinal sheets for flexural strengthening in addition to shear strengthening. Malvar et al. (1995) tested beams that were strengthened with FRP for flexure or flexure and shear. The beams that were strengthened for flexure and shear performed better because they failed in flexure and were more ductile than the beams strengthened only for flexure. Alexander et al. (1996) tested beams in shear and found that adding longitudinal sheets did not contribute significantly to the ultimate shear capacity of the beam.

Varying amounts of internal shear reinforcing steel and external FRP reinforcement were used by many researchers, providing information about the interaction of internal and external reinforcement. Triantafillou (1998) tested beams with no internal steel reinforcement and found a dramatic shear strength increase on the beams that were strengthened with CFRP over unstrengthened beams. Li et al. (2001) and Khalifa et al. (2002) also found that FRP had a greater strengthening effect on beams with little or no internal shear reinforcement than on beams with more stirrups. Deniaud et al. (2001) conducted tests on beams with different amounts of internal shear reinforcement. They found that the relative contribution of the FRP to the total shear resistance decreased as the amount of internal shear reinforcement increased. As expected, the ultimate shear strength for specimens with more internal reinforcement was higher than for specimens with less internal reinforcement. The magnitude of the FRP contribution remained the same, causing the relative contribution of the FRP to decrease. Umezu et al. (1997) conducted tests in which beams were strengthened with different amounts of FRP in a total wrapping scheme. The beams with smaller amounts of FRP failed by rupture of the sheet, while the beams with larger amounts of FRP failed in shear only in the concrete, showing that the tensile capacity of the sheets was not reached. Chaallal et al. (2002) tested beams with varying amounts of internal steel reinforcement and one, two, or three plies of FRP in a U-wrap configuration. They found that the greatest increase in strength for a single layer of FRP was for a beam with 24 in. stirrup spacing, while the greatest increase in strength for a double layer of FRP was for a beam with 16 in. stirrup spacing. Therefore, they determined that there is an optimum amount of FRP reinforcement that is different depending on the amount of internal shear reinforcement. Uji (1992) found that the strains in the FRP were higher than the strains in the stirrups at the same location, due to the fact that the FRP carries most of its strain over the effective bond length, while the steel distributes the strain more uniformly. Sato et al. (1996) also found that the ratio of strain carried by CFRP to stirrups was 1.3 times the stiffness ratio of the materials because of higher localized FRP strains around the shear crack.

2.2.2 Experimental Research Using NSM FRP

Tensile bond tests conducted by Blaschko et al. (1999) indicated that applying FRP in slits greatly increased the ultimate load over applying FRP to the surface of the concrete. Hassan et al. (2002) compared the cost and effectiveness of rectangular NSM reinforcement to round NSM bars and EB sheets. Externally bonded sheets and rectangular NSM strips were found to be the most cost effective repair methods. Carolin et al. (2001) conducted tests on seven beams strengthened in flexure with square NSM reinforcement, and found that the strength of the beam

was more than doubled, demonstrating the effectiveness of the method. Cross sections of the various types of FRP used for strengthening are shown in Figure 2-5.

De Lorenzis et al. (2004) conducted a bond test on round NSM bars using groove filling material as a variable. It was found that tests with epoxy-filled grooves had higher strength than tests with cement paste-filled grooves. Carolin et al. (2001) tested beams strengthened with square NSM rods and recommended using cement mortar instead of epoxy for improvement of health and environmental conditions on site.

Fiber type and surface treatment of the bars were variables in bond tests conducted by De Lorenzis et al. (2004). CFRP and GFRP bars were tested. Specimens with CFRP bars were found to have higher ultimate strengths than those with GFRP bars. Specimens containing bars with a spirally wound surface deformation pattern had higher bond strengths than specimens containing bars with a ribbed surface. De Lorenzis et al. (2002) found that deformed bars were more likely to cause a splitting failure of the surrounding material, while sandblasted rods were more likely to pull out.

Surface preparation of the groove was also a variable in bond tests conducted by De Lorenzis et al. (2004). The specimens with rougher grooves made by saw cutting achieved higher loads than the specimens with smooth grooves as formed.

Groove width was a variable in bond tests performed by De Lorenzis et al. (2001, 2002). They found that increasing the size of the groove increased the strength when the failure occurred by splitting of the epoxy cover, but not when failure occurred by pullout of the bars. De Lorenzis et al. (2004) found that increasing the groove size increased the bond strength by delaying the splitting failure.

Several researchers investigated the effects of different bond lengths. Yan et al. (1999) and De Lorenzis et al. (2001, 2004) conducted bond tests with round NSM FRP bars and found that increasing the bonded length of the NSM reinforcement increased the ultimate load. Sena-Cruz et al. (2004) performed a bond test using rectangular NSM CFRP strips. They found that increasing the bond length increased the ultimate strength, but the average bond strength over the length of the FRP decreased. This showed that an increase in bonded length of FRP results in an increase in strength that is not proportional to the amount of additional material used. Hassan et al. (2003) conducted beam tests using rectangular NSM tape to strengthen beams in flexure. They found that bonded lengths of less than 250 mm did not result in a significant load increase over the control beam with no FRP. Bonded lengths between 250 mm and 850 mm resulted in a load increase of approximately 15 to 45% over the control beam, but eventually failed by debonding of the FRP tape. Bonded lengths greater than 850 mm had the highest loads, with a load increase of approximately 53% over the control beam, and failed by rupture of the strips. This indicated that the development length for the NSM bars on the beams in the study was approximately 850 mm. They also noted that the development length of the NSM bars could depend on the amount of internal steel reinforcement and the width of the groove.

Some researchers strengthened beams in shear with NSM FRP rods with rod spacing as a variable. Khalifa et al. (2000) conducted tests on two beams with different rod spacings and found an increase in the ultimate load of 30% for the larger spacing, and 44% for the smaller spacing compared to the unstrengthened beam. De Lorenzis et al. (2001) conducted three tests on T-shaped beams and found that NSM reinforcement was able to increase the shear capacity of the beams by 28 to 41% over beams without NSM reinforcement. Valerio et al. (2003) tested ten

beams in shear using one to five round aramid NSM bars. They found that using one or two bars enhanced the shear capacity somewhat by changing the geometry of the shear crack, but the failure was eventually by shear. Using three to five bars resulted in the highest load and prevented shear failure, forcing the beams to fail in flexure.

De Lorenzis et al. (2000) conducted eight shear tests on T-shaped beams with fiber orientation as a variable. They found that fibers at an angle of 45 degrees to the beam (perpendicular to the crack) were most effective. They also found that the strength could be enhanced further by anchoring the rods into the compression flange of the beam.

Nordin et al. (2001) conducted tests on four beams in flexure using prestressed square NSM reinforcement. They found that all of the beams failed by fracture of the fibers with an increase of up to 70% in the ultimate load over the control beam with no NSM reinforcement. The beams strengthened with prestressed fibers had the same ultimate load as those without prestressed fibers, but a smaller displacement at failure.

It is difficult to directly compare the results of the tests on NSM FRP because several different types and shapes of bars were used in the tests. There were very few test results available for rectangular NSM FRP tape, indicating that much more research needs to be undertaken to gain a better understanding of that type of reinforcement.

Chapter 3 Experimental Program

3.1 Introduction

This chapter presents the details of the experimental tests conducted at the University of Minnesota regarding the use of FRP for shear strengthening of beams. The testing program consisted of two parts. The first part was a series of eighteen bond tests conducted on small-scale specimens. The objective of these tests was to gain a greater understanding of the bond behavior of FRP. The second part of the experimental testing program was a series of tests conducted on two large-scale beam specimens. The objective of the beam tests was to evaluate the behavior of FRP when used to repair shear cracks. The design and materials used in the large-scale beam tests were determined from the results of the small-scale bond tests. The test type, parameters, specimen design, materials used, construction, instrumentation, and procedure for the small-scale bond tests are presented in Section 3.2. The corresponding details are presented for the large-scale beam tests in Section 3.3.

3.2 Bond Tests

3.2.1 Test Type

Before using FRP to repair shear cracks in a structure, it is important to understand the bond behavior between FRP and concrete. The test type for the small-scale tests was chosen to investigate the effects of several variables on bond behavior between FRP and concrete. The test setup is shown in Figure 3-1. Two concrete blocks were placed adjacent to each other to simulate a crack between them. The blocks were loaded in a direction perpendicular to the crack to simulate crack opening. The blocks were attached by one ply of FRP bonded across the crack on two sides, eliminating any steel or concrete contribution. An advantage of this test setup was the ability to test the FRP without gripping it directly, which eliminated a possible stress concentration. This test setup also allowed tensile load to be applied to FRP on both sides of the block at one time while keeping the moment in the strips to a minimum.

The tests were performed using a 600 kip universal load frame. One half of the specimen was attached to a stiffened steel beam that was attached to the laboratory floor. The other half was seated on top of the first half and attached to a similar steel beam connected to the cylinder of the load frame. Grout was used at the interface between each block and steel beam to ensure a tight fit and prevent vertical rotation of the blocks. Petroleum jelly was applied to the edges of the adjoining surfaces of the beams to keep the epoxy resin from gluing the crack shut. An upwards force was applied to the top block to open the crack.

3.2.2 Parameters

Two different types of FRP were used in the small-scale bond tests. They were externally bonded CFRP sheets and near surface mounted CFRP tape. A total of 18 tests were completed with the two types of FRP. The parameters for each test are shown in Table 3-1.

For the EB FRP sheets, the variables investigated were strip width and spacing, strip orientation, and unbonded region at the crack. The total amount of FRP on each specimen was the same to facilitate comparisons between tests.

The system for the EB FRP sheets consisted of a roll of carbon fabric and an epoxy resin matrix. The fabric could be cut to any desired size and shape before being applied to the structure. Previous research had indicated that the area of concrete substrate removed was proportionally larger for sheets of smaller widths (Ueda et al., 1999). The variable of strip width and spacing was chosen to investigate the possibility that using smaller strips with spaces between them may be more efficient than using one strip with the same total width, because a larger total area of concrete substrate could be removed with multiple strips.

Strip orientation was chosen as a variable because of the possible advantages with shear cracks where the crack is opening and sliding simultaneously. It was expected that a strip with fibers oriented 90 degrees to the crack would be the most effective in the crack opening tests because the loading would be in the fiber direction. Specimens with fibers oriented 45 degrees to the crack were also tested. In previous research, beams had been strengthened in shear with FRP oriented at 45 or 90 degrees to the crack (Uji, 1992, Chaallal et al, 1998, Hutchinson et al, 1999). However, none of the bond tests had tested fibers at an angle to the loading direction to determine if there was any impact on the effective bond length.

An unbonded region near the crack was also chosen as a variable for the EB FRP. It was thought that leaving an unbonded region near the crack would reduce the stress concentration in the FRP at the crack, increasing the effectiveness of the strip. An unbonded region had not been used as a variable in any of the bond tests discussed in Chapter 1.2.1.

The variables addressed with the NSM FRP tape were strip orientation, adhesive type, and vibrations during cure of the epoxy. The NSM FRP tape was packaged as a roll of tape that could be cut to the desired length before being applied to a structure, but the width of the tape was constant. Two strips of tape were used on each side of every specimen to facilitate comparisons between tests.

Strip orientation was a variable for the NSM tape. As with the externally bonded sheets, it was expected that tests with fibers oriented at 90 degrees to the crack would be the most effective, but a test with fibers at 45 degrees to the crack was also performed.

The adhesive type was also chosen as a variable for the tests on NSM FRP, because the tape was not a part of a commercially available system. After completing the first three tests with NSM tape, it was determined that an additional study of adhesives from several different manufacturers needed to be completed to determine which adhesives were best for use with FRP tape. The details and results of that study can be found in Appendix B. The adhesive that performed best in that study was used in the remaining tests on NSM FRP. In Table 3-1, the FRP type for the tests with the first adhesive (Sika Anchorfix-3) is listed as NSM-A, while the FRP type for the tests with the second adhesive (3M DP460 NS) is listed as NSM-B.

One specimen with NSM FRP was loaded with a small cyclic load while the epoxy was curing. This was done to investigate the possible effects of traffic vibrations during cure of the adhesive on the effectiveness of the NSM FRP repair.

The specimen labeling system used for the bond tests references the variables in that particular test. Tests beginning with an E have externally bonded sheets, while those beginning

with an N have near surface mounted tape. An A or B denoting which adhesive was used follows the N for the near surface mounted specimens. The next number states the testing order. After the first dash, a 45 or 90 signifies the angle of the fibers to the crack. The next number represents the number of strips on each side of the specimen. For the specimens with an unbonded region, the last number with the U is the total number of unbonded inches. The specimen with vibrations has a V at the end of the designation. For example, test E3-90-1-U2 is the third externally bonded test; it had one strip at 90 degrees to the crack and two total inches of unbonded region at the crack.

3.2.3 Specimen Design

Each half specimen was a rectangular shape, 2 x 1 x 1 ft. The two halves joined together to form a square shape 2 x 2 x 1 ft. Specimen drawings can be found in Figure 3-2. A square shape was chosen to allow investigation of different strip orientations. The dimensions of the specimen were chosen to be larger than the effective bond length of the EB FRP sheets. The effective bond length was found in previous research to be in the range of 3 to 4 in. for a single ply of CFRP (Iketani et al., 1997, Bizindavyi et al., 1999, Chajes et al., 1996). Therefore, a length of 12 in. on each side of the crack was determined to be sufficient.

The gap between the two halves of the specimen simulated the crack opening, so sufficient reinforcement was used in the specimen to prevent cracks from occurring elsewhere in the specimen. Threaded rods embedded into the specimen attached the specimen to the loading frame. There was not enough room inside the half specimen to anchor the rods through bond, so a nut was placed in the middle of the half specimen to serve as mechanical anchorage. The reinforcement inside each half specimen was designed to ensure that there would be no cracking of the core concrete when the FRP fibers were oriented at 90 or 45 degrees to the crack.

Two unbonded 1.25 in. diameter steel rods extended through both halves of the specimen and acted as linear bearings to ensure that the crack opened evenly with no rotation of the blocks. Two PVC pipe sleeves were cast into each half specimen to accommodate these rods. The rods fit snugly into the PVC pipes and were greased to ensure that friction from the rods did not interfere with the test.

3.2.4 Materials

The concrete for the small-scale specimens was delivered from a ready-mix plant. The mix design specified normal weight concrete with a compressive strength of 4000 psi at 28 days. A slump of 5 in. was specified to ensure that the concrete penetrated all of the gaps between the reinforcing steel. A slump test (ASTM C143) was performed prior to concrete pouring to verify the properties. Initially, the measured slump of the concrete was 4 in. Plasticizer was added to the mix to increase the workability. A second slump test was performed, and the measured slump was 5 in. Test cylinders were also made during the concrete pour. Compressive and split tensile strength tests (ASTM C39 and ASTM C496) were conducted at the beginning, middle, and end of the bond tests. Values for these tests are given in Table 3-2. The values represent the average of three tests on 4 x 8 in. cylinders. Coefficients of variation for the tests are also given in the table.

The threaded rods for the longitudinal bars were Grade B7. The rebar for the internal reinforcement were #3 and #4 Grade 60.

The FRP system used for the externally bonded sheets was a Tyfo Fibrwrap by Fyfe Co. This system consisted of SCH-35 Composite with Tyfo S epoxy. SCH-35 was a unidirectional carbon fiber fabric packaged in a 24 in. wide roll. The Tyfo S epoxy was a two-component epoxy matrix material that could be thickened to any desired consistency and could also be used as a primer and finish coat. The composite laminate thickness was approximately 0.035 in. The ultimate strength given by the manufacturer was 143,700 psi in the fiber direction and the tensile modulus was 11,400 ksi. The manufacturer specified ultimate strain of the laminate was 1.26%. There were several manufacturers that made similar systems consisting of a unidirectional carbon fiber fabric and an epoxy matrix. The Tyfo system was chosen because the epoxy only required a 72 hour cure. All of the other available systems required a 7 or 14 day cure, which would significantly impact the time required to complete all of the tests. Bond tests on concrete cylinders were completed to confirm the cure time of the epoxy and ensure that the Tyfo system could be confidently tested after 72 hours. The details and results of these tests can be found in Appendix C. Tensile tests were performed to determine the ultimate strength of the FRP laminate. The tensile strength, shown in Table 3-3, is the average of six tests. The coefficient of variation for the tests is also given in the table.

The FRP system chosen for the near surface mounted tests was Aslan 500 CFRP tape by Hughes Brothers. It was made from 700 ksi carbon fiber, 60% by volume in a bisphenol epoxy vinyl ester resin matrix. The tape was 2 x 16 mm (0.079 x 0.63 in) with a cross-sectional area of 0.05 in^2. The manufacturer specified guaranteed tensile strength of the tape was 300,000 psi and the modulus was 19,000 ksi. The manufacturer specified ultimate strain of the tape was 1.7 %. Aslan 500 Tape was chosen for the near surface mounted tests because it was the only rectangular near surface mounted tape available. Tensile tests were also performed to determine the ultimate strength of the FRP tape. The tensile strength, shown in Table 3-3, is the average of six tests. The coefficient of variation for the tests is also given in the table.

The adhesives chosen for use with the Aslan 500 FRP tape were Sika Anchorfix-3 (adhesive A) and 3M DP-460 NS (adhesive B). The Anchorfix-3 was initially chosen based on cost, availability, and ease of application, but after testing several different adhesives, it was found that the DP-460 NS had superior bond characteristics. The shear strength of Sika Anchorfix-3 given by the manufacturer was 4900 psi. The tensile strength was 4700 psi, and the tensile modulus was 120 ksi. The manufacturer specified elongation to failure was given as 1.2%. The shear strength of the 3M DP-460 NS was given by the manufacturer as 4500 psi. The tensile strength was 5100 psi and the tensile modulus was 360 ksi. The elongation to failure was not supplied by the manufacturer, but previous research had indicated a measured value of 2.1% elongation to failure (Nozaka, 2002). The cure time for both epoxies was 24 hours at room temperature.

3.2.5 Construction

Three separate sets of forms were constructed for the small-scale specimens. Each set of forms contained ten half blocks, or five specimens. Figure 3-3 shows a set of forms. The forms were fabricated from 0.375, 0.5 and 0.75 in. plywood and 2 x 4 in. bracing. Each end of a specimen had holes for four threaded rods to extend out 6 in. beyond the concrete. Each end also had two holes for 1.25 in. PVC pipes that held the place of the steel bearing rods until testing. PVC sleeves fit snugly over the PVC pipes. The pipes were greased for ease of removal. A piece of plywood between the two half blocks also had holes with 1 in. long PVC pipe sleeves to

support the inside ends of the threaded rods during concrete casting, because the rods could not extend through both halves of the specimen. The middle piece of plywood also contained holes for the PVC pipe to extend through. Ends of all PVC pipes inside the forms were taped to keep concrete from getting inside. The forms were oiled before the reinforcement was placed inside to prevent oil from coming into contact with the reinforcement.

The specimens were cast on the University of Minnesota Civil Engineering loading dock. The concrete was placed in two lifts, each approximately 12 in. deep. The first lift was placed in each form and vibrated, and then the second lift was placed in each form and vibrated. The tops of the specimens were then finished with a float. The specimens for the bond test were cast on the afternoon of 3/13/03. The specimens were kept in the forms for seven days covered with wet burlap and plastic tarps to keep them moist. After seven days, the burlap was removed and the specimens were removed from the forms. They were then stored in the laboratory until testing.

3.2.6 Instrumentation and Data Acquisition

A computer data acquisition system was used to record time, displacement, and load from every test. Data was taken at a rate of 1 Hz. All of the tests were displacement-controlled to allow data to be collected for FRP on both sides of the specimen.

In every test, four linear variable differential transformers (LVDTs) were used to measure the crack opening on each corner of the block. The LVDTs were glued to the top and bottom halves of the block approximately 5 in. from the edge. The LVDTs were located approximately 1 in. out from the surface of the concrete. Therefore, the distance between two LVDTs on the same side or opposite one another was 14 in.

On most of the specimens with EB FRP sheets, strain gages were also used. The strain gages were placed on the surface of the FRP at a 1 in. spacing to capture the effective bond length as it shifted away from the crack. The gages extended 6 in. on either side of the crack. The gages were oriented in the same direction as the fibers, and were placed all in the same line of fibers. The fibers are sewn together with threads that run perpendicular to the fiber direction. The strain gages were placed to avoid these threads to minimize the influence of the surface irregularities on the strain readings. The instrumentation plan for a typical specimen can be seen in Figure 3-4.

The specimens with the NSM FRP did not have any surface strain gages.

3.2.7 Procedure

The testing procedure for the tests on EB FRP was slightly different from the procedure followed for the tests on NSM FRP due to the different preparations required. In addition, the procedure changed slightly for some of the specimens to remedy problems that were encountered. Several changes were also made to fine tune the procedure in a series of pilot bond tests that were completed prior to beginning the primary bond tests. The details of the pilot tests can be found in Appendix D.

The basic procedure for the setup and testing of the specimens with EB FRP was as follows:

Each specimen was brought to the test frame as one unit. They were lifted with threaded rods that were placed in the PVC pipe sleeves. Once the specimen was set near the test frame,

the top half of the specimen was lifted off with the crane, and the plywood was removed from between the two halves. The PVC pipes inside the sleeves were also removed at that time.

The specimen was then placed into the load frame. The bottom half of the specimen was lifted into the frame using chain hoists. It was aligned with the bottom steel beam and set into place. The top half of the specimen was then picked up with the chain hoists and set on top of the bottom half. The two steel rods were then dropped into the PVC pipe sleeves to line up the two halves. The crosshead was lowered onto the top half of the specimen. If the alignment was off, shims were placed at the corners of the bottom specimen to level it and align the threaded rods with the holes in the top steel beam.

Once the top and bottom halves were sufficiently aligned with each other and with the steel beams, grout was placed. The crosshead was lifted, and the edges of the specimen were taped to reduce dripping. The grout was mixed with enough water to achieve a workable consistency. It was poured on the top half block and the crosshead was lowered until the beam squeezed grout out from each side to ensure complete coverage. The grout was allowed to harden for approximately one half hour. Nuts were then placed on the threaded rods and torqued to 600 ft-lb. The bottom half of the specimen was then lifted up snug to the top half with the chain hoists. The bottom half was prepared and grout was placed in the same way. After the grout was completely cured and all nuts were fully torqued, the crosshead was raised and lowered a few times to ensure everything moved smoothly.

Surface preparation was required to remove any excess loose concrete from the surface and ensure that the vertical exterior surface between the two blocks was even. Any unevenness on the vertical exterior surface between the two blocks at the crack could cause a stress concentration in the FRP during testing. The surface was evened out by grinding. Wire brushing followed to roughen up the surface for better adhesion. Any remaining dust was then blown away with pressurized air until the surface was clean. Before the FRP was applied, petroleum jelly was spread on the inside edges of the blocks to keep the adhesive from gluing the cracks together. Masking tape was applied to the edges to ensure that no petroleum jelly got on the specimens where the FRP was to be applied. On the specimens with an unbonded region, petroleum jelly or an anti-adhesive tape was applied over the desired unbonded area.

The two parts of the epoxy were measured and mixed at a ratio of 34.5 to 100 by weight. The epoxy was thoroughly mixed with a paddle mixer and a base layer was applied to both sides of the specimen with a foam roller as a primer. The primer layer was given approximately one half hour to seep into the pores of the concrete. The FRP fabric was cut to the desired length and width and saturated with the remaining epoxy. Strips for all tests were 22 in. long. The excess epoxy was pushed out of the fabric with a roller. The fabric was applied to each side of the specimen and a level was used to ensure that the fibers were oriented at the desired angle. A final coat of epoxy was applied to the FRP.

The hydraulics were turned on and the load was set to 1 kip in compression in order to maintain a constant position while the FRP cured. The load was held for at least 72 hours until testing began. Keeping the load constant was more successful than keeping the displacement constant, possibly due to shrinkage in the hydrocal.

After the FRP had cured for at least 24 hours, the strain gages were applied to the FRP surface. The LVDT supports were also glued onto the concrete surface. The instrumentation was checked to ensure it was working properly.

After at least 72 hours, the bond test began. The tests were monotonic with a crosshead loading rate of 0.00005 in./sec. The tests continued until the FRP on both sides had peeled off. The FRP and concrete failure surfaces were then photographed, the hydraulics were shut off, and the blocks were removed from the testing machine.

Several changes in procedure were required for the specimens with NSM FRP tape. Instead of the surface preparations, two grooves were cut into the full length of the specimens on each side. The 0.25 x 0.75 in. grooves were cut with a diamond tuck-pointing blade on a circular saw. The grooves were then brushed out and blown out with pressurized air to remove any dust or debris.

The adhesives used came in two-part cartridges that were mixed using a static mixing nozzle and dispensed with a manual or pneumatic gun. A small amount of adhesive was discarded at the beginning of each cartridge to ensure that only well-mixed adhesive was applied. The FRP tape was cut to 24 in. and one piece of tape was coated with epoxy. The grooves were masked with tape to prevent excess epoxy on the surface of the concrete. One groove was then filled with epoxy and the tape was inserted so that it was centered in the groove. Any remaining voids were filled with epoxy and the excess epoxy was removed with a trowel. The surface was smoothed, and the masking tape was removed. The same procedure was then followed for the other three grooves.

One specimen had cyclic loading applied while the adhesive was curing. For that specimen, the load was set to cycle between 1 and 5 kips in compression at a frequency of 1 Hz. The loading began as soon as the FRP had been applied to the specimen, and continued for 3 days until the specimen was tested.

3.3 Beam Tests

3.3.1 Test Type

The large-scale specimens were intended to have loading conditions similar to the cantilevered bridge pier caps with flexure-shear cracks. Therefore, the test setup needed to produce a shear failure in a region of high moment. A simply-supported beam was chosen for the specimen, because the middle region of a simply supported beam with a point load in the center has similar loading conditions to a cantilever with high moment and shear. The simply supported beam was chosen for the beam tests because it provided an opportunity to test two different shear detailing schemes with one test specimen. The test setup can be seen in Figure 3-5.

Lateral bracing was provided at each end of the beam near the reaction blocks. The lateral bracing consisted of a steel beam bolted to the floor, and steel beams bolted to the floor beam on either side of the specimen. The space between the bracing was set at 12.5 in. so that it would be greater than the width of the beam. The lateral bracing was in place to prevent the beam from tipping to the side in the case of an unexpected type of failure.

The tests were performed using a 600 kip universal load frame. The ends of the specimen were supported on bearing pads on concrete reaction blocks, and a point load was applied to a steel bearing plate in the center of the beam.

3.3.2 Parameters

The amount of internal shear reinforcement was a variable in the tests. Each beam had one shear span with stirrups and one without so that shear strengthening in both types of regions could be investigated. Beam B1 was cracked and retrofitted with FRP on both shear spans. Beam B2 was used as a control to try to determine the strength of the shear span with minimum stirrups.

3.3.3 Specimen Design

Each specimen was 12 x 32 x 192 in. The longitudinal reinforcement and the cross-sectional dimensions of the beam were chosen to provide a higher moment capacity than shear capacity. The depth of the section was made larger than the small-scale specimens to ensure that there was sufficient length to develop at least one FRP tape across a shear crack. The length of the specimen was chosen to provide a shear span to effective depth ratio of at least 3. The actual shear span to effective depth ratio of the beam was 3.

There were five #10 Grade 60 bars in each specimen for longitudinal reinforcement. Stirrups were placed in the beam to ensure that there would be a shear failure in the center region of the beam, where the moment was also high. Each specimen also had #3 stirrups spaced at 4 in. in the end regions, where shear failure was not desired. The end regions extended 1.5 times the effective depth from the end supports of the beam. The center regions extended 1.5 times the effective depth from the center of the beam. In the center region on one side, #3 stirrups were spaced at 14 in., the maximum spacing. The stirrup spacing to satisfy A_{vmin} would have been 22 in., but the maximum spacing of one half the effective depth controlled the design. In the center region on the other side, there were no stirrups. Concrete cover of 2 in. was provided on all faces of the beam. Figure 3-6 shows drawings of the specimen.

3.3.4 Materials

The concrete for the large-scale specimens was delivered from a ready-mix plant. The mix design specified normal weight concrete with a compressive strength of 4000 psi at 28 days. Test cylinders were made during the concrete pour. Compressive and split tensile strength tests (ASTM C39 and ASTM C496) were conducted at 28 days as well as at the beginning and end of the tests. Values for these tests are given in Table 3-4. The values in the table represent the average of three tests on 4 x 8 in. cylinders. The coefficients of variation are also given in the table.

The rebar for the longitudinal reinforcement was #10 Grade 60, and the rebar for the transverse reinforcement was #3 Grade 60.

Aslan 500 CFRP tape by Hughes Brothers was used for the near surface mounted reinforcement. The adhesive chosen for use with the Aslan 500 FRP tape was 3M DP-460 NS.

3.3.5 Construction

Two sets of forms were constructed for the large-scale specimens. The beams were cast together using separate forms to ensure that they would have the same strength concrete. Each set of forms contained one beam. The forms were fabricated from 0.75 in. plywood and 2 x 4 in. bracing as shown in Figure 3-7. The forms were oiled before the reinforcement was placed inside to prevent oil from coming into contact with the reinforcement.

The specimens were cast on the University of Minnesota Civil Engineering loading dock. The concrete was placed in two lifts and vibrated. The tops of the specimens were then finished with a float. The specimens for the beam tests were cast on 2/24/04. The specimens were kept in the forms for seven days covered with wet burlap and plastic tarps to keep them moist. After seven days, the burlap was removed and the specimens were removed from the forms. They were then stored in the laboratory until testing.

3.3.6 Instrumentation and Data Acquisition

A computer data acquisition system was used to record time, displacement, and load from each test. Data was taken at a rate of 1Hz. The tests were displacement controlled.

LVDTs measured the relative displacement between the bottom of the beam and the reaction block at each end of the beam. LVDTs also measured the relative displacement between the bottom of the beam and the floor at the center of the beam.

Internal strain gages were placed on selected stirrups in each beam. The typical stirrup instrumentation is shown in Figure 3-8. The strain gages were placed on both legs of all stirrups located in the center region. In the end regions, every other stirrup had strain gages placed on one leg. On each leg that had strain gages, there were three gages. One was placed at midheight of the stirrup and the other two were 8 in. above and below midheight. The internal strain gages were waterproofed with a butyl rubber tape and an epoxy coating and the wires were secured to the stirrup legs to prevent damage to the gages or wires during pouring.

3.3.7 Procedure

There were several differences between the testing procedures of the two beams. The setup and testing procedure for the first test was as follows:

The beam specimen was stored in the laboratory until testing. The beam was lifted with the crane into one side of the testing frame. A pallet jack and crane were used to position the beam in the center of the testing frame. Once the beam was positioned on the concrete reaction blocks, chain hoists were used to accurately align the beam with the bearing pads on both ends and with the crosshead in the center.

Grout was used to attach a steel bearing plate to the center of the top of the beam. The crosshead was lifted, and shims were used to level the plate with the crosshead. The plate was lifted, and grout was poured onto the beam. The plate was then placed on top of the grout.

Lateral bracing was set up near the reaction blocks on each end of the beam. The bracing was checked to ensure that the beam was not bearing on the bracing.

The LVDTs were attached to the bottom of the beam on each end and in the center. The strain gages were connected to the data acquisition system, and all of the instrumentation was checked to ensure that it was working properly.

The hydraulics were turned on and the crosshead was lowered to the surface of the bearing plate. A small amount of compression was applied to the beam to close the gap between the crosshead and the bearing plate.

The first testing phase began. The testing was monotonic with a crosshead loading rate of 0.01 in./min. Testing was stopped at several points to inspect the crack growth. Testing was

terminated when significant flexure-shear cracks were detected on the side of the beam without stirrups. The cracks were determined to be significant when they had turned diagonally toward the loading point and extended approximately two-thirds of the depth of the beam. The specimen was then unloaded and photographed.

The side of the beam with no internal shear reinforcement was retrofit with NSM FRP. Four grooves were cut at a 45 degree angle to the beam. The 0.25 x 0.75 in. grooves were cut with a diamond tuck-pointing blade on a circular saw. The grooves extended approximately six inches past the center of the beam, and six inches past the end of the region without stirrups. The grooves were brushed out and blown out with high pressure air to remove any dust or debris.

The adhesive used to apply the FRP came in two-part cartridges that were mixed using a static mixing nozzle and dispensed with a pneumatic gun. A small amount of adhesive was discarded at the beginning of each cartridge to ensure that only well-mixed adhesive was applied. The FRP tape was cut to the length of the groove and one piece of tape was coated with epoxy. The grooves were masked with tape to prevent excess epoxy on the surface of the concrete. One groove was then filled with epoxy and the tape was inserted so that it was centered in the groove. Any remaining voids were filled with epoxy and the excess epoxy was removed with a trowel. The surface was smoothed, and the masking tape was removed. The same procedure was then followed for the other seven grooves.

After allowing the adhesive at least 48 hours to cure, the second testing phase began. The crosshead was brought back into contact with the plate and a small amount of compression was applied. The second phase of testing was identical to the first phase except that testing continued until significant flexure-shear cracks were observed on the side of the beam with stirrups at the maximum spacing. The specimen was then unloaded and photographed.

The side of the beam with stirrups at the maximum spacing was then retrofit with NSM FRP tape. Two grooves were cut on each face at a 45 degree angle to the beam. The groove preparation and application of the FRP tape was completed as on the other side of the beam.

After allowing the adhesive at least 48 hours to cure, the third testing phase began. The crosshead was again brought back into contact with the plate and a small amount of compression was applied. The third phase of testing was similar to the other two phases. The testing was continued until failure of the beam occurred and the load dropped. The beam was then unloaded and photographed. The beam was removed from the testing frame.

The setup and testing procedure for the second beam was different because the beam was intended to be used as a control specimen. It was intended to have a shear failure to compare to the flexural failure of the first beam.

While the beam was stored in the lab, NSM FRP tape was applied to the side of the beam with no stirrups. Shear failure was desired on the side of the beam with minimum stirrups so there was no FRP applied to that side.

The groove preparation and FRP application procedure were similar to the other beam. Four grooves were cut on each side of the beam at a 45 degree angle. The grooves were cleaned out with high pressure air. FRP was applied to the first four grooves using the same procedure as the other beam. At this point, all of the large tubes of adhesive had been used. For the remaining four grooves, multiple small cartridges of adhesive were used for each groove. The small cartridges were dispensed with a static mixing nozzle and a manual gun.

After allowing the adhesive to cure for at least 48 hours, the beam was lifted into the loading frame. For this beam, the adhesive actually cured for several weeks due to delays in the laboratory. The same procedure as used for Beam 1 was used to position and align the beam, attach the steel bearing plate, and set up the instrumentation.

The hydraulics were turned on and the crosshead was lowered to the surface of the bearing plate. A small amount of compression was applied to the beam to close the gap between the crosshead and the bearing plate.

The testing then began. The testing was monotonic with a crosshead loading rate of 0.01 in./min. Testing continued until failure of the beam occurred and the load dropped. The specimen was then unloaded, photographed, and removed from the testing frame.

Chapter 4 Experimental Results and Discussion

4.1 Introduction

The results for the eighteen bond tests and the two beam tests are presented and discussed in this chapter. The results for the bond tests are explained in Section 4.2. A discussion of the results and the effects of the variables are discussed in Section 4.3. The results of the beam tests are presented in Section 4.3 and discussed in Section 4.5. Detailed summaries for each individual bond test can be found in Appendix E. Graphs showing the load vs. stroke, load vs. LVDT displacement, and strain graphs for each bond test are shown in Appendix F. The photographs of the failure surfaces of each bond test specimen are shown in Appendix G.

4.2 Bond Test Results

Table 4-1 gives the maximum load achieved in each of the bond tests with externally bonded (EB) sheets, and the maximum load achieved for the east and west sides of the specimen. For specimens with multiple strips, the loads for each strip were determined from the difference between the recorded load before and after failure of that strip. The strips are identified with their respective location on the east and west sides, with N denoting the strip on the north side, C for center, and S for south. If more than one strip failed simultaneously, the total load for that failure was divided equally among the strips that failed at that time. These loads are denoted by an s in the table.

Table 4-2 gives the maximum strain reading for each side of each specimen. The maximum strain reading is the highest strain value of any gage at any load level for the entire test. The maximum strain did not usually occur at failure, so the strain at failure is also listed. The maximum strain at failure was the highest strain value of any gage at the last load recorded before failure. The average strain at debonding for each side is also given in the table. The average strain at debonding was also taken at the last load recorded before failure. It was taken as the average of all of the strain readings on gages that were in the debonded region of the sheet. The debonded region was defined as the region near the crack where there was less than 200 microstrain change from one gage to the next. The strips that did not have strain gages have an ND, indicating that no data was available.

Table 4-3 presents the failure surface areas for the eighteen externally bonded specimens. Figure 4-1 shows a diagram of the two types of failure surfaces: concrete substrate failure and shear failure at the crack. The concrete substrate failure area is the surface concrete area where the FRP sheet was attached to the concrete. The shear failure area is a piece of concrete at the crack that extended to the side beyond where the FRP was attached to the concrete and extended deeper into the concrete block. The estimated percentage of concrete substrate failure area on each side is given in Table 4-3. The estimated concrete substrate surface areas were estimated from the pictures of the failure surfaces of concrete and FRP shown in Appendix G. The substrate failure area is taken as a percentage of the area over which the FRP sheet was attached to the concrete. The estimated crack projection area for each side is also given in the table. The estimated crack projection area was found by assuming a triangular shape for the concrete piece taken out at the crack. The area of the triangle was estimated from the measured height and length of the concrete shear failure surface. The specimens were divided into two groups depending on the estimated concrete substrate failure area. If the concrete substrate failure area

was at least 30% of the failure area for at least one side of the specimen, then a significant amount of concrete substrate had been removed for that specimen, and the specimen was placed in group 1. If less than 30% of the failure area was concrete substrate, then it was not significant, and the specimen was placed in group 2. The last column of Table 4-3 lists the group in which each specimen was placed.

Table 4-4 shows the effective bond lengths that were estimated from the strain graphs. The effective bond length of an FRP sheet is the length over which most of the load is transferred from the FRP into the concrete. For each strip that had strain gages, an effective bond length was measured for several different loads. The largest and smallest effective bond lengths on each side of the specimen are given in the table.

Table 4-5 gives the results of the tests for the near surface mounted (NSM) FRP. The first column gives the maximum load reached in the test. The table also gives the maximum load reached for each tape on each side. An s indicates that two or more strips failed simultaneously and the total load was divided equally among the strips.

4.3 Discussion of Bond Tests

4.3.1 Discussion of Bond of EB FRP

Table 4-1 shows a fair amount of variability in the loads of some similar specimens. Specimens E1-90-1, E2-90-1, and E6-90-1 were all control tests with one 6 in. strip of FRP on each side. The loads for the three tests varied from 13.4 to 16.9 kips. The average for the tests was 15.1 kips with a standard deviation of 1.8 kips. The three tests on specimens with an unbonded region were more consistent. They exhibited loads of 11.8 to12.2 kips. The average load was 12.0 kips with a standard deviation of 0.2 kips. The tests with strips at 45 degrees had maximum loads of 9.7 to 13.0 kips, with an average of 11.7 kips and a standard deviation of 1.7 kips. A large variability was expected in the tests with strips at 45 degrees because the specimens had different numbers of strips. The tests with multiple strips at 90 degrees to the crack had maximum loads of 16.1 to 20.4 kips. The average was 18.6 kips, with a standard deviation of 2.3 kips. A large variability was also expected in these tests because the specimens had different numbers of strips. However, the two tests with two 90 degree strips on each side also had very different loads, 16.1 and 20.4 kips.

The reason that the variability was low for the specimens with the unbonded region near the crack was because each of the tests exhibited the same type of failure. No concrete substrate was removed over the area of the sheet, nor was any large piece of concrete broken off near the crack. There was a progressive failure in the adhesive interface. This suggests that a stress concentration caused by the unbonded region between the adhesive and concrete may have reduced the strength of the adhesive interface to 12 kips. The other groups of tests had various amounts of concrete substrate removed over the area of the sheets and various size pieces of concrete removed at the crack. The specimens with larger amounts of concrete removed through substrate failure or shear failure at the crack had higher ultimate loads.

With the exception of the unbonded region specimens, the amount of concrete substrate removed over the area of the sheet varied over all specimens with no correlation to any of the variables: however, it had a large effect on the test results. In an attempt to minimize this effect, the externally bonded tests have been split into two categories, depending on the amount of concrete substrate removed. The specimens were divided into these groups because the bond

had a large effect on the results, but the bond varied throughout the tests without respect to the variables. Some specimens with 90 degree standard strips had better bond than others although there was no variable between the tests. Some 45 degree tests and multiple strip tests also had better bond than others. Although efforts were made to ensure that the surface preparation was the same for each specimen, it is assumed that surface preparation had something to do with the bond variations observed in the tests. It is possible that the surface preparation of grinding, wire brushing, and high pressure air was not always sufficient for the bond of EB sheets, which caused it to work better in some areas than in others. In all tests, independent of the quality of the bond, the failure type was generally the same. There was a progressive peeling failure in some combination of the adhesive interface and the concrete substrate. When the peeling progressed to the end of the sheet, the sheet peeled off abruptly and a chunk of concrete was removed at the crack.

The specimens were placed in group 1 if significant concrete substrate was removed, otherwise they were placed in group 2. Tables 4-6 and 4-7 give the maximum loads for the two groups of specimens, the average loads for each test series, and the percentage increase in load over the average load of the control specimens in each group. Considering the Group 1 specimens with significant concrete substrate removed, the control specimen had an ultimate load of 16.9 kips. The 45 degree specimen had a load of 13 kips. The multiple strip specimens had loads of 19.4 to 20.4 kips, with an average of 19.9 kips. Considering the Group 2 specimens without significant concrete substrate removed, the control specimens had loads of 13.4 to 15.0 kips. The average was 14.2 kips. The multiple strip specimen had a load of 16.1 kips. The 45 degree specimens had loads of 9.7 to 12.2 kips with an average of 11.0 kips. When the tests are divided into these groups, it becomes easier to see the effects of the strip orientation, width and spacing because the impact of the bond failure mode variability is lessened.

The amount of concrete shear failure at the crack had some correlation to the variable of strip width and spacing. For example, specimen E10-90-3 with three 2 in. strips at 1 in. spacing had a total of 8 in. between the outermost edges of FRP, while the control specimen only had 6 in. It is likely that the extra 2 in. caused the total failure area at the crack to be larger. Specimen E9-90-2 with two strips at 3 in. spacing was an exception to this. The failure area at the crack was not larger for that specimen, but it was most likely caused by insufficient bond in that particular specimen. The specimens with multiple strips at 45 degrees to the crack displayed the same trend of a larger number of strips resulting in a larger shear failure area on a much smaller scale. This was because much less concrete was removed at the crack for specimens with strips at 45 degrees, regardless of whether or not they had good bond over the area.

The specimens with the largest failure surfaces at the crack, and the largest concrete substrate failure area carried the largest loads. Increasing the quality of the bond increases the amount of concrete removed, and the variables of unbonded region, fiber orientation, and strip width and spacing all had some influence as well.

4.3.2 Effect of Unbonded Region for EB FRP

The concept of leaving an unbonded region near the crack was to reduce the stress concentration in the fibers near the crack by distributing the strain in the FRP over a larger area. It was thought that the ultimate strength of the system would be increased. This is not what was observed. Instead, the ultimate loads for the specimens with the unbonded region were the lowest of any of the tests with strips at 90 degrees to the crack. The average maximum loads of

the unbonded region tests was 12.0 kips, which was a 29% decrease in strength from the average of the control specimen with good bond. It represents an approximately 15% decrease in strength from the average of the control specimens without good bond.

There were three specimens with an unbonded region. Two specimens had an unbonded region of 1 in. on either side of the crack, formed by petroleum jelly or anti-adhesive tape. These specimens were denoted by a U2 at the end of the specimen number, such as E3-90-1-U2. This refers to 2 in. of total unbonded area. One specimen had an unbonded region of 0.5 in. on each side of the crack, formed by anti-adhesive tape. This specimen was denoted by a U1 at the end of the specimen number. The specimens with an unbonded region all had very similar ultimate loads. The specimens with unbonded regions all exhibited the same type of failure, and as a result, were not affected by the variability of the bond failure mode. The specimens all failed completely in the concrete/adhesive interface, with no concrete substrate removed over the area of the sheet and no piece of concrete removed at the crack. The failure surfaces of a typical specimen with an unbonded region are shown in Figure 4-2a. The failure surfaces of a typical specimen with one strip of FRP at 90 degrees to the crack and no unbonded region is shown in Figure 3-2b. The concrete failure near the crack is visible in Figure 4-2b. Figure 4-2a shows that no concrete substrate was removed at failure on the specimens with an unbonded region. The size of the unbonded region did not have a significant effect on the failure load. The specimens with a 1 in. unbonded region on each side of the crack had decreases in strength of 17% from the control specimen when petroleum jelly was used and 15% when anti-adhesive tape was used. The specimen with a 0.5 in. unbonded region on each side of the crack had a decrease in strength of 14%.

This type of failure is believed to have been caused by a stress concentration formed between the FRP and the concrete at the point where the unbonded region ended. It is likely that this stress concentration initiated the debonding process at a lower load than in the control specimens.

It may be true that leaving an unbonded region at the crack reduces the stress concentration in the fibers at that location. However, in these externally bonded FRP bond tests, the highest stresses reached in the FRP did not come close to the strength of the laminate. The FRP did not fracture in any of the tests, and it was not the weak link in the system. Therefore, reduction of the stress concentration in the fibers did not increase the ultimate load of the test. All of the tests failed by peeling off at the adhesive interface or the concrete substrate. These were the weak links in the system. Therefore, causing a stress concentration at the concrete/adhesive interface reduced the ultimate load of the test.

Leaving an unbonded region at the crack effectively moved the stress concentration from a stronger element to a weaker element in the system, resulting in a lower strength for these specimens. Leaving an unbonded region might be beneficial in some situations. If anchorage or total wrapping is used so that the full strength of the FRP is reached, and the failure occurs by fracture of the sheets, then leaving an unbonded region may be beneficial.

4.3.3 Effect of Fiber Orientation for EB FRP

The concept of changing the fiber orientation from 90 to 45 degrees was not to increase the strength of the specimen. It was clear that applying load at an angle to the fibers would not result in a higher ultimate load. In a shear crack, the crack is opening as well as sliding. If the

fibers are placed perpendicular to the crack, there will be a transverse force on the fibers. To have the resultant of the force acting perpendicular to the fibers, it may be necessary to place the fibers at some angle to the crack. Also, when reinforcing a beam in shear with EB FRP, it is often desirable to wrap the beam in a total or U-wrap. When this is done, the fibers have to be at 45 degrees to the crack, assuming a crack angle of 45 degrees. It was of interest in the bond tests to see whether placing the strip at an angle to the load could improve ductility, because FRP generally fails in a very brittle manner. It was also of interest to investigate if placing fibers at an angle to the load had an impact on the effective bond length of the sheet.

There were three tests with fibers at 45 degrees to the crack. The load was also applied at 45 degrees to the fibers because the crack remained perpendicular to the loading. The first test had one strip on each side of the specimen, the second test had two, and the third test had three. The failure loads ranged from 9.7 to 13.0 kips. The single strip reached the highest load because it had the best bond. When compared to the control specimen that had good bond, the 45 degree specimen had a 23% decrease in strength. The specimen with two strips attained a maximum load of 9.7 kips, and the specimen with three strips reached a maximum load of 12.2 kips. Neither exhibited good bond. A 26% increase in strength was observed when increasing the number of strips from two to three. The test with two strips had a 32% decrease in strength from the average of the control specimens without good bond, and the test with three strips had a 14% decrease. The average of the two tests was 11.0 kips. This represents a 23% decrease in strength from the average of the control specimens without good bond.

The 45 degree specimens had different amounts of concrete substrate removed over the area, but all of them had very small amounts of concrete removed at the crack. Because the fibers were being pulled at an angle to the crack, the shear failure in the concrete substrate did not form over as large an area as it did in the 90 degree specimens. The concrete pieces that were removed at the crack were usually from the inside of the angle of the FRP where the concrete was put in tension. The failure area for a typical 45 degree strip specimen is shown in Figure 4-2c. The photograph is rotated to a 90 degree position. In the actual test setup, the crack was horizontal.

The specimens with fibers at 45 degrees to the crack were less stiff compared to the 90 degree specimens. The displacements at peak load for the 45 degree specimens were between 0.1 and 0.2 in. while the displacements at peak load obtained with the 90 degree specimens were between 0.03 and 0.06 in. This was because as the FRP debonded, the fibers began splitting in the transverse direction and straightening out over the crack. The flexibility of the FRP allowed for a much greater crack opening at failure for the 45 degree specimens than with the 90 degree specimens. Typical Load vs. Displacement curves for the 45 and 90 degree specimens are shown in Figure 4-3.

The 45 degree specimens showed fairly good strength and large deformations in this loading scheme. The ultimate failures were very sudden, as in the 90 degree specimens, so there did not appear to be greater ductility. However, the behavior should be further evaluated in tests on beams in shear to assess the behavior when the shear crack is sliding as well as opening.

4.3.4 Effect of Strip Width and Spacing for EB FRP

In previous research, it had been suggested that the amount of concrete substrate removed at failure of the sheet was not proportional to the size of the sheet, and it was proportionally

larger for smaller sheets (Ueda et al., 1999). None of the previous bond tests had used strip width as a variable while keeping the area of FRP constant. The hypothesis was that using a larger number of smaller strips would allow the strips to be more efficient by removing more concrete than they would if fewer larger strips were used. Keeping the total amount of FRP constant allowed the direct investigation of this hypothesis. The strip spacing was chosen as a variable to investigate whether behavior would be further enhanced by engaging a larger area of concrete when the strips were moved further apart.

There were three tests with multiple strips at 90 degrees to the crack with various strip widths and spacings. There were also three tests with a single 6 in. strip at 90 degrees to the crack. There was one test with two 3 in. strips at 1 in. spacing. There was one test with two 3 in. strips at 3 in. spacing. The third test had three 2 in. strips at 1 in. spacing. The tests with 1 in. spacing were put into group 1 because they both had good bond. The failure loads for the tests were 19.4 kips for the test with two strips and 20.4 kips for the test with three strips. This indicates a 5% increase when spreading out the FRP over three narrow strips. The test with two strips had an increase of 15% from the strength of the control specimen, and the test with three strips had an increase of 21% over that of the control specimen. The average of these two tests was 19.9 kips, which was an increase of 18% over the control specimen with good bond. The test with 3 in. spacing did not have good bond. The maximum load in the test was 16.1 kips. This was an increase of 13% over the average strength of the control specimens without good bond. These results show that spreading out the FRP by using multiple smaller strips is more efficient than using one larger strip. Unfortunately, the specimen with 3 in. spacing cannot be compared to the specimens with 1 in. spacing because of the different observed bond conditions, so an optimal strip spacing cannot be determined from these tests.

The tests with multiple strips carried greater loads than the control specimens because of the larger amount of concrete removed at the crack. The failure area for a typical multiple strip specimen is shown in Figure 4-2d.

4.3.5 Measurement of Effective Bond Length for EB FRP

The effective bond length was measured for each strip that had strain gages. For each strain profile at a given load, effective bond length was determined as the distance between the debonded region and the point at which the strain reached within 200 microstrain of zero. The effective bond length represents the distance over which the significant portion of the strain is transferred from the debonded portion of the FRP into the concrete. The end point of the effective bond length farthest from the crack was taken at the gage nearest to zero strain in which there was at least a change of 200 microstrain between that and the adjacent gage. The end point of the effective bond length closest to the crack was taken at the gage for which there was less than a 200 microstrain change between that gage and the adjacent one. A change in strain less than 200 microstrain was assumed to be insignificant because of the variability of the strain gages due to surface irregularities on the FRP. This value corresponds to approximately 5 to 10% of the highest measured strains. Therefore, the effective bond lengths measured in this manner represent the lengths over which 80 to 100% of the load was transferred from the FRP to the concrete. The strain gage data plots for each strip with strain gages are shown in Appendix F. An example of a strain graph with effective bond lengths determined is shown in Figure 4-4. In the graph, the effective bond lengths are denoted for several loads. At each load there is a tick mark on the line indicating each end point of the effective bond length.

At the lower loads, before debonding began, effective bond lengths of 1 to 2 in. were observed for all of the specimens. The highest load where the effective bond length could be measured generally had the largest effective bond length. The largest effective bond length ranged from 2 to 5 in. The largest effective bond lengths for the control specimens ranged from 2 to 4 in. with an average of 3.3 in. For the specimens with an unbonded region, the range was 2 to 3 in. with an average of 2.3 in. The 45 degree specimens had a range of 3 to 4 in. with an average of 3.3 in. The 90 degree specimens with multiple strips had a range of 3 to 5 in. with an average of 3.7 in. These results show that the specimens with the unbonded region had the lowest effective bond lengths as well as the lowest ultimate loads. The specimens at 45 degrees to the crack had much lower loads than the control specimens, but the effective bond lengths were similar to those of the control specimens. It is possible that the effective bond lengths do not correlate to the loads for specimens with the fibers at an angle to the loading. The specimens with multiple strips at 90 degrees had the largest effective bond lengths, and also had the highest loads overall. This could be because they engaged the most concrete. The average of the largest effective bond length for all strips was 3.2 in.

4.3.6 Discussion of Bond of NSM FRP

The variability in bond between the first two NSM tests was high. The tests were identical, but the adhesive on the first test was not cured properly in at least two locations. For this reason, the loads for these two tests were not averaged together. The second test, with an ultimate load of 38.1 kips, was taken as the control specimen for adhesive A. The two identical tests using adhesive B did not have a high variability.

The variability for the bond of the NSM FRP tests was expected to be smaller than for the EB FRP tests because it was not as dependent on surface preparation and amount of concrete substrate removed. It was dependent upon the adhesive used. The failure type for NSM FRP tape was different from the EB FRP sheets. In the tests with NSM FRP, the failure began with cracking of the epoxy that extended into the surrounding concrete. Large pieces of concrete were broken off of the specimen. The specimens with adhesive A had failures between the FRP tape and the epoxy, and the tape eventually pulled out of the epoxy. In these specimens, the matrix of the FRP tape was damaged in most tests. After the failure of the bond between the tape and the epoxy, the specimens still held some load through friction between the tape and the epoxy. The specimens with adhesive B had failure in the concrete directly surrounding the groove. There was no failure between the FRP and adhesive or in the adhesive. Figure 4-5 shows the FRP tape after failure with adhesive B and concrete attached as well as the tape after failure for adhesive A.

4.3.7 Effect of Adhesive Type for NSM FRP

The adhesive became a variable in these tests after testing three specimens with adhesive A (Sika Anchorfix-3). The adhesive was not curing consistently in all tests. Also, the failures in all tests were between the adhesive and the FRP tape. It became clear that the maximum strength of the FRP tape was not being reached because of premature adhesive failure. A bond test was performed with several different adhesives to determine which had the highest strength. The results of this study are given in Appendix B. The adhesive with the highest strength (3M DP460 NS) was used in the bond tests as adhesive B.

The specimens with adhesive B exhibited much higher loads than those with adhesive A. The maximum load for the 90 degree specimen with adhesive A was 38.1 kips. The average maximum load for three 90 degree specimens with adhesive B was 55.3 kips, with a coefficient of variation of 2.0%. This corresponds to a 45% difference in strength when changing adhesive type.

As mentioned previously, the specimens with different adhesives had different failure types. The specimens with adhesive A ultimately failed between the FRP tape and the adhesive. The specimens with adhesive B ultimately failed in the concrete adjacent to the groove. Specimens with adhesive B had higher strengths because they were able to take better advantage of the strength of the FRP tape. When both adhesives were fully cured, adhesive B was less brittle than adhesive A, and had a larger elongation to failure. From these tests, it appears that a tougher, less brittle adhesive is more effective in bonding the dissimilar substrates of FRP and concrete. The failure surfaces for typical NSM specimens with both adhesives are shown in Figure 4-6a and 4-6b.

4.3.8 Effect of Fiber Orientation for NSM FRP

The concept of changing the fiber orientation for the NSM FRP specimens was the same as that for the EB FRP specimens. In a shear crack, the crack is opening as well as sliding, and it may be desirable to place the reinforcement at a 45 degree angle to the crack. It was also of interest to see if it could demonstrate good ductility while still carrying a considerable amount of load. It was also of interest to determine if the tape would fracture at the crack because it was not possible for the NSM reinforcement to peel off like the externally bonded sheets.

The specimen with the NSM reinforcement oriented 45 degrees to the crack had a much lower ultimate load than the specimen with the reinforcement oriented 90 degrees to the crack using adhesive A. The 45 degree test reached a load of 22.3 kips, 59% of the strength of the 90 degree specimen. Like the EB tests, the NSM test with fibers oriented 45 degrees to the crack was less stiff than the tests with fibers oriented 90 degrees to the crack, and had a larger displacement at peak load. The 45 degree specimen had approximately twice the displacement of the 90 degree specimen with the same adhesive at peak load. However, after reaching peak load, the 45 degree NSM specimen continued to hold approximately 90% of the peak load while undergoing an additional 0.05 in. displacement. This shows that the 45 degree NSM specimen had a more ductile failure than the other tests. The Load vs. Displacement plot for a 45 and two 90 degree NSM tests are shown in Figure 4-3.

The failure surface of the 45 degree specimen, shown in Figure 4-6c, lost much less concrete than the 90 degree specimen. This was similar to what was observed for the externally bonded specimens. The FRP tape did not fracture at the crack, but its flexibility allowed it to bend as the crack opened. There was significant damage at failure in the matrix of the tape near the crack. The failure surface for the 45 degree specimen is shown in Figure 4-6c.

4.3.9 Effect of Vibrations During Cure of Adhesive on NSM FRP

One of the specimens with NSM FRP was loaded with a small amplitude cyclic load while the adhesive was curing. The cyclic load was intended to represent vibrations caused by car traffic on a bridge. This test was done to investigate the effect of traffic vibrations during adhesive curing on the strength of FRP repair on a bridge.

The cyclic load that was applied to the specimen ranged between 1 and 5 kips in compression. The corresponding displacement of the crack was 0.002 in. The frequency of the load was 1 Hz. This load was determined from the actual truck loading on a pier cap of MN Bridge 19855/56. The shear stress in the concrete from car traffic was estimated to be 20% of the stress caused by truck traffic. The stress was then applied to the bond test specimen in compression. It was not possible to apply any tension to the specimen while the adhesive was curing because there was nothing else holding the two halves of the specimen together.

The test NB18-90-2V with adhesive B and cyclic loading had a maximum capacity of 54.5 kips. The average of the control tests NB-16-90-2 and NB17-90-2 with the adhesive B was 55.3 kips. This shows that there was an insignificant change in strength when cyclic loading was applied to the specimen while the adhesive was curing. The failure surface of the specimen with vibrations was similar to that of the control specimens with adhesive B. The failure surfaces are shown in Figure 4-6d.

4.3.10 Comparison of EB FRP with NSM FRP

The tests on specimens with EB FRP indicated that using multiple strips at 90 degrees to the crack was the most efficient. The maximum load reached was 20.4 kips. The maximum load that could have been reached if the tests had failed by fracture of the fibers was 67 kips, based on the average tensile strength of 160 ksi from tensile tests conducted on the EB FRP. The measured tensile strength of the sheets matches the tensile strength provided by the manufacturer. This calculation assumes that the total width of FRP on the specimen was 12 in. The best EB FRP configuration was only able to use 30% of the capacity of the FRP.

The control test with adhesive B on the NSM FRP had the highest load, 56.3 kips. The maximum load that could have been reached if the tests had failed by fracture of the fibers was 72 kips, based on the average tensile strength of 360 ksi from the tensile tests conducted on the NSM FRP. The measured tensile strength was 20% higher than the guaranteed tensile strength provided by the manufacturer. Therefore, this NSM FRP configuration reached 78% of the strength of the tape.

It is clear that the near surface mounted FRP tape was more efficient than the externally bonded FRP sheets at developing the most of its capacity. It is possible that higher strengths could have been achieved with either type of FRP if a longer embedment length was provided, but no tests were performed with a different embedment length. There are several other notable differences between the two types of FRP.

The NSM FRP tape had greater displacements at peak load than the EB sheets. It also had a lower stiffness. It is possible that the lower stiffness resulted from the larger area of adhesive between the concrete and the FRP. The behavior of the NSM FRP depends on the type of adhesive used. The NSM specimens using a less brittle adhesive had higher ultimate loads, but did not carry any load after failure, because the failure was in the concrete. These specimens were able to develop much higher loads because a more flexible adhesive allowed the concrete to transfer load into the FRP tape more efficiently. This was similar to the behavior of the EB sheets. The NSM specimens using a more brittle adhesive failed in the interface between the adhesive and the FRP. The ultimate loads were lower, but approximately half of the ultimate load was held by friction between the FRP tape and adhesive after failure. These specimens were not able to transfer the load from the concrete into the FRP as effectively because the

adhesive was not flexible enough. However, a failure between the FRP and adhesive is able to hold more load after failure due to friction. A Load vs. Stroke plot comparing 45 and 90 degree tests of each type of FRP as well as both types of NSM adhesive is shown in Figure 4-3. In the graph, E10-90-3 and E-11-45-2 represent EB tests at 90 and 45 degrees, and NA14-90-2, NA15-45-2, and NA17-90-2 represent NSM tests at 45 and 90 degrees, as well as one test with adhesive B.

4.4 Beam Test Results

Beam tests were performed using the most effective FRP configuration from the bond tests, NSM tape applied with 3M DP-460 NS. Two simply supported beam test specimens were constructed. Three tests were performed on the first beam specimen, B1. Test 1 was performed before any external FRP shear reinforcement was applied to the beam. There were two separate periods of loading in Test 1. The first run, Test 1A, was stopped when it was observed that the beam had begun bearing on the lateral bracing. Test 1B was run after the problem was fixed. Test 2 was performed after external FRP reinforcement was applied to the side of the beam with no stirrups (NS). Test 3, the final test, was completed after external FRP shear reinforcement had been applied to the side of the beam with minimum stirrups (MS). One test (Test 4) was performed on the second beam specimen, B2. Test 4 was performed after FRP had been applied to the NS span of Beam B2. For Tests 1 and 2, the beam was loaded only until the shear cracks had developed sufficiently for retrofit, so the beam was not loaded to failure. The beam was loaded to failure in Test 3. The beam was also loaded to failure in Test 4. The Load vs. Displacement plots for Tests 1 to 3 are shown in Figure 4-7. The Load vs. Displacement plot for test 4 is shown in Figure 4-8.

Table 4-8 tabulates the calculated capacities of the beams for each test, and the loads at which the tests were terminated. The calculated capacities for Tests 1 and 2 represent the shear capacities of the NS and MS spans respectively before FRP shear reinforcement was applied. The calculated capacity for Test 3 was the smaller of the shear capacities of the NS and MS spans after retrofit with FRP. The shear and flexural capacities of the beams before retrofit with FRP were based on ACI 318-99. The capacities were calculated using measured concrete strengths from cylinder tests. The capacities were calculated using a nominal steel strength of 60 ksi, because no tensile tests were performed on the steel reinforcement. The shear capacities of the spans after retrofit with NSM FRP were calculated based on the proposed addition to ACI 440.2R-02 regarding strengthening with NSM FRP. The calculations for the capacities of each beam test are in Appendix H. The flexural and shear strengths of the beam are calculated, as well as the shear strengths of each span of the beam after retrofit.

Table 4-9 gives the calculated shear capacities of the NS and MS spans after FRP retrofit, as well as the calculated flexural capacity of the beam. The capacities for Tests 1 to 3 were all calculated using a concrete compressive strength of 6320 psi, the strength of the test cylinders prior to testing of Beam B1. The capacity for Test 4 was calculated using a concrete compressive strength of 6870 psi, the strength of the test cylinders prior to testing of Beam B2. The shear capacities of the NS and MS spans after retrofit with FRP were designed to equal the flexural capacity of the beam. This was done to achieve the maximum increase in shear strength without using excess FRP. The number and spacing of FRP bars to achieve that strength were calculated using the proposed addition to ACI 440.2R-02. The calculations are shown in Appendix H.

Strain gages were placed in three locations on each side of each stirrup in the center region of the beam. Gages were also placed in three locations on one side of every other stirrup in the end region of the beam. Figure 4-9 shows the placement of the strain gages on the stirrups in the beam. The number of the strain gage is the number of the stirrup as shown in the figure. The letters following the number indicate whether it was at the bottom, middle, or top of the stirrup, denoted by b, m, and t. For the stirrups with gages on each leg, l and r denote whether the gage was on the right or left side of the stirrup. Any strain reading of less than 200 microstrain was not considered to be significant. Most of the gages did not show any significant strain during Test 1. The gages that did show significant strains during Test 1 are listed in Table 4-10. The gages are listed along with their strains at 105 kips, the end of Test 1. The strains in the gages at 105 kips in Test 2 are also given, to determine whether the added FRP reinforcement on the NS side had an effect on the strains. The gages with significant strain in Test 1 were in the end regions of the NS span. The percentage decrease in strain is given for each gage. Table 4-11 lists the gages that had significant strain at the end of Test 2. The gages are listed along with their strain at 140 kips, the end of Test 2. The strains in the gages at 140 kips in Test 3 are also given, to determine whether the added FRP reinforcement on the MS side had an effect on the strains in those stirrups. The percentage decrease in strain is also given for each gage. Table 4-12 lists the gages that had significant strain at the end of Test 3, the last test on Beam B1. The strain is given at 200 kips, before the flexural reinforcement yielded. The strain at 200 kips in Test 4 on Beam B2 is also given in the table, to determine whether the additional FRP on the MS span during Test 3 had an effect on the strain in those stirrups after 140 kips. Tests 3 and 4 were performed on different beams but both failed in flexure. The strains in the gages are being compared for the two tests to determine if the shear reinforcement in the MS side experienced larger strains when there was no FRP on that side as the beams approached flexural failure. The percentage decrease in strain from Test 4 to Test 3 is given in the table. The strains in the stirrups are also given at 250 kips for Tests 3 and 4. The plots of all strain gages with significant strain in each test are given in Figure 4-19 and 4-20.

4.5 Discussion of Beam Tests

4.5.1 Effect of FRP Shear Strengthening on NS Span

The calculated strength of the span without stirrups (NS) was 107 kips. In Test 1, this span was loaded to 105 kips and the test was suspended. The NS span was then strengthened in shear with NSM FRP to a calculated capacity of 224 kips. In Test 1, there were only two strain gages that had a significant strain at 105 kips. After retrofit of the NS side, one gage showed a slight increase in strain at the same load, and one showed a 10% decrease at 105 kips. The two strain gages were both in the end region of the NS span of the beam, so the FRP reinforcement did not have a great effect on the strain in those stirrups. Because there were no stirrups in the center region of the span where the FRP was applied, it was not possible to determine what effect the additional FRP shear reinforcement had on strain in that region.

The FRP shear reinforcement clearly strengthened the NS span. The ultimate load reached was 259 kips, 2.4 times the calculated capacity of the span with no stirrups. Although the actual strength of the NS span without FRP was not determined, it was evident that the FRP was effective in strengthening the span in shear.

4.5.2 Effect of FRP Shear Strengthening on MS Span

The calculated strength of the span with minimum stirrups (MS) was 160 kips. In Test 2, this span was loaded to 140 kips. The MS span was then strengthened in shear with NSM FRP to a nominal calculated capacity of 218 kips. In Test 2, there were several strain gages that had a significant strain at 140 kips. After retrofit of the MS side, the strain gages in the MS span showed decreases of 8 to 46% at 140 kips. Higher strains did not necessarily have larger reductions. Before retrofit of the MS side, a main shear crack had developed that crossed stirrup 3 at the bottom, stirrup 2 between the bottom and the middle, and stirrup 1 near the top. The crack diagrams for Beam B1 at 140 kips are shown in Figure 4-10. The NSM FRP tape crossed this crack in two locations, between stirrup 1 and 2, and between stirrup 2 and 3. After the retrofit, the strain in the eight strain gages closest to the crack was reduced by an average of 29% at 140 kips. The highest strain in the MS span at 140 kips was reduced by 23%.

In Test 3, the last test on Beam B1, the MS span and NS span were both strengthened with NSM FRP to calculated capacities of 218 and 224 kips, respectively. The beam was tested to an ultimate load of 259 kips, at which time the test failed in flexure. In Test 4 on Beam B2, the NS span was strengthened with FRP to a calculated capacity of 228 kips, but the MS span was not strengthened with FRP. The unstrengthened MS span of the beam had a calculated capacity of 164 kips. The beam was tested to an ultimate load of 255 kips, at which time the beam failed in flexure. By comparing the strain gages in the MS spans of the beams at 200 and 250 kips in Tests 3 and 4, one can investigate whether the additional FRP caused a reduction in strain at higher loads. At 200 kips, the strains in the gages on the MS span in Test 3 showed decreases in strain of 0 to 100% over the strains in Test 4. Gages with larger strains did not necessarily show larger decreases. This large range appears to be due to the fact that the cracks did not form in exactly the same location in the two beams, so the decrease in strain in any individual gage is not necessarily meaningful. Crack diagrams of Beam B1 at 259 kips, B2 at 140 kips, and B2 at 255 kips are shown in Figures 4-11, 4-12, and 4-13. However, the average decrease in strain of the gages in the MS spans at 200 kips was 39% in Test 4. Out of 28 gages with significant strain on the MS span, only 4 gages showed an increase in strain in the test with NSM FRP reinforcement. However, 19 gages showed a decrease in strain of at least 20%. The highest strain in the MS span at 200 kips was reduced by 68%. This data shows that adding FRP to the MS span of the beam generally reduced strains in the stirrups on that side at higher loads. In the end region of the NS span of the beam, there were 14 gages with significant strain. Half of them had higher strains in Test 3 and half had higher strains in Test 4. This shows that the additional FRP on the MS span did not have a noticeable effect on the strain in the NS span. At 250 kips, the strains in the gages on the MS span in Test 3 showed decreases in strain of 0 to 94% over Test 4. The average decrease in strain of the gages in the MS spans at 250 kips was 36% over Test 4. Out of 32 gages with significant strain on the MS span, 7 gages showed an increase in strain in Test 3 over Test 4. However, 22 gages showed a decrease in strain of at least 20% in Test 3 over Test 4. The highest strain in Test 4 in the MS span at 250 kips was reduced by 89% in Test 3. Adding FRP to the MS span of the beam generally reduced strains in the stirrups on that side at 250 kips. In the end region of the NS span of the beam, there were 16 gages with significant strain. Four of them had higher strains in Test 3 and 12 had higher strains in Test 4. At 250 kips, it appeared that the test with additional FRP reinforcement on the MS span also exhibited reduced strains in the NS span.

The amount of shear strengthening provided by the NSM FRP reinforcement on the MS side could not be determined because Beams B1 and B2 both failed in flexure. However, the strain gages on the MS side showed that there were significantly lower strains in most locations on Beam B1. The decrease in strain shows that the FRP carried some of the load that would otherwise be carried by the stirrups, and therefore provided some additional strength to the beam.

4.5.3 Discussion of Failure

Figures 4-10 through 4-13 show crack diagrams of the two beams. Each diagram of B1 shows one face of the beam from the load application point to the support, a distance of 7 ft. Each diagram of B2 shows the face of the beam from support to support, a distance of 14 ft. In addition to the cracks, the diagrams show vertical lines where the stirrups were located and diagonal lines where the FRP reinforcement was located. Along the vertical lines symbolizing the stirrups, dots in three locations indicate which stirrups were equipped with strain gages, and show the placement of strain gages on the stirrups. The hatched area on the diagrams corresponds to the location of the lateral bracing. Cracks could not be marked in this area because the bracing was covering the face of the beam. The diagrams show the crack pattern at 140 kips, when there was no FRP reinforcement on the MS side of the beam. The load level of 140 kips corresponds to the end of Test 2 on Beam B1. Cracks were drawn at the same load level on Beam B2 for comparison purposes. The diagrams also show the crack pattern at 259 kips on Beam B1 and 255 kips on Beam B2, after flexural failure occurred. Figures 4-14 to 4-16 show photographs of Beam B1 at the end of Tests 1, 2, and 3. Photographs of Beam B2 at 140 kips and at the end of Test 4 are shown in Figures 4-17 and 4-18.

Throughout Test 1, flexural cracks originated on the bottom edge of the beam and propagated vertically. The cracks were spaced approximately 8-10 inches apart. When the loads approached 100 kips, the outer cracks began to turn diagonally toward the load point. The cracks were all small, with maximum crack widths of 0.004 to 0.006 in.

During Test 2, the flexure cracks continued to develop and turn diagonally toward the load point. At approximately 127 kips, the main shear crack on the MS span formed. The formation of this crack resulted in significant jumps in strains in the eight strain gages nearest to the crack. A slight jump in displacement was also observed. The crack was nearly vertical in the center of the beam where it had formed as a flexural crack, but turned nearly horizontal near the top and bottom of the beam, and had a crack width of 0.02 in. Figure 4-10 shows the crack diagrams at the end of Test 2. The main cracks are indicated by bolder lines in the diagrams. This flexure-shear crack was repaired with NSM FRP tape. Cracks also continued to grow on the NS span, but crack growth on that side was slower and less sudden. It is likely that this is because the NS side was heavily reinforced in shear with NSM FRP. Shear crack widths on the NS span had maximum widths of 0.012 to 0.016 in. The flexure cracks were all small, with maximum crack widths of 0.006 to 0.008 in.

Both spans were strengthened in shear with NSM FRP when Test 3 began. The existing cracks continued to grow on both spans, with cracks branching off and connecting to other cracks. At approximately 147 kips, another main shear crack formed on the MS side, farther from the center. This crack resulted in significant jumps in the strain of the seven strain gages closest to the crack. The crack diagram showing Beam B1 at the end of Test 3 is shown in Figure 4-11. The main cracks are indicated by bolder lines on the diagram. A slight jump in displacement was also observed. A main crack also developed on the NS side, but it developed

slowly and did not cause any significant jumps in strain or displacement. At approximately 240 kips, the flexural reinforcement began to yield, and the load vs. displacement curve became nearly horizontal. All of the cracks, especially the flexure cracks, widened significantly while the flexural reinforcement was yielding. At 259 kips, ultimate failure of the beam occurred by crushing of the concrete near the loading point. At this time, the flexural cracks had maximum widths of 0.1 to 0.15 in. The shear cracks on the NS span had maximum widths of 0.025 to 0.04 in., and the shear cracks on the MS span had maximum widths of 0.035 to 0.06 in. A crack was observed in the concrete at the center of the beam that followed the groove of one FRP strip on the NS side for approximately 6 in. The crack then curved around the end of the FRP strip from the MS side before extending vertically up the center of the beam. This crack was observed on both faces of the beam. It was the only failure observed along the adhesive. It is possible that the MS span had larger cracks because there was less FRP crossing the cracks on that side. There were only two strips of FRP tape on each face of the MS span, and four strips of FRP tape on each face of the NS span. Figure 4-11 shows the locations of the cracks at the end of Test 3 for each face of the beam.

Early in Test 4, flexure cracks began to form on the bottom edge of the beam and propagate vertically. The cracks continued to develop and turn diagonally toward the load point. At approximately 126 kips, the main shear crack on the MS span formed, branching off from a flexural crack. Figure 4-12 shows the crack diagrams of Beam B2 at 140 kips. Larger cracks are indicated by bolder lines on the diagram. A slight jump in displacement was also observed at the formation of the crack. The crack was nearly vertical in the center of the beam where it had formed as a flexural crack, but turned nearly horizontal near the top of the beam. Cracks also formed on the NS span, but crack growth on that side was slower and less sudden, because the NS side was already reinforced in shear with NSM FRP. At approximately 142 kips, another main shear crack formed on the MS side, farther from the center. This crack resulted in significant jumps in the strain of the several strain gages closest to the crack. A slight jump in displacement was also observed. At 170 kips, shear cracks on the NS span had a maximum width of 0.018 in. Shear cracks on the MS span had maximum widths of 0.020 to 0.022 in. The flexure cracks were all small, with maximum crack widths of 0.006 to 0.008 in. At approximately 230 kips, the flexural reinforcement began to yield, and the load vs. displacement curve became nearly horizontal. All of the cracks, especially the flexure cracks, widened significantly while the flexural reinforcement was yielding. At 255 kips, ultimate failure of the beam occurred by crushing of the concrete near the loading point. At this time, the flexural cracks had maximum widths of 0.1 to 0.15 in. The shear cracks on the NS span had maximum widths of 0.020 to 0.026 in., and the shear cracks on the MS span had maximum widths of 0.08 to 0.10 in. Figure 4-13 shows the locations of the cracks at the end of Test 4 for each face of the beam.

The final capacities of both beams at failure were significantly higher than the calculated shear and flexural capacities of the beams. Because the FRP was oriented at 45 degrees to the beam, it crossed or diverted some flexural cracks in addition to crossing shear cracks. This could have increased the ultimate flexural capacity of the beams. In addition, the shear capacity of the MS span of Beam B2 was much higher than it should have been. This could be due to a significantly higher strength steel or concrete than was specified. Also, there was a possibility that arching action in the beam caused the shear strength to be greater than the calculated shear strength. The shear capacities of each span of Beam B1 with the FRP reinforcement were unknown, since the beam failed in flexure. However, they are significantly higher than the

capacities calculated using the proposed addition to ACI 440.2R-02, which suggests that the equations for shear strength of NSM FRP are conservative. Additional research is needed to accurately determine the increase in strength provided by NSM FRP tape.

4.5.4 Beam Test Details

Specimen B1 was the first beam tested. The longitudinal axis of the beam was oriented in the east-west direction, so the side faces were north and south. Initially, there was no FRP on the beam. The first test on the beam was completed on 7/8/04. The specimen was loaded monotonically until approximately 85 kips, at which time it was observed that the lateral bracing had begun to bear on the beam in one spot. This test is referred to as Test 1A in the Load vs. Displacement graph in Figure 4-7. The beam was unloaded and the lateral bracing was moved further from the sides of the beam to prevent further interference. The beam was then loaded again to 105 kips. This test is referred to as Test 1B in Figure 4-7. For unknown reasons, the stiffness of Beam B1 increased the second time it was loaded. The loading was stopped approximately every 5 kips between 80 and 105 kips to inspect and mark the crack growth. At 105 kips, the test was terminated. After all cracks were marked, the beam was unloaded and the cracks closed. The beam was then retrofit with FRP on the side with no stirrups (NS).

Beam B1 was tested again after near surface mounted FRP tape was used to retrofit the side of the beam without stirrups. This test is denoted as Test 2 in Figure 4-7. There were four strips of FRP tape at an angle of 45 degrees to the beam. The strips were spaced 13 in. apart. The strips extended approximately 6 in. past the point where the stirrups began, and 6 in. past the load point in the center of the beam. This caused the outer strips to be shorter in length. There was one 22 in. strip, one 38 in. strip, and two 42 in. strips on each face of the beam. Aslan 500 CFRP tape and 3M DP 460 NS adhesive were used for the retrofit. The beam was tested after 5 days. The loading procedure was the same as the first test. The beam was loaded to approximately 140 kips. The test was stopped once at approximately 120 kips to inspect the crack growth. The test was terminated at a load of 140 kips. After all cracks were marked, the beam was unloaded. Some of the cracks were still visible after the beam was unloaded. The MS span of the beam was then retrofit with FRP.

Beam B1 was tested a third time after near surface mounted FRP tape was used to retrofit the span of the beam with stirrups. This test is denoted as Test 3 in Figure 4-7. There were two strips of FRP tape on each face of the MS span, placed at a 45 degree angle. The strips were spaced 26 inches apart. The strips extended approximately 6 in. beyond the end of the MS region towards the end region of the beam. In the center of the beam, the strips were extended to the edge of the FRP retrofit from the NS span, at the centerline of the beam. There was one 42 in. strip and one 36 in. strip on each face of the beam. The beam was tested after 4 days. The loading procedure was the same as the other tests. The beam was loaded until failure, without stopping. The flexural reinforcement began to yield at approximately 241 kips. The test continued until approximately 258 kips, at which time there was a crushing failure of the concrete at the top of the beam near the support. The maximum load reached on the beam was 259.2 kips.

Specimen B2 was the second beam tested. The longitudinal axis of the beam was oriented in the east-west direction, so the side faces were north and south. The beam was intended to be used as a control beam to find the shear strength of the side of the beam with minimum stirrups. The concept was to determine how much increase in strength was achieved

by adding FRP to that side. Because the side of the beam with no stirrups had a lower capacity than the side with minimum stirrups, NSM FRP was applied to the NS side before testing to strengthen that side. The retrofit scheme was identical to the NS side of Beam B1. There were four strips of FRP tape at an angle of 45 degrees to the beam. The strips were spaced 13 in. apart. The strips extended approximately 6 in. past the point where the stirrups began, and 6 in. past the load point in the center of the beam. The beam was moved into the testing frame after the adhesive had cured. The testing procedure for Beam B2 was the same as for Beam B1. The beam was tested on 8/25/04. Monotonic load was applied to the beam until failure. The test was stopped every 10 kips between 140 and 210 kips to check the crack growth. At approximately 240 kips, the Load vs. Displacement graph leveled out. The flexural cracks grew large as the steel yielded, and the failure occurred by crushing of the concrete at the top of the beam near the load point. The maximum load reached in the test was 254.6 kips. Because a flexural failure occurred, it was not possible to determine the increase in strength provided by the FRP on the MS side of the beam.

Chapter 5: Conclusions and Recommendations

5.1 Conclusions and Recommendations for Bridges 19855 and 19856

- The cracked, but undeteriorated, pier cap overhangs of Bridges 19855/56 are not prone to structural failure under current traffic loading conditions.
- Further research examining more bridges is required to determine why the pier cap overhangs of Bridges 19855/56 have cracked while overhangs of similar design in other bridges have not.
- The ultimate capacity provisions used to design the pier cap overhangs were found to be conservative when applied to experimentally tested pier cap overhangs. Ultimate capacity provisions currently found in the ACI 318-02 and 1998 AASHTO LRFD specifications were also found to be conservative.
- Shallow beam flexural provisions satisfactorily predicted the ultimate capacity of the pier cap overhangs even tough they are classified as deep beams in current specifications (ACI, 2002 AASHTO 1998).
- Strut and tie-based provisions provide adequate predictions of the ultimate capacity of pier cap overhangs.
- The estimated cracking load of the pier cap overhangs is less than the calculated service load supporting the fact that the overhangs have cracked.
- The estimated cracking load is only slightly larger than the calculated dead load of the bridge superstructure supporting the possibility that the bridge cracked shortly after being opened to traffic or under construction loads.
- Drastic measures would be required to prevent the cap from cracking such as increasing the height of the overhang by 20%
- Crack widths can possibly be controlled by increasing the amount of tensile reinforcing steel by 33% which could be achieved by designing the pier cap overhang for the moment at the center of the column rather than the face of the column.

5.2 Conclusions on Laboratory testing

The eighteen bond tests provided valuable information about the behavior of externally bonded and near surface mounted FRP. The tests on EB and NSM FRP showed that a fiber orientation of 90 degrees to the crack was stronger and stiffer than a fiber orientation of 45 degrees to the crack. Unbonding a portion of the EB strip over the crack reduced the effectiveness of the strip. Using multiple smaller strips of EB FRP instead of one larger strip of the same total width was more effective. The effectiveness of NSM FRP was increased by using a more flexible adhesive. The bond tests using EB FRP were able to achieve 30% of the tensile strength of the laminate, while the bond tests using NSM FRP were able to achieve 78% of the tensile strength of the tape. Overall, the NSM FRP specimens had more consistent bond than the EB FRP specimens and were able to take better advantage of the strength of the FRP. Because the NSM FRP was more effective, it was used to retrofit the beam specimens for shear.

Two beam specimens were tested to evaluate the effectiveness of FRP when used to repair shear cracks in beams. One beam was cracked in shear in a high moment region of the span with no stirrups (NS span). NSM FRP was used to retrofit the cracks. The beam was then cracked in shear in a high moment region of the span with stirrups at the maximum allowable spacing of d/2 (MS span). NSM FRP was used again to retrofit the cracks. After strengthening both spans in shear, the beam was tested to failure. The ultimate failure of the beam was by yielding of the flexural reinforcement and crushing of the concrete near the loading point. Another beam was tested to failure with FRP reinforcement on the NS span but not on the MS span. This beam also ultimately failed in flexure. Because both beams failed in flexure, it was not possible to determine how much shear strength was provided by the FRP reinforcement. Average reductions in strains of 36% and 39% were seen at 200 kips and 250 kips respectively when additional FRP reinforcement was applied to the beam. This suggests that some additional strength is provided by the FRP, although the exact amount could not be determined.

5.3 Recommendations

Based on the results of the experimental program, NSM FRP is recommended over EB FRP for repairing shear cracks in reinforced concrete beams. The NSM FRP should be installed perpendicular to the shear cracks. The 3M adhesive DP 460 NS is recommended for use with the NSM FRP. The recommended procedure for application of NSM FRP is contained in Appendix I.

The bond and beam tests have demonstrated that NSM FRP is a promising retrofit technique. The beam tests have indicated that additional FRP reinforcement reduces the strains in the stirrups, yet it is unclear how much additional shear strength is provided. Future beam tests using different amounts and spacings of NSM FRP to strengthen beams in shear while ensuring an ultimate failure in shear could provide more information. The equations for shear strengthening with NSM FRP from the proposed addition to ACI 440.2R-02 regarding strengthening with NSM FRP appeared to be conservative in this situation. More research is necessary to develop equations that accurately calculate the strength of NSM FRP used to retrofit shear cracks.

References

AASHTO, 1977. Standard Specifications for Highway Bridges, Washington D.C. 1977.

AASHTO, 1998. LRFD Design Specification for Bridges, Washington D.C. 1998.

ACI, 1983. Building Code Requirements for Structural Concrete (ACI 318-83) and Commentary (ACI 318R-83). American Concrete Institute. Farmington Hills. 1983.

ACI, 2002. Building Code Requirements for Structural Concrete (ACI 318-02) and Commentary (ACI 318R-02). American Concrete Institute. Farmington Hills. 2002.

Alexander, J. G. S., and J. J. R. Cheng, "Shear Strengthening of Small Scale Concrete Beams with Carbon Fibre Reinforced Plastic Sheets," CSCE 1st Structural Specialty Concrete, 1996, Alberta, Canada, pp. 167-177

Al-Sulaimani, G., A. Sharif, I. A. Basunbul, M. H. Baluch, and B. N. Ghaleb, "Shear Repair for Reinforced Concrete by Fiberglass Plate Bonding," ACI Structural Journal, Vol. 91, No. 3, July-August 1994

Araki, N., Y. Matsuzaki, K. Nakano, T. Katoaka, and H. Fukuyama, "Shear Capacity of Retrofitted RC Members with Continuous Fiber Sheets," Proceedings of the Third International Symposium on Non-Metallic Reinforcement for Concrete Structures, October, 1997, Vol. 1, pp. 515-522

Bizindavyi, L., and K. W. Neale, "Transfer Lengths and Bond Strengths for Composites Bonded to Concrete," ASCE Journal of Composites for Construction, Vol. 3, No. 4, November, 1999, pp. 153-160

Blaschko, M., and K. Zilch, "Rehabilitation of Concrete Structures with Strips Glued into Slits," Proceedings of the Twelfth International Conference on Composite Materials, 1999

Bousselham, A., and O. Chaallal, "Shear Strengthening Reinforced Concrete Beams with Fiber-Reinforced Polymer: Assessment of Influencing Parameters and Required Research," ACI Structural Journal, March-April 2004, Vol.101, No. 2, pp. 219-227

Carolin, A., M. Nordin, and B. Taljsten, "Concrete Beams Strengthened with Near Surface Mounted Reinforcement of CFRP," Proceedings of the International Conference on FRP Composites in Civil Engineering, 2001, pp. 1059-1066

Chaallal, O., M. J. Nollet, and D. Perraton, "Shear Strengthening of RC Beams by Externally Bonded Side CFRP Strips," ASCE Journal of Composites for Construction, Vol. 2, No. 2, May 1998, pp. 111-114

Chaallal, O., M. Shahawy, and M. Hassan, "Performance of Reinforced Concrete T-Girders Strengthened in Shear with Carbon Fiber-Reinforced Polymer Fabrics," ACI Structural Journal, May-June 2002, Vol. 99, No. 3, pp. 335-343

Chajes, M. J., W. W. Finch, T. F. Januszka, and T. A. Thomson, "Bond and Force Transfer of Composite Material Plates Bonded to Concrete," ACI Structural Journal, Vol. 93, No. 2, March-April 1996, pp. 208-217

Chajes, M. J., T. F. Januszka, D. R. Mertz, T. A. Thomson, and W. W. Finch, "Shear Strengthening of Reinforced Concrete Beams Using Externally Applied Composite Fabrics," ACI Structural Journal, Vol. 92, No. 3, May-June 1995, pp. 295-303

De Lorenzis, L., K. Lundgren, and A. Rizzo, "Anchorage Length of Near-Surface Mounted Fiber-Reinforced Polymer Bars for Concrete Strengthening-Experimental Investigation and Numerical Modeling," ACI Structural Journal, March-April 2004, Vol. 101, No. 2, pp. 269-278

De Lorenzis, L., and A. Nanni, "Characterization of FRP Rods as Near-Surface Mounted Reinforcement," ASCE Journal of Composites for Construction, May 2001, Vol. 5, No. 2, pp. 114-121

De Lorenzis, L., and A. Nanni, "Bond between Near-Surface Mounted Fiber-Reinforced Polymer Rods and Concrete in Structural Strengthening," ACI Structural Journal, March-April 2002, Vol. 99, No. 2

De Lorenzis, L., A. Nanni, and A. La Tegola, "Flexural and Shear Strengthening of Reinforced Concrete Structures with Near Surface Mounted FRP Rods," Proceedings of the Third International Conference on Advanced Composite Materials in Bridges and Structures, August 2000, pp. 521-528

Deniaud, C, and J. J. Roger Cheng, "Shear Behavior of Reinforced Concrete T-Beams with Externally Bonded Fiber-Reinforced Polymer Sheets," ACI Structural Journal, Vol. 98, No. 3, May-June 2001, pp. 386-394

Ferguson, P.M. Design Criteria for Overhanging Ends of Bent Caps, Report, Center for Highway Research, University of Texas, 1964.

Ferguson, P.M and Liao, H.M. Shear Strength of Bent Caps Between Columns. Report, Center for Highway Research, University of Texas, 1966.

FHWA, Federal Highway Administration National Bridge Inventory (NBI), 2003

Funakawa, I., K. Shimono, T. Watanabe, S. Asada, and S. Ushijima, "Experimental Study on Shear Strengthening with Continuous Fiber Reinforcement Sheet and Methyl Methacrylate Resin," Proceedings of the Third International Symposium on Non-Metallic Reinforcement for Concrete Structures, October 1997, Vol. 1, pp. 475-482

Hassan, T., and S. Rizkalla, "Investigation of Bond in Concrete Structures Strengthened with Near Surface Mounted CFRP Strips," ASCE Journal of Composites for Construction, 2003, Vol. 7, No. 3, pp. 248-257

Hassan, T., and S. Rizkalla, "Flexural Strengthening of Post-Tensioned Bridge Slabs with FRP Systems," PCI Journal, 2002, Vol. 47, No. 1, pp.76-93

Hutchinson, R. L., "The Use of Externally Bonded CFRP Sheets for Shear Strengthening of I-Shaped Prestressed Concrete Bridge Girders," PhD Thesis, University of Manitoba, 1999

Hutchinson, R. L., and S. H. Rizkalla, "Shear Strengthening of AASHTO Bridge Girders Using Carbon Fiber Reinforced Polymer Sheets," Proceedings of the Fourth International Symposium on Fiber Reinforced Polymer Reinforcement for Reinforced Concrete Structures, 1999, pp. 945-958

Iketani, J., and Y. Jinno, "Adhesive Properties of a Carbon Fiber Blanket on to the Concrete Surfaces," 42nd International SAMPE Symposium, May 1997, pp. 109-116

Izumo, K., T. Asamizu, N. Saeki, and K. Shimura, "Shear Strengthening of PRC Members by Fiber Sheets," Transactions of the Japan Concrete Institute, Vol. 19, 1997, pp. 105-112

Kachlakev, D. I., and W. A. Barnes, "Flexural and Shear Performance of Concrete Beams Strengthened with Fiber Reinforced Polymer Laminates," Proceedings of the Fourth International Symposium on Fiber Reinforced Polymer Reinforcement for Reinforced Concrete Structures, 1999, pp. 959-972

Kage, T., M. Abe, H. Lee, and F. Tomosawa, "Effect of CFRP Sheets on Shear Strengthening of C Beams Damaged by Corrosion of Stirrup," Proceedings of the Third International Symposium on Non-Metallic (FRP) Reinforcement for Concrete Structures, October 1997, Vol. 1, pp. 443-450

Kamiharako, A., K. Maruyama, K. Takada, and T. Shiomura, "Evaluation of Shear Contribution of FRP Sheets Attached to Concrete Beams," Proceedings of the Third International Symposium on Non-Metallic (FRP) Reinforcement for Concrete Structures, October 1997, Vol. 1, pp. 467-474

Khalifa, A., L. De Lorenzis, and A. Nanni, "FRP Composites for Shear Strengthening of RC Beams," Proceedings of the Third International Conference on Advanced Composite Materials in Bridges and Structures, August 2000, pp. 137-144

Khalifa, A. and A. Nanni, "FRP Rehabilitation of Rectangular Simply Supported RC Beams with Shear Deficiencies Using CFRP Composites," Construction and Building Materials, 2002, Vol. 16, No. 3, pp. 135-146

Khalifa, A., G. Tumialan, A. Nanni, and A. Belarbi, "Shear Strengthening of Continuous Reinforced Concrete Beams Using Externally Bonded Carbon Fiber Reinforced Polymer Sheets," Proceedings of the Fourth International Symposium on Fiber Reinforced Polymer Reinforcement for Reinforced Concrete Structures, 1999, pp. 995-1008

Li, A., C. Diagana, and Y. Delmas, "CFRP Contribution to Shear Capacity of Strengthened RC Beams," Engineering Structures, 2001, Vol. 23, pp. 1212-1220

Maeda, T., Y. Asano, Y. Sato, T. Ueda, and Y. Kakuta, "A Study on Bond Mechanism of Carbon Fiber Sheet," Proceedings of the Third International Symposium on Non-Metallic Reinforcement for Concrete Structures, October 1997, Vol. 1, pp. 279-286

Malvar, L. J., G. E. Warren, and C. Inaba, "Rehabilitation of Navy Pier Beams with Composite Sheets," Non-Metallic Reinforcement for Concrete Structures, 1995, pp. 534-540

Miyauchi, K., S. Inoue, S. Nishibayashi, and Y. Tanaka, "Shear Behavior of Reinforced Concrete Beam Strengthened with CFRP Sheet," Transactions of the Japan Concrete Institute, Vol. 19, 1997, pp. 97-104

Nakaba, K., T. Kanakubo, T. Furuta, and H. Yoshizawa, "Bond Behavior between Fiber-Reinforced Polymer Laminates and Concrete," ACI Structural Journal, Vol. 98, No. 3, May-June 2001, pp. 359-367

Nordin, H., B. Taljsten, and A. Carolin, "Concrete Beams Strengthened with Prestressed Near Surface Mounted Reinforcement," Proceedings of the International Conference on FRP Composites in Civil Engineering, 2001, pp. 1067-1075

Norris, T., H. Saadatmanesh, and M. R. Ehsani, "Shear and Flexural Strengthening of R/C Beams with Carbon Fiber Sheets," ASCE Journal of Structural Engineering, Vol. 123, No. 7, July 1997, pp. 903-911

Nozaka, K., "Repair of Fatigued Steel Bridge Girders with Carbon Fiber Strips," PhD Thesis, Department of Civil Engineering, University of Minnesota, 2002

Ono, K., M. Matsumura, S. Sakanishi, and K. Miyata, "Strength Improvement of RC Bridge Piers by Carbon Fiber Sheet," Proceedings of the Third International Symposium on Non-Metallic (FRP) Reinforcement for Concrete Structures, Vol. 1, October 1997, pp. 563-570

Pellegrino, C., and C. Modena, "Fiber Reinforced Polymer Shear Strengthening of RC Beams with Transverse Steel Reinforcement," Journal of Composites for Construction, 2002, Vol. 6, No. 2, pp. 104-111

Sato, Y., H. Katsumata, and Y. Kobatake, "Shear Strengthening of Existing Reinforced Concrete Beams by CFRP Sheet," Proceedings of the Third International Symposium on Non-Metallic Reinforcement for Concrete Structures, October 1997, Vol. 1, pp. 507-514

Sato, Y., T. Ueda, Y. Kakuta, and S. Ono, "Ultimate Shear Capacity of Reinforced Concrete Beams with Carbon Fiber Sheet," Proceedings of the Third International Symposium on Non-Metallic Reinforcement for Concrete Structures, October 1997, Vol. 1, pp. 499-506

Sato, Y., T. Ueda, Y. Kakuta, and T. Tanaka, "Shear Reinforcing Effect of Carbon Fiber Sheet Attached to Side of Reinforced Concrete Beams," Advanced Composite Materials in Bridges and Structures, 1996, pp. 621-627

Sena-Cruz, J. M., J. A. O. Barros, "Bond between Near-Surface Mounted CFRP Laminate Strips and Concrete in Structural Strengthening," Journal of Composites for Construction, 2004

Taerwe, L., H. Khalil, and S. Matthys, "Behavior of RC Strengthened in Shear by External CFRP Sheets," Proceedings of the Third International Symposium on Non-Metallic Reinforcement for Concrete Structures, October 1997, Vol. 1, pp. 483-490

Taljsten, B., "Defining Anchor Lengths of Steel and CFRP Plates Bonded to Concrete," International Journal of Adhesion and Adhesives, 1997, Vol. 17, pp. 319-327

Triantafillou, T., "Shear Strengthening of Reinforced Concrete Beams Using Epoxy-Bonded FRP Composites," ACI Structural Journal, Vol. 95, No. 2, March-April 1998, pp. 107-115

Ueda, T., Y. Sato, and Y. Asano, "Experimental Study on Bond Strength of Continuous Carbon Fiber Sheet," Proceedings of the Fourth International Symposium on Fiber Reinforced Polymer Reinforcement for Reinforced Concrete Structures, 1999, pp. 407-416

Uji, K., "Improving Shear Capacity of Existing Reinforced Concrete Members by Applying Carbon Fiber Sheets," Transactions of the Japan Concrete Institute, Vol. 14, 1992, pp. 253-266

Umezu, K., M. Fujita, H. Nakai, and K. Tamaki, "Shear Behavior of RC Beams with Aramid Fiber Sheets," Proceedings of the Third International Symposium on Non-Metallic Reinforcement for Concrete Structures, October 1997, Vol. 1, pp. 491-498

Valerio, P. and T. J. Ibell, “Shear Strengthening of Existing Concrete Bridges,” Structures and Buildings, February 2003, Issue 1, pp. 75-84

Yan, X., B. Miller, A. Nanni, and C. Bakis, “Characterization of CFRP Rods Used as Near-Surface Mounted Reinforcement,” Proceedings of the Eighth International Structural Faults and Repair Conference, 1999

Yazdani, N. Prevention of Cracking in Pier Caps. Report, Department of Civil Engineering, FAMU/FSU College of Engineering, 1990.

Yazdani, N. and Mesidor, E. “Flexural and Shear Behavior of Bridge Pier Caps,” Structural Engineering Review, Elsevier Science Ltd., Vol 8, No 1, 1996.

Young, B.S. Cracking in Reinforced Concrete Bent Caps. Thesis, Texas A&M University, 2000.

Young B.S., Bracci, J.M., Keating, P.B., and Hueste, M.D. “Cracking in Reinforced Concrete Bent Caps,” ACI Structural Journal, American Concrete Institute, Vol. 99, No. 4, July-Aug 2002.

Tables

Table 1-1: Correction factors and standard deviations for ultimate capacity provisions

Provision	Correction Factor	Standard Deviation	No. of Tests
ACI 318-02 Shallow Flexure	1.11	0.08	6
ACI 318-81 Shallow Flexure	1.11	0.08	6
1977 AASHTO Shallow Flexure	1.11	0.08	6
1998 AASHTO LRFD Shallow Flexure	1.11	0.08	6
ACI 318-02 Shallow Shear (using Eqn 1-1)	1.23	0.16	14
ACI 318-03 Shallow Shear (using Eqn 1-1)	1.23	0.16	14
1977 AASHTO Shallow Shear (using Eqn 1-1)	1.23	0.16	14
ACI 318-02 Shallow Shear (using Eqn 1-2)	1.27	0.18	14
ACI 318-03 Shallow Shear (using Eqn 1-2)	1.27	0.18	14
1977 AASHTO Shallow Shear (using Eqn 1-2)	1.27	0.18	14
1998 AASHTO LRFD MCFT	1.32	0.15	14
ACI318-02 Strut and tie	1.23	0.15	20
1998 AASHTO LRFD Strut and Tie	1.23	0.15	20

Table 1-2: Estimated ultimate capacities for pier cap overhang of Bridge 19855

Provision	Predicted Ultimate Capacity (kips)	Correction Factor	Estimated Ultimate Capacity (kips)
ACI 318-02 Shallow Flexure	1178	1.11	1308
ACI 318-81 Shallow Flexure	1178	1.11	1308
1977 AASHTO Shallow Flexure	1178	1.11	1308
1998 AASHTO LRFD Shallow Flexure	1178	1.11	1308
ACI 318-02 Shallow Shear (using Eqn 1-1)	1329	1.23	1635
ACI 318-03 Shallow Shear (using Eqn 1-1)	1329	1.23	1635
1977 AASHTO Shallow Shear (using Eqn 1-1)	1329	1.23	1635
ACI 318-02 Shallow Shear (using Eqn 1-2)	1300	1.27	1651
ACI 318-03 Shallow Shear (using Eqn 1-2)	1300	1.27	1651
1977 AASHTO Shallow Shear (using Eqn 1-2)	1300	1.27	1651
1998 AASHTO LRFD MCFT	1303	1.32	1720
ACI318-02 Strut and tie	1124	1.23	1383
1998 AASHTO LRFD Strut and Tie	1124	1.23	1383

Table 1-3: Reduced ultimate capacities for pier cap overhang of Bridge 19855

Provision	Estimated Ultimate Capacity (kips)	Resistance Factor	Reduced Ultimate Capacity (kips)
ACI 318-02 Shallow Flexure	1308	0.9	1177
ACI 318-81 Shallow Flexure	1308	0.9	1177
1977 AASHTO Shallow Flexure	1308	0.9	1177
1998 AASHTO LRFD Shallow Flexure	1308	0.9	1177
ACI 318-02 Shallow Shear (using Eqn 4-1)	1635	0.75	1226
ACI 318-83 Shallow Shear (using Eqn 4-1)	1635	0.85	1390
1977 AASHTO Shallow Shear (using Eqn 4-1)	1635	0.85	1390
ACI 318-02 Shallow Shear (using Eqn 4-2)	1651	0.75	1238
ACI 318-83 Shallow Shear (using Eqn 4-2)	1651	0.85	1403
1977 AASHTO Shallow Shear (using Eqn 4-2)	1651	0.85	1403
1998 AASHTO LRFD MCFT Shear	1720	0.9	1548
ACI 318-02 Strut and Tie	1383	0.75	1037
1998 AASHTO LRFD Strut and Tie *	1383	1.00*	1383

*Although 1998 AASHTO LRFD prescribes different resistance factors for strut and tie design depending on the failing component, in all overhangs examined in this research the tie capacity was much smaller than either the strut of nodal region capacity resulting in the uniform resistance factor of 1.00.

Table 1-4: Average correction factors and standard deviations for cracking provisions

Provision	Correction Factor	Standard Deviation	No. of Tests
Gross Section	1.32	0.20	16
Transformed Section	1.19	0.17	16
Finite Element	0.93	0.14	16

Table 1-5: Estimated cracking loads for pier cap overhang of Bridge 19855

Provision	Predicted Load (kips)	Correction Factor	Estimated Load (kips)
Gross Section	273	1.32	361
Transformed Section	315	1.19	375
Finite Element	354	0.93	329

Table 1-6: Estimated cracking loads for pier cap overhang of Bridge 19856

Provision	Predicted Load (kips)	Correction Factor	Estimated Load (kips)
Gross Section	317	1.32	419
Transformed Section	360	1.19	428
Finite Element	411	0.93	382

Table 2-1 Comparison of Steel and Fiber Properties

Material	Tensile Strength (ksi)	Tensile Modulus (10^6 psi)	Density (lb/in^3)
E-glass	500	10.5	0.092
Carbon	580-730	33-42	0.064-0.065
Aramid	550	9-19	0.052-0.053
Steel	50-120	28-30	0.284

Table 2-2 Comparison of Steel and CFRP Strength-to-Density Ratios

Material	Strength to Density Ratio (10^4 in)
Steel (Grade 50)	17.6
CFRP (Tyfo SCH-35/Tyfo S)	332

Table 3-1 Parameters for Bond Tests

Test	FRP Type	Strips on Each Side	Strip Width (in)	Spacing Between Strips (in)	Fiber Orientation to Crack (deg)	Unbonded Length at Crack (in)
E1-90-1	EB	1	6	-	90	0
E2-90-1	EB	1	6	-	90	0
E3-90-1-U2	EB	1	6	-	90	2
E4-90-1-U2	EB	1	6	-	90	2
E5-90-1-U1	EB	1	6	-	90	1
E6-90-1	EB	1	6	-	90	0
E7-45-1	EB	1	6	-	45	0
E8-90-2	EB	2	3	1	90	0
E9-90-2	EB	2	3	3	90	0
E10-90-3	EB	3	2	1	90	0
E11-45-2	EB	2	3	1	45	0
E12-45-3	EB	3	2	1	45	0
NA13-90-2	NSM-A	2	-	6	90	0
NA14-90-2	NSM-A	2	-	6	90	0
NA15-45-2	NSM-A	2	-	6	45	0
NB16-90-2	NSM-B	2	-	6	90	0
NB17-90-2	NSM-B	2	-	6	90	0
NB18-90-2V	NSM-B	2	-	6	90	0

Table 3-2 Concrete Strengths for Bond Tests

Test Date (age of concrete)	Compressive Strength (psi)	Coefficient of Variation (%)	Tensile Strength (psi)	Coefficient of Variation (%)
4/10/03 (28 days)	6150	3.4	620	3.9
11/20/03 (224 days)	7840	2.3	640	10.0
6/20/04 (437 days)	8700	3.1	660	7.3

Table 3-3 Tensile Test Strengths of NSM and EB FRP

FRP Type	Tensile Strength (ksi)	Coefficient of Variation (%)
Near Surface Mounted Tape (Aslan 500)	360	4.5
Externally Bonded Sheet (Tyfo SCH-35 /Tyfo S)	160	13.6

Table 3-4 Concrete Strengths for Beam Tests

Test Date (age of concrete)	Compressive Strength (psi)	Coefficient of Variation (%)	Tensile Strength (psi)	Coefficient of Variation (%)
3/23/04 (28 days)	5990	3.0	440	6.7
6/20/04 (117 days)	6320	2.1	450	8.0
8/24/04 (182 days)	6870	5.1	460	7.5

Table 4-1 Maximum Loads for EB FRP Tests

Test	Max. Load (kips)	Max. Load East (kips)	Max. Load West (kips)
E1-90-1	16.9	8.4	8.4
E2-90-1	13.4	6.0	7.3
E3-90-1-U2	12.2	5.6	6.3
E4-90-1-U2	12.1	5.9	6.0
E5-90-1-U1	11.8	5.6	6.3
E6-90-1	15.0	7.7	6.9
E7-45-1	13.0	4.7	11.7
E8-90-2	19.4	N 5.0s S 5.0s	N 5.0s S 4.1
E9-90-2	16.1	N 3.8 S 3.9	N 4.2 S 4.4
E10-90-3	20.4	N 3.3 C 3.0 S 3.7	N 3.2 C 3.8 S 4.0
E11-45-2	9.7	N 4.5s S 4.5s	N 2.0 S 4.0
E12-45-3	12.2	N 4.1s C 4.1s S 4.1s	N 2.4s C 2.4s S 2.4s

Table 4-2 Maximum Strains for EB FRP Tests

Test	Max. Strain East	Strain at Failure East	Average Strain at Debonding East	Max. Strain West	Strain at Failure West	Average Strain at Debonding West
E1-90-1	2916	2810	1801	2395	2319	1816
E2-90-1	2726	2153	1984	3476	3374	2671
E3-90-1-U2	1838	1766	1704	2035	1986	1573
E4-90-1-U2	NA	NA	NA	NA	NA	NA
E5-90-1-U1	NA	NA	NA	1765	1765	1594
E6-90-1	NA	NA	NA	NA	NA	NA
E7-45-1	3436	3226	2194	3003	2869	2225
E8-90-2	N NA S NA	N NA S NA	N NA S NA	N 3995 S 3130	N 3895 S 2814	N 2585 S 2642
E9-90-2	N NA S NA	N NA S NA	N NA S NA	N NA S NA	N NA S NA	N NA S NA
E10-90-3	N NA C NA S NA	N NA C NA S NA	N NA C NA S NA	N NA C 4176 S NA	N NA C 3928 S NA	N NA C 3508 S NA
E11-45-2	N NA S NA	N NA S NA	N NA S NA	N NA S 3930	N NA S 3628	N NA S 2336
E12-45-3	N NA C 3858 S NA	N NA C 3858 S NA	N NA C 2450 S NA	N NA C 3569 S NA	N NA C 3557 S NA	N NA C 2442 S NA

Table 4-3 Failure Surface Areas for EB FRP Tests

Test	Estimated Concrete Substrate Failure Area East (%)	Estimated Crack Projection Area East (in^2)	Estimated Concrete Substrate Failure Area West (%)	Estimated Crack Projection Area West (in^2)	Group
E1-90-1	5	10.5	70	12.0	1
E2-90-1	5	5.3	5	5.6	2
E3-90-1-U2	0	0.0	0	0.0	2
E4-90-1-U2	0	0.0	0	0.0	2
E5-90-1-U1	0	0.0	0	0.0	2
E6-90-1	10	13.8	10	11.9	2
E7-45-1	50	1.6	10	1.3	1
E8-90-2	30	14.4	5	6.4	1
E9-90-2	5	9.5	5	2.5	2
E10-90-3	10	10.5	60	17.5	1
E11-45-2	5	1.0	5	2.5	2
E12-45-3	25	2.0	5	4.0	2

Table 4-4 Effective Bond Lengths for EB FRP Tests

Test	Smallest Effective Bond Length East (in)	Largest Effective Bond Length East (in)	Smallest Effective Bond Length West (in)	Largest Effective Bond Length West (in)
E1-90-1	1	2	1	4
E2-90-1	1	3	1	4
E3-90-1-U2	1	2	1	2
E4-90-1-U2	NA	NA	NA	NA
E5-90-1-U1	NA	NA	1	3
E6-90-1	NA	NA	NA	NA
E7-45-1	1	3	1	4
E8-90-2	N NA S NA	N NA S NA	N 1 S 1	N 3 S 3
E9-90-2	N NA S NA	N NA S NA	N NA S NA	N NA S NA
E10-90-3	N NA C NA S NA	N NA C NA S NA	N NA C 1 S NA	N NA C 5 S NA
E11-45-2	N NA S NA	N NA S NA	N NA S 1	N NA S 3
E12-45-3	N NA C 1 S NA	N NA C 3 S NA	N NA C 1 S NA	N NA C 3 S NA

Table 4-5 Maximum Loads for NSM FRP Tests

Test	Maximum Load (kips)	Maximum Load East (kips)	Maximum Load West (kips)
NA13-90-2	27.7	N 8 S NA	N NA S NA
NA14-90-2	38.1	N 10 S 4.1	N 2.9 S 7.1
NA15-45-2	22.3	N 4.8s S 4.8s	N 7.6s S 7.6s
NB16-90-2	54.3	N 18.3 S 13.5	N 13.3s S 13.3s
NB17-90-2	56.3	N 14.4 S 14.3	N 13.6 S 15.0
NB18-90-2V	54.5	N 11.5 S 15.2	N 15.0 S 15.0

Table 4-6 EB Specimens with Significant Concrete Removed

Test Series	Test Numbers	Maximum Loads (kips)	Increase from Average Standard Load (%)	Average Load (kips)	Increase from Average Standard Load (%)
Standard	E1-90-1	16.9		16.9	
45 Degree	E7-45-1	13.0	-23	13.0	-23
Multiple Strips	E8-90-2 E10-90-3	19.4 20.4	15 21	19.9	18

Table 4-7 EB Specimens without Significant Concrete Removed

Test Series	Test Numbers	Maximum Loads (kips)	Increase from Average Standard Load (%)	Average Load (kips)	Increase from Average Standard Load (%)
Standard	E2-90-1 E6-90-1	13.4 15.0		14.2	
Unbonded Region	E3-90-1-U2 E4-90-1-U2 E5-90-1-U1	11.8 12.1 12.2	-17 -15 -14	12.0	-15
45 Degree	E11-45-2 E12-45-3	9.7 12.2	-32 -14	11.0	-23
Multiple Strips	E9-90-2	16.1	13	16.1	13

Table 4-8 Capacities of Beam Tests and Loads at which Tests were Terminated

Test	Calculated Capacity (kips)	Load at which Test was Terminated (kips)
1 (B1 with no FRP)	107 (controlled by shear strength of NS span with no FRP)	105
2 (B1 with FRP on NS span only)	160 (controlled by shear strength of MS span with no FRP)	140
3 (B1 with FRP on both spans)	218 (controlled by shear strength of MS span with FRP)	259
4 (B2 with FRP on NS span only)	164 (controlled by shear strength of MS span with no FRP	255

Table 4-9 Final Capacities of Beam B1

	Calculated Capacity (kips)	Maximum Load at Failure (kips)
Calculated Shear Capacity of NS span with FRP	224	259
Calculated Shear Capacity of MS span with FRP	218	
Calculated Flexural Capacity of Beam	224	

Table 4-10 Strains for Tests 1 and 2

Strain Gage	Distance from Load Point (in)	Microstrain at 105 kips (Test 1)	Microstrain at 105 kips (Test 2)	Decrease in Strain (%)
18m	48	467	471	0
20b	56	554	498	10

Table 4-11 Strains for Tests 2 and 3

Strain Gage	Distance from Load Point (in)	Microstrain at 140 kips (Test 2)	Microstrain at 140 kips (Test 3)	Decrease in Strain (%)
1ml	9	263	241	8
1tl	9	230	134	42
1tr	9	917	608	34
2bl	23	417	270	35
2ml	23	1394	1104	21
2br	23	477	309	35
2mr	23	1407	1063	25
3bl	37	415	322	22
3br	37	392	326	17
7b	56	469	323	31
7m	56	439	237	46
9b	64	541	312	42
11b	72	314	242	23
17bl	44	280	234	16
17br	44	398	363	9
18m	48	781	768	2
20b	56	791	802	0
22b	64	297	272	8
22m	64	804	492	39
24b	72	1522	1155	24

Table 4-12 Strains for Test 3 and 4

Strain Gage	Distance from Load Point (in)	Microstrain at 200 kips (Test 3)	Microstrain at 200 kips (Test 4)	Decrease in Strain (%)
1ml	9	569	103	0
1tl	9	396	1402	72
1br	9	591	42	0
1tr	9	1090	1567	30
2bl	23	469	698	33
2ml	23	1390	2107	34
2tl	23	1223	1370	11
2br	23	616	633	3
2mr	23	1486	1549	4
2tr	23	951	1129	16
3bl	37	856	1849	54
3ml	37	685	1606	57
3br	37	1314	1638	20
3mr	37	995	1104	10
4bl	44	2283	1576	0
4ml	44	38	836	95
4tl	44	358	462	23
4br	44	1165	2159	46
4mr	44	172	586	71
5b	48	658	1784	63
5m	48	198	502	61
5t	48	215	1055	80
7b	56	515	848	39
7m	56	888	2341	62
7t	56	-1	222	100
9b	64	987	3094	68
9m	64	204	390	48
11b	72	2047	2001	0
17bl	44	928	1921	52
17ml	44	304	127	0
17tl	44	267	631	58
17br	44	997	1960	49
17tr	44	142	1036	86
18b	48	594	699	15
18m	48	1218	999	0
18t	48	586	417	0
20b	56	1487	1113	0
20m	56	375	80	0
20t	56	338	703	52
22b	64	972	1639	41
22m	64	1021	263	0
24b	72	2191	1125	0

Table 4-12 Strains for Test 3 and 4 cont.

Strain Gage	Distance from Load Point (in)	Microstrain at 250 kips (Test 3)	Microstrain at 250 kips (Test 4)	Decrease in Strain (%)
1bl	9	298	377	21
1ml	9	1618	122	0
1tl	9	619	3253	81
1br	9	1226	39	0
1mr	9	1469	83	0
1tr	9	1298	1608	19
2bl	23	707	1034	32
2ml	23	1661	2472	33
2tl	23	2173	2897	25
2br	23	911	1145	20
2mr	23	1832	1929	5
2tr	23	1721	2290	25
3bl	37	1350	2247	40
3ml	37	772	1983	61
3tl	37	252	193	0
3br	37	1693	2170	22
3mr	37	1594	1674	5
4bl	44	2443	3943	38
4ml	44	109	1774	94
4tl	44	746	718	0
4br	44	1976	2678	26
4mr	44	270	1003	73
4tr	44	311	433	28
5b	48	2358	6898	67
5m	48	338	692	51
5t	48	379	1576	76
7b	56	788	1773	56
7m	56	1345	4640	71
7t	56	40	419	90
9b	64	1465	13700	89
9m	64	650	576	0
11b	72	5335	2663	0
17bl	44	1774	3194	44
17ml	44	658	1595	59
17tl	44	661	848	22
17br	44	1694	5403	69
17mr	44	432	1617	73
17tr	44	412	1338	69

Table 4-12 Strains for Tests 3 and 4 cont.

Strain Gage	Distance from Load Point (in)	Microstrain at 250 kips (Test 3)	Microstrain at 250 kips (Test 4)	Decrease in Strain (%)
18b	48	1870	1999	6
18m	48	1692	3284	48
18t	48	977	1069	9
20b	56	2284	2976	23
20m	56	761	363	0
20t	56	678	1059	36
22b	64	2003	2424	17
22m	64	1422	561	0
24b	72	3806	1792	0
24m	72	366	18	0

Figures

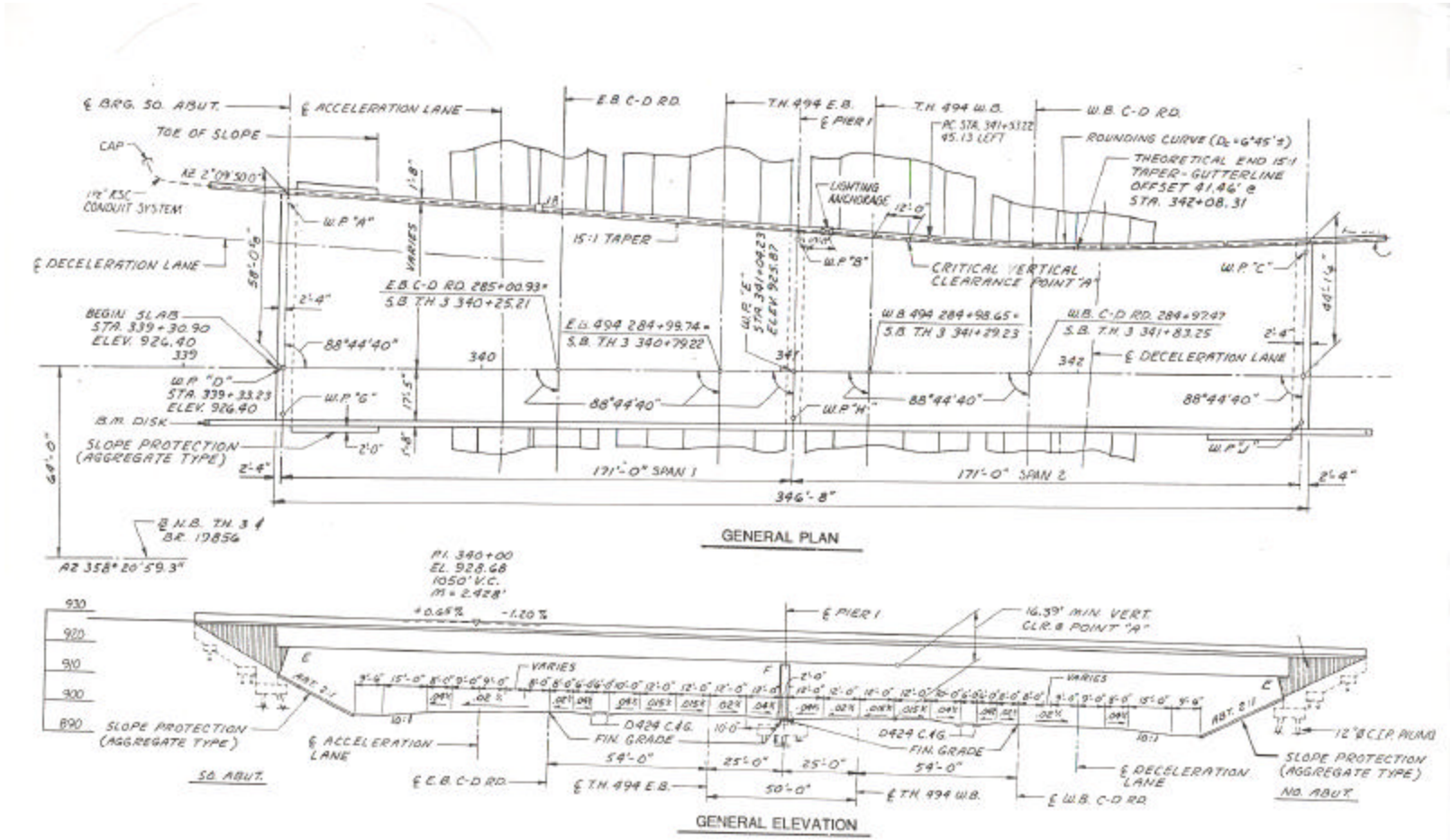

Figure 1-1 Plan and elevation view of Bridge 19855.

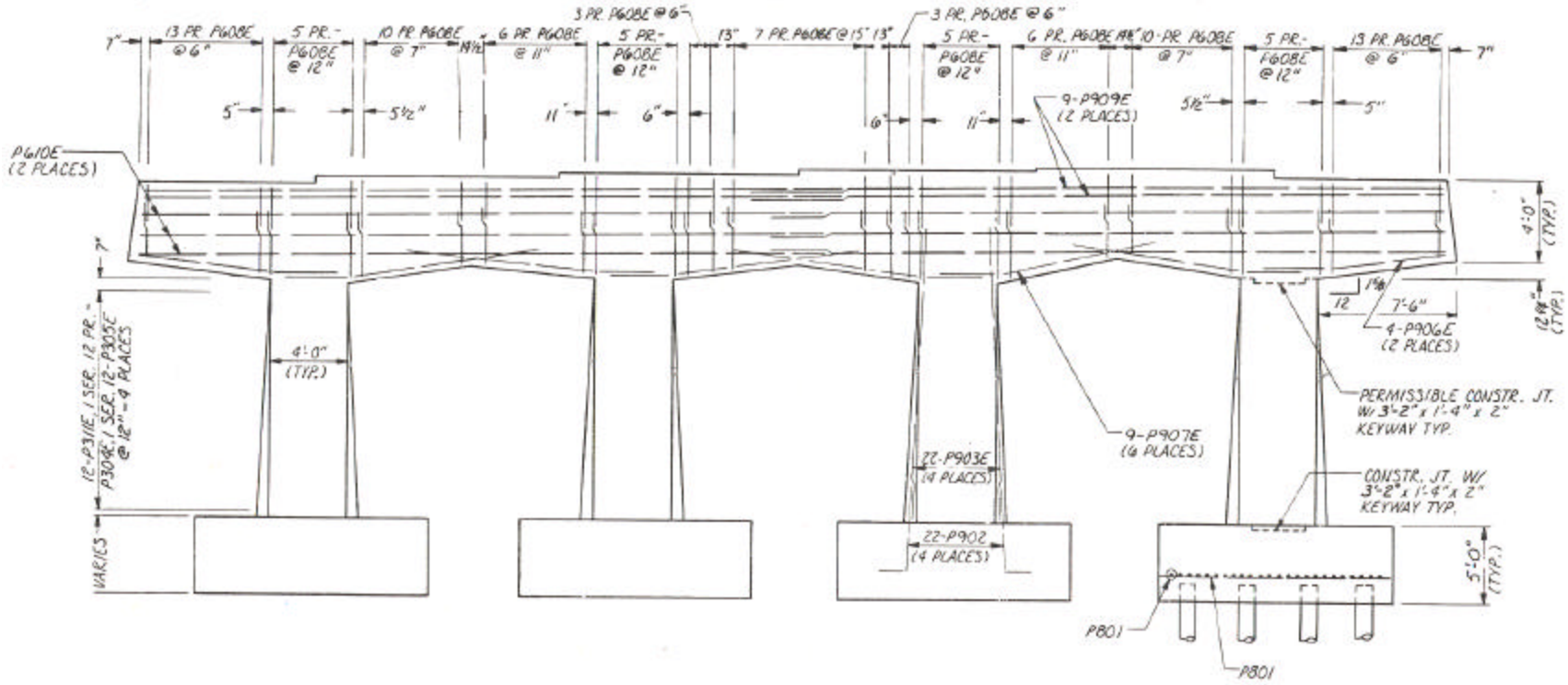

Figure 1-2 Elevation view of pier cap.

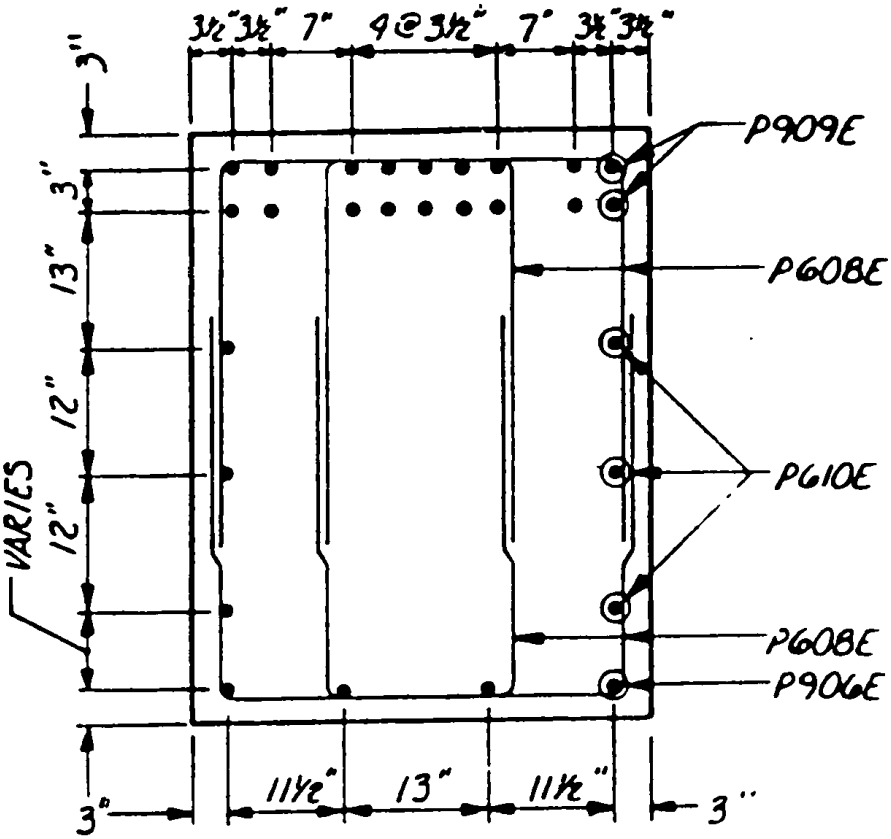

Figure 1-3 Standard reinforcing detail cross-section of pier cap overhang.

Figure 1-4 Cracked overhang of Bridge 19855.

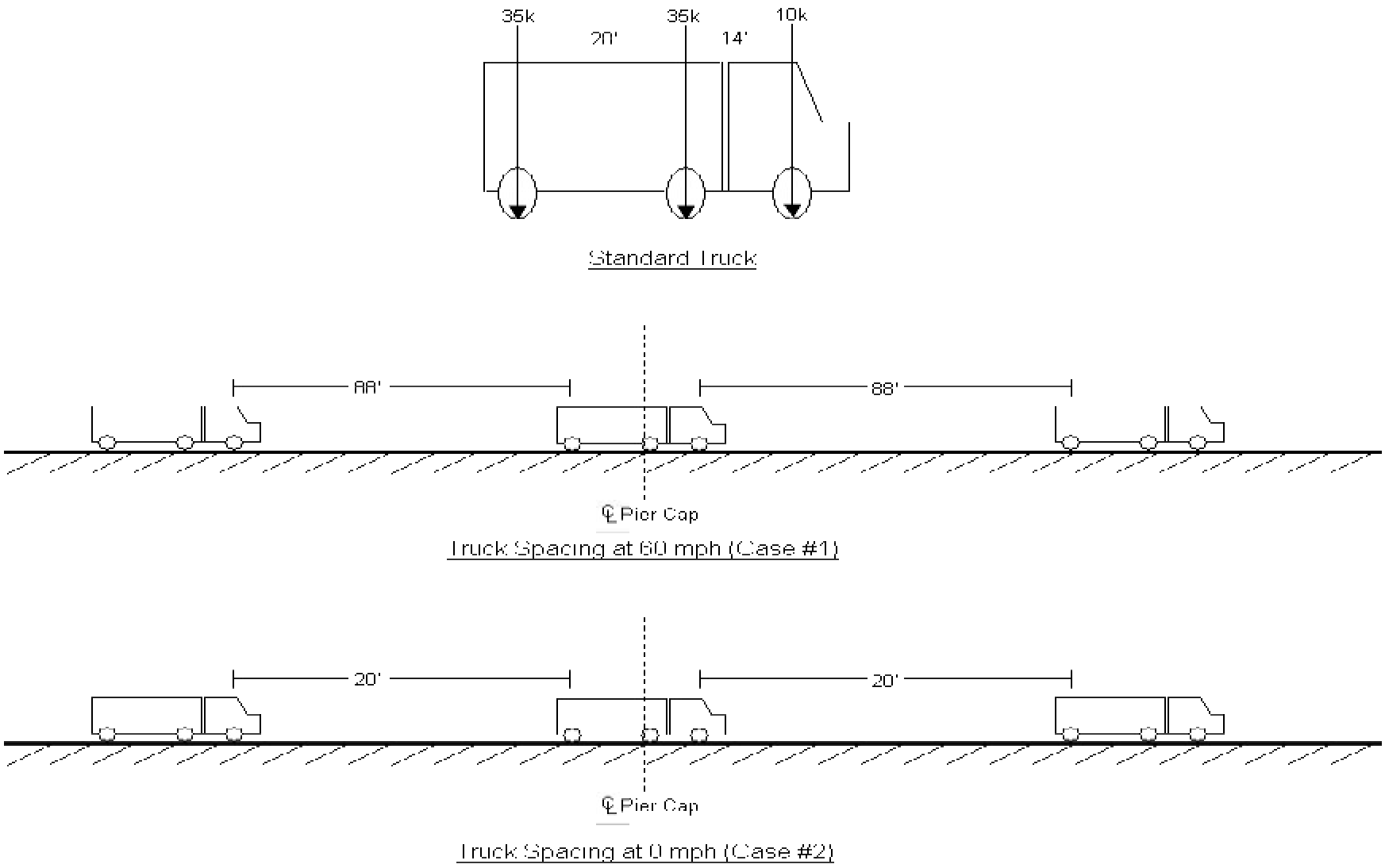

Figure 1-5 Truck and traffic loads and spacings used to determine service load.

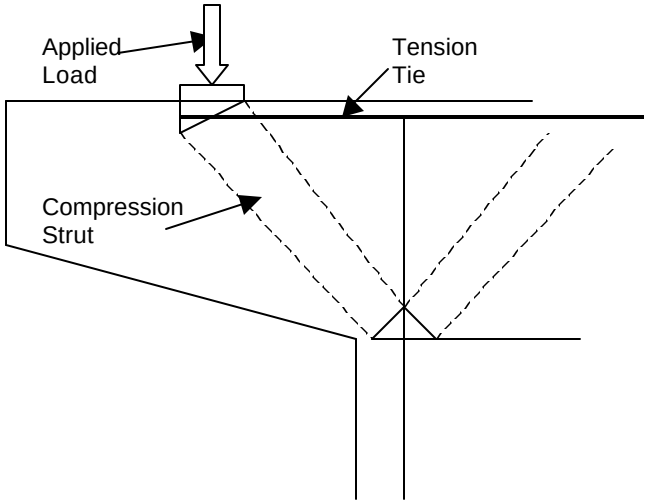

Figure 1-6 Truss Model used in Strut and Tie Method

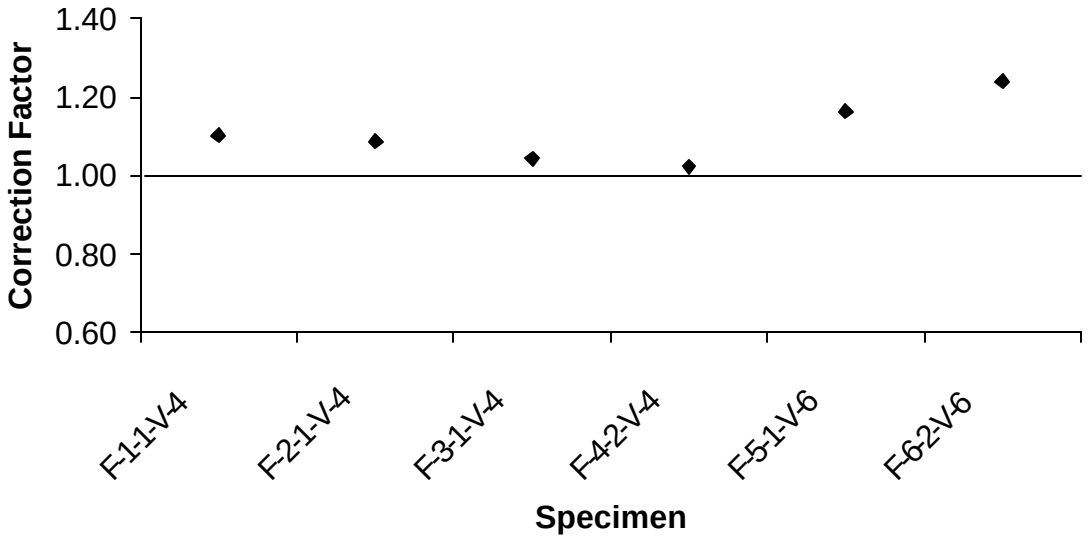

Figure 1-7 Ultimate strength correction factors for shallow beam flexural provision (ACI 318-02, ACI 318-81, 1998 AASHTO LRFD, 1977 AASHTO)

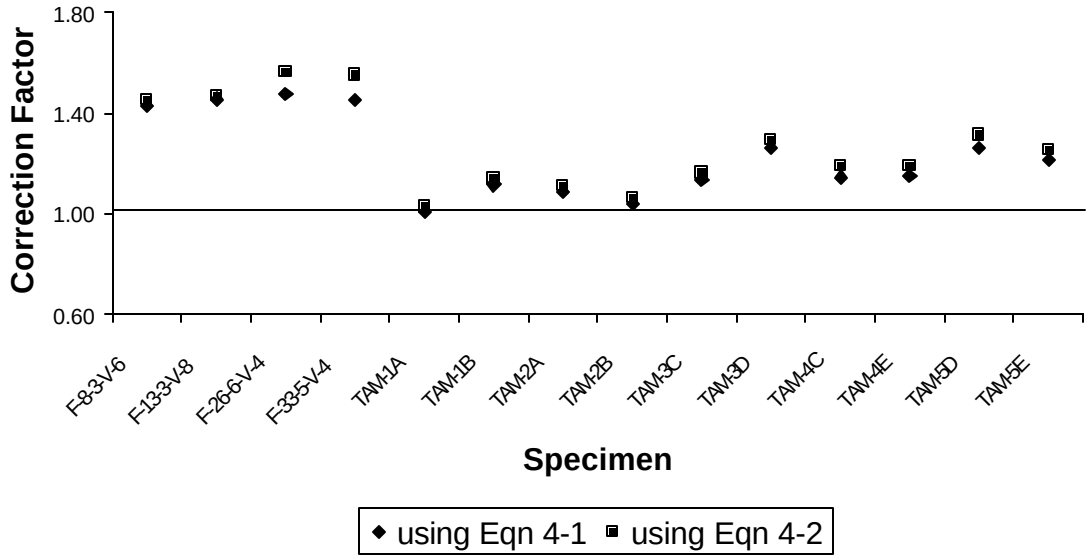

Figure 1-8 Ultimate Strength correction factors for shallow beam shear provision (ACI 318-02, ACI 318-81, 1977 AASHTO)

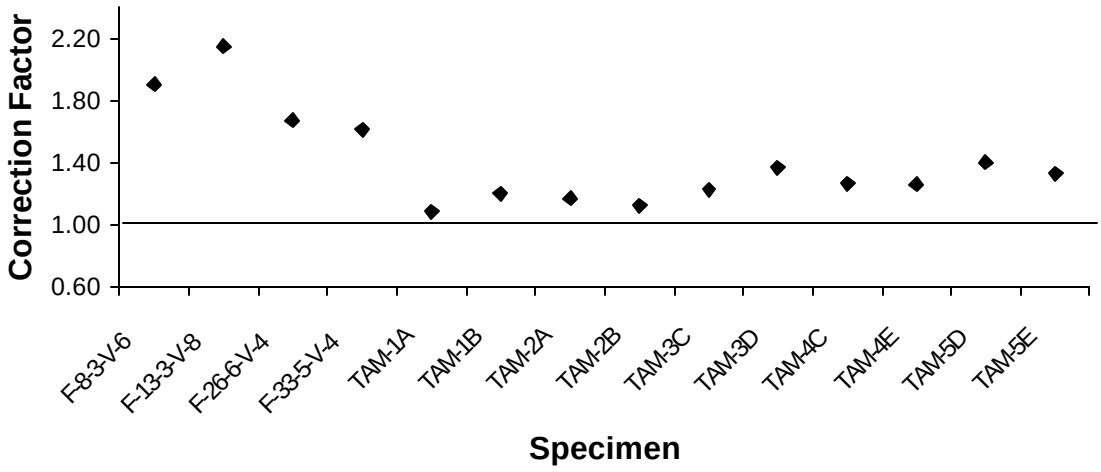

Figure 1-9 Ultimate strength correction factors for 1998 AASHTO LRFD shear provision using MCFT

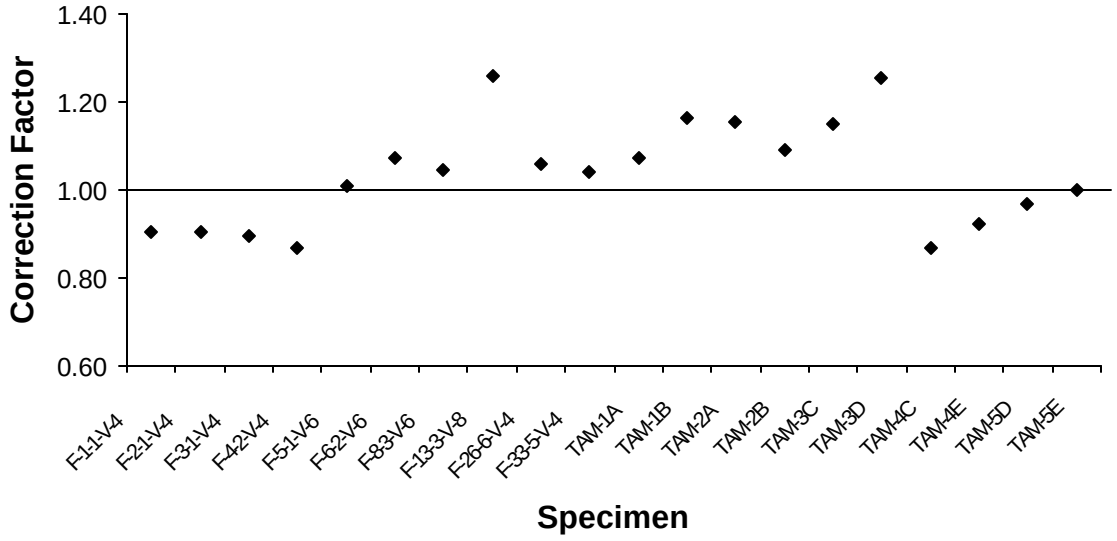

Figure 1-10 Ultimate strength correction factors for ACI 318-02 strut and tie provision

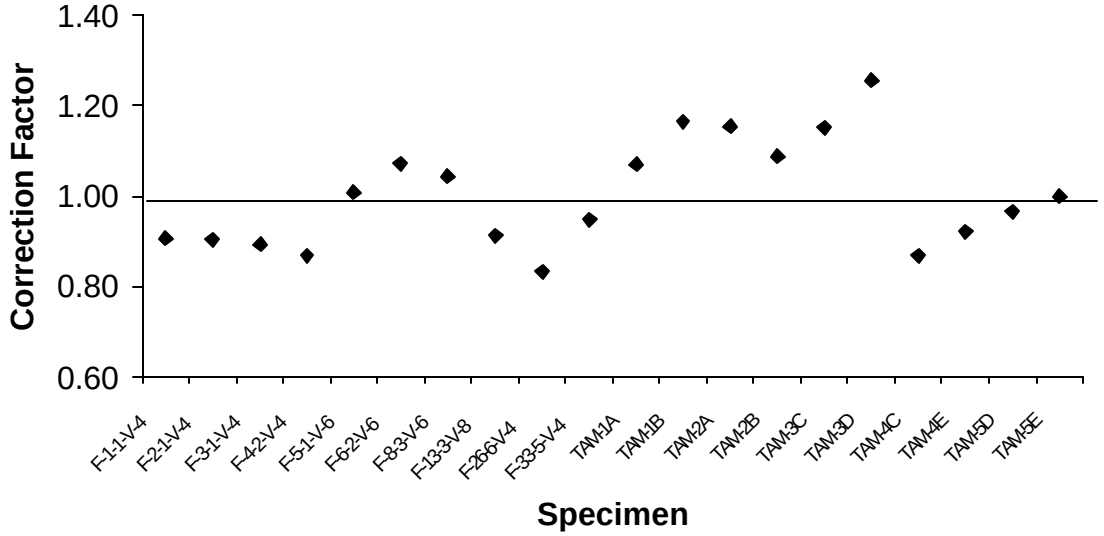

Figure 1-11 Ultimate strength correction factors for 1998 AASHTO LRFD strut and tie provision

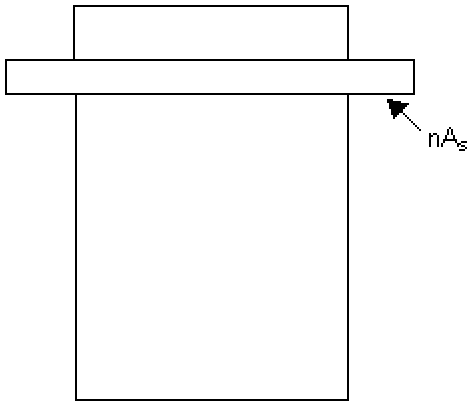

Figure 1-12 Transformed section of pier cap overhang

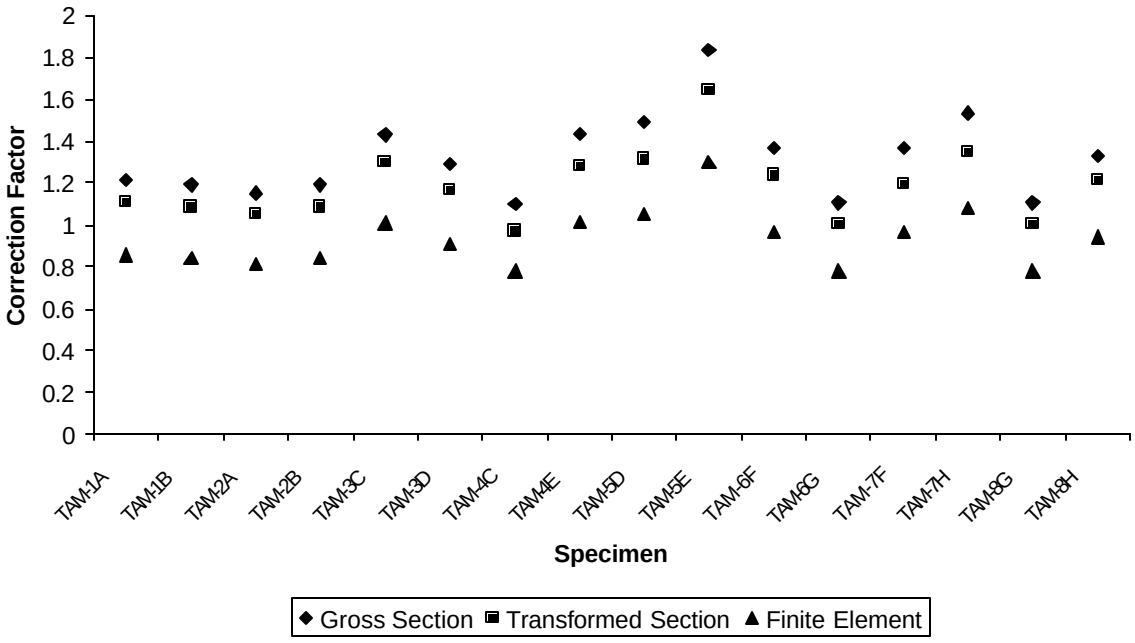

Figure 1-13 Cracking load correction factors for gross section, transformed section, and finite element models

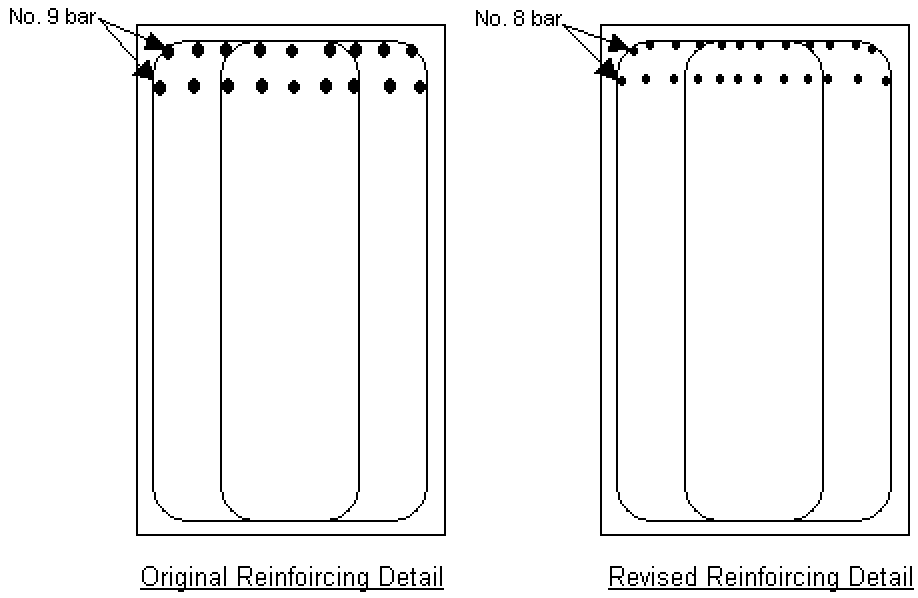

Figure 1-14 Reinforcing details of original cross-section and cross section modified to meet bar distribution serviceability requirements.

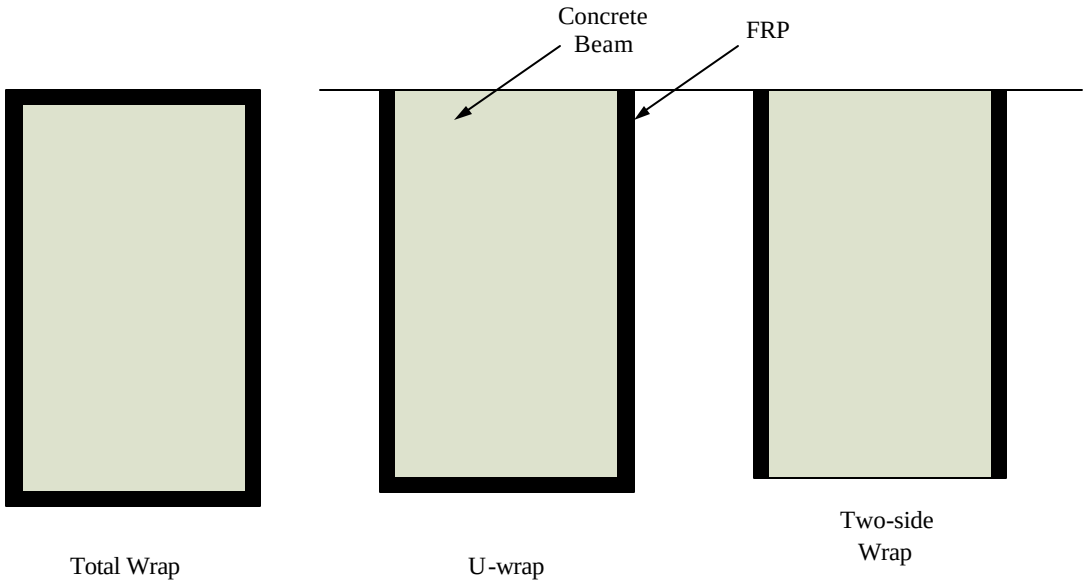

Figure 2-1 Wrapping Schemes

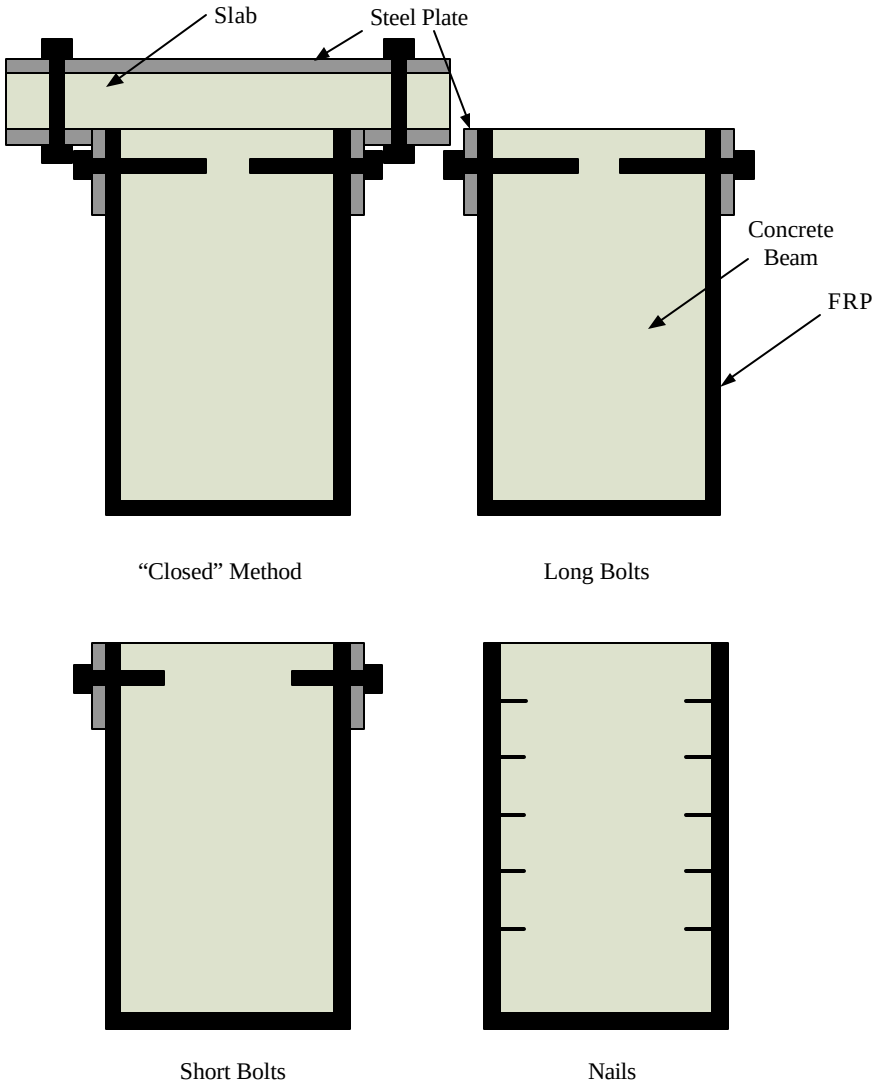

Figure 2-2 Anchoring Methods

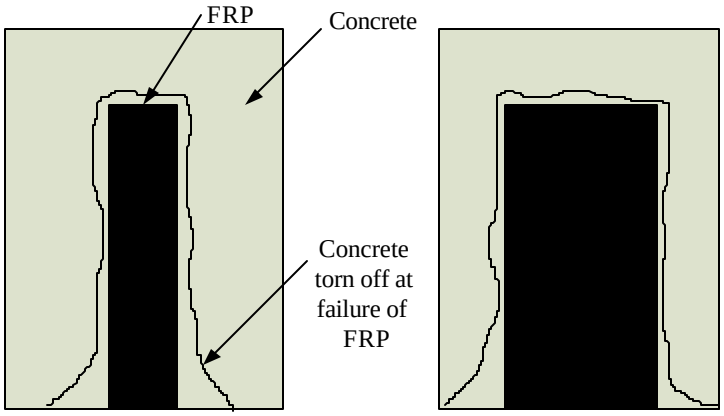

Figure 2-3 Effect of Strip Width

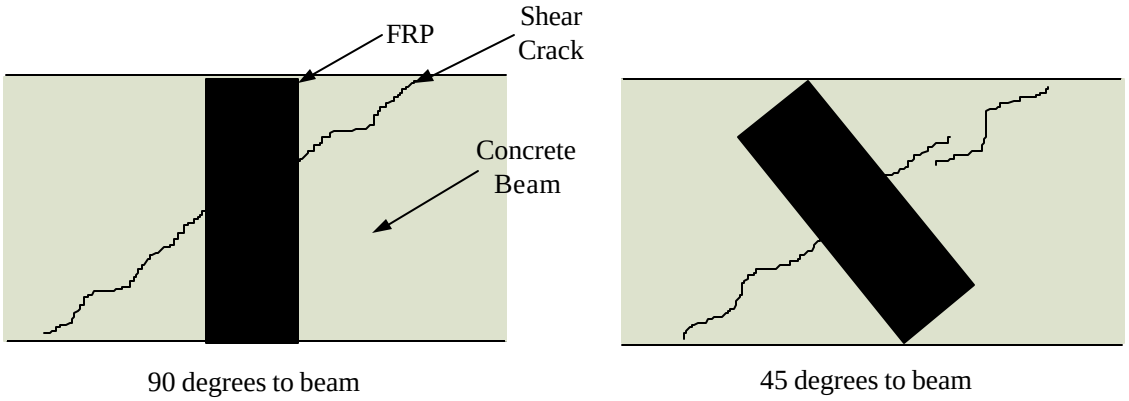

Figure 2-4 Fiber Orientations

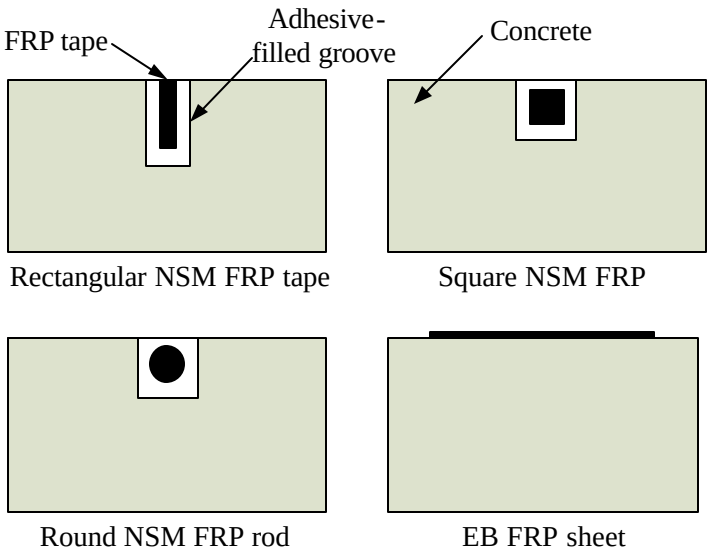

Figure 2-5 FRP Strengthening Methods

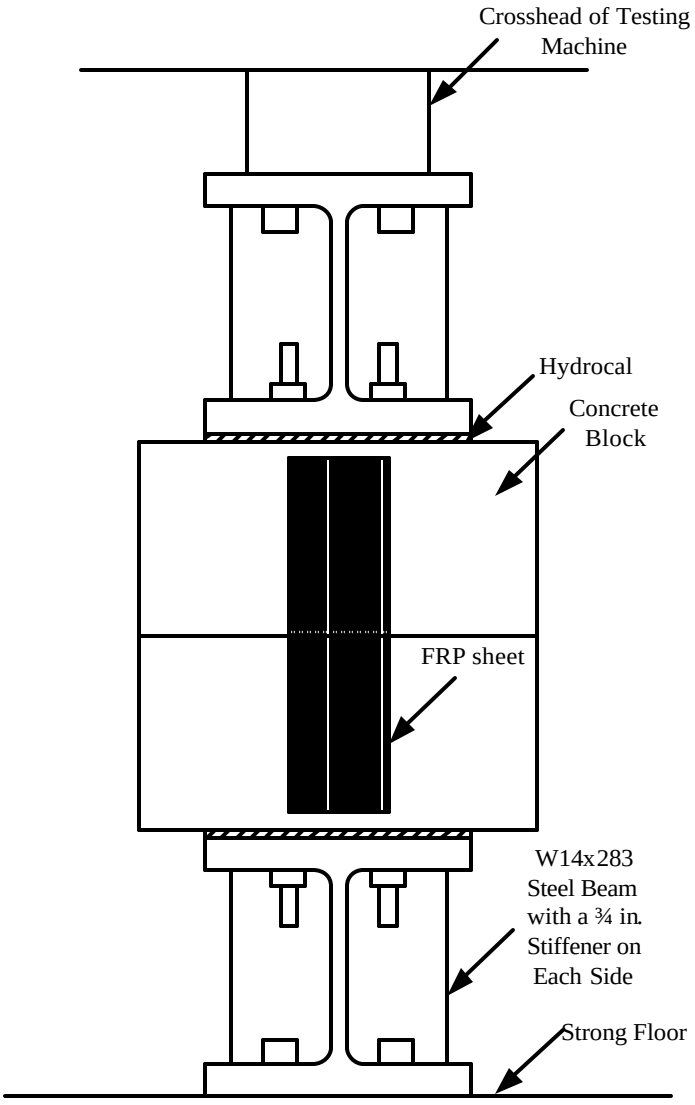

Figure 3-1 Bond Test Setup

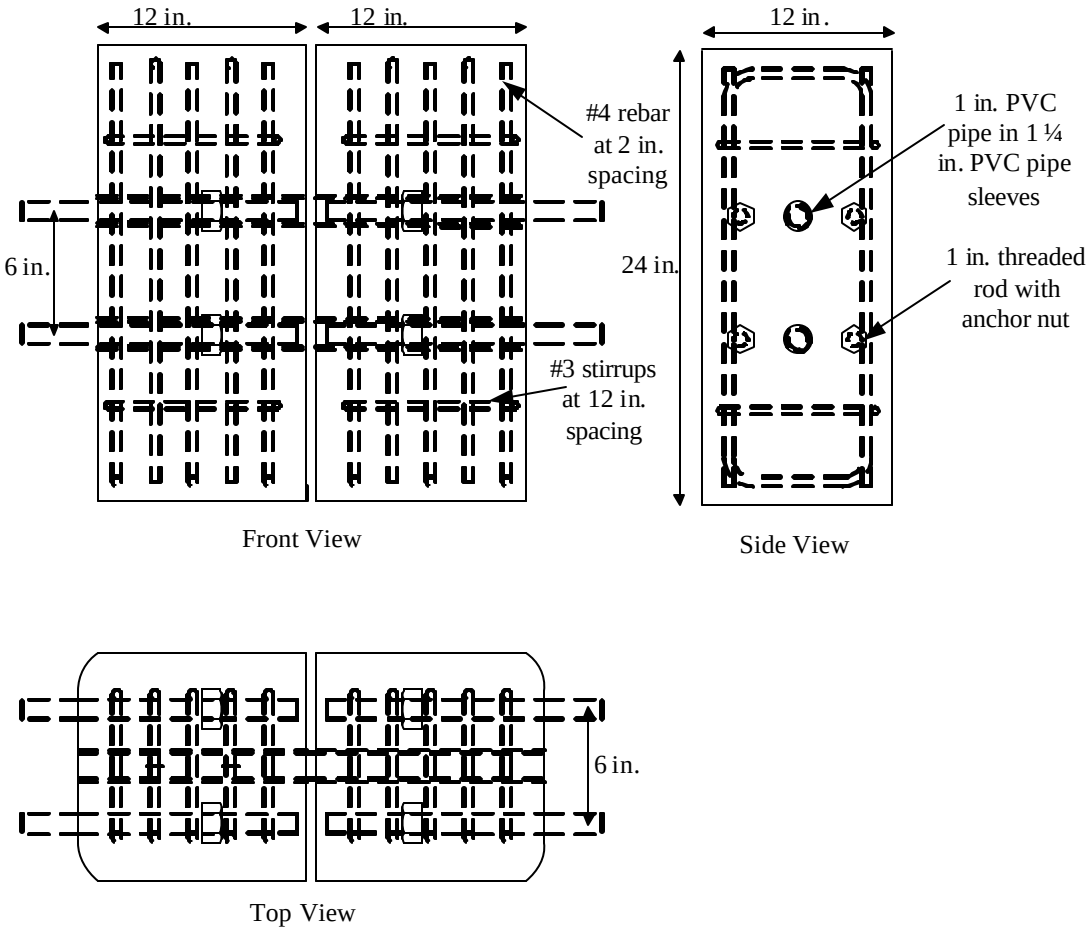

Figure 3-2 Bond Test Specimen Drawings

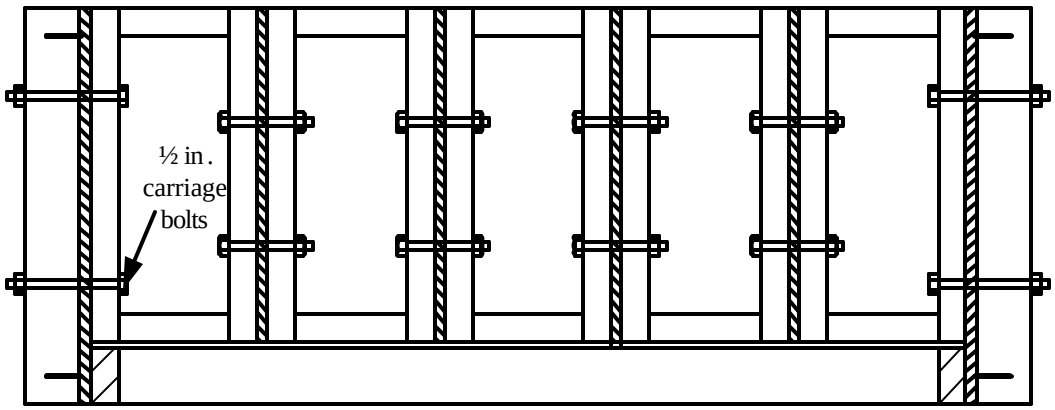

Side View

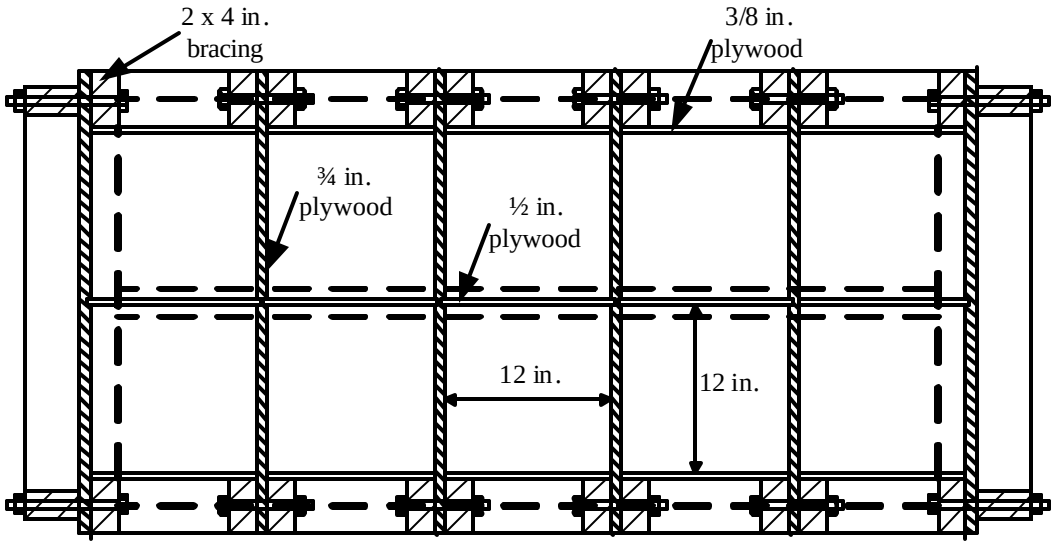

Top View

Figure 3-3 Forms for Bond Test Specimens

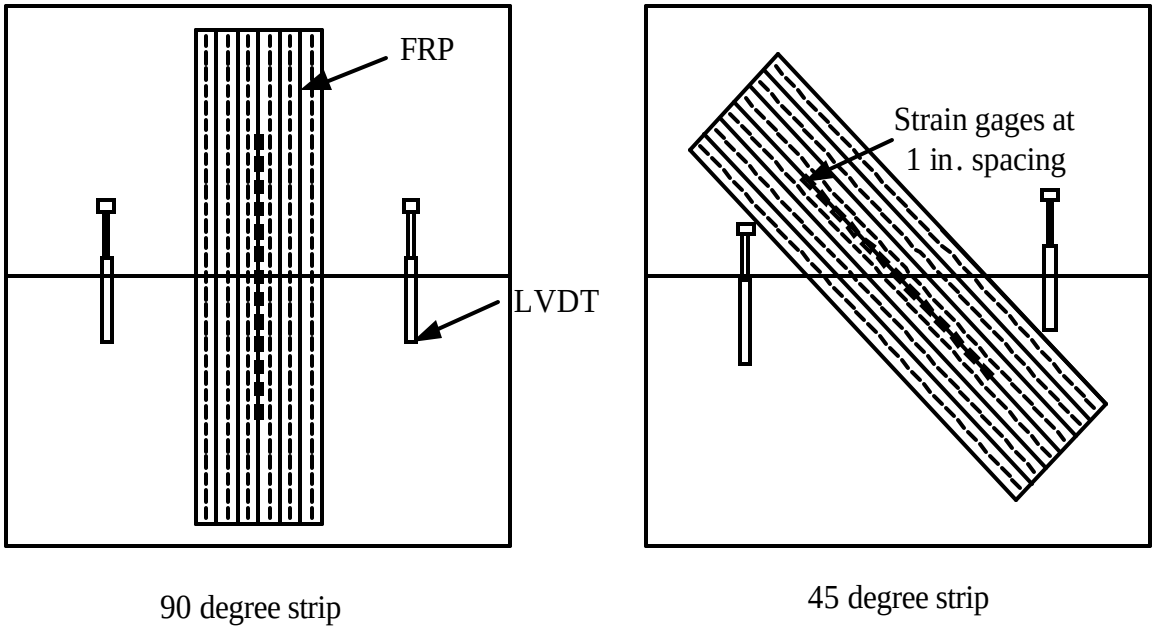

Figure 3-4 Typical Bond Test Instrumentation

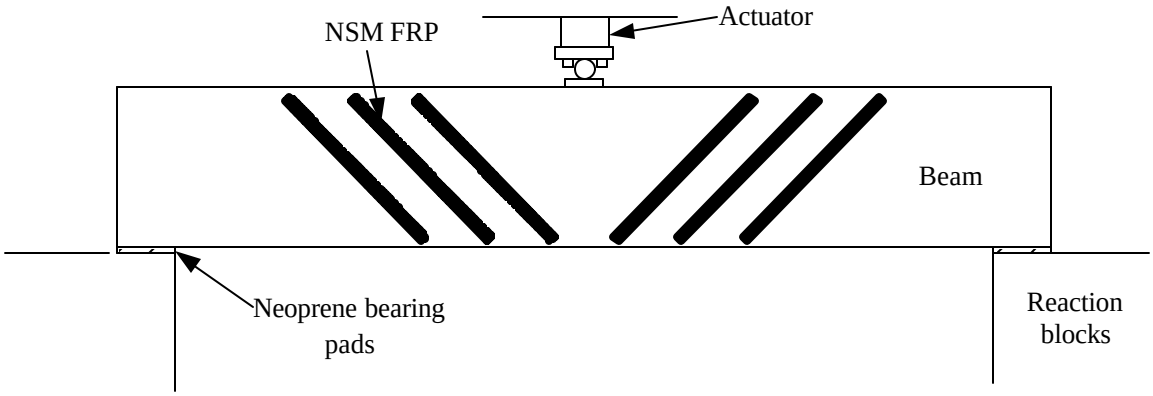

Figure 3-5 Beam Test Setup

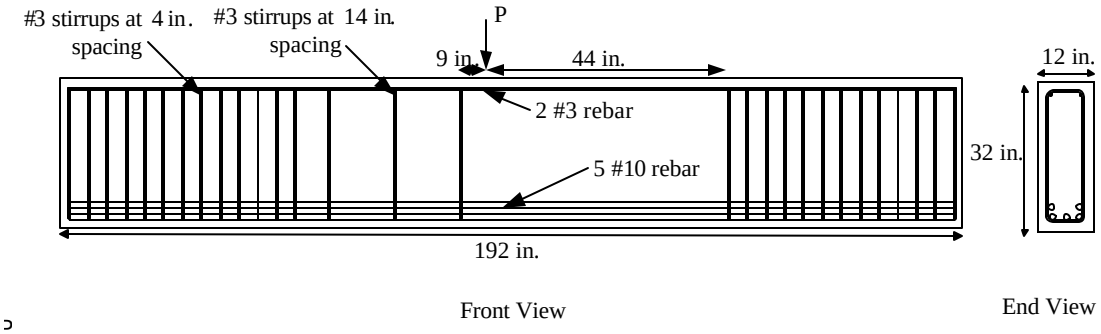

Figure 3-6 Beam Test Specimen Drawings

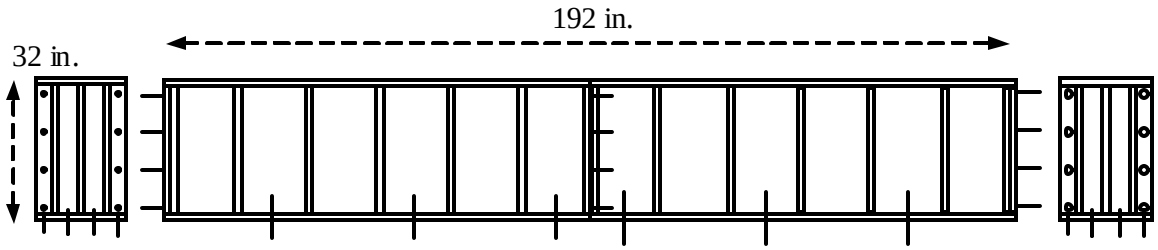

Side and End Panels

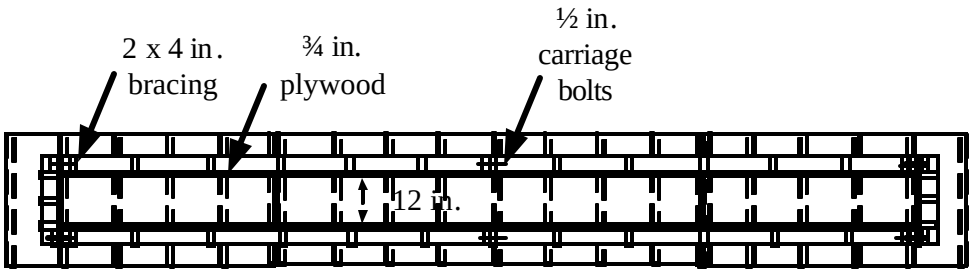

Top View

Figure 3-7 Forms for Beam Test Specimens

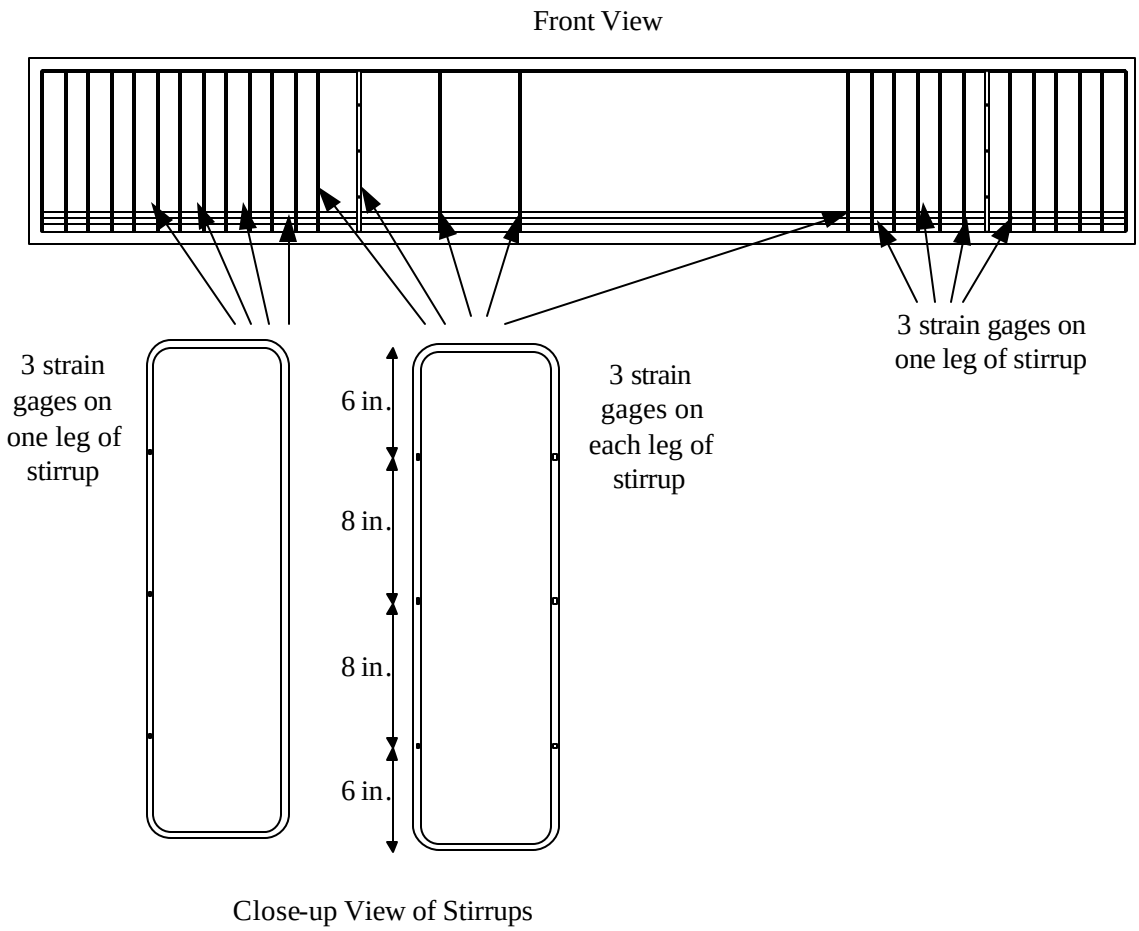

Figure 3-8 Beam Test Instrumentation

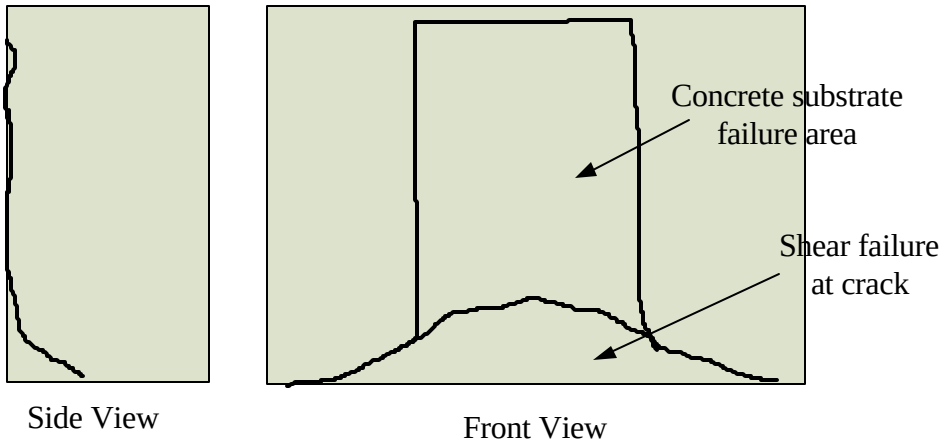

Figure 4-1 Failure Surfaces

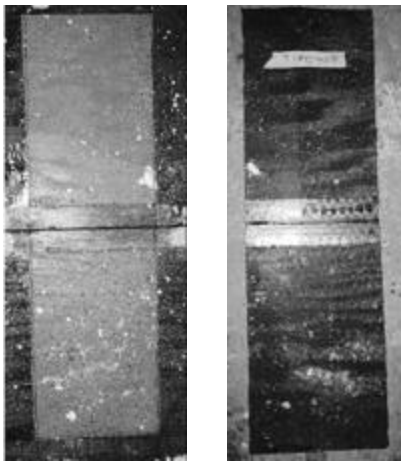

Concrete FRP

a) Specimen E4-90-1-U2

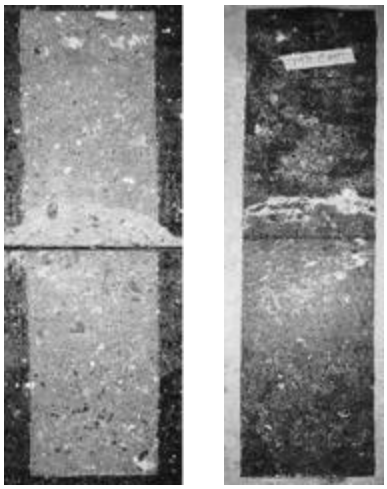

Concrete FRP

b) Specimen E6-90-1

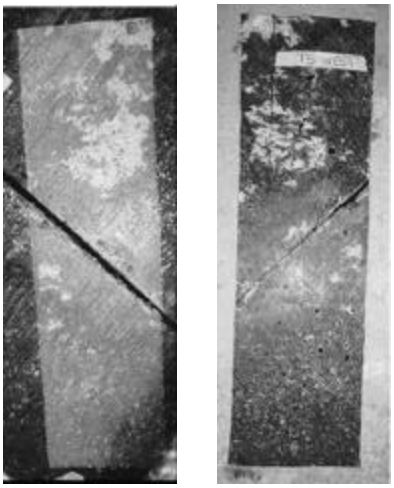

Concrete FRP

c) Specimen E7-45-1

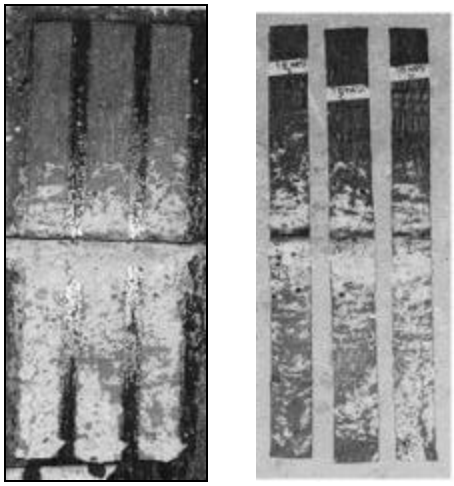

Concrete FRP

d) Specimen E10-90-3

Figure 4-2 Comparison of EB Failure Surfaces

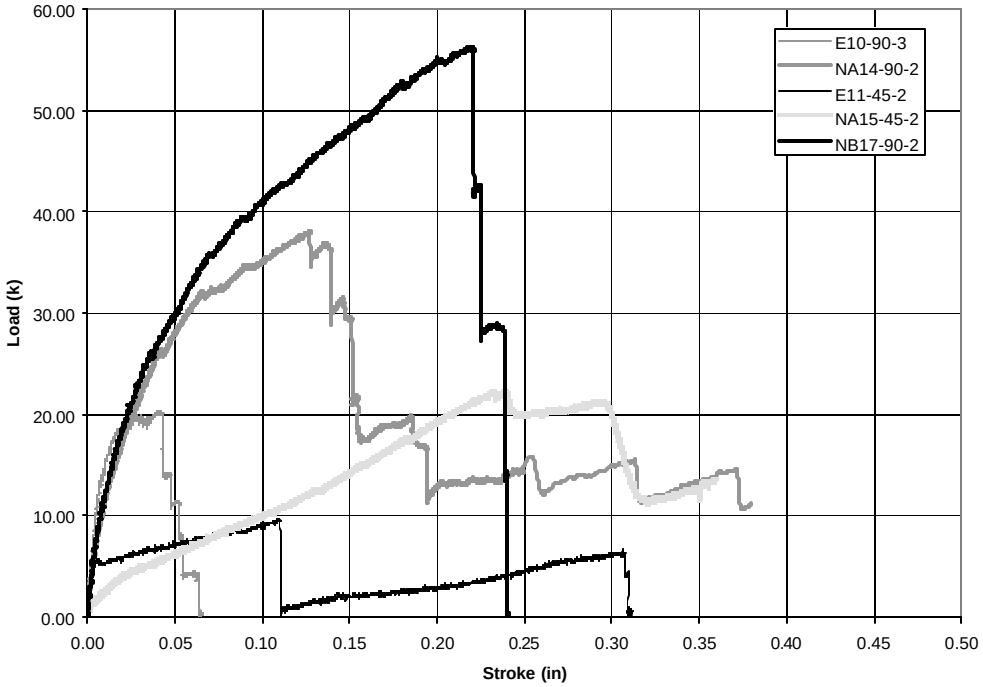

Figure 4-3 Comparison of EB and NSM FRP

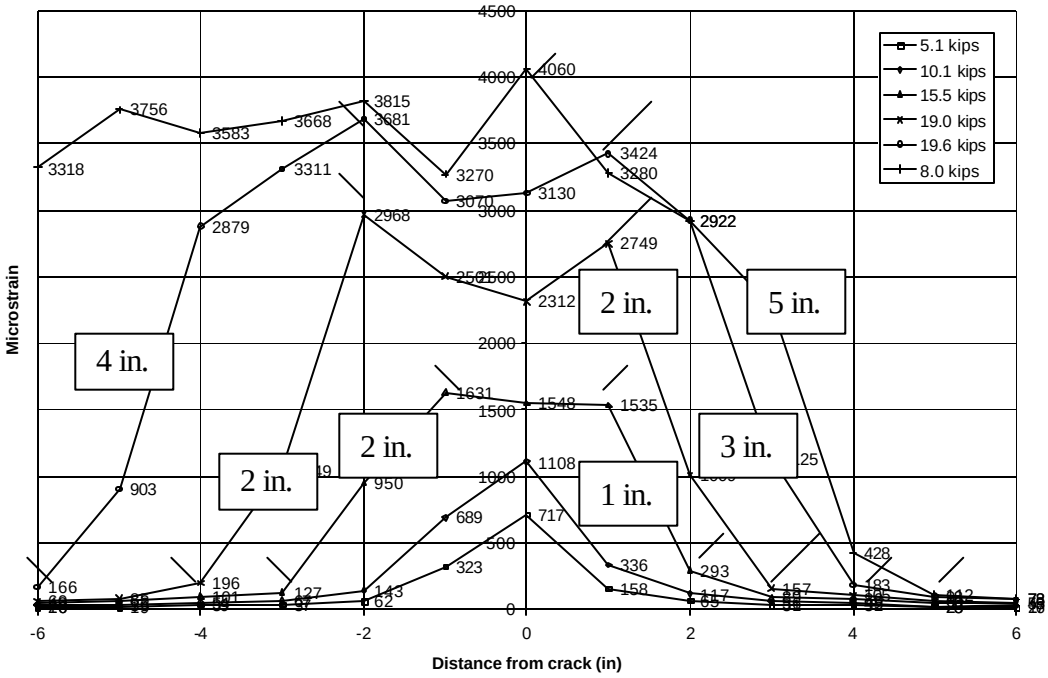

Figure 4-4 Typical Effective Bond Length Measurement

a) Tape Using Adhesive A

b) Tape Using Adhesive B

Figure 4-5 Comparison of Tapes after Failure

a) Specimen NA14-90-2

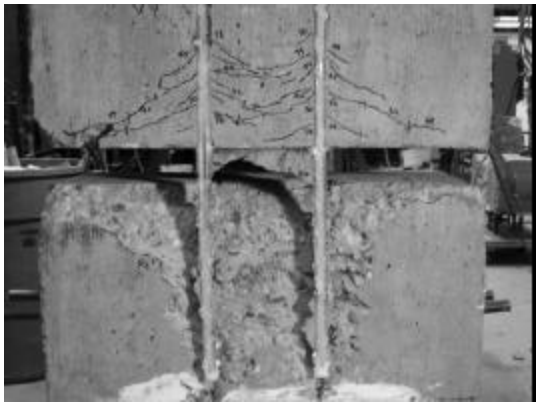

b) Specimen NB17-90-2

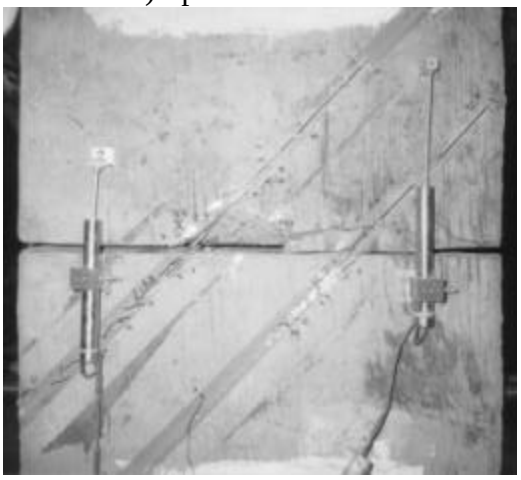

c) Specimen NA15-45-2

d) Specimen NB18-90-2V

Figure 4-6 Comparison of NSM Failure Surfaces

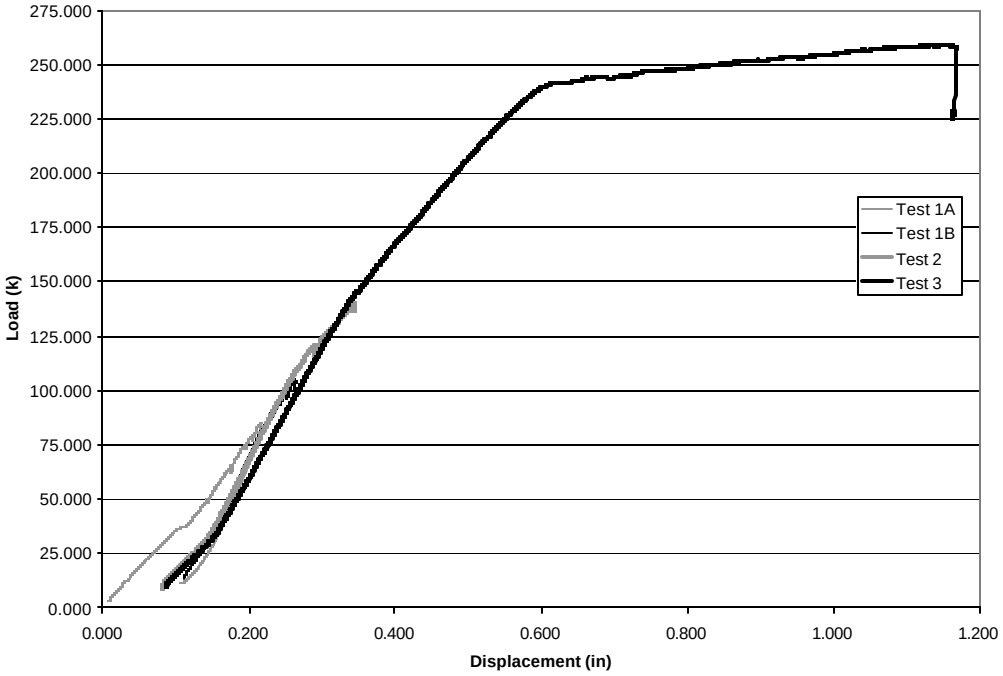

Figure 4-7 B1 Load vs. Displacement

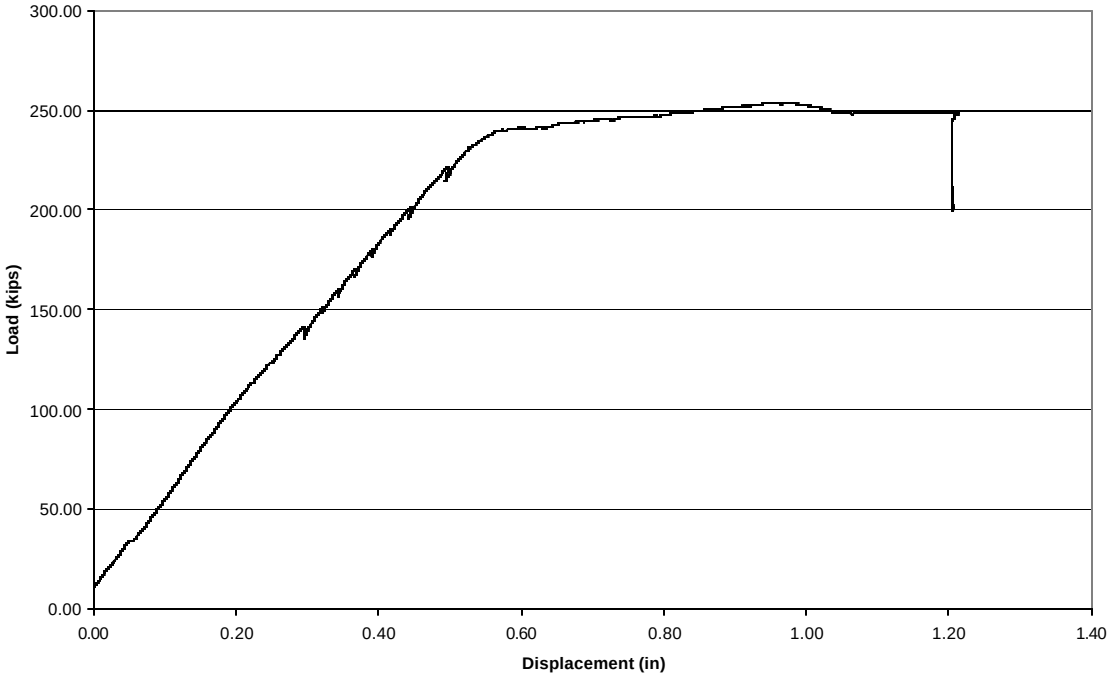

Figure 4-8 B2 Load vs. Displacement

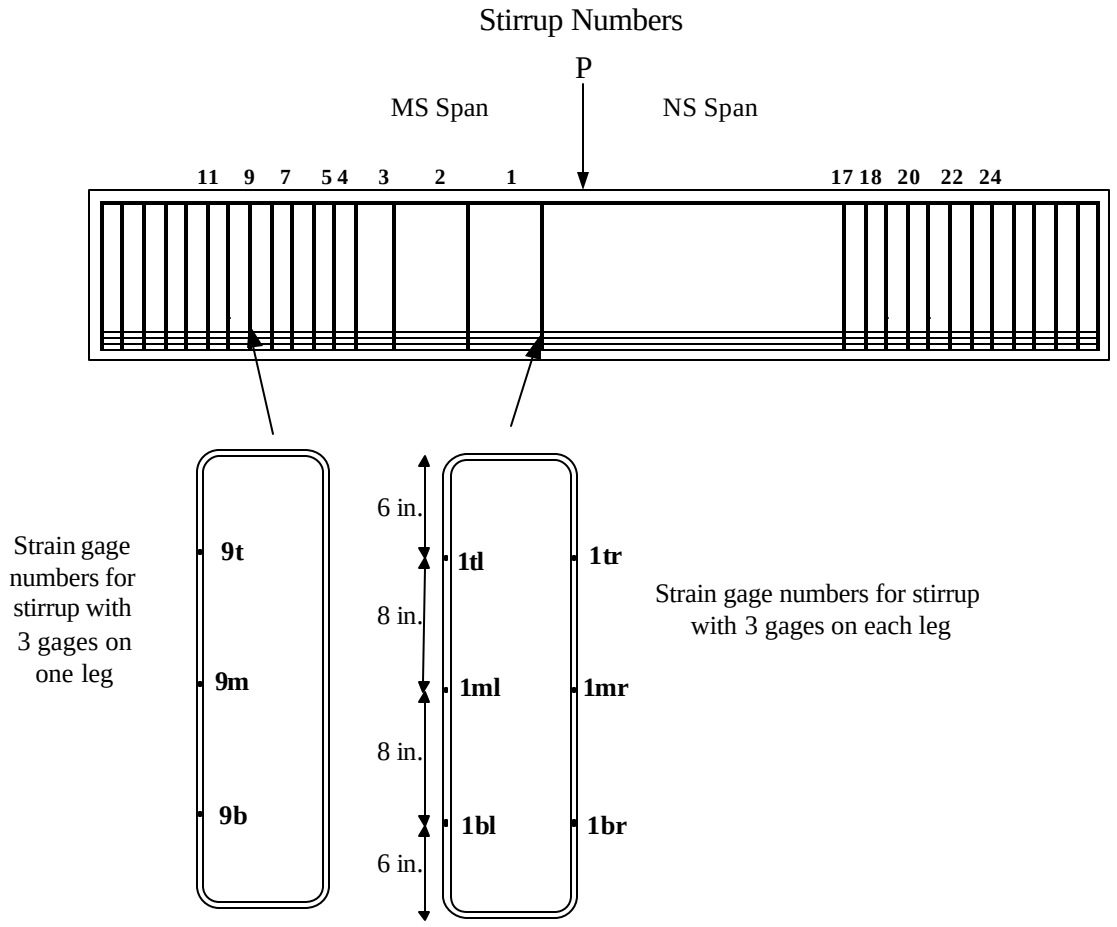

Figure 4-9 Strain Gage Locations

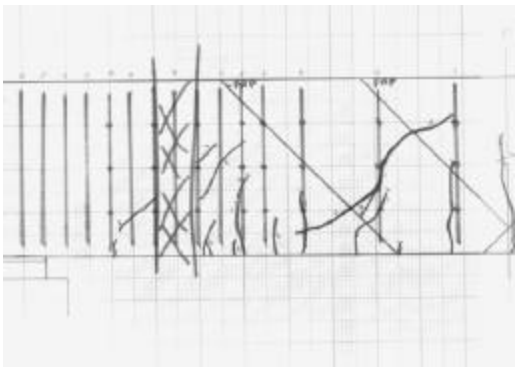

a) Northeast

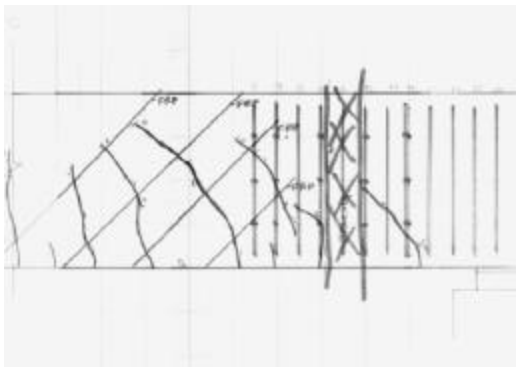

b) Northwest

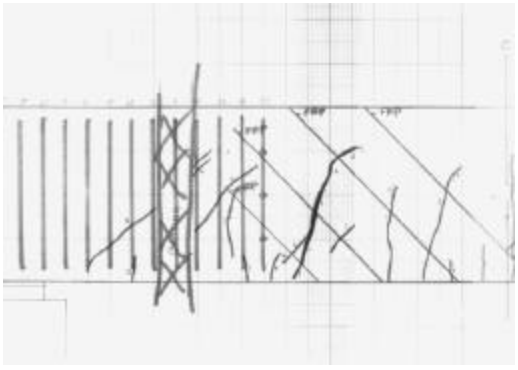

c) Southwest

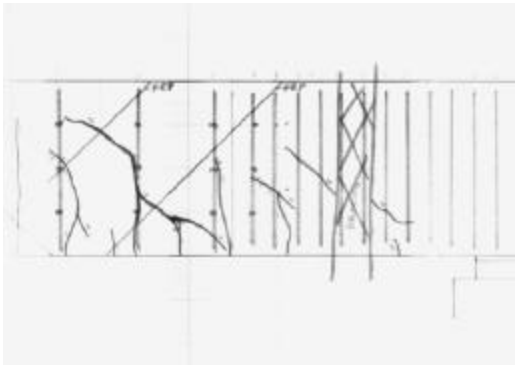

d) Southeast

Figure 4-10 B1 Crack Diagrams at 140 kips

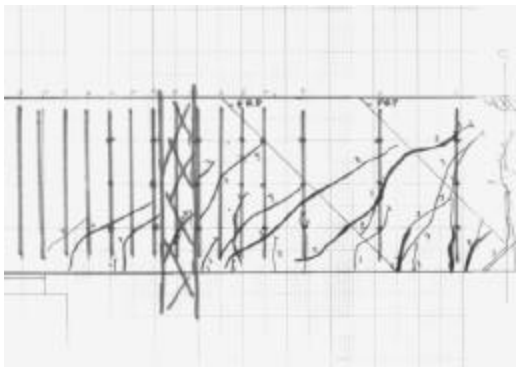

a) Northeast

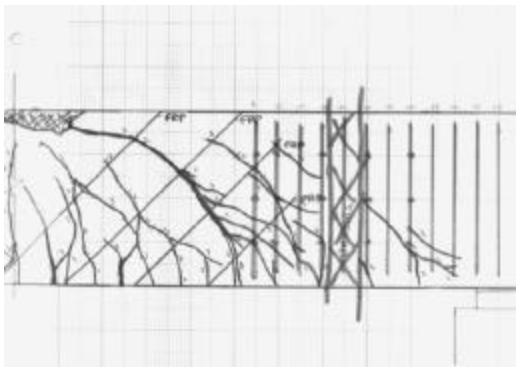

b) Northwest

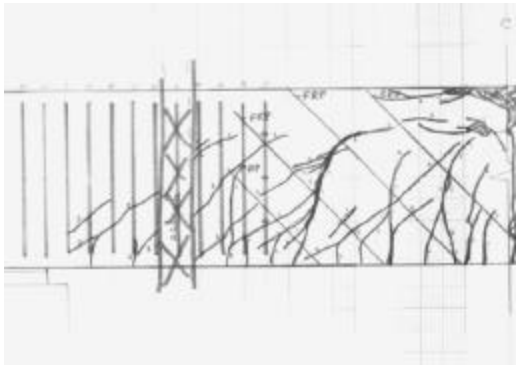

c) Southwest

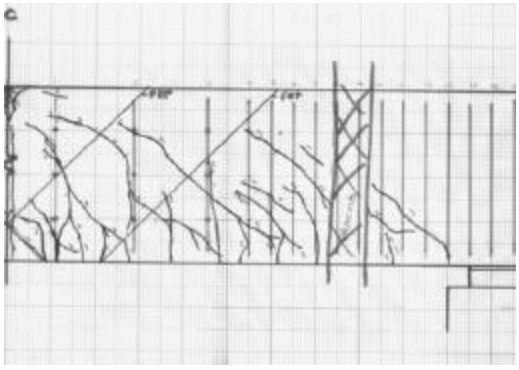

d) Southeast

Figure 4-11 B1 Crack Diagrams at 259 kips

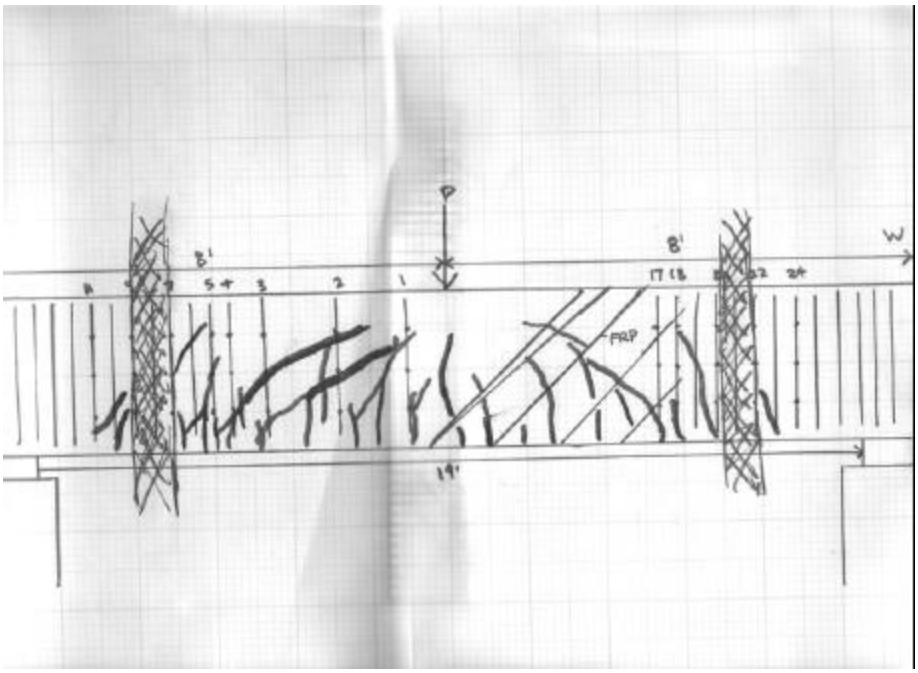

a) North

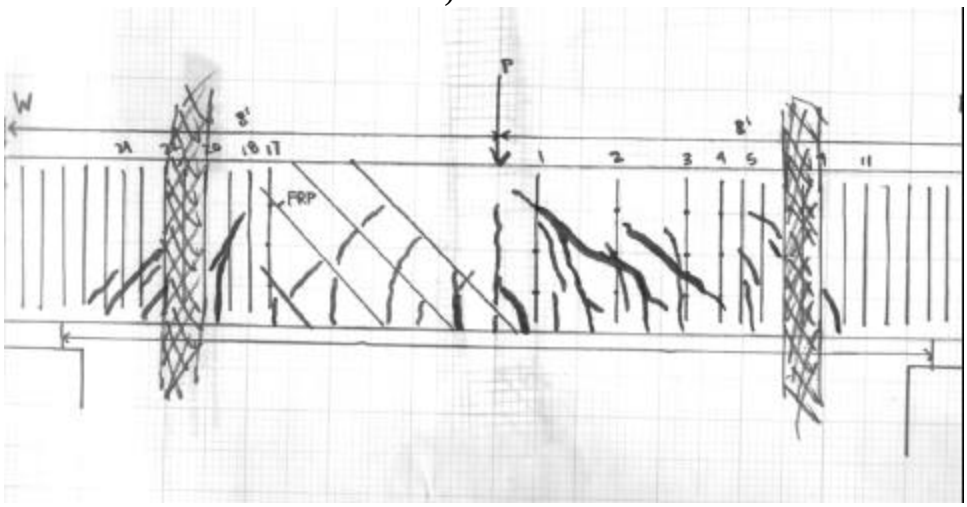

b) South

Figure 4-12 B2 Crack Diagrams at 140 kips

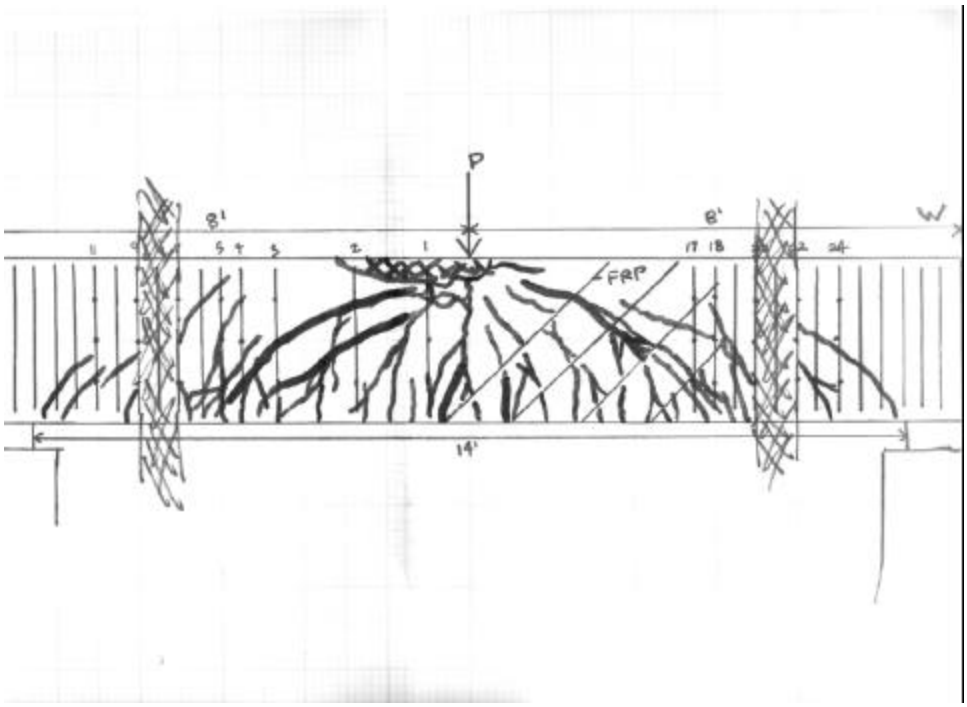

a) North

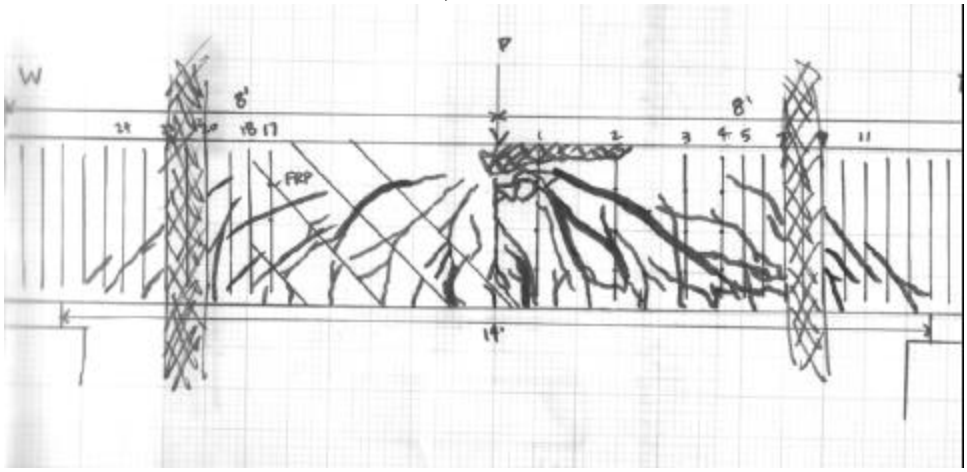

b) South

Figure 4-13 B2 Crack Diagrams at 255 kips

a) South

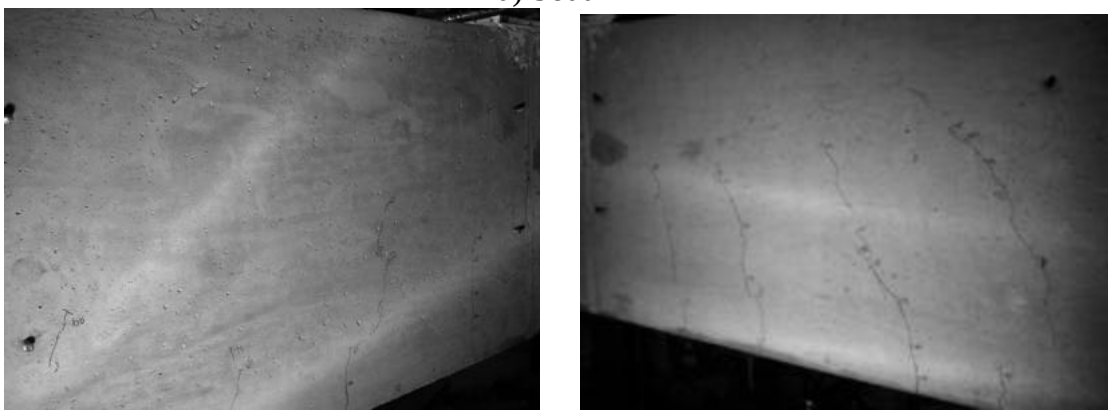

b) North

Figure 4-14 B1 at 105 kips (End of Test 1)

a) South

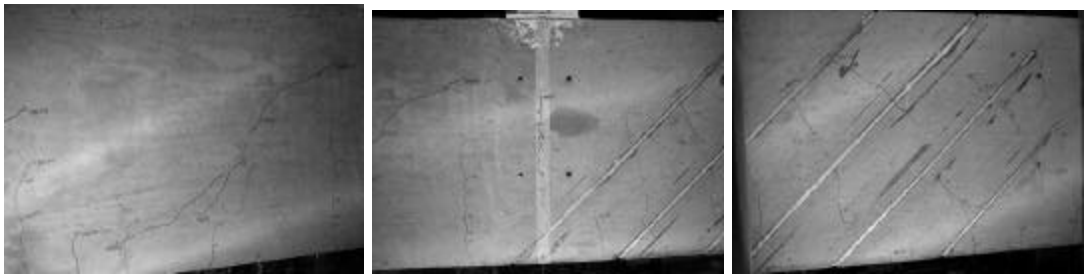

b) North

Figure 4-15 B1 at 140 kips (End of Test 2)

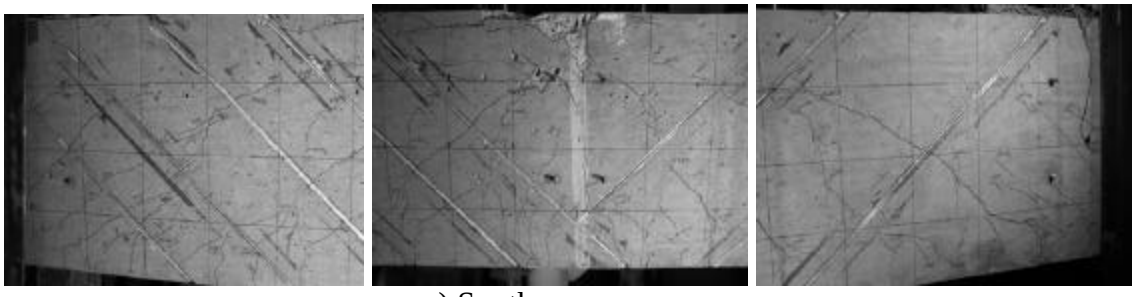

a) South

b) North

Figure 4-16 B1 at 259 kips (End of Test 3)

a) South

b) North

Figure 4-17 B2 at 140 kips

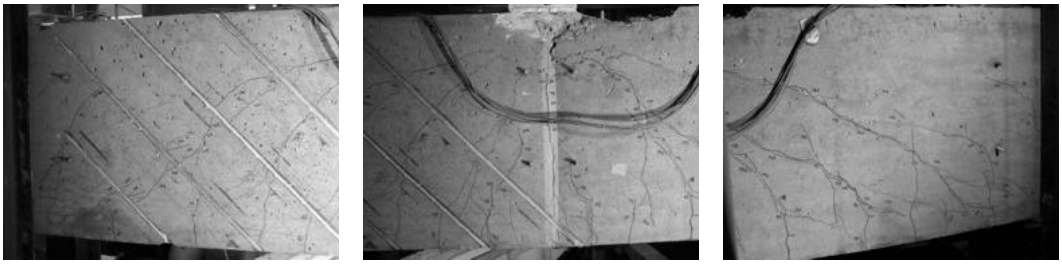

a) South

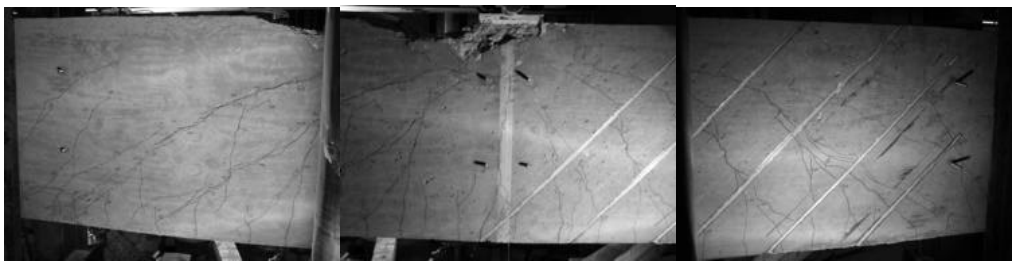

b) North

Figure 4-18 B2 at 255 kips (End of Test 4)

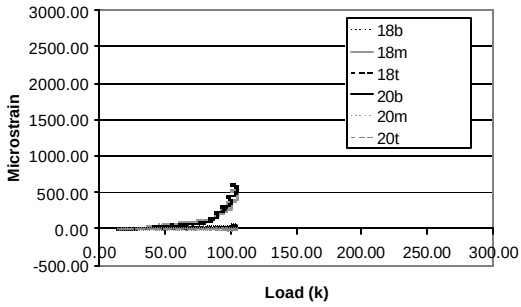

a) Stirrup 18 and 20 gages Test 1B

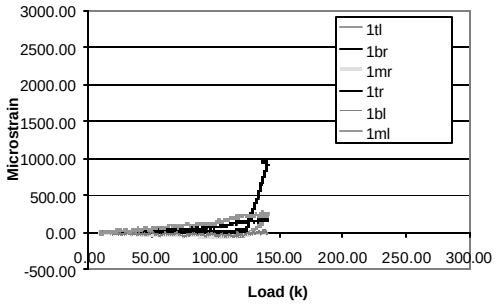

b) Stirrup 1 gages Test 2

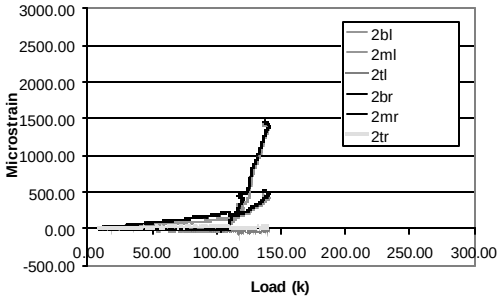

c) Stirrup 2 gages Test 2

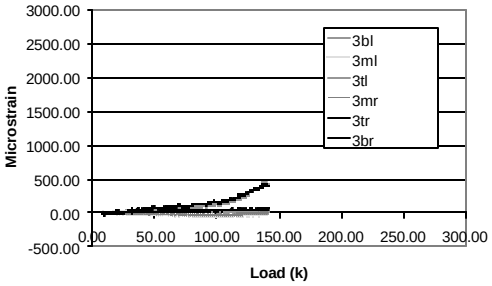

d) Stirrup 3 gages Test 2

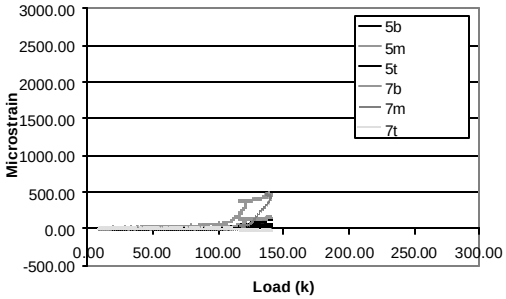

e) Stirrup 6 and 7 gages Test 2

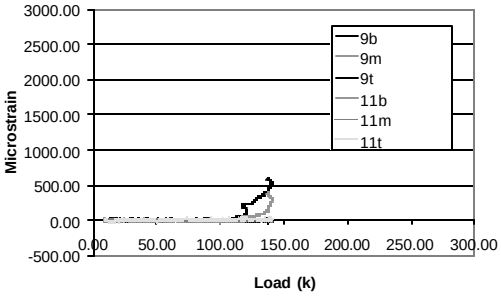

f) Stirrup 9 and 11 gages Test 2

Figure 4-19 B1 Strain Plots

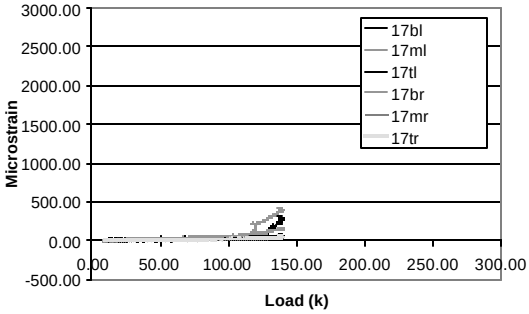

g) Stirrup 17 gages Test 2

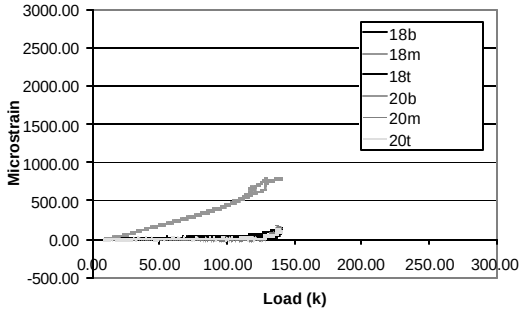

h) Stirrup 18 and 20 gages Test 2

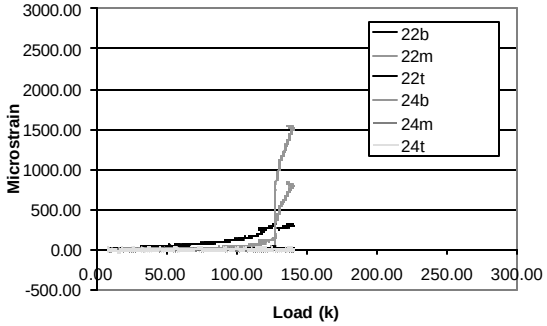

i) Stirrup 22 and 24 gages Test 2

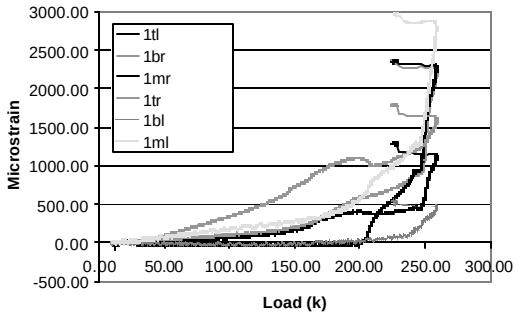

j) Stirrup 1 gages Test 3

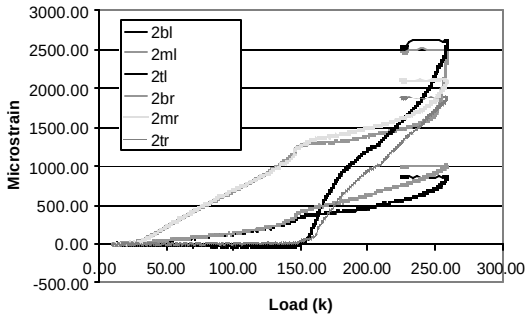

k) Stirrup 2 gages Test 3

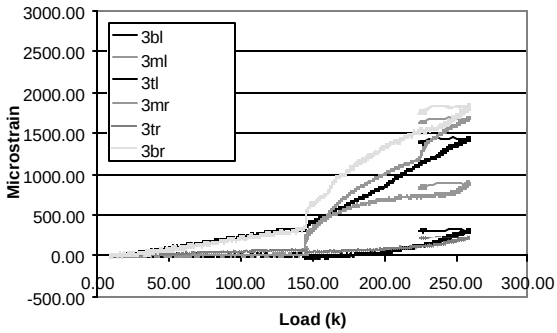

l) Stirrup 3 gages Test 3

Figure 4-19 B1 Strain Plots cont.

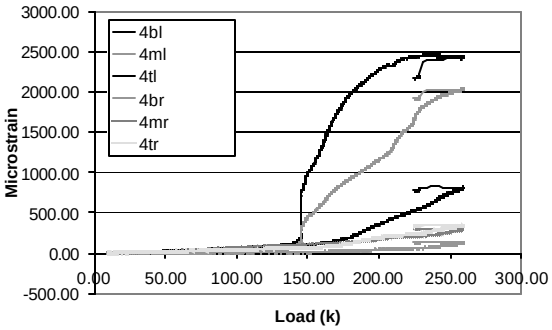

m) Stirrup 4 gages Test 3

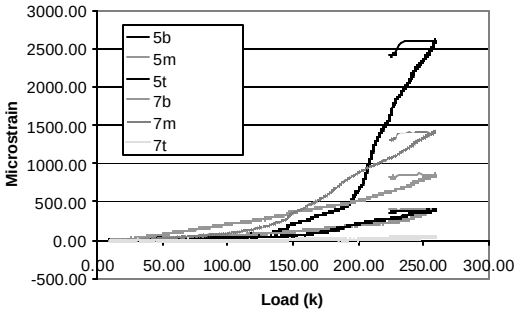

n) Stirrup 5 and 7 gages Test 3

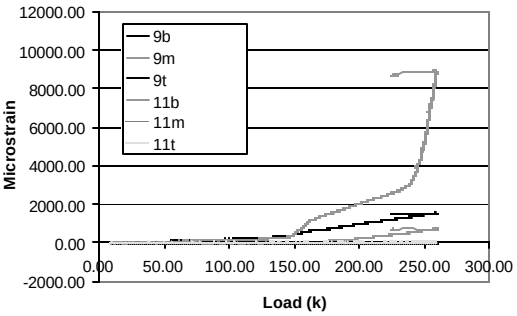

o) Stirrup 9 and 11 gages Test 3

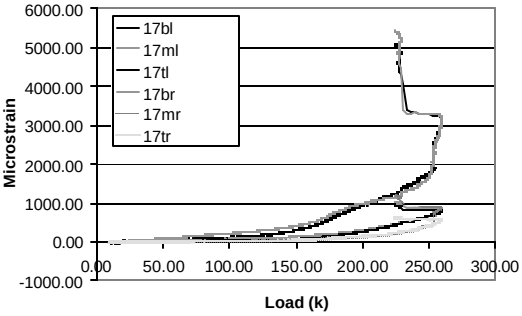

p) Stirrup 17 gages Test 3

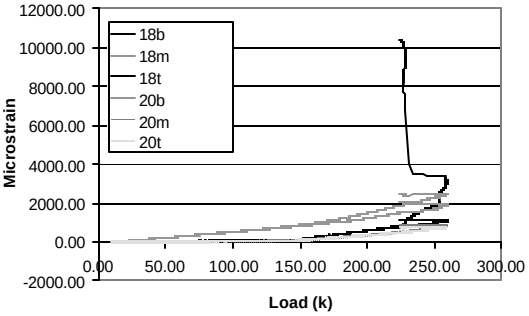

q) Stirrup 18 and 20 gages Test 3

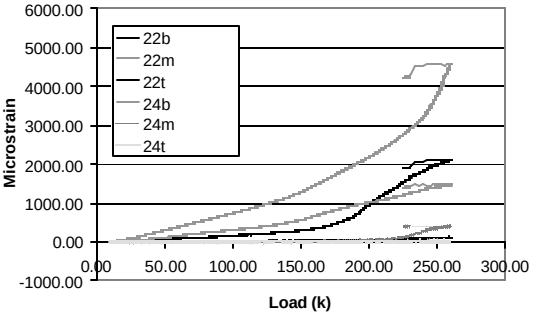

r) Stirrup 22 and 24 gages Test 3

Figure 4-19 B1 Strain Plots cont.

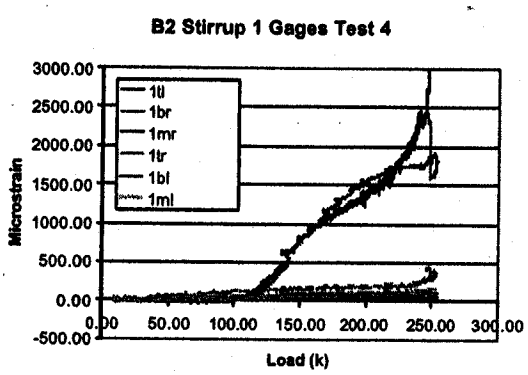

a) Stirrup 1 gages Test 4

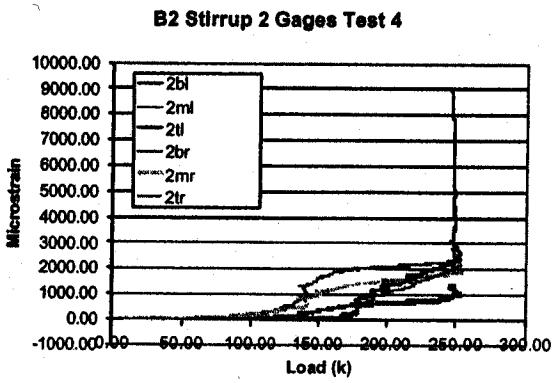

b) Stirrup 2 gages Test 4

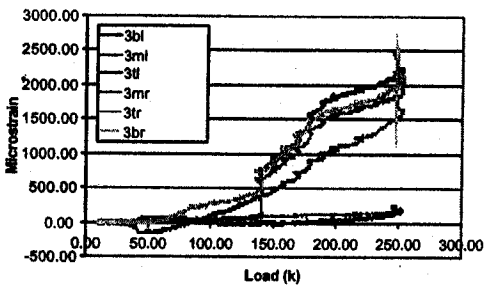

c) Stirrup 3 gages Test 4

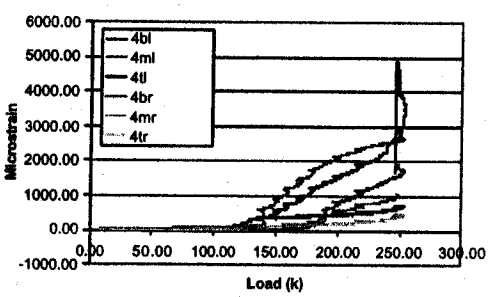

d) Stirrup 4 gages Test 4

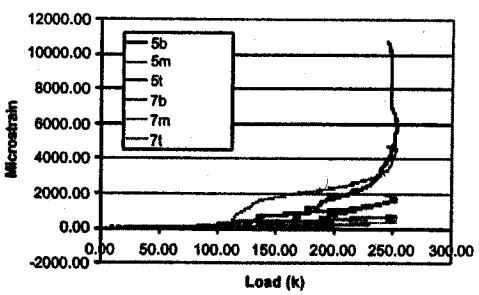

e) Stirrup 5 and 7 gages Test 4

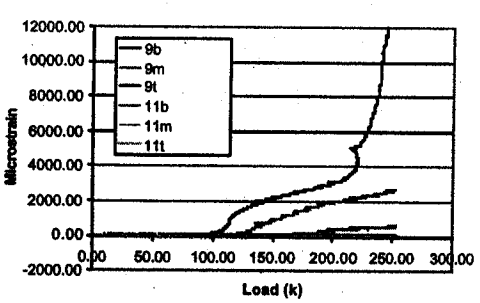

f) Stirrup 9 and 11 gages Test 4

Figure 4-20 B2 Strain Plots

Appendix A Sample Calculations for Ultimate Capacity

Shallow Beam Flexure (ACI 318-02, 1998 AASHTO, ACI 318-83, 1977 AASHTO)

The predicted ultimate capacity is calculated as follows if the longitudinal steel in the compression area of the cap is included and additional skin steel is excluded. The nominal moment capacity is calculated assuming the tensile steel yields and compression steel does not yield. This must be verified later. Similar triangles can be used on the strain diagram to find the strains in reinforcement in terms of the ultimate compressive concrete strain.

$$e'_s = e_{cu}(\frac{x-d'}{x}) \tag{A-1}$$

$$e_s = e_{cu}(\frac{d-x}{x}) \tag{A-2}$$

By assuming that the steel behaves linear-elastically until yielding occurs, the stress in the compression steel can be determined by using Hooke's Law.

$$f'_s = E_s e'_s \tag{A-3}$$

The steel is assumed to behave as a perfect plastic after yielding allowing the tensile steel strength to be calculate as:

$$T_s = A_s f_y \tag{A-4}$$

The strength of the compression steel is calculated as:

$$C_s = A'_s f'_s \tag{A-5}$$

The compressive strength of the concrete is determined using the Whitney stress block and expressed as the following:

$$C_c = 0.85 f'_c (xbb - A'_s) \tag{A-6}$$

To preserve internal moment equilibrium, the following relationship must be upheld:

$$T_s = C_c + C_s \tag{A-7}$$

Substituting equations (A-4), (A-5) and (A-6) into (A-7) produces the following expression that can be solved for the distance from the extreme compression face to the neutral axis.

$$A_s f_y = 0.85 f'_c (xbb - A'_s) + A'_s Ee_{cu}(\frac{x-d'}{x}) \tag{A-8}$$

$$(18in^2)(60ksi) = 0.85(4.8ksi)((.85*42"*x - 4in^2) + (4in^2)(29000)(0.003)\frac{(x-3")}{x}$$

x=6.99"

The assumption that the tensile steel yields and the compressive steel does not yield must now be checked to assure a proper design.

$$e'_s = 0.003\frac{(6.99"-3")}{6.99"} = 0.00171 \le 0.0022 = e_y$$

$$e_s = 0.003(\frac{55.5"-6.99"}{6.99"}) = 0.0208 \ge 0.0022 = e_y$$

The nominal moment capacity can be calculated by determining the moment associated with the internal resisting forces.

$$M_n = C_c(d - \frac{xb}{2}) + C_s(d - d') \tag{A-9}$$

$$M_n = .85(4.8ksi)(6.99"*0.85*42" - 4in^2)(55.5" - \frac{6.99"(0.85)}{2}) + (4in^2)(29000ksi)(0.00171)*(55.5" - 3")$$

$$M_n = 63{,}039k" = 5253k'$$

The nominal load capacity of a pier cap overhang with a point load applied at a distance from the face of the column support can be calculated using the following relationship.

$$P_n = \frac{M_n}{a} \tag{A-10}$$

$$P_n = \frac{5253kft}{4\,ft} = 1313kips$$

The maximum and minimum constraints on reinforcing steel according to the ACI 318-83, 1977 AASHTO and 1998 AASHTO LRFD specifications are as follows.

$$r = \frac{A_s}{bd} \tag{A-11}$$

$$r = \frac{18in^2}{42"(55.5")} = 0.00772$$

$$r_{\min} = \max(\frac{3\sqrt{f'_c}}{f_y}, \frac{200}{f_y}) \tag{A-12}$$

$$r_{\min} = \max(\frac{3\sqrt{4000ksi}}{60000ksi}, \frac{200}{60ksi}) = 0.00333$$

$$r_{\max} = 0.75\,r_{bal} = 0.75\frac{0.85\,f'_c\,b_1}{f_y}\frac{87{,}000}{87{,}000 + f_y} \tag{A-13}$$

$$r_{bal} = \frac{0.85(4000\,psi)(0.85)}{60{,}000\,psi}\frac{87{,}000}{87{,}000 + 60{,}000\,psi} = 0.02851$$

$$r_{\max} = 0.75(0.02851) = 0.02138$$

$$r_{\min} \le r \le r_{\max} \tag{A-14}$$

$$r_{\min} = 0.00333 \le r = 0.00772 \le r_{\max} = 0.02138$$

The ACI 318-02 specification uses the same limit on minimum reinforcing steel as above. The maximum limit on reinforcing steel is regulated by making the resistance factor dependent on ductility. A resistance factor of 0.9 may only be used if the strain in the longitudinal tension steel is greater than 0.5% at failure. This is determined as follows.

$$e_s = e_{cu}(\frac{d-x}{x}) > 0.005 \quad \text{(A-15)}$$

$$e_s = 0.003(\frac{55.5in - 7.32in}{7.32in}) = 0.020 > 0.005$$

use $f = 0.9$

If the longitudinal steel in compression is neglected, the equations above can be used by simply setting A'$_s$ equal to zero. This results in the following expression for the nominal load capacity of a pier cap overhang in flexure.

$$P_n = \frac{0.85 f'_c \, bxb(d - \frac{xb}{2})}{a} \quad \text{(A-16)}$$

$$(18in^2)(60ksi) = 0.85(4.8ksi)(0.85)(42in)x$$

$$x = 7.41in$$

$$P_n = \frac{0.85 * 4.8ksi * 0.85 * 7.41in * 42in(55.5in - \frac{7.41in * 0.85}{2})}{48in} = 1177kips$$

Multiplying the nominal capacity by the appropriate resistance factor yields the design capacity. If the longitudinal compression steel is included in calculations the design capacity is.

$$fP_n = 0.9(1313kips) = 1182kips$$

If the longitudinal compression steel is excluded the design capacity is.

$$fP_n = 0.9(1177kips) = 1059kips$$

Shallow Beam Shear Design (ACI318-02, ACI 318-83, 1977 AASHTO)

The pier cap overhang has a point load located within one effective depth from the face of the column. Accordingly, the cross section of the overhang at the face of the column is used in designing the pier cap for shear. The shear resistance component due to concrete can be calculated using ACI318-02 Eqn (11-3) as follows.

$$V_c = 2\sqrt{f'_c} b_w d \quad \text{(A-17)}$$

$$V_c = 2\sqrt{4800psi}(42in)(55.5in) = 323kips$$

In lieu of using Eqn (11-3), the shear resistance component due to concrete can also be calculated using ACI 318-02 Eqn (11-5) as follows.

$$V_c = (1.9\sqrt{f'_c} + 2500 r_w \frac{V_u d}{M_u}) b_w d \le 3.5\sqrt{f'_c} b_w d \quad \text{where:} \quad \frac{V_u d}{M_u} \le 1 \quad \text{(A-18)}$$

$$\frac{V_u d}{M_u} \le 1 \Rightarrow \frac{(52.1 * P)}{24P} = 2.17$$

$$V_c = (1.9\sqrt{4800\,psi} + 2500(0.0082)(1))(42in)(55.5in) = 355kips \le 3.5\sqrt{4800\,psi}(42in)(55.5in) = 565kips$$

The shear resistance component due to transverse reinforcement can be computed using the ACI 318-02 Eqn (11-15).

$$V_s = \frac{A_s f_y d}{s} \le 8\sqrt{f'_c} b_w d \qquad \text{(A-19)}$$

$$V_s = \frac{4(0.44in^2)(60ksi)(55.5in)}{6in} = 977kips \le 8\sqrt{4000psi}(42in)(55.5in) = 1179kips$$

The total shear capacity is the sum of the individual resistances and is calculated as follows:

$$V_n = V_c + V_s \qquad \text{(A-20)}$$

$V_n = 323k + 977k = 1300kips$ Using ACI 318-02 Eqn (11-3)

$V_n = 355k + 977k = 1332kips$ Using ACI 318-02 Eqn (11-5)

The transverse reinforcement stirrups must not be spaced in excess of the following limits.

$$\text{If } V_s \le 4\sqrt{f'_c} bd, \text{ then } s \le \min(\frac{d}{2}, 24in) \qquad \text{(A-21)}$$

$$\text{If } 4\sqrt{f'_c} bd \le V_s \le 8\sqrt{f'_c} bd, \text{ then } s \le \min(\frac{d}{4}, 12in) \qquad \text{(A-22)}$$

$$\text{Since } 4\sqrt{f'_c} bd \le V_s \le 8\sqrt{f'_c} bd, \; s \le \min(\frac{55.5in}{4}, 12in) = 12in$$

The design load capacity is equal to the design shear capacity and is calculated as follows for the ACI318-83 and 1977 AASHTO specifications.

$fP_n = 0.85(1300kips) = 1105kips$ Using ACI 318-02 Eqn (11-3)

$fP_n = 0.85(1332kips) = 1132kips$ Using ACI 318-02 Eqn (11-5)

For the ACI 318-02 the design load capacity is calculated as follows.

$fP_n = 0.75(1300kips) = 975kips$ Using ACI 318-02 Eqn (11-3)

$fP_n = 0.75(1332kips) = 999kips$ Using ACI 318-02 Eqn (11-5)

Modified Compression Field Shear Design (1998 AASHTO LRFD)

Due to the presence of a point load near the face of the column, the pier cap overhangs are designed for shear at the face of the column. The effective shear depth is the distance between the resultant tensile and compressive forces in a cross section and is found using the following equations derived from 1998 AASHTO LRFD Article 5.8.2.7.

$$d_v = h - d' - \frac{xb}{2} \qquad \text{(A-23)}$$

$$d_v \ge \max(0.9d, 0.72h) \qquad \text{(A-24)}$$

$$d_v = 60" - 4.5" - \frac{7.32"}{2} = 51.8"$$

$$d_v \ge \max(0.9(55.5in), 0.72(60in)) = 50.0in$$

The nominal shear resistance can be found using AASHTO Eqns (5.8.3.3-1,2,3&4).

$$V_n = V_c + V_s \le 0.25 f'_c bd_v \qquad \text{(A-25)}$$

for which:

$$V_c = 0.0316 b \sqrt{f'_c} b d_v \quad \text{(A-26)}$$

$$V_s = \frac{A_v f_y d_v (\cot q + \cot a) \sin a}{s} \quad \text{(A-27)}$$

AASHTO Eqns (5.8.2.5-1) and (5.8.3.5-1) must be followed to assure that a minimum amount of longitudinal and transverse reinforcing steel is included in design.

$$A_v \geq 0.0316 \sqrt{f'c} \frac{b_v s}{f_y} \quad \text{(A-28)}$$

$$A_v = 1.76 in^2 \geq 0.0316 \sqrt{4 ksi} \frac{42"(6")}{60 ksi} = 0.265 in^2$$

$$A_s f_y \geq \left[\frac{M_u}{d_v f_f} + \left(\frac{V_u}{f_s} - 0.5 V_s \right) \cot q \right] \quad \text{(A-29)}$$

$$A_s f_y = 18 in^2 (60 ksi) = 1080 kips \geq \left[\frac{22{,}080 k"}{51.8"(0.9)} + \left(\frac{920 kips}{0.9} - 0.5(1166.9 kips) \right) \cot 38° \right] = 1035.2 kips$$

The values of θ and β in the equations above are determined from Figure 5.8.3.4.2-1 in the 1998 AASHTO LRFD specification using the following variables:

$$v = \frac{V_u}{f b d_v} \quad \text{(A-30)}$$

$$v = \frac{920 kips}{0.9(42")(51.8")} = 0.470$$

$$e_x = \frac{\frac{M_u}{d_v} + 0.5 V_u \cot q}{E_s A_s} \quad \text{(A-31)}$$

$$e_x = \frac{\frac{22{,}080 k"}{51.84"} + 0.5(920 kips) \cot(40°)}{29{,}000 ksi (1.76 in^2)} = 0.0197$$

Because θ is present in both the input and output from the graphs, iterations must be performed until a stable value is obtained.

The values of β and θ can then be substituted into equations (A-25), (A-26), and (A-27) above to determine the nominal shear resistance of the pier cap overhang.

$$b = 0.9$$

$$q = 38.5°$$

$$V_c = 0.0316(.9) \sqrt{4.8 ksi} (42")(51.8") = 136 kips$$

$$V_s = \frac{1.76 in^2 (60 ksi)(51.8")(\cot 38°)}{6"} = 1167 kips$$

$$V_n = 136 kips + 1167 kips = 1303 kips$$

$$V_n \le 0.25 f'_c b_v d_v = 0.25(4.8ksi)(42")(51.8") = 2611kips$$

The design load capacity is equal to the design shear capacity and is calculated as follows.

$$fP_n = 0.9(1303kips) = 1173kips$$

ACI318-02 Strut and Tie Method

A pier cap overhang is considered a deep beam if either the clear span is less than four times the member depth or a point load is located within a distance of twice the effective depth from the column face. The ACI 318-02 specification allows deep beams to be designed using the strut and tie method. The entire overhang is considered to be a disturbed region. Shown below is the truss model used in design.

The angle between the compressive strut and the global horizontal axis is determined using assumed geometry and basic trigonometry.

$$q = \tan^{-1}\left(\frac{50in}{48in}\right) = 46.2°$$

The axial forces in the strut and tie (T1 and S1) can be determined by applying force equilibrium to the node. The forces in the truss members in terms of the applied load are:

$$F_{us} = \frac{P}{\sin q} \qquad \text{(A-32)}$$

$$F_{us} = \frac{P}{\sin 46.2°} = 1.39P$$

$$F_{ut} = P\cot(q) \qquad \text{(A-33)}$$

$$F_{ut} = P\cot 46.2° = 0.96P$$

The dimensions of the critical node must be determined. The node is a hydrostatic C-C-T node and is shown in Figure A.3. The top boundary of the node is equal to the width of the bearing plate through which the load is applied.

$$l_b = 20in \text{ =width of bearing pad}$$

The side boundary is determined by the effective tie width which is equal to twice the distance from the extreme tension face to the centriod of the flexural longitudinal reinforcing steel in this application.

$$h_a = 2(h-d) \qquad \text{(A-34)}$$

$$h_a = 2*(60in - 55.5in) = 9in$$

The dimensions of the slanted face can be determined using the following equation.

$$w_a = h_a \cos q + l_b \sin q \qquad \text{(A-35)}$$

$$w_a = 9in(\cos 46.2°) + 20in(\sin 46.2°) = 20.67in$$

The following relationship must be valid to use the greater value of β_s in ACI 318-02 A.3.2.2. for the bottle-shaped strut.

$$\sum \frac{A_{si}}{b_{si}} \sin g_i \geq 0.003 \tag{A-36}$$

$$\sum \frac{A_{si}}{b_{si}} \sin g_i = \frac{A_v}{bs_1} \sin(90° - q) + \frac{A_{sk}}{bs_2} \sin q \geq 0.003$$

$$\frac{1.76in^2}{42in(6in)} \sin(43.8°) + \frac{0.88in^2}{42in(12in)} \sin(46.2°) = 0.0061 \geq 0.003$$

The nominal capacity of the tensile tie (T1) is calculated using ACI 318-02 Eqn (A-6).

$$F_{nt} = A_s f_y \tag{A-37}$$

$$F_{nt} = (60ksi)(18in^2) = 1080kips$$

The nominal capacity of the compression strut (S1) is determined using ACI 318-02 Eqn (A-3).

$$F_{ns} = 0.85 b_s f'_c w_a b \tag{A-38}$$

$$F_{ns} = (0.85)(0.75)(4.8ksi)(20.7in)(42in) = 2660kips$$

The nominal capacities of the three faces of the nodal zone are calculated using ACI 318-02 Eqns (A-7&8).

$$F_{nl} = 0.85 b_n f'_c l_b b \tag{A-39}$$

$$F_{nl} = 0.85(0.8)(4.8ksi)(20in)(42in) = 2742kips$$

$$F_{nh} = 0.85 b_n f'_c h_a b \tag{A-40}$$

$$F_{nh} = 0.85(0.8)(4.8ksi)(9in)(42in) = 1234kips$$

$$F_{nw} = 0.85 b_n f'_c w_a b \tag{A-41}$$

$$F_{nw} = 0.85(0.8)(4.8ksi)(20in)(42in) = 2742kips$$

The maximum load that can be placed on each component is determined by setting the nominal capacity of the component multiplied by the appropriate resistance factor equal to the force in the component. The smallest maximum load controls the design and is the design load capacity.

For the tension tie:

$$fF_{nt} = F_{ut}$$

$$P = \frac{0.75(1080kips)}{0.96} = 844kips$$

For the compression strut:

$$fF_{ns} = F_{us}$$

$$P = \frac{0.75(2660kips)}{1.39} = 1435kips$$

For the top surface of the node:

$$fF_{nl} = P$$

$$P = 0.75(2742kips) = 2057kips$$

For the side surface of the node:

$$fF_{nh} = F_{ut}$$

$$P = \frac{0.75(1234kips)}{0.96} = 964kips$$

For the slanted surface of the node:

$$fF_{nw} = F_{us}$$

$$P = \frac{0.75(2742kips)}{1.39} = 1478kips$$

The nominal load capacity of the pier cap overhang is 844 kips and is controlled by failure of the tie.

1998 AASHTO LRFD Strut and Tie Design

A pier cap is considered to be a deep beam according to the 1998 AASHTO LRFD if the distance from the point of zero moment to the face of the support is less that twice the effective depth or if a load causing more than half of the shear at the face of the support is within twice the effective depth from the face of the support. The truss model and components of loads in the strut and tie are identical to those calculated above for the ACI 318-02 strut and tie method. The method for proportioning the node is also identical except that the effective tie width is taken to be the distance from the extreme face to six times the bar diameter past the innermost longitudinal bar.

$l_b = 20in$ =width of bearing pad

$$h_a = 6in + 6(1.128in) = 12.75in$$

$$w_a = 12.75in(\cos 46.2°) + 20in(\sin 46.2°) = 23.3in$$

The minimum requirement for crack control reinforcement in both the longitudinal and transverse directions is as follows. Maximum bar spacing must be less than 12in.

$$\frac{A_v}{A_c} \geq 0.003 \qquad \text{(A-42)}$$

$$\frac{4(0.44in^2)}{42in(60in)} = 0.00087 \leq 0.003$$

$$\frac{A_{sk}}{A_c} \geq 0.003 \qquad \text{(A-43)}$$

$$\frac{0.88in^2(5)}{42in(60in)} = 0.0017 \leq 0.003$$

The nominal capacity of a tension tie is calculated as:

$$F_{nt} = A_s f_y \qquad \text{(A-44)}$$

$$F_{nt} = (60ksi)(18in^2) = 1080kips$$

The nominal capacity of a compression strut is calculated as:

$$F_{ns} = f_{cu} w_a b \tag{A-45}$$

where:

$$f_{cu} = \frac{f'_c}{0.8 + 170 e_1} \le 0.85 f'_c \tag{A-46}$$

$$e_1 = (e_s + 0.002) \cot^2 a_s \tag{A-47}$$

$$e_s = \frac{0.96P}{EA} = \frac{0.96P}{29000ksi(18in^2)} = 1.83x10^{-6}$$

$$e_1 = (1.83x10^{-6} + 0.002) \cot^2 (46.2°) = 0.0018$$

$$f_{cu} = \frac{4.8ksi}{0.8 + 170(0.0018)} = 4.34ksi \le 0.85(4ksi) = 3.4ksi$$

$$F_{ns} = 3.4ksi(23.3in)(42in) = 3327kips$$

The nominal capacity of each face of a nodal region anchoring one tension tie can be calculated as:

$$F_{nl} = 0.75 f'_c l_b b \tag{A-48}$$

$$F_{nl} = 0.75(4.8ksi)(20in)(42in) = 3024kips$$

$$F_{nh} = 0.75 f'_c h_a b \tag{A-49}$$

$$F_{nh} = 0.75(4.8ksi)(12.75in)(42in) = 1928kips$$

$$F_{nw} = 0.75 f'_c w_a b \tag{A-50}$$

$$F_{nw} = 0.75(4.8ksi)(23.3in)(42in) = 3523kips$$

The design load capacity of the pier cap overhang is determined with the same method as for ACI318-02 strut and tie design as shown above.

For the tie:

$$fF_{nt} = F_{ut}$$

$$P = \frac{1.0(1080kips)}{0.96} = 1125kips$$

For the Strut:

$$fF_{ns} = F_{us}$$

$$P = \frac{0.70(3327kips)}{1.39} = 1675kips$$

For the top surface of the node:

$$fF_{nl} = P$$

$$P = 0.7(3024kips) = 2117kips$$

For the side surface of the node:

$$fF_{nh} = F_{ut}$$

$$P = \frac{0.7(1928kips)}{0.96} = 1406kips$$

For the slanted surface of the node:

$$fF_{nw} = F_{us}$$

$$P = \frac{0.7(3523kips)}{1.39} = 1774kips$$

The design load capacity of the pier cap overhang is 1125 kips and is controlled by failure of the tension tie.

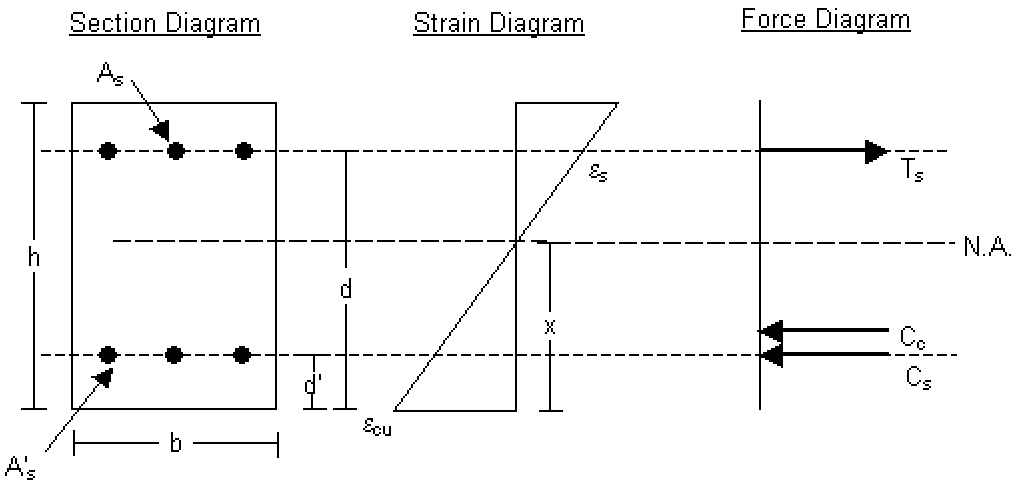

Figure A.1 Diagram of pier cap overhang cross-section including strains and internal forces at ultimate.

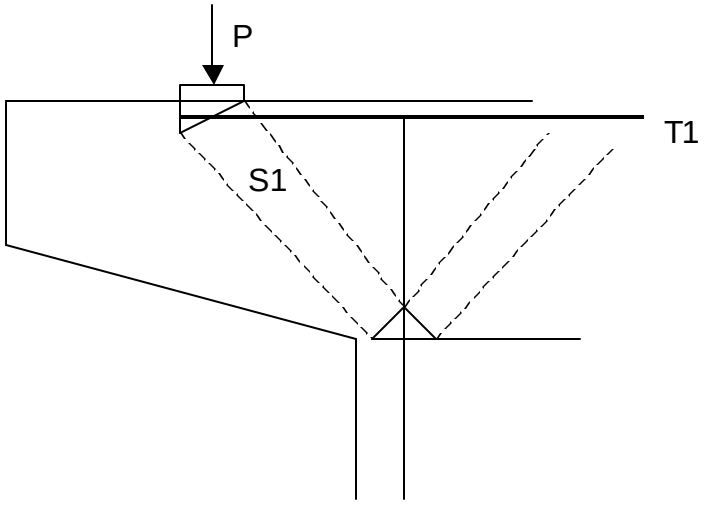

Figure A.2 Diagram of truss model used in strut and tie calculations.

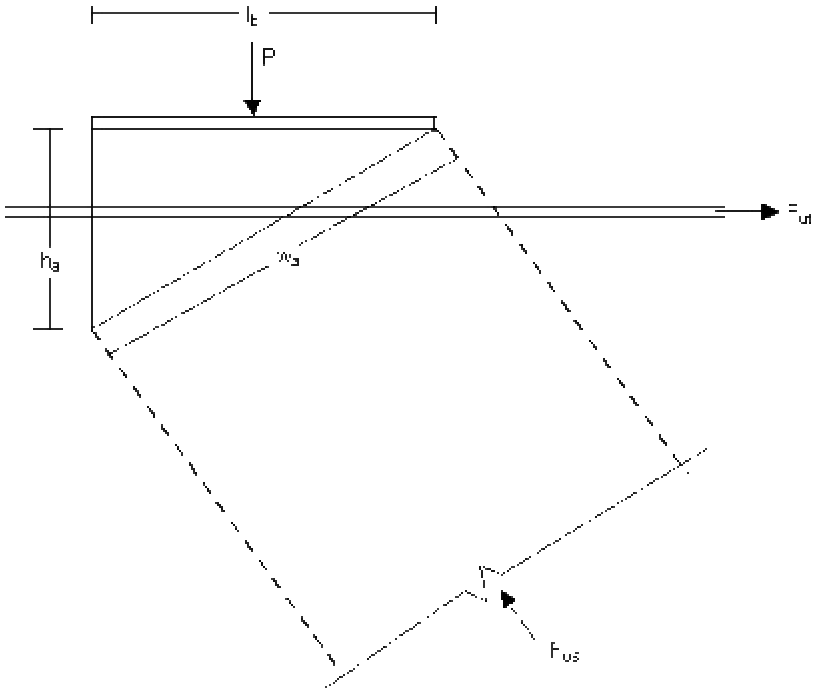

Figure A.3 Detail of critical node

Appendix B NSM Adhesive Tests

List of Tables

List of Figures

Adhesive tests were performed prior to completing the NSM FRP testing. Because the Aslan 500 tape did not come as a part of a system, there were several choices of adhesives to be used with the tape. Seven different adhesives were chosen for evaluation. Six specimens were tested for each of the adhesives. The adhesive exhibiting the best behavior was then used for the remaining NSM FRP bond tests.

The tensile test setup chosen for the tests is shown in Figure B-1. The specimens were tested in a 200-kip MTS testing machine. The FRP tape was inserted into a 0.25 x 0.75 in. saw-cut groove in a 6 x 6 in. concrete block 6 to 10 in. in length. The groove was filled with one of the seven adhesives as described later in this appendix. The block with the NSM tape was placed in the testing machine and the top face of the block bore against a plate that was clamped to two steel tubes. The steel tubes were bolted to the bottom plate. The top plate kept the block from rotating when the tensile force was applied to the FRP tape, which was located on one side of the block. The plate also put the concrete in a state of compression which generally caused an adhesive failure rather than a concrete failure. An adhesive failure was desirable for comparison of the different adhesives. A fixed hydraulic grip system gripped aluminum tabs affixed to the FRP tape and an actuator applied a tensile force.

The specimens were cast in modulus of rupture beam molds manufactured from steel. Plywood spacers were set in the molds while casting to divide the beams into three pieces approximately 8 in. in length. The plywood spacers moved slightly during casting, causing the lengths of the blocks to vary between 6 and 10 in. All of the blocks had a 6 x 6 in. cross section which were the dimensions of importance to the test.

The adhesives that were chosen for testing were Sikadur Anchorfix-3, Master Builders/Chemrex Concresive 1420, 3M DP600 NS, 3M DP460 NS, Sonneborn Epofil, Sikadur 35 Hi-Mod LV, and Sikadur 32 Hi-Mod. Cure time, consistency, tensile strength, tensile modulus, elongation to failure, and shear strength of these adhesives are given in Table B-1. All information in the table was provided by the manufacturer except the elongation to failure for 3M DP 460 NS, which was determined in previous research (Nozaka, 2002). A dash in the table indicates that that information was not provided by the manufacturer. A non-sag adhesive is indicated by NS in the table.

The concrete for the blocks was mixed and cast in the laboratory. Half of the beams were cast at one time because of the limitations associated with placing concrete by hand. The other half of the specimens were poured the following day. The specimens were cast on 2/18/04 and 2/19/04. Test cylinders were also cast with each set of specimens. Compressive and split tensile strength tests (ASTM C39 and ASTM C496) were conducted at the beginning of the adhesive tests. Values for these tests are given in Table B-2. The values represent the average of three tests on 4 x 8 in. cylinders. Coefficients of variation for the tests are also presented in the table.

To prepare the concrete blocks for the tests, a groove was cut into one side of each specimen with a tuck pointing blade on a circular saw. The groove was cut perpendicular to the top side of the block. The grooves were then brushed clean and high pressure air was used to remove any remaining dust or debris. The FRP tape was cut to a length of 16 in. It was lightly sanded and wiped with acetone to remove any dust or grease from the surface.

The procedure for applying the adhesive differed depending on the consistency of the adhesive. Epofil, Sikadur 32, and Sikadur 35 were two-component liquid adhesives. To apply

them to the specimens, the FRP tape was inserted into the center of the groove. Small pieces of tape were used as spacers to keep the FRP in the center of the groove. The groove was then sealed with duct tape, leaving the top of the groove open. For Sikadur 32 and Sikadur 35, the two components of the adhesive were measured and a drill with a mixing attachment was used to mix them together thoroughly. The adhesive was then transferred to a squeeze bottle and dispensed into the groove from the top until it was full. Epofil was a two-component cartridge that was mixed with a static mixing nozzle and dispensed into the top of the groove using a manual gun. Sikadur Anchorfix-3, Concresive 1420, 3M DP 600 NS and 3M DP 460 NS were non-sag two-component adhesives that were supplied in cartridges. They were mixed with static mixing nozzles and applied using manual guns. The grooves were not taped for application of the non-sag adhesives. The grooves were filled from the front with the adhesive. The FRP tape was then coated with the adhesive and inserted into the center of the groove. The surface of the adhesive was smoothed with a trowel.

After application of the adhesive, the FRP tape was clamped to a steel tube and angle seated on top of the block. The angle kept the FRP tape perpendicular to the top of the block while the adhesive cured.

Approximately 24 hours prior to testing, aluminum tabs were attached to the top end of the FRP tape. The 0.625 x 4 in. tabs were cut from 0.125 in. thick aluminum. They were lightly sanded and wiped with acetone before bonding them to the FRP tape with a fast-curing epoxy.

After the epoxy had cured, the specimen was inserted into the test frame. Shims were used under the block to position the top of the block tightly against the plate. The crosshead was lowered until the grips covered approximately 3 in. of the tabs. The grips were closed and the testing began. The loading was displacement-controlled with a rate of 0.01 in./min. Testing continued until the load dropped suddenly due to failure of bond between the tape and the adhesive, failure of the concrete, failure of the adhesive, or fracture of the FRP tape. If the FRP tape had not broken, it was pulled out of the concrete block before both parts were removed from the test frame.

Some of the blocks were re-used for a second round of testing. A groove was cut in the side opposite the first groove. The same procedure was followed for preparation and testing.

There were several different types of failures observed in the adhesive tests. Most of the adhesive tests on the Anchorfix-3, Concresive 1420, Sikadur 32, Sikadur 35, and Epofil failed by a loss of bond between the FRP tape and the adhesive. This usually occurred in a very sudden fashion. In some of these tests, shock from the abrupt loss of bond immediately caused the FRP tape to break. In these cases, the FRP broke off cleanly with no fraying of the fibers. The tests using 3M DP 600 NS all failed by loss of bond between the adhesive and the concrete. The tests using 3M DP 460 NS failed in various ways including loss of bond between the tape and the adhesive, failure in the adhesive, failure in the concrete, and fracture of the FRP tape. When failure occurred by fracture of the FRP tape, it was not a clean break. The fibers began to fray and break off individually until the tape completely deteriorated. Figure B-2 shows a photograph of a typical failure for each adhesive type.

Table B-3 shows the maximum loads reached in each of the tests. A dash in the table indicates that the test was not valid because of a failure due to the gripping method. Figure B-3 shows a graph comparing the average and highest load of each of the seven adhesives. The tests using Sika Anchorfix-3 had the lowest ultimate strengths with an average load of 6.8 kips and a

maximum load of 7.7 kips. The tests using 3M DP 460 NS had the highest ultimate strengths with an average load of 16.5 kips and a maximum load of 18.3 kips. The other adhesives all performed comparably, with maximum loads between 11.3 and 13.6 kips. Based on its superior strength in the adhesive tests, 3M DP 460 NS was the adhesive chosen to continue the bond tests on NSM FRP tape.

Table B-1 Properties of Adhesives

Adhesive	Cure Time	Consistency	Tensile Strength (psi)	Tensile Modulus (ksi)	Elongation to Failure (%)	Shear Strength (psi)
3M DP 600 NS	1 hour	NS[1]	-	-	-	3580
Sikadur Anchorfix-3	24 hours	NS	4700	120	1.2	4900
MBT/Chemrex Concresive 1420	24 hours	NS	4000	-	1.0	-
Sikadur 32 Hi Mod	7 days	2800 cps	5100	320	1.8	5900
Sikadur 35 Hi Mod LV	> 7 days	375 cps	8900	410	5.4	5100
Sonneborn Epofil	> 7 days	750 cps	7300	450	8.0	8800
3M DP 460 NS	24 hours	NS	5100	360	2.1	4500

1 NS = Non Sag

Table B-2 Concrete Strengths for Adhesive Tests

Specimen Set Date Tested (age of concrete)	Compressive Strength (psi)	Coefficient of Variation (%)	Split Tensile Strength (psi)	Coefficient of Variation (%)
Set 1 4/19/04 (58 days)	8080	6.8	610	8.6
Set 2 4/19/04 (59 days)	9350	6.3	660	5.0

Table B-3 Maximum Loads for Adhesive Tests

Adhesive Type (Age at Testing)	Test 1 Load (kips)	Test 2 Load (kips)	Test 3 Load (kips)	Test 4 Load (kips)	Test 5 Load (kips)	Test 6 Load (kips)	Ave. Load (kips)	Max. Load (kips)
Anchorfix-3 (4 days)	6.7	7.7	6.8	6.0	6.6	6.8	6.8	7.7
Concresive 1420 (3 days)	9.5	8.5	11.3	9.6	7.7	8.5	9.2	11.3
Epofil (18 days)	13.2	-	11.9	12.1	13.3	13.3	12.8	13.3
Sikadur 35 (17 days)	-	-	11.8	12.1	11.2	12.0	11.8	12.1
Sikadur 32 (16 days)	12.0	12.0	12.4	-	13.6	12.7	12.5	13.6
DP 600 NS (4 days)	9.8	12.2	11.4	9.4	10.8	10.8	10.7	12.2
DP 460 NS (4 days)	17.1	14.1	18.3	17.1	17.9	14.7	16.5	18.3

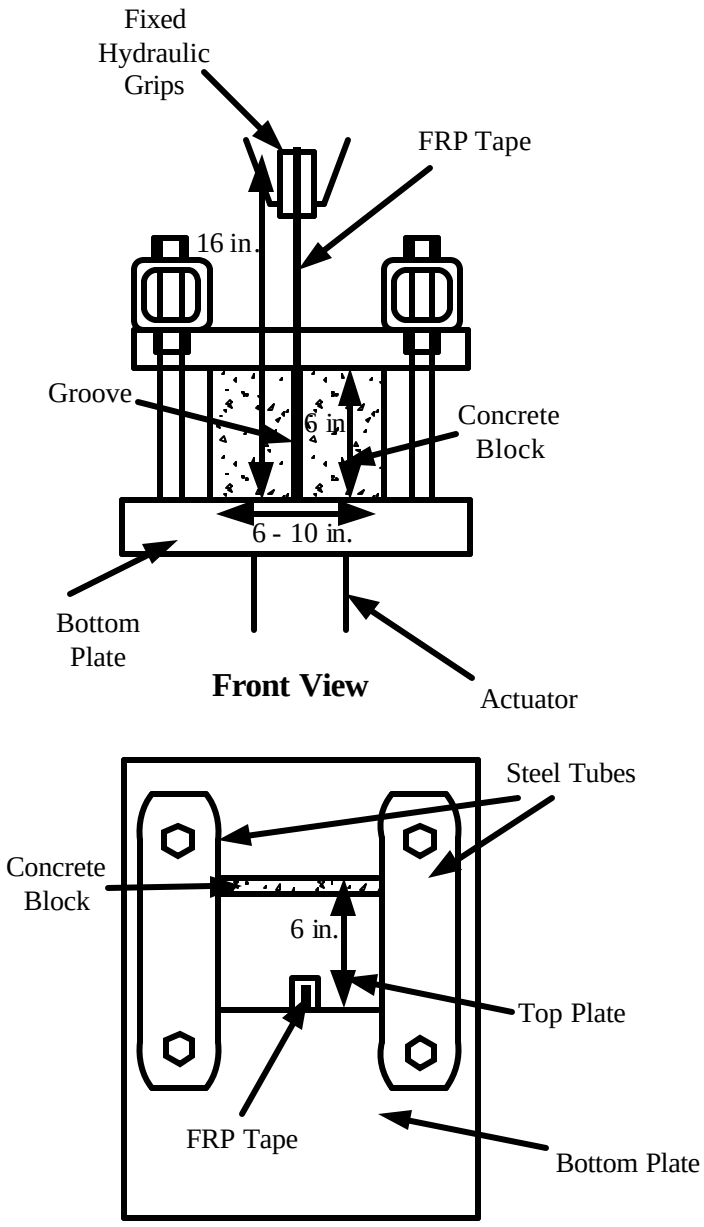

Figure B-1 Adhesive Test Setup

a) Sika Anchorfix-3

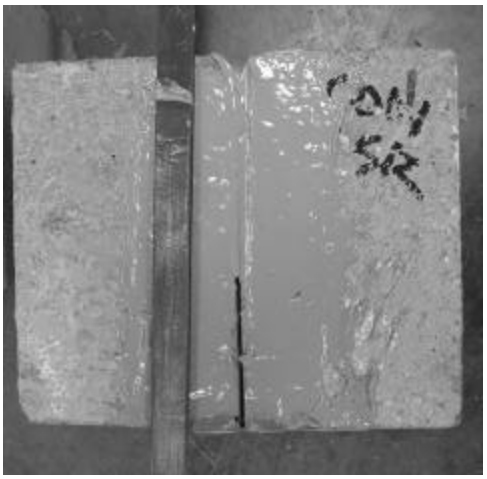

b) Concresive 1420

c) Sikadur 35

d) Sikadur 32

Figure B-2 Adhesive Test Specimens after Failure

e) 3M DP 600 NS

f) 3M DP 460 NS

g) Epofil

Figure B-2 Adhesive Test Specimens after Failure (cont.)

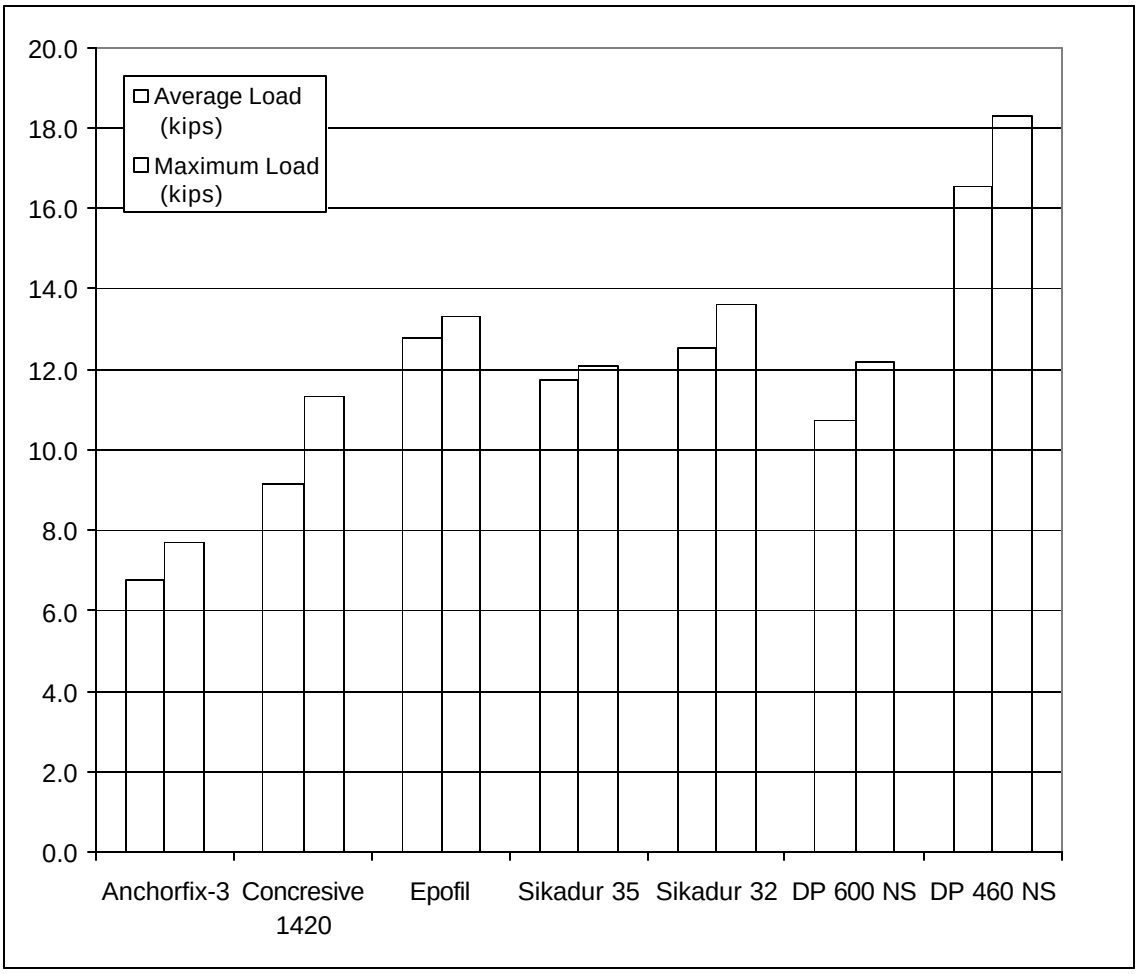

Figure B-3 Adhesive Test Load Comparison Graph

Appendix C Epoxy Cure Time Tests

List of Tables

List of Figures

The pilot bond tests demonstrated that the particular epoxy used in those tests required a cure time exceeding 3 days. Consequently, a new FRP system that could be tested within a shorter time frame was sought for the primary bond tests. An epoxy cure time test was conducted to ensure that the new system could be confidently tested after 3 days of curing. Three tests were done each after one, two, three, four, and five days of curing.

The test setup is shown in Figure C-1. It consisted of a 6 by 12 in. concrete cylinder in two halves with a 1 in. threaded rod extending longitudinally through each half of the cylinder, and sticking approximately six inches out of each end. The threaded rod served to attach the cylinder to the testing machine and allowed a tensile force to be applied to the concrete cylinder. Two 2 in. wide strips of FRP were applied between the two parts, on opposite sides. Tensile force was applied using a 200-kip MTS testing machine.

The concrete cylinders were created at the same time as the bond test specimens, using the same concrete. They were formed in cylinder molds with holes drilled in the top and bottom for the threaded rod to extend through. After curing, the cylinders and threaded rods were removed from the molds and cut in half with a concrete saw. The cylinders were then fastened into plywood frames as shown in Figure C-2 to keep the two halves from moving with respect to each other after the FRP was applied. The FRP was applied with the same surface preparation and application procedure as the bond tests.

The specimens were set into the testing machine while still in the plywood frames. The threaded rod on the top half was fastened into the top of the load frame, and a hex nut was screwed onto the bottom rod. The hex nuts on the bottom rod were tightened as uniformly as possible to minimize the amount of initial compression or tension in the specimen. The plywood frames were then removed and the testing began. The tests were displacement controlled, with a loading rate of 0.0001 in./sec.

The results from the epoxy cure time tests exhibited an interesting trend. The results are shown in Figure C-3, as well as Table C-1. The strength of the FRP was highest at 24 hours. After 24 hours, the load decreased, and then held approximately constant after 72 hours. It is possible that this was due to the stiffening of the epoxy as it reached full cure. This showed that testing done at or after 3 days could be compared with confidence. It also showed that earlier testing might show misleadingly high results.

Based on the results of this test, all epoxy for the bond tests was allowed at least 3 days to cure prior to testing to ensure consistent results.

Table C-1 Epoxy Cure Time Results Table

Cure Time (days)	Load (kips) Test 1	Load (kips) Test 2	Load (kips) Test 3	Load (kips) Average	Standard Deviation
1	5.7	6.6	6.3	6.2	0.4
2	4.2	3.9	-	4.1	0.2
3	4.3	4.2	3.9	4.2	0.2
4	4.5	4.6	4.2	4.4	0.2
5	4.5	3.4	-	3.9	0.7

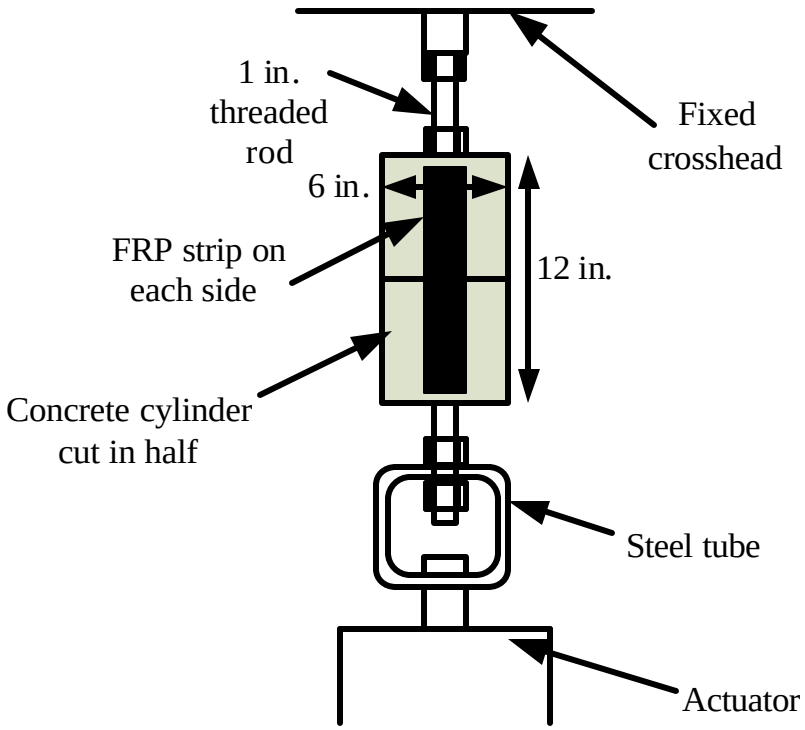

Figure C-1 Epoxy Cure Time Test Setup

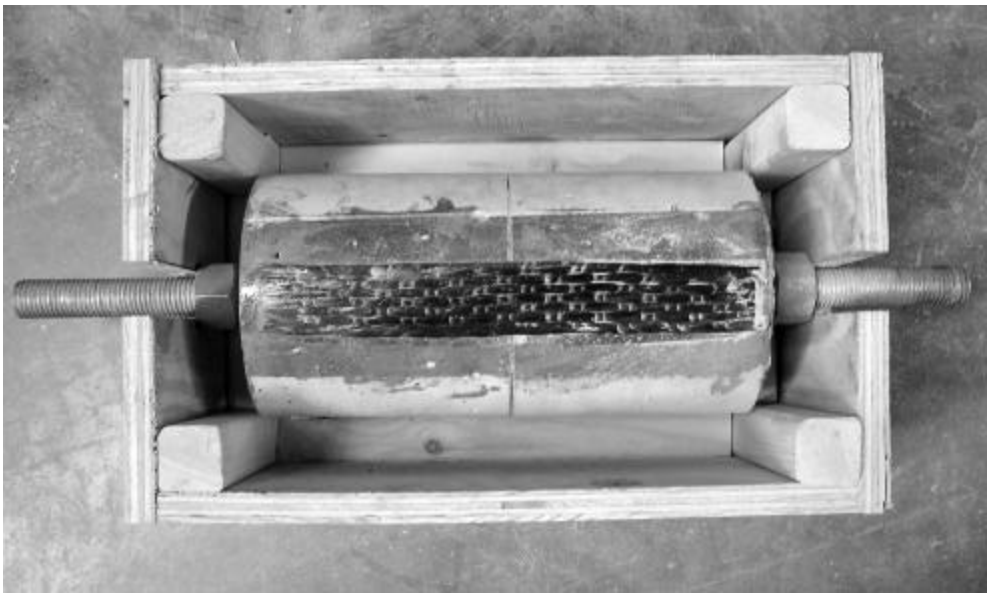

Figure C-2 Epoxy Test Specimen Frames

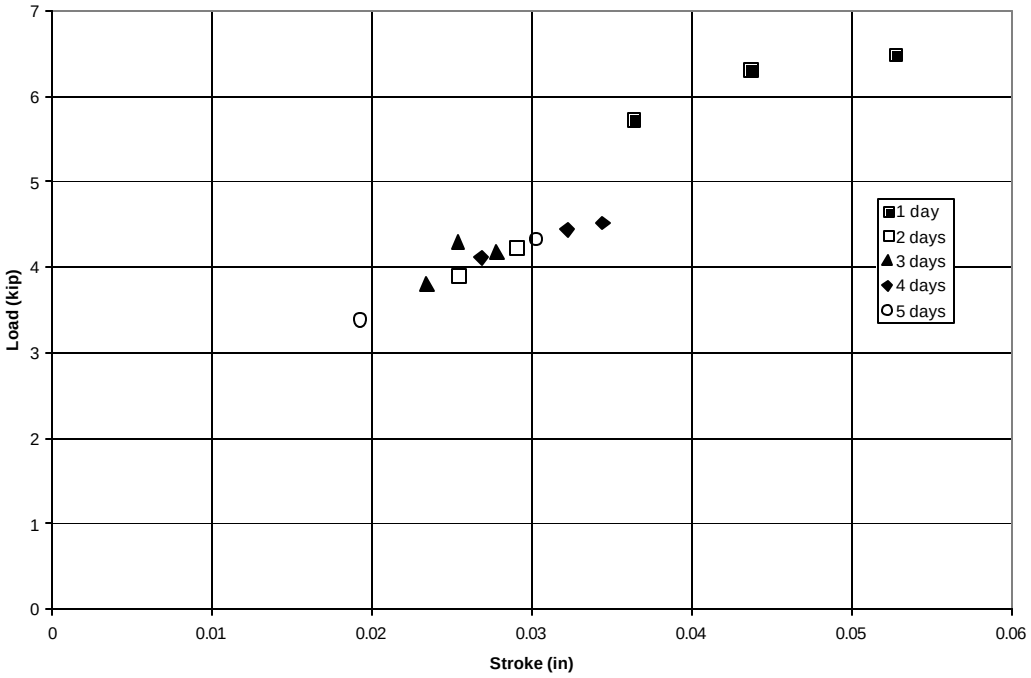

Figure C-3 Epoxy Cure Time Results Graph

Appendix D Pilot Bond Tests

List of Figures

A pilot test was completed before the eighteen bond specimens were cast. The purpose was to identify and fix any potential problems with the proposed test method. The test type and specimen design were the same as planned for the bond tests.

There were a total of seven specimens that were tested as a part of the pilot test. All of the specimens were tested with a single 6 in. strip of FRP on each side. There were no variables in the pilot tests.

The pilot test specimens were cast in the same forms to be used for the bond tests. The concrete for the first two specimens was mixed and placed by hand in the laboratory. The concrete for the other five specimens was delivered from a local ready-mix concrete plant. The specified concrete strength was 4000 psi for all specimens. The FRP system that was used for the pilot test was SikaWrap Hex 103C. It was a unidirectional carbon fiber fabric system similar to the Tyfo system but the full cure time on the Sika system was 14 days, compared to 3 days for the Tyfo system. Consequently, the Tyfo system was chosen for the primary bond tests because it enabled testing to be completed in a reasonable time frame.

Several problems were identified with the initial procedure. Initially, the top block had not been tightened to the beam, and there was no grout between the blocks and the beams. Large rotations occurred after the FRP failed on one side, causing moment in the FRP on the opposite side. This only allowed one side to be tested accurately. The problem was solved by using grout between the half blocks and the steel beams to which they were attached and torquing the bolts connecting the blocks to the steel beams.

In one of the pilot bond tests, part of the crack was accidentally glued together by the adhesive used to attach the FRP so that a new crack formed in the concrete at a different location. This prevented the attainment of accurate strain data. To prevent this from occurring in the primary bond tests, Vaseline was applied to the inside surface of the crack to prevent the two inside faces of the blocks from becoming glued together.

Large load fluctuations occurred when turning on the hydraulics and controller in some of the pilot tests due to warm-up of the system. To eliminate those load fluctuations, the controller was turned on in advance and set to hold a small compressive load on the blocks while the FRP cured.

A test was also conducted to determine the strain gage configuration to be used. It was determined that the strain gages should be no more than 1 in. apart, and should extend at least 6 in. from the crack to capture the effective bond length as it shifts. Three vertical lines of strain gages were placed on a single sheet to evaluate the variability. They showed that there can be a great deal of variability in the gages because of the surface irregularities of the FRP. It was determined that a change in strain smaller than 200 microstrain was insignificant because of the high irregularity of the FRP fabric surface. A diagram in Figure D-1 shows the locations of the strain gages on the specimen. A graph showing the variability between lines of strain gages is shown in Figure D-2.

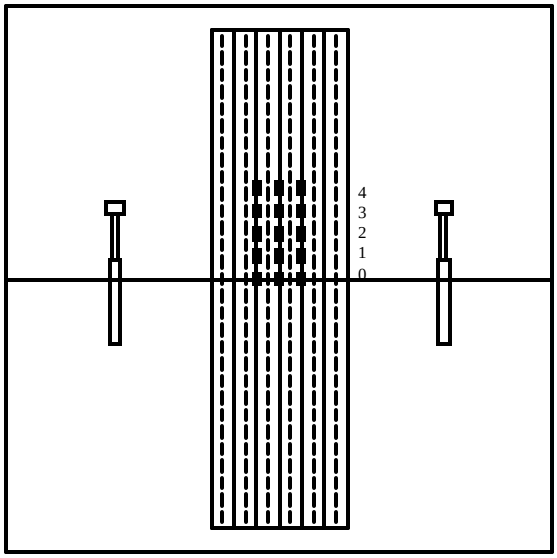

Figure D-1 Strain Gage Locations

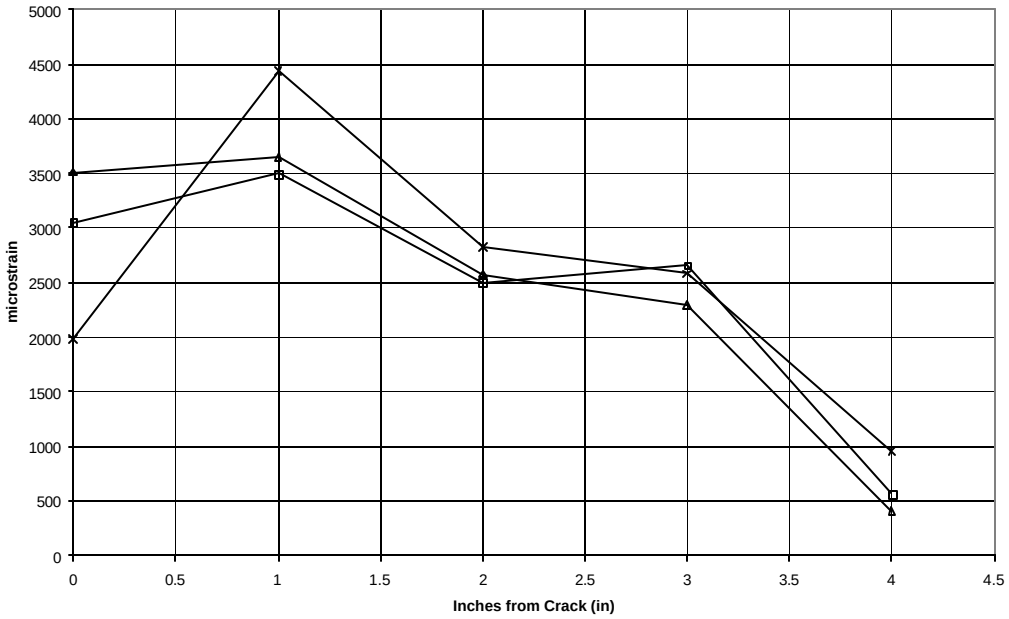

Figure D-2 Strain Gage Variability Graph

Appendix E Bond Test Details

Table of Contents

Sections E-1 through E-18 present the details of the externally bonded and near surface mounted bond tests. Appendix F contains the load vs. stroke and load vs. LVDT plots for these tests, as well as strain data plots. Photographs of the specimens after failure are shown in Appendix G. In this appendix, a failure is described as an adhesive interface failure if the sheet peeled off from the concrete with no concrete attached. A concrete substrate failure occurred if the sheet peeled off from the concrete and a small amount of concrete came off with the sheet. A concrete substrate failure was shallow and did not involve large aggregate. When a concrete shear failure occurred at the crack, a large piece of concrete was broken off of the specimen. The piece of concrete included large aggregate and could be over an inch in depth. The loads for each strip or tape of FRP are determined by the drop in load that occurred after failure of that strip or tape.

E-1 E1-90-1

E1-90-1 was the control test. The specimen had one strip of EB FRP sheet on each side of the specimen. The strips were each 6 in. wide with fibers oriented at 90 degrees to the crack. There was no unbonded region at the crack. The test was performed on 6/2/03 after allowing three days for the FRP to cure. The maximum load measured during the first test was 16.9 kips. The FRP on both sides peeled off with a combination of concrete substrate failure, adhesive interface failure, and concrete shear failure near the crack. The bottom west side failed first under a load of 8.4 kips, and the bottom east side failed second carrying 8.4 kips.

The procedure was different for this test than the others because the emergency stop on the hydraulics was accidentally pushed approximately 48 hours after FRP application. This caused a compressive load of three kips to be put on the specimen for approximately 24 hours before the test. In addition, when the hydraulics were turned back on prior to testing, several kips of compression and tension were applied to the specimen before the load could be steadied. Some tiny cracks in the adhesive were noticed before the test began. It was difficult to determine whether the early load fluctuations had a significant effect on the results of the test.

E-2 E2-90-1

E2-90-1 was another control test with one strip of EB FRP sheet on each side of the specimen. The strips were each 6 in. wide with fibers oriented at 90 degrees to the crack. There was no unbonded region at the crack. The test was performed on 6/7/03 after allowing three days for the FRP to cure. The maximum load reached during the second test was 13.4 kips. The FRP on both sides peeled off with mostly adhesive interface failure and some concrete substrate failure near the ends of the sheet, as well as concrete shear failure near the crack. The bottom west side failed first carrying 7.3 kips, and the bottom east failed second carrying 6.0 kips.

The procedure for this test differed from the typical test procedure. To prevent load fluctuations like those observed in the testing of E1-90-1, the controller was turned on right before testing, at a compressive load of approximately three kips, the weight of the cylinder. This was also the load that had been on the specimen over the FRP cure time.

This block had also been dropped on the floor from the load frame while it was being positioned, resulting in chips on the top corners of the top block. It did not appear to have significantly damaged the block, and did not appear to have an effect on the test. Petroleum jelly from between the blocks also appeared to have leaked out onto the surface of the blocks because

tape had not been applied to prevent this from occurring yet. This could have had some effect on the test by encouraging a failure between the concrete and adhesive.

E-3 E3-90-1-U2

The specimen for test E3-90-1-U2 had a 6 in. strip of EB FRP on each side. The fibers were oriented 90 degrees to the crack, and there was a 1 in. wide unbonded region on either side of the crack. The unbonded region was formed by coating the region with petroleum jelly. The test was performed on 6/15/03 after allowing three days for the FRP to cure. The maximum load reached was 12.2 kips. The sheets peeled off entirely at the adhesive interface with no substrate or shear failure of the concrete. The bottom east side failed first carrying a load of 5.6 kips, and the top west side failed second carrying 6.3 kips.

The procedure for this test also differed from the standard procedure. A new controller was used to allow a constant load to be held on the specimen while the FRP cured and to prevent the load fluctuations that were occurring with the old controller. However, the gain settings on the new controller were not set correctly, so the controller became unstable approximately ten hours after the FRP was applied, causing the load to fluctuate between 2.5 kips in compression and 0.5 kips in tension. The gain setting was adjusted to fix the problem, and there did not appear to be any damage to the specimen from the low load levels.

E-4 E4-90-1-U2

Test E4-90-1-U2 was a repeat of test E3-90-1-U2. The specimen had a 6 in. strip of EB FRP on each side. The fibers were oriented 90 degrees to the crack, and there was a 1 in. wide unbonded region on either side of the crack. The unbonded region was formed by anti-adhesive tape instead of petroleum jelly for this test. The test was performed on 7/7/03 after allowing the FRP three days to cure. The maximum load reached during this test was 12.1 kips. The failure was entirely in the adhesive interface. No concrete substrate was removed. The bottom east side failed first carrying 5.9 kips and the bottom west failed second carrying 6.0 kips.

This test was done on the same block that was used for test E3-90-1-U2. Because no concrete had been removed from the block it was able to be reused after grinding off all remaining epoxy from the surface.

E-5 E5-90-1-U1

Test E5-90-1-U1 had one 6 in. strip of FRP on either side. The fibers were oriented 90 degrees to the crack. There was an unbonded region of 0.5 in. on either side of the crack. The unbonded region in this test was formed with anti-adhesive tape, as in test E4-90-1-U2. The test was performed on 7/11/03 after allowing three days for the FRP to cure. The maximum load reached in this test was 11.8 kips. Again, the failure was entirely in the adhesive interface, with no concrete substrate or shear failure. The top west side failed first carrying 5.6 kips and the bottom east failed second carrying 6.3 kips.

Test 5 was also performed on the same concrete block that was used for tests E3-90-1-U2 and E4-90-1-U2. No concrete had been removed from the block on any of those tests, so the block was reused after grinding away all excess epoxy from the surface

E-6 E6-90-1

Test E6-90-1 was a repeat of the control test. The specimen had one 6 in. strip of EB FRP on each side. The fibers were oriented at 90 degrees to the crack, and there was no unbonded region. The test was performed on 7/18/03 after allowing the FRP to cure for three days. The maximum load reached during the test was 15.0 kips. The failure was a combination of adhesive interface and concrete substrate failure. Shear failure of the concrete also occurred near the crack. The top east side failed first carrying 7.7 kips, and the top west failed second carrying 6.9 kips.

Test E6-90-1 was also performed on the same concrete block as tests E3-90-1-U2, E4-90-1-U4, and E5-90-1-U1. The specimen was reused after grinding off all excess epoxy from the surface. The test was performed to ensure that it was not a problem with the block that was causing no concrete to be removed at failure.

E-7 E7-45-1

The specimen for test E7-45-1 had one 6 in. wide strip of FRP on either side. The strips were oriented at 45 degrees to the crack, and there was no unbonded region. The test was performed on 7/25/03 after allowing the FRP three days to cure. The maximum load reached in this test was 13.0 kips. The failure occurred in the adhesive interface and the concrete substrate, but very little concrete was taken out near the crack. The top west side failed first, but it was not possible to determine what portion of the load the top west side was carrying when it failed, because the specimen rotated and the load dropped from 13.0 kips to 1.3 kips. The specimen rotated because the loading became eccentric after one side failed, and the actuator that was attached to the top half of the specimen could not resist rotation. The bottom east failed second carrying a load of 4.7 kips.

The procedure for this test differed from the standard procedure because the 45 degree specimen took on load much more slowly. The loading rate was changed from the standard rate of 0.00005 in./sec to 0.0001 in./sec after approximately 30 minutes. The loading rate was increased again to 0.0005 in./sec after the top west side failed.

E-8 E8-90-2

The specimen for test E8-90-2 had two 3 in. strips of FRP on each side. The strips were spaced 1 in. apart, and were oriented 90 degrees to the crack. There was no unbonded region. The test was performed on 8/3/03 after allowing the FRP to cure for four days. The maximum load reached during this test was 19.4 kips. The failure type was a combination of concrete substrate and adhesive interface with some concrete shear failure at the crack. The top northeast, top southeast, and bottom northwest sides failed almost simultaneously carrying a total load of 15 kips, but it was not possible to determine how much of the load was carried by each strip. The top southwest side failed last carrying a load of 4.1 kips.

Test E8-90-2 followed the standard procedure.

E-9 E9-90-2

The specimen for test E9-90-2 had two 3 in. strips on each side. The strips were separated by 3 in. spacing. The strips were oriented at 90 degrees to the crack and there was no unbonded region. The test was performed on 8/12/03 after allowing the FRP to cure for seven

days. The maximum load reached during the test was 16.1 kips. The failure occurred in the adhesive interface and the concrete substrate with some concrete shear failure near the crack. The top southwest side failed first carrying a load of 4.4 kips. The bottom northwest side failed second carrying 4.2 kips. The bottom southeast side failed third carrying 3.9 kips, and the top northeast side failed last carrying 3.8 kips.

This test followed the standard procedure. However, the strain and LVDT data for this test were lost due to accidental deletion of a computer file.

E-10 E10-90-3

The specimen for test E10-90-3 had three strips of FRP on each side. The strips were 2 in. wide at a 1 in. spacing. The strips were oriented 90 degrees to the crack and there was no unbonded region. The test was performed on 8/25/03 after allowing the FRP to cure for four days. The maximum load achieved was 20.4 kips. The failure was a combination of adhesive interface and concrete substrate, with some concrete shear failure near the crack. The bottom center east side failed first carrying 3.7 kips. The bottom southeast side failed second carrying 3.0 kips. The bottom northeast side failed third carrying 3.3 kips. The bottom northwest side failed fourth carrying 3.2 kips. The bottom center west side failed fifth carrying 3.8 kips, and the bottom southwest side failed last carrying 4.0 kips

Test E10-90-3 followed the standard procedure for testing.

E-11 E11-45-2

The specimen for test E11-45-2 had two strips on each side. The strips were 3 in. wide with 1 in. spacing, and were oriented 45 degrees to the crack. There was no unbonded region at the crack. The test was performed on 9/03/03 after allowing the FRP to cure for six days. The maximum load reached was 9.7 kips. The failure was mostly in the adhesive interface with some concrete substrate and a small amount of concrete shear failure at the crack. The top northeast and southeast sides failed simultaneously carrying a total load of 9.0 kips. The specimen experienced some rotation after the first strips failed. The top northwest side failed third carrying 2.0 kips, and the bottom southwest side failed fourth, carrying 4.0 kips. The maximum load carried by the strips that failed first cannot be directly compared to the maximum load carried by the strips that failed last for the 45 degree specimens. This is because the rotation that these specimens experience after the first strip fails could cause some damage to the remaining strips, in addition to causing misalignment of the system.

The loading rate was changed prior to testing this specimen to .0001 in./sec, because the specimens with strips at 45 degrees were known to undergo much larger deformations.

E-12 E12-45-3

The specimen for test E12-45-3 had three strips on each side. The strips were 2 in. wide at a 1 in. spacing. The strips were oriented at 45 degrees to the crack, and there was no unbonded region at the crack. The test was performed on 12/14/03 after allowing the FRP to cure for four days. The maximum load reached in the test was 12.2 kips. The failure was mostly in the adhesive interface with some concrete substrate failure and a small amount of concrete shear failure near the crack. All three strips on the bottom west side failed simultaneously with a

total load of 12.2 kips. The beam then encountered some rotation. The east side top south, top center, and bottom north side all failed simultaneously carrying a total load of 7.1 kips.

The loading rate for this test was 0.0001 in./sec until the displacement reached approximately 0.25 in. At that time, the displacement was advanced manually to approximately 0.4 inches to speed up the test.

E-13 NA13-90-2

This was the first test using near surface mounted FRP tape. The adhesive used for this test was Sika Anchorfix-3. There were two 24 in. long tapes on each side of the block. They were spaced 6 in. apart, and were oriented at 90 degrees to the crack. The test was completed on 11/13/03, after allowing one day for the adhesive to cure. The maximum load reached in this test was 27.7 kips. The failure began with progressive cracking of the surface epoxy and concrete, followed by a loss of bond between the FRP tape and epoxy. A large piece of concrete near the crack was broken off at failure. There was also significant damage to the tape. The northeast side failed first, carrying 8.0 kips, and the remaining load was held by friction between the tapes and epoxy. The test continued until a displacement of approximately 0.25 in. was reached, at which time the displacement was advanced manually up to the maximum displacement of 0.5 in. All of the tapes slipped up to 0.5 in., at which time the test was ended.

Inspection of the adhesive after this test showed that the epoxy was not fully cured in at least two locations. This resulted in changing the cure time from one to two days for the other tests, as well as ensuring that all potentially improperly mixed epoxy from the beginning of each cartridge was discarded.

E-14 NA14-90-2

The specimen for test NA14-90-2 was identical to that of test NA13-90-2. The adhesive used was Sikadur Anchorfix-3. There were two tapes on each side oriented at 90 degrees to the crack. The test was performed on 11/20/03 after allowing the adhesive to cure for two days. The maximum load reached during the test was 38.1 kips. The failure began with progressive cracking of the surface epoxy and the concrete, followed by shear failure of the concrete near the crack, and a loss of bond between the FRP tape and the epoxy. Significant damage to the tape was observed. The northwest side failed first carrying a load of 2.9 kips, the southwest side failed second carrying 7.1 kips, the northeast side failed third carrying 10.0 kips, and the southeast side failed fourth, carrying 4.1 kips.

This test followed the same procedure as test NA13-90-2. The test continued until a displacement of approximately 0.25 in., and then displacement was advanced manually up to 0.5 in.

E-15 NA15-45-2

The specimen for this test had two tapes on each side at 6 in. spacing. The tapes were oriented 45 degrees to the crack. The adhesive used was Sika Anchorfix-3. The test was performed on 11/23/03 after allowing the adhesive to cure for two days. The maximum load reached during this test was 22.3 kips. The failure began with progressive cracking of the concrete and epoxy on the surface, followed by shear failure of the concrete near the crack and a loss of bond between the FRP tape and the adhesive. Again, the FRP tapes were significantly

damaged. The northeast and southeast side failed simultaneously carrying a total load of 9.5 kips, and then the northwest and southwest sides failed simultaneously carrying a total load of 15.1 kips.

Test NA15-45-2 followed the same procedure as test NA13-90-2 and NA14-90-2. The test was run until approximately 0.25 in. displacement, then the displacement was advanced manually up to 0.5 in.

E-16 NB16-90-2

The specimen for test NB16-90-2 was similar to that of tests NA13-90-2 and NA14-90-2. The adhesive used was 3M DP640 NS. There were two tapes on each side oriented at 90 degrees to the crack. The test was performed on 5/30/04 after allowing the adhesive to cure for two days. The maximum load reached during the test was 54.3 kips. The failure began with progressive cracking of the concrete, followed by shear failure of the concrete near the crack, and failure of the concrete along the groove. A large portion of concrete was broken off of the specimen at failure. There was no failure in the adhesive. The northwest and southwest sides failed first carrying a combined load of 26.6 kips, the southeast side failed second carrying 13.5 kips, and the northeast side failed third, carrying 18.3 kips.

E-17 NB17-90-2

The specimen for test NB17-90-2 was identical to that of tests NB16-90-2. The adhesive used was 3M DP640 NS. This adhesive was chosen subsequent to the adhesive tests because it performed better than the other adhesives tested. There were two tapes on each side oriented at 90 degrees to the crack. The test was performed on 6/3/04 after allowing the adhesive to cure for two days. The maximum load reached during the test was 56.3 kips. The failure began with progressive cracking of the concrete, followed by shear failure of the concrete near the crack, and shear failure of the concrete along the groove. A large portion of concrete was broken off of the specimen at failure. There was no adhesive failure. The southeast side failed first carrying a load of 14.3 kips. The southwest side failed second carrying a load of 15.0 kips, the northwest side failed third carrying 13.6 kips, and the northeast side failed fourth, carrying 14.4 kips.

E-18 NB18-90-2V

The specimen for test NB18-90-2V was identical to that of tests NB16-90-2 and NB17-90-2. The adhesive used was 3M DP640 NS. There were two tapes on each side oriented at 90 degrees to the crack. The procedure for this test was different than the other tests with near surface mounted FRP tape. The specimen was loaded with a cyclic load varying from 1 to 5 kips in compression at a frequency of 1 Hz. The cyclic load was applied from the time the FRP was applied until testing began. The loading was intended to mimic the vibrations caused by car traffic traveling over a bridge. The test was performed on 6/7/04 after allowing the adhesive to cure for three days. The maximum load reached during the test was 54.5 kips. The failure began with progressive cracking of the concrete, followed by shear failure of the concrete near the crack, and shear failure of the concrete along the groove. A large portion of concrete was broken off of the specimen at failure. There was no adhesive failure. The southwest side failed first carrying a load of 15.0 kips. The northwest side failed second carrying a load of 15.0 kips, the northeast side failed third carrying 11.5 kips, and the southeast side failed fourth, carrying 15.2 kips.

Appendix F Bond Test Plots

List of Figures

This appendix contains the graphs of Load vs. Stroke and Load vs. LVDT Displacements for all of the bond tests, and Surface Strain vs. Distance from Crack for each test with strain data. The effective bond lengths are indicated on the strain plots.

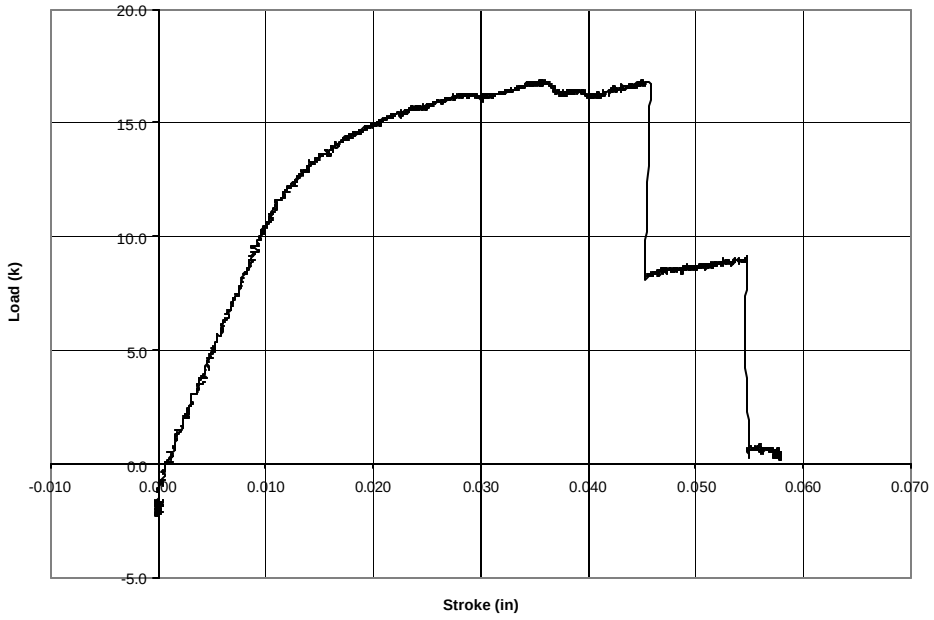

a) Load vs. stroke

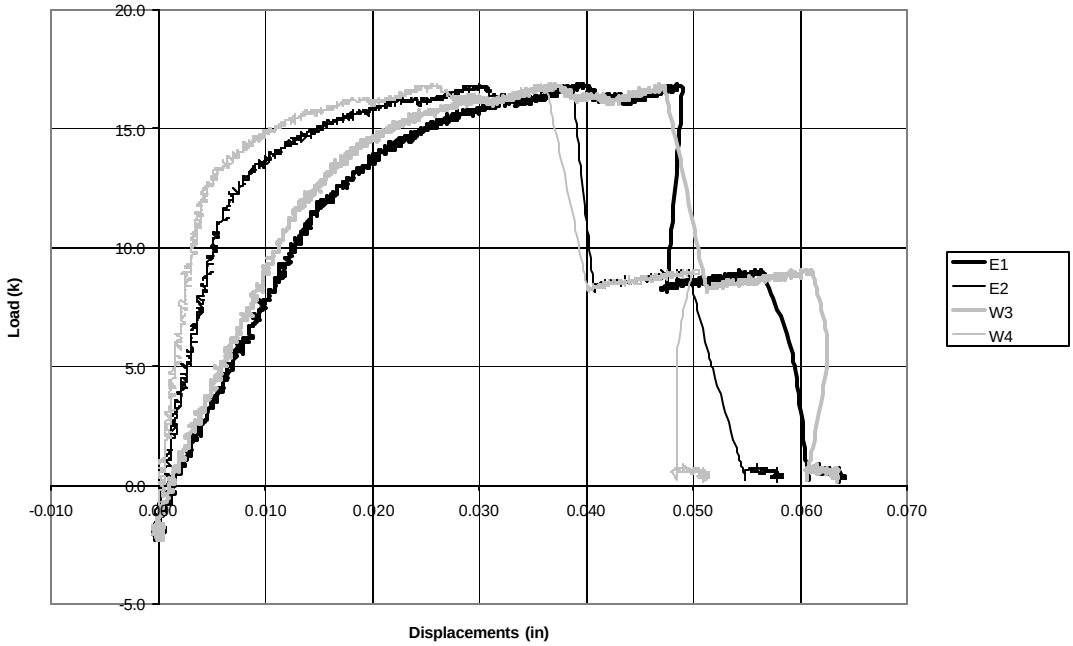

b) Load vs. LVDT Displacements

Figure F-1 E1-90-1 Data Plots

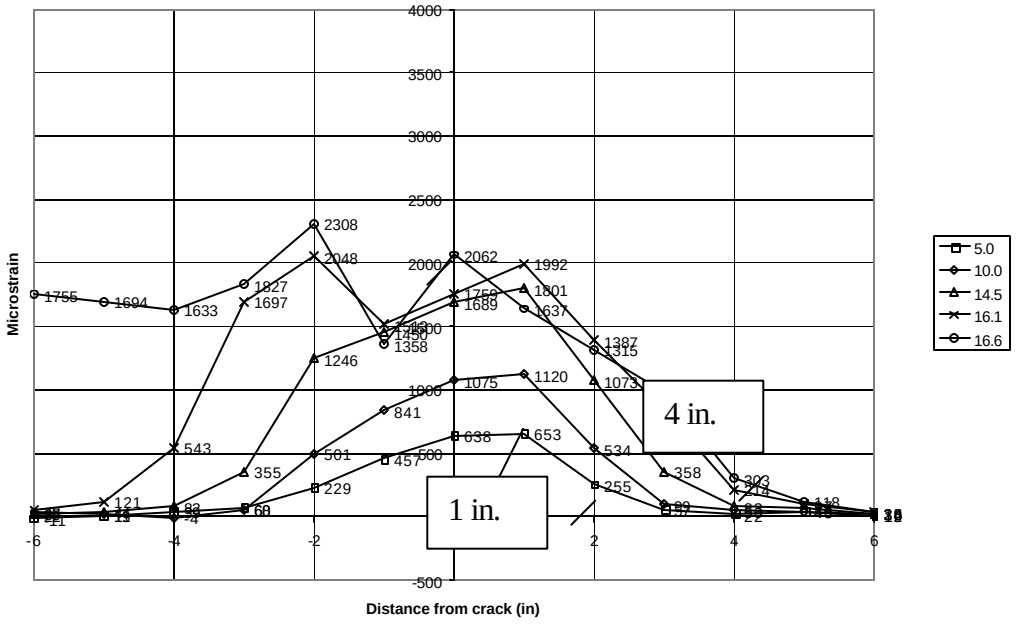

c) West surface gages

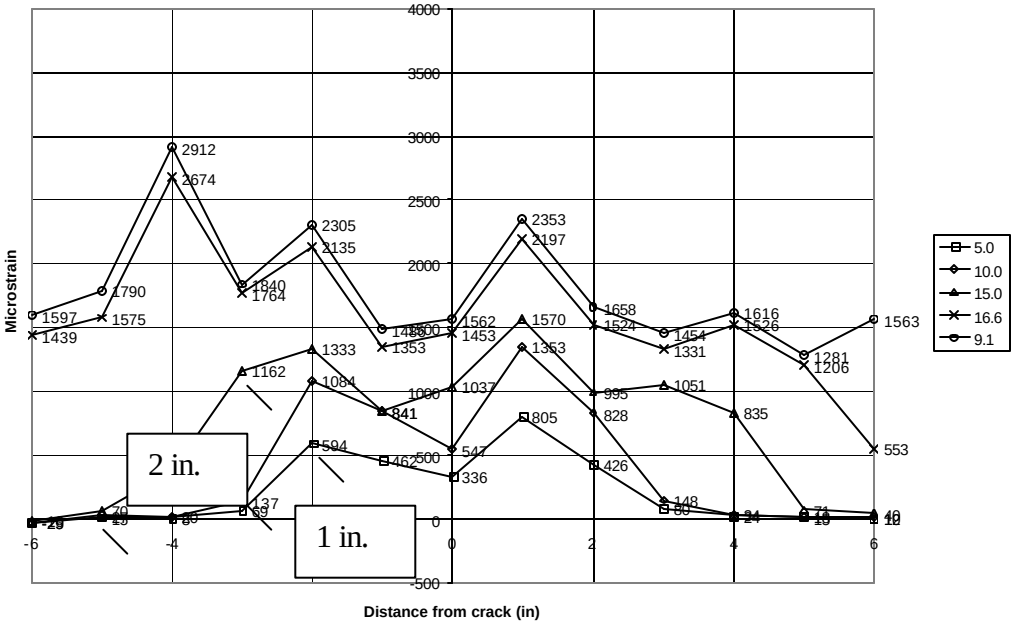

d) East surface gages

Figure F-1 E1-90-1 Data Plots cont.

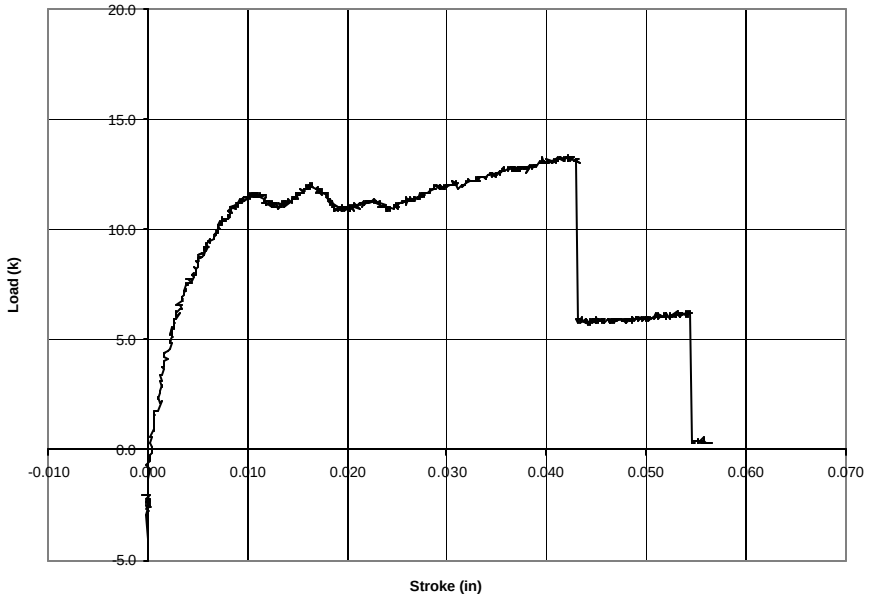

a) Load vs. stroke

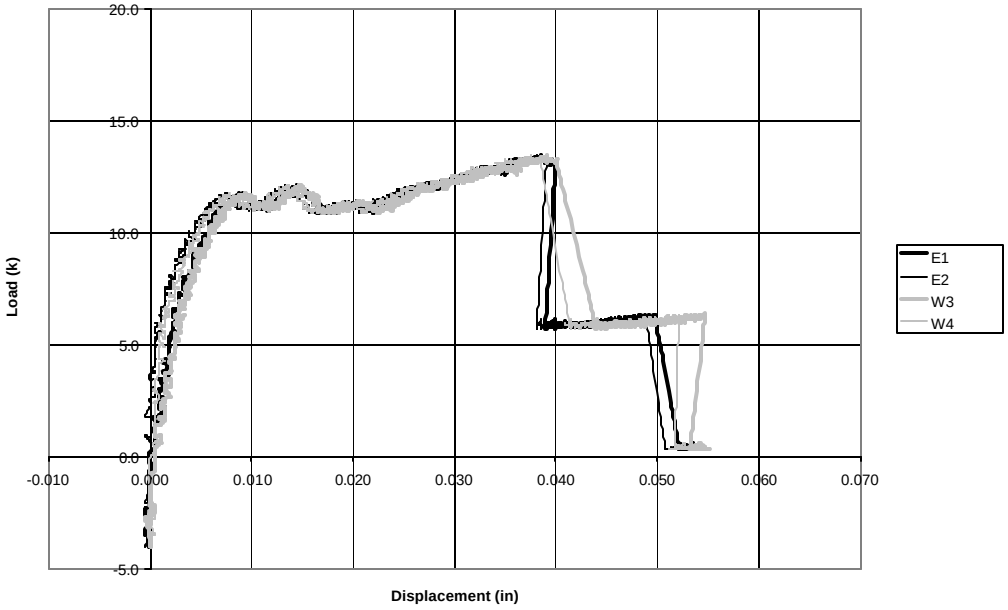

b) Load vs. LVDT Displacements

Figure F-2 E2-90-1 Data Plots

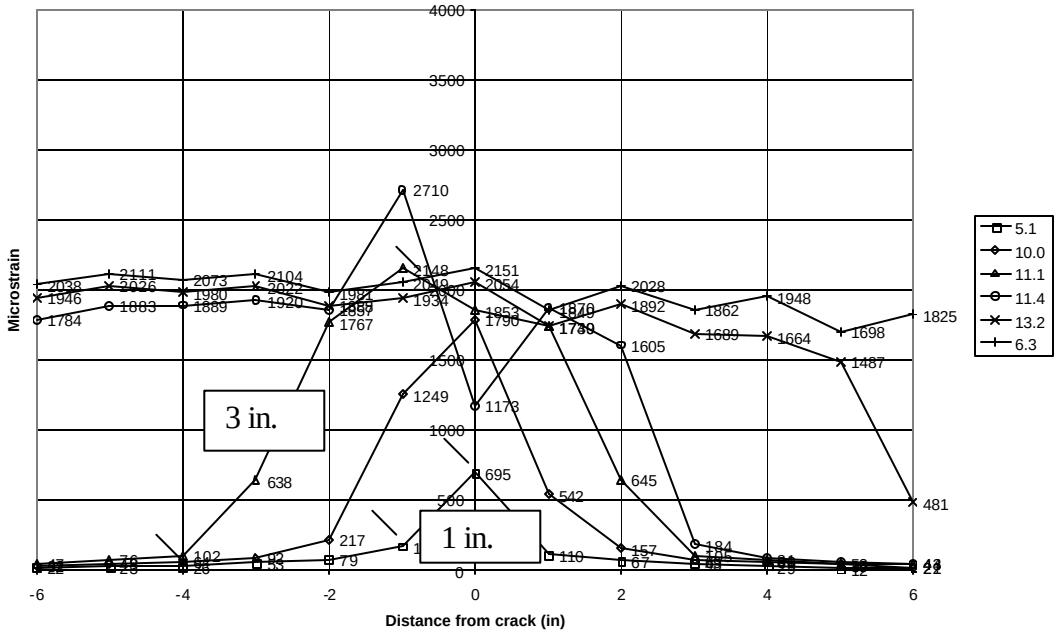

c) East surface gages

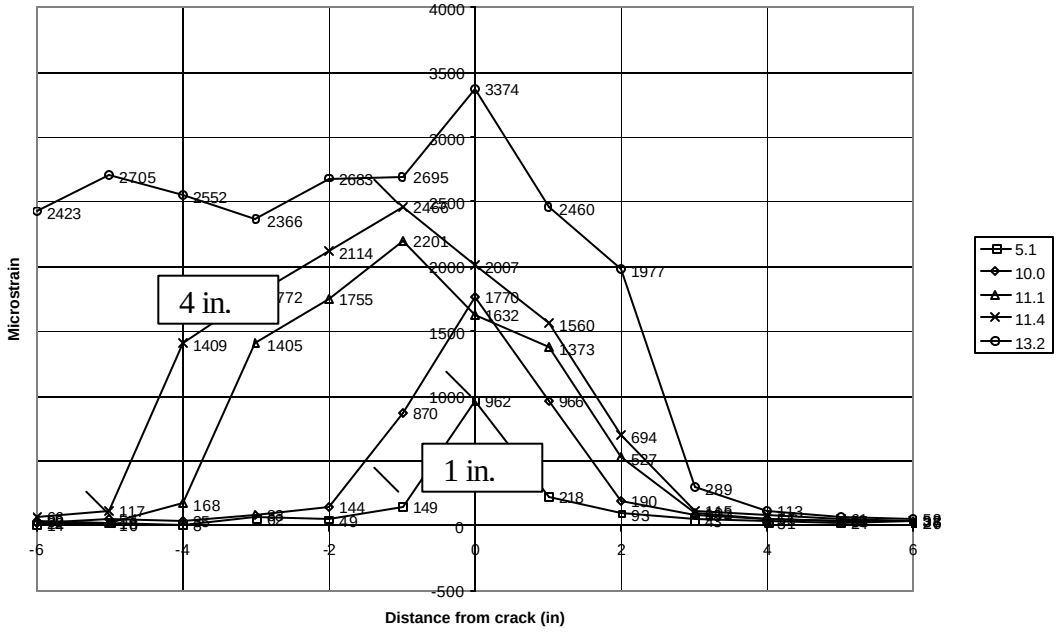

d) West surface gages

Figure F-2 E2-90-1 Data Plots cont.

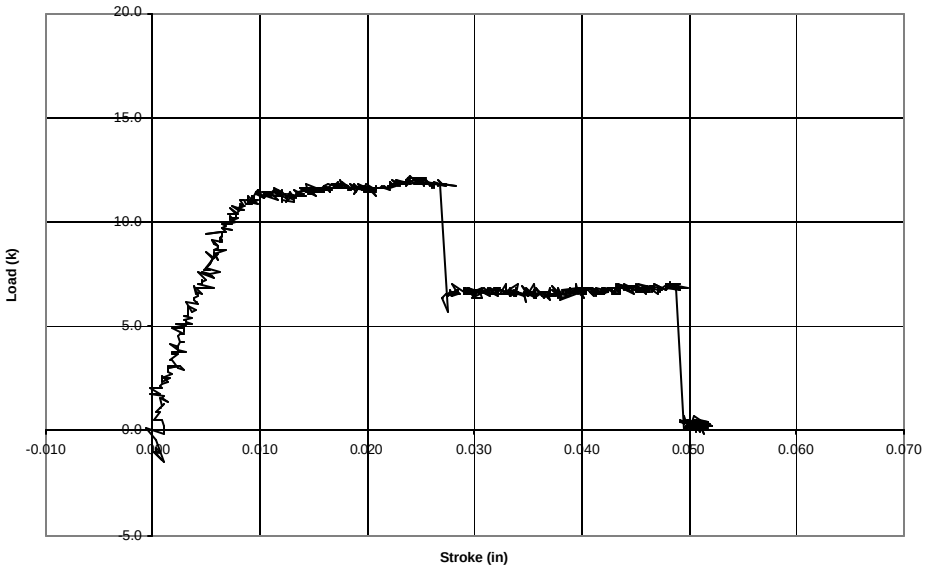

a) Load vs. stroke

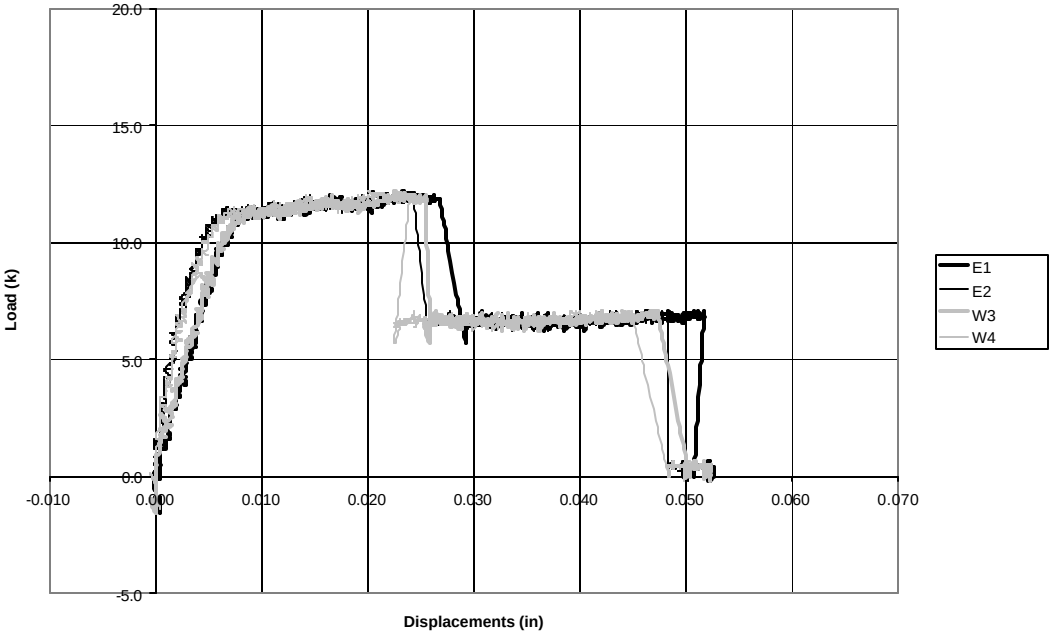

b) Load vs. LVDT Displacements

Figure F-3 E3-90-1-U2 Data Plots

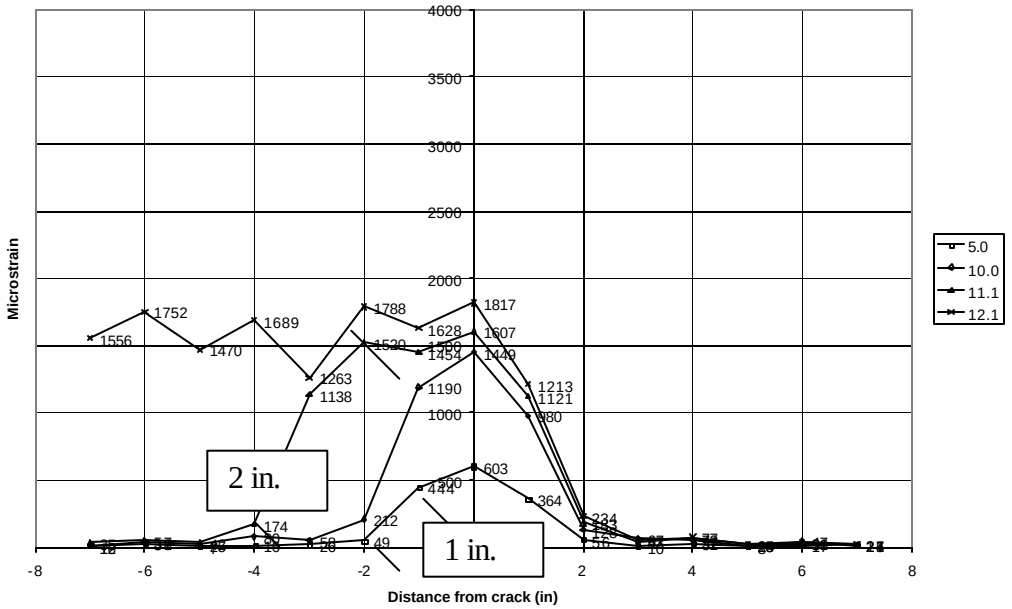

c) East surface gages

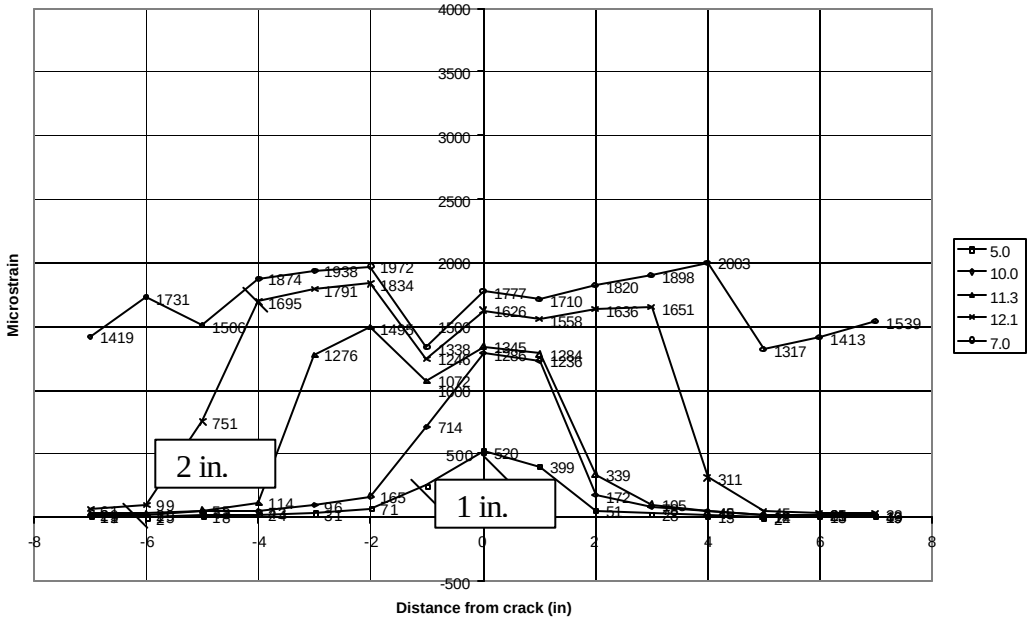

d) West surface gages

Figure F-3 E3-90-1-U2 Data Plots cont.

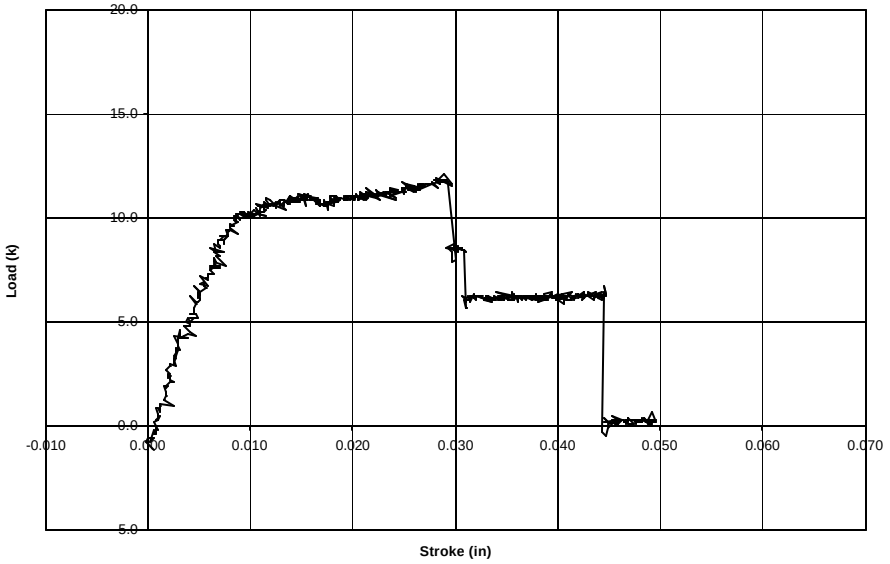

a) Load vs. stroke

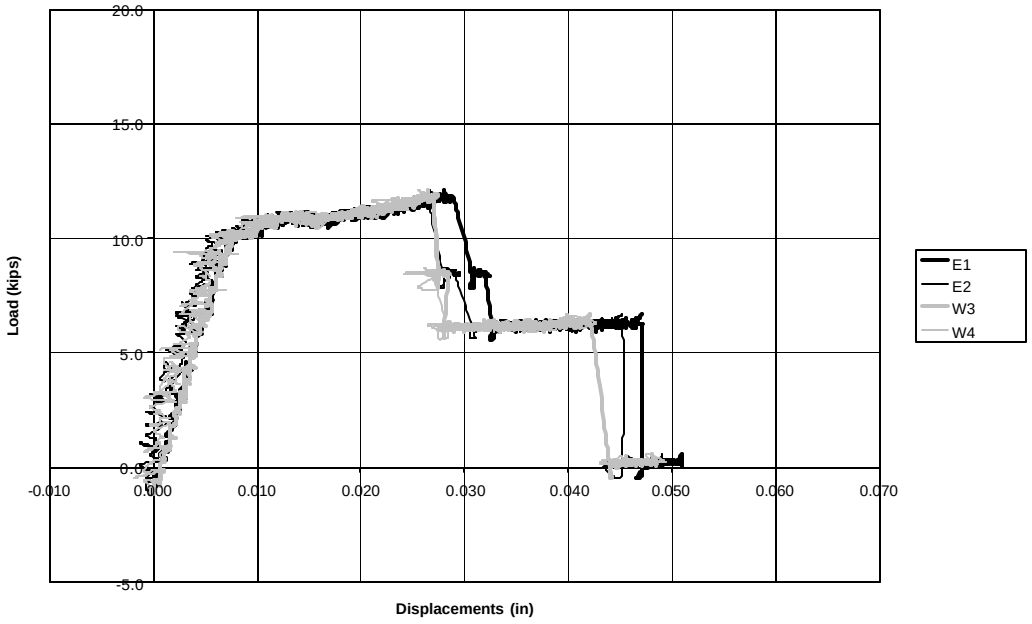

b) Load vs. LVDT Displacements

Figure F-4 E4-90-1-U2 Data Plots

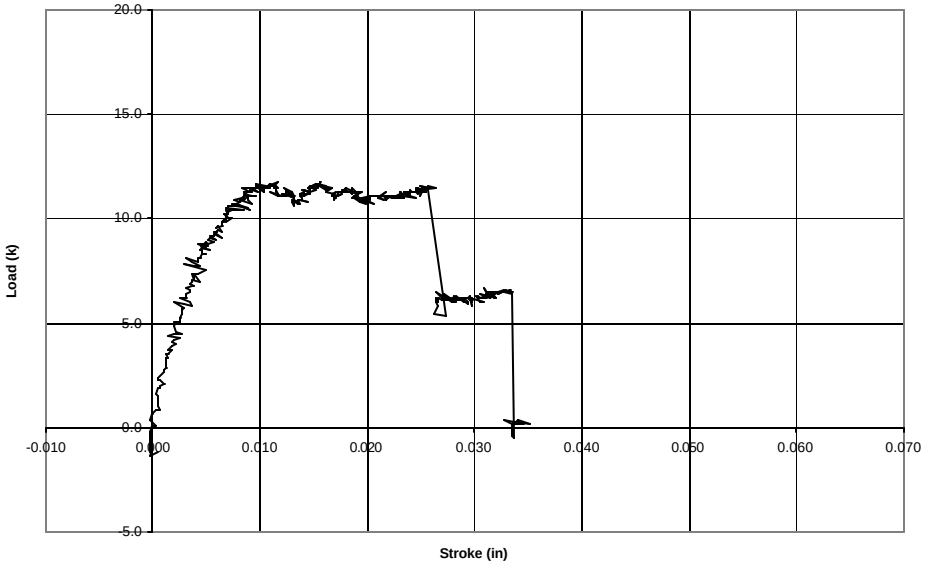

a) Load vs. stroke

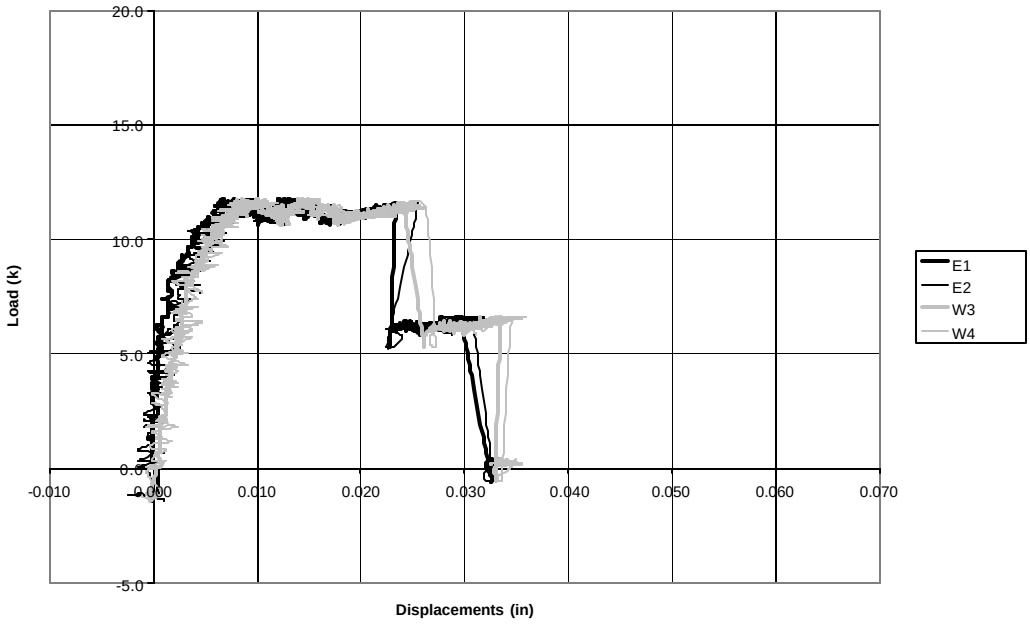

b) Load vs. LVDT Displacements

Figure F-5 E5-90-1-U1 Data Plots

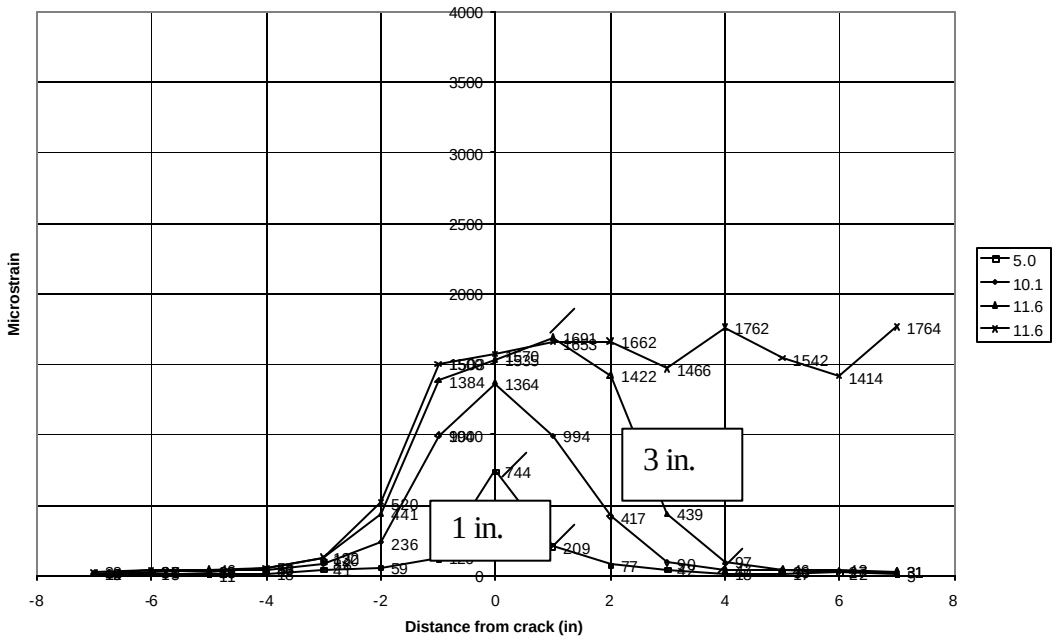

c) West surface gages

Figure F-5 E5-90-1-U1 Data Plots cont.

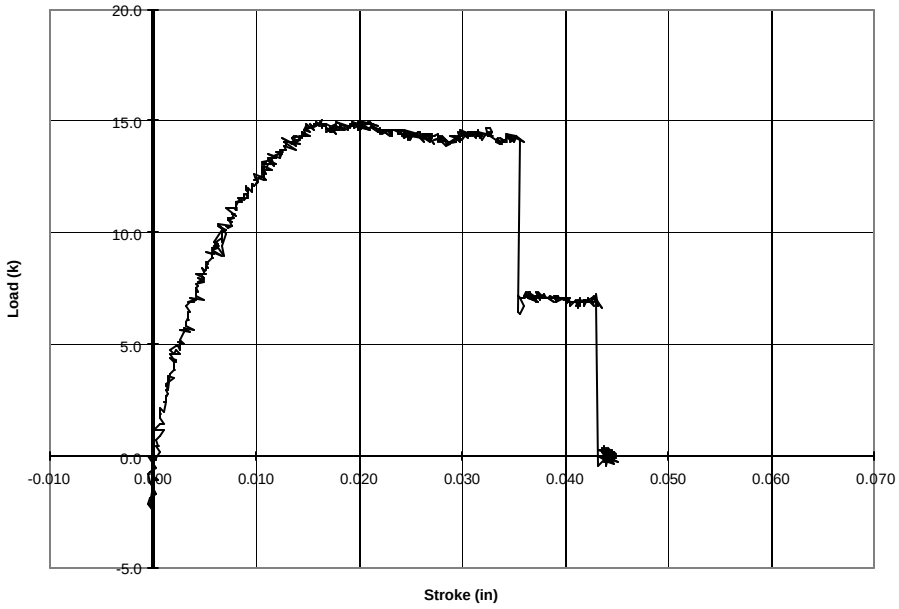

a) Load vs. stroke

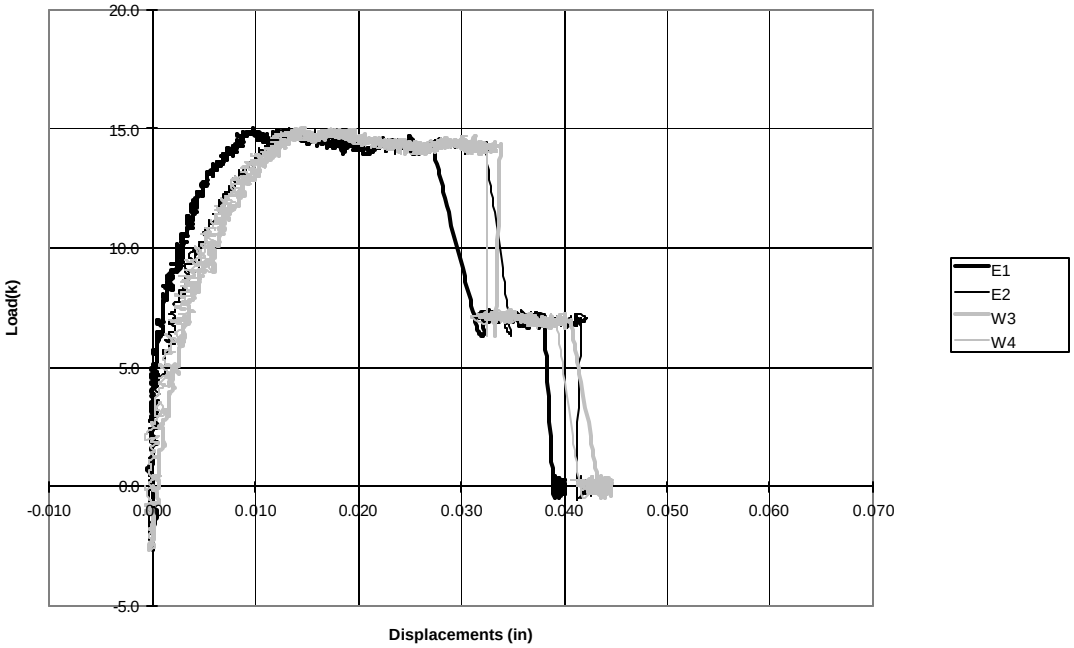

b) Load vs. LVDT Displacements

Figure F-6 E6-90-1 Data Plots

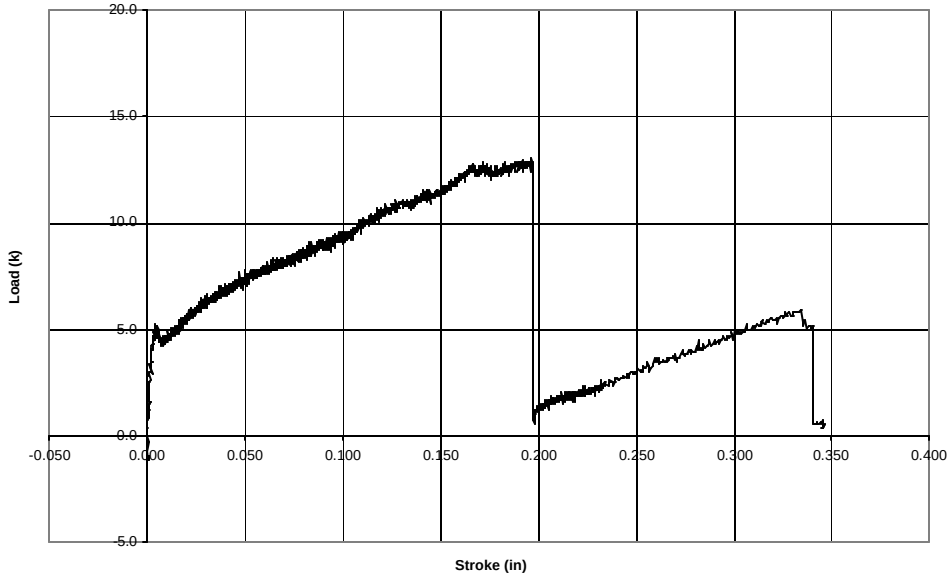

a) Load vs. stroke

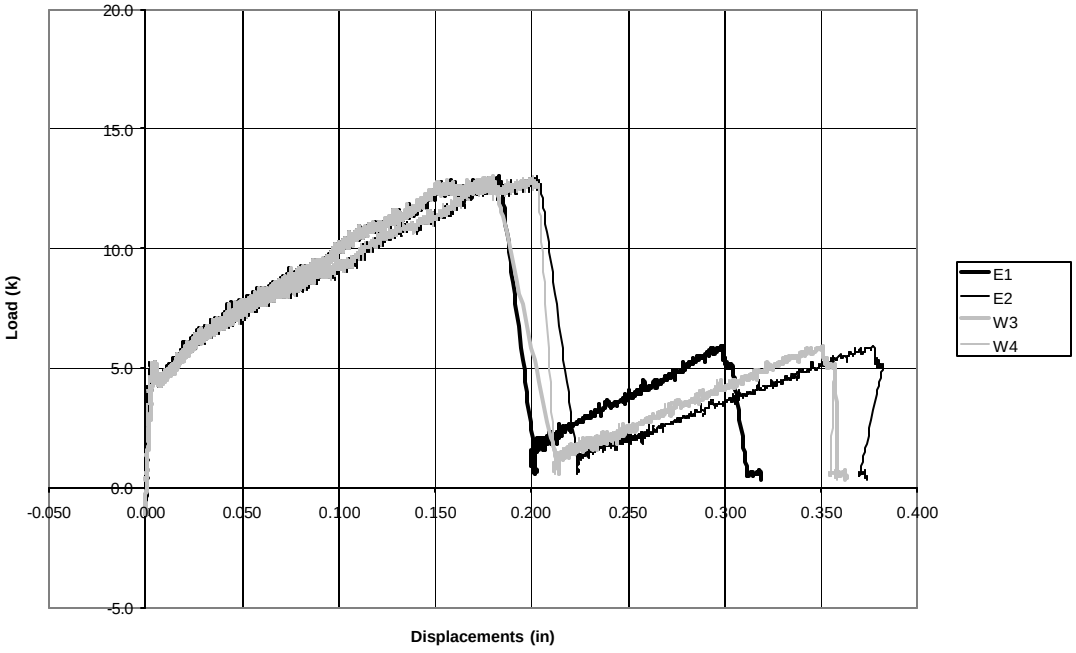

b) Load vs. LVDT Displacements

Figure F-7 E7-45-1 Data Plots

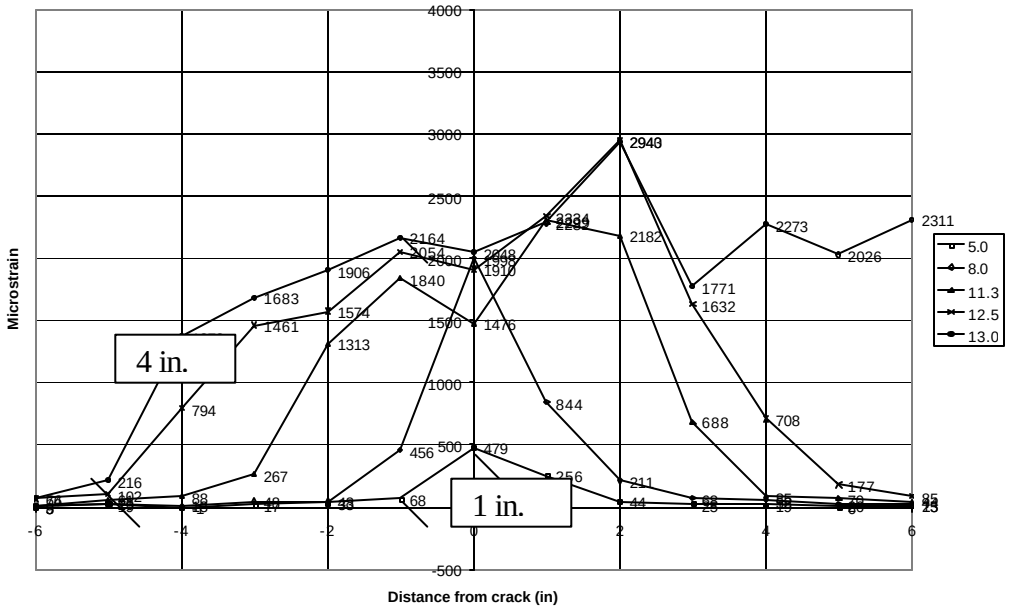

c) West surface gages

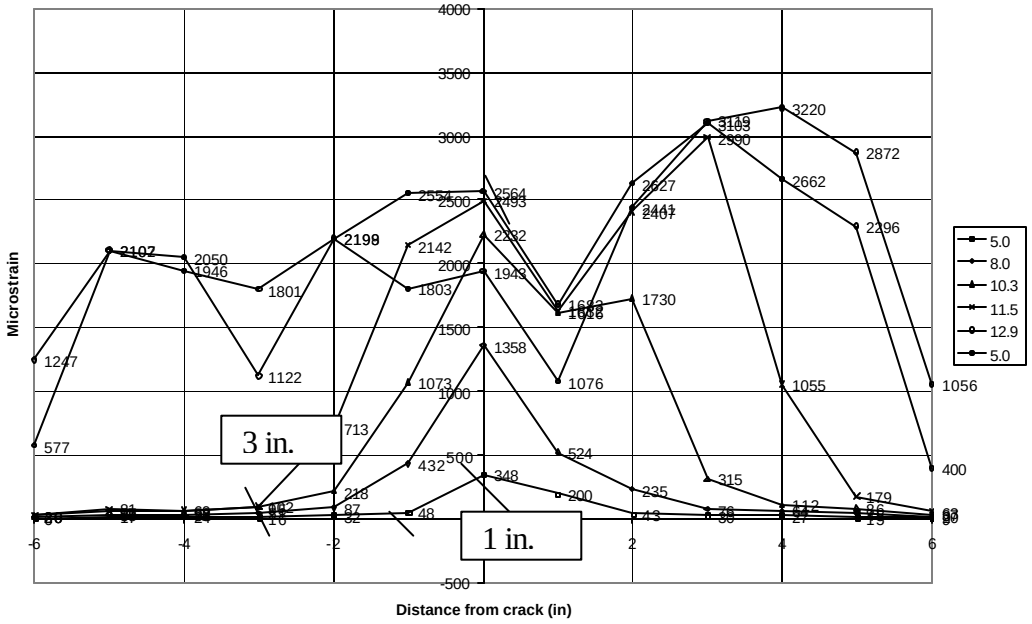

d) East surface gages

Figure F-7 E7-45-1 Data Plots cont.

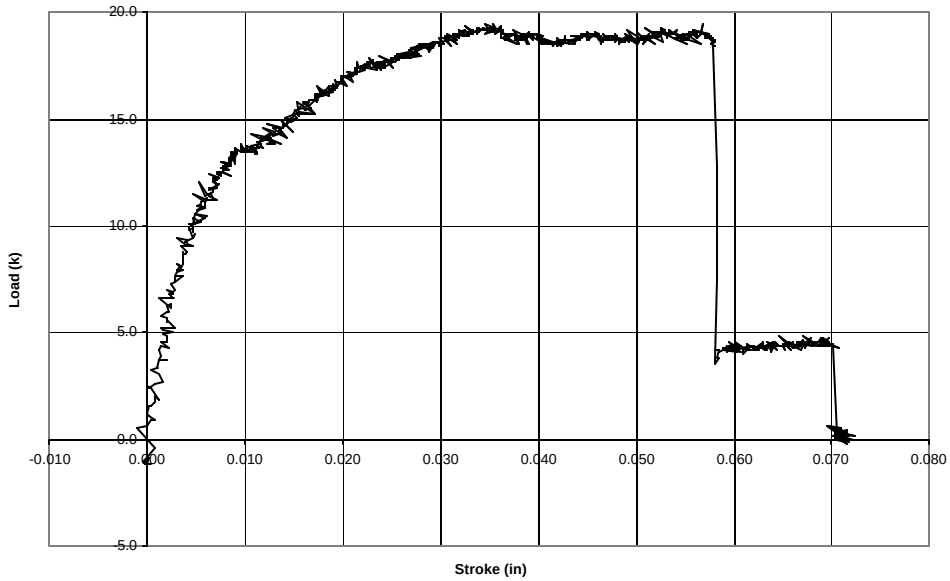

a) Load vs. stroke

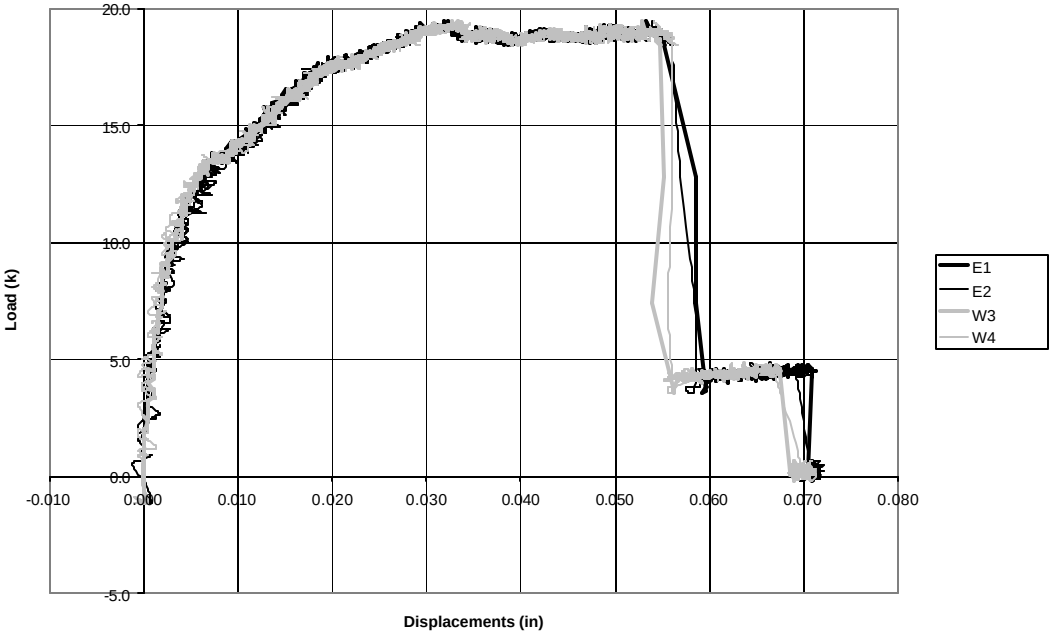

b) Load vs. LVDT Displacements

Figure F-8 E8-90-2 Data Plots

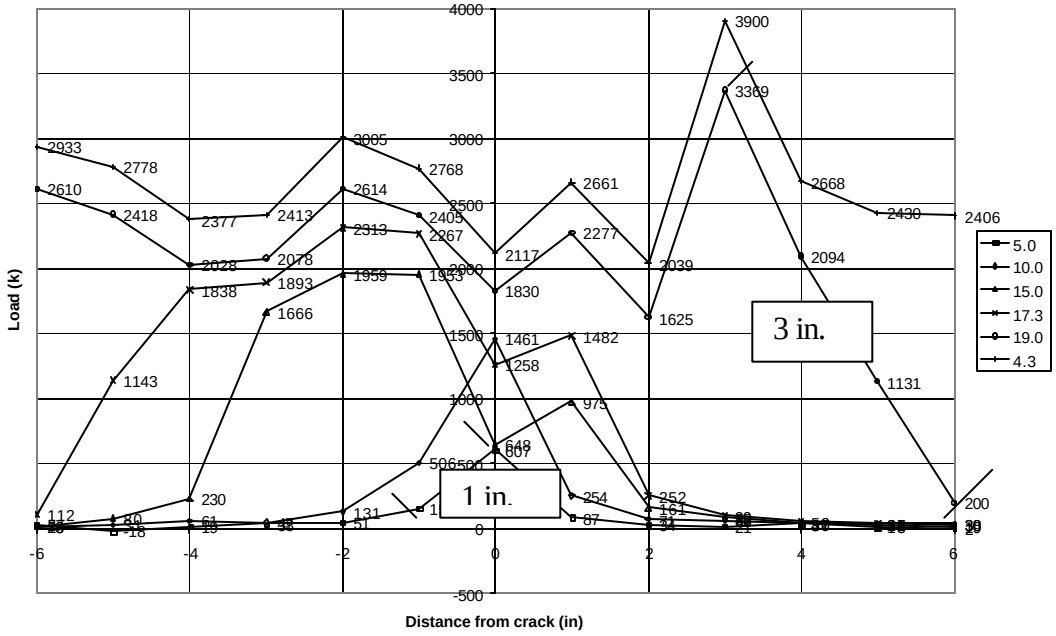

c) West south surface gages

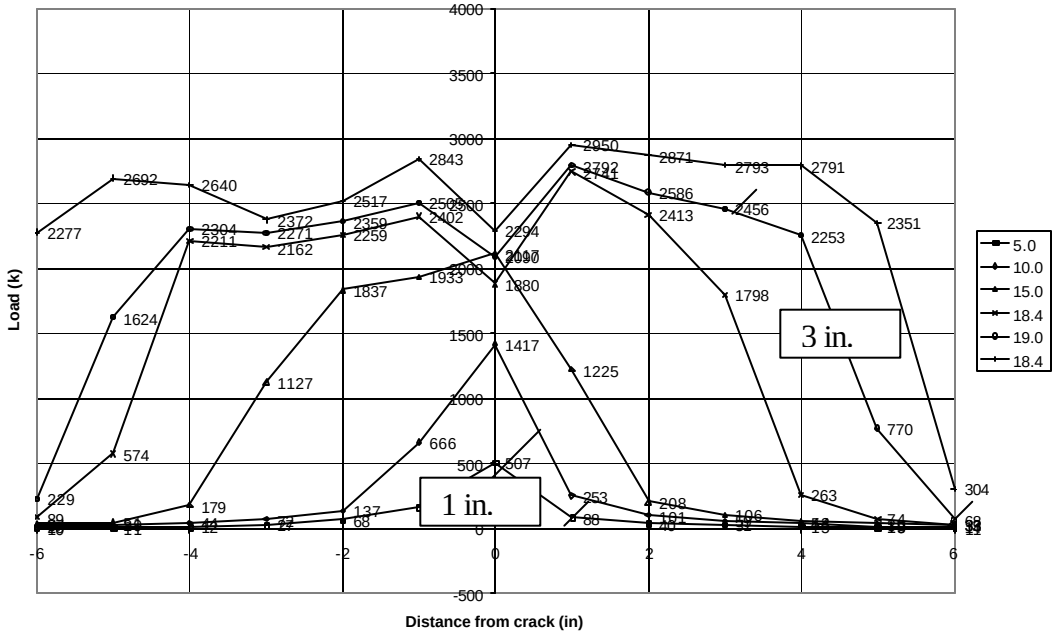

d) West north surface gages

Figure F-8 E8-90-2 Data Plots cont.

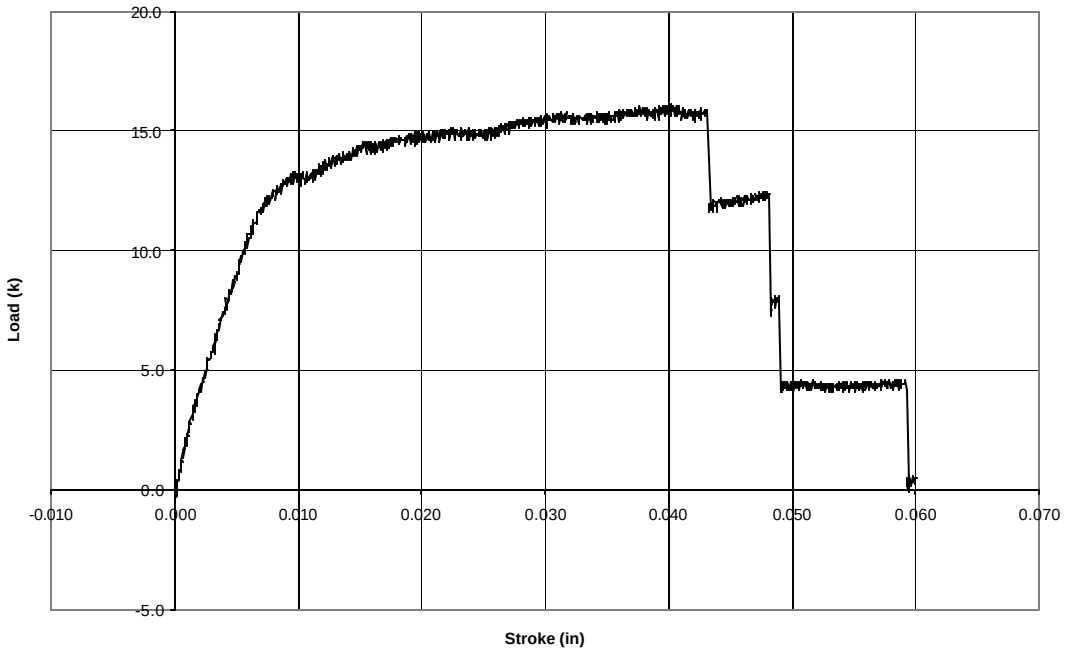

a) Load vs. stroke

Figure F-9 E9-90-2 Data Plots

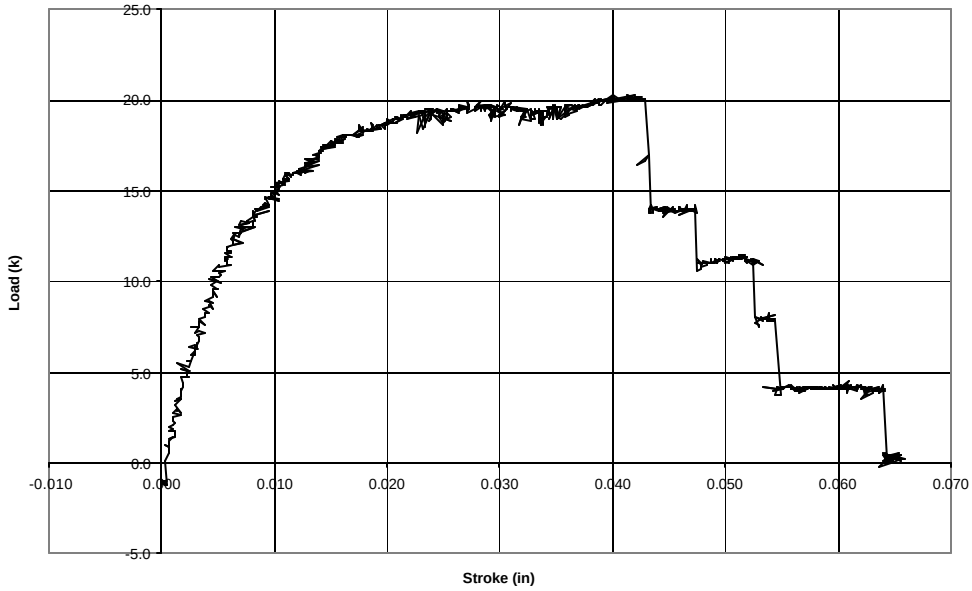

a) Load vs. stroke

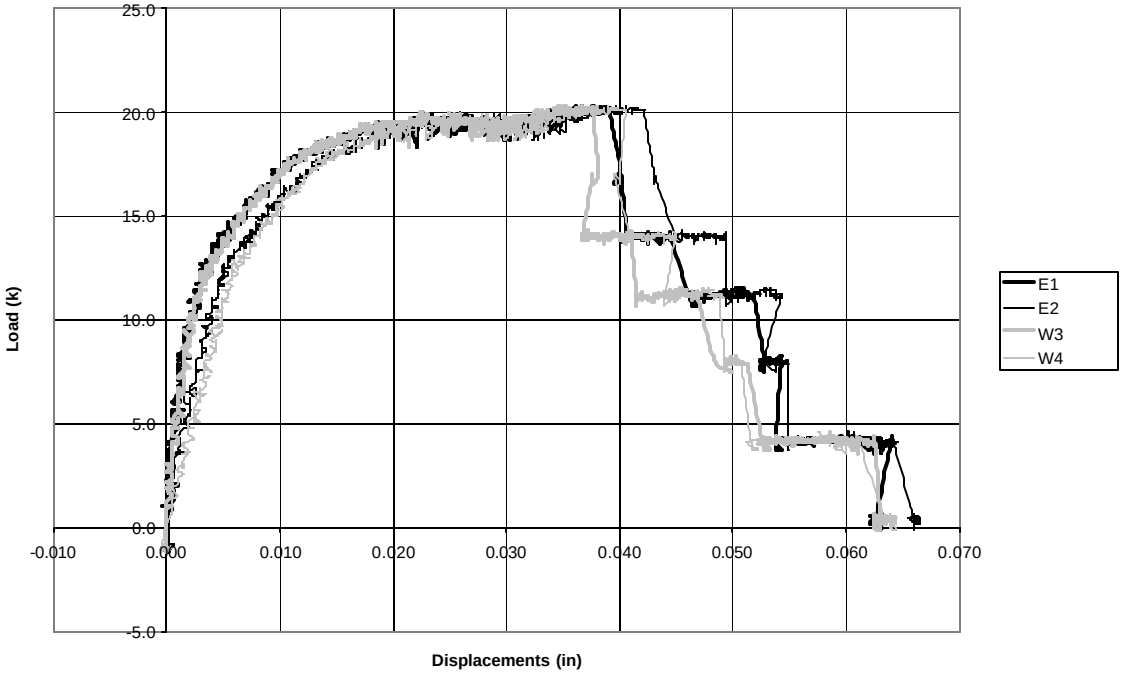

b) Load vs. LVDT Displacements

Figure F-10 E10-90-3 Data Plots

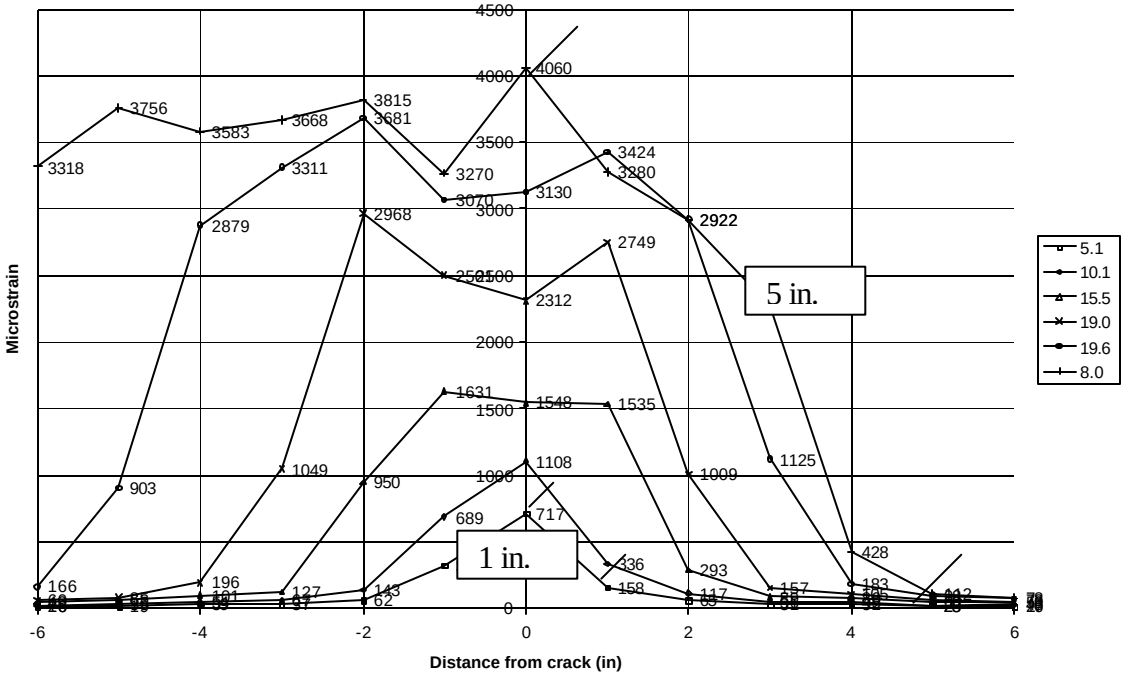

c) West center surface gages

Figure F-10 E10-90-3 Data Plots cont.

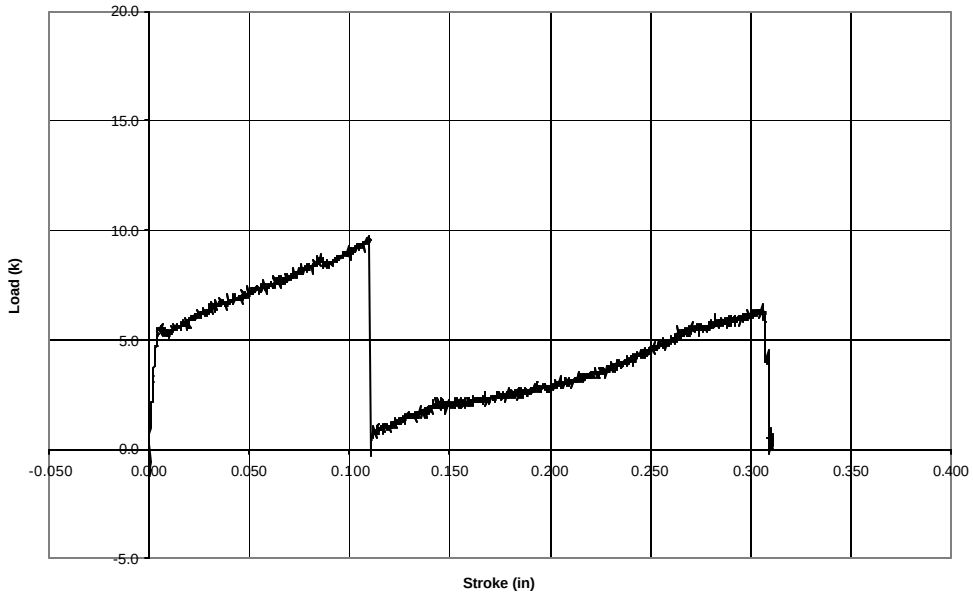

a) Load vs. stroke

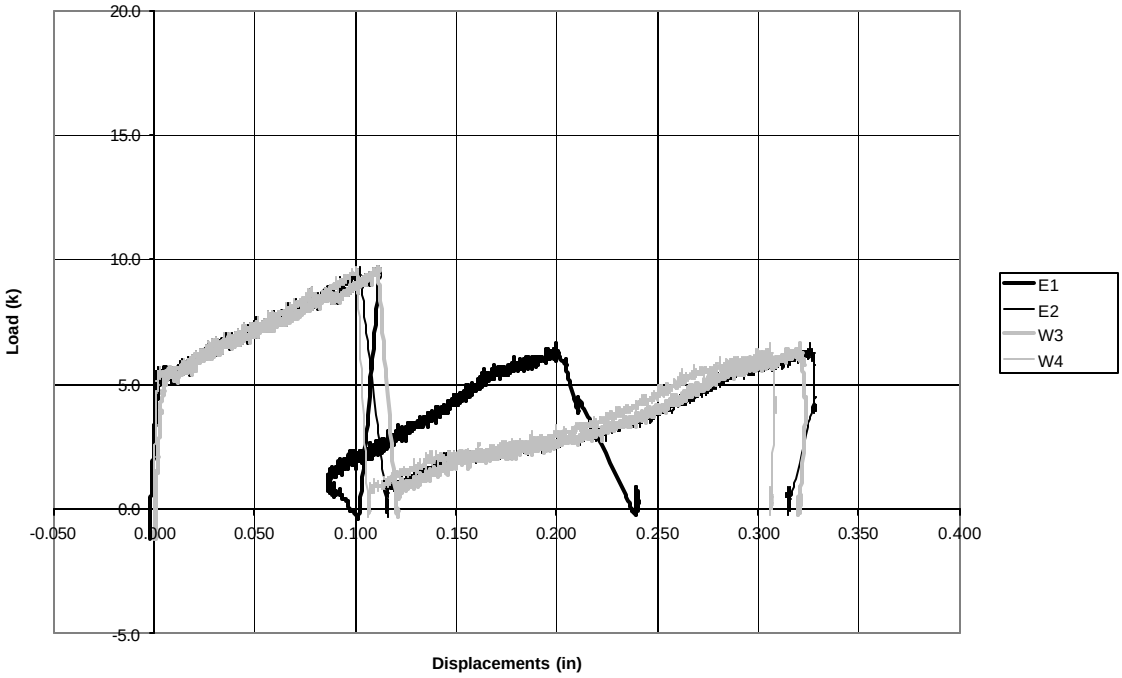

b) Load vs. LVDT Displacements

Figure F-11 E11-45-2 Data Plots

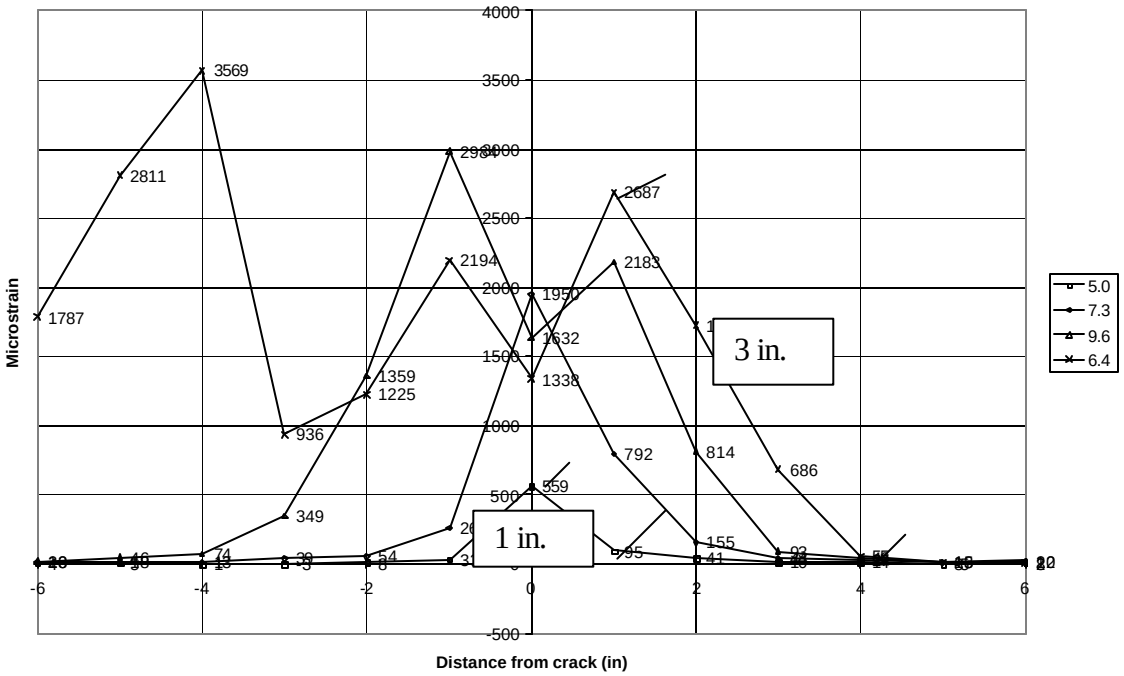

c) West south surface gages

Figure F-11 E11-45-2 Data Plots cont.

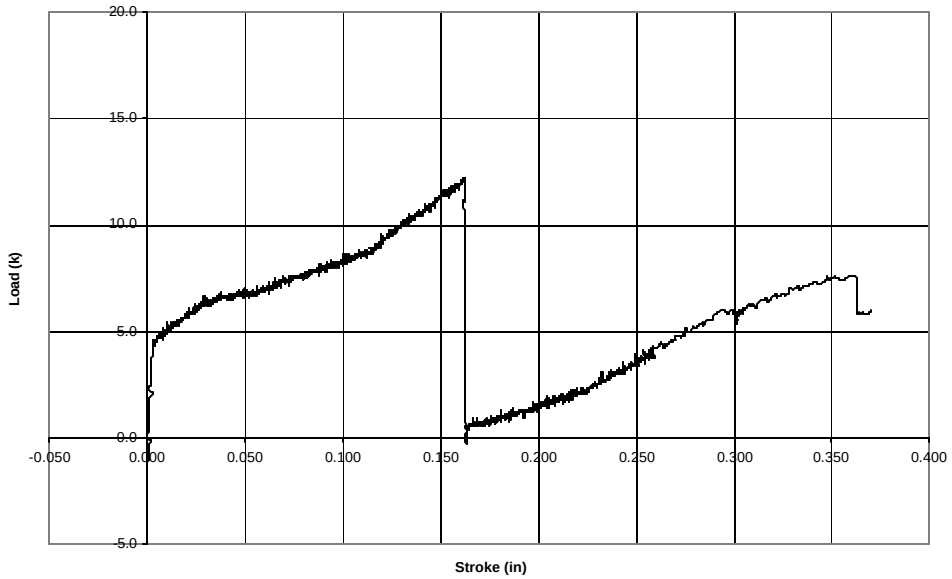

a) Load vs. stroke

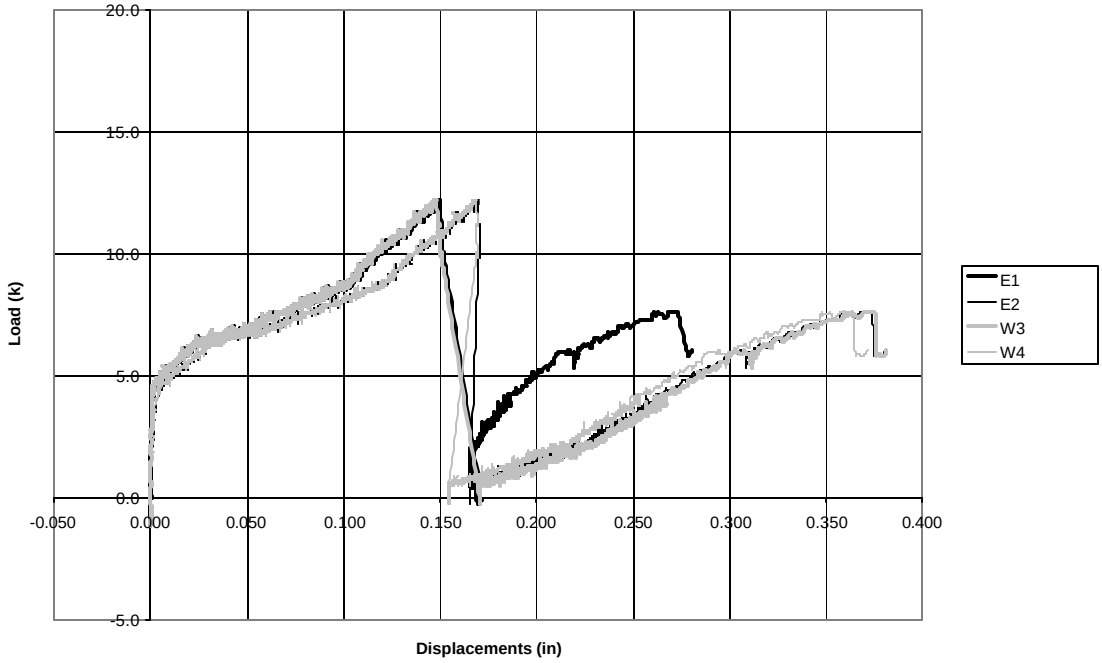

b) Load vs. LVDT Displacements

Figure F-12 E12-45-3 Data Plots

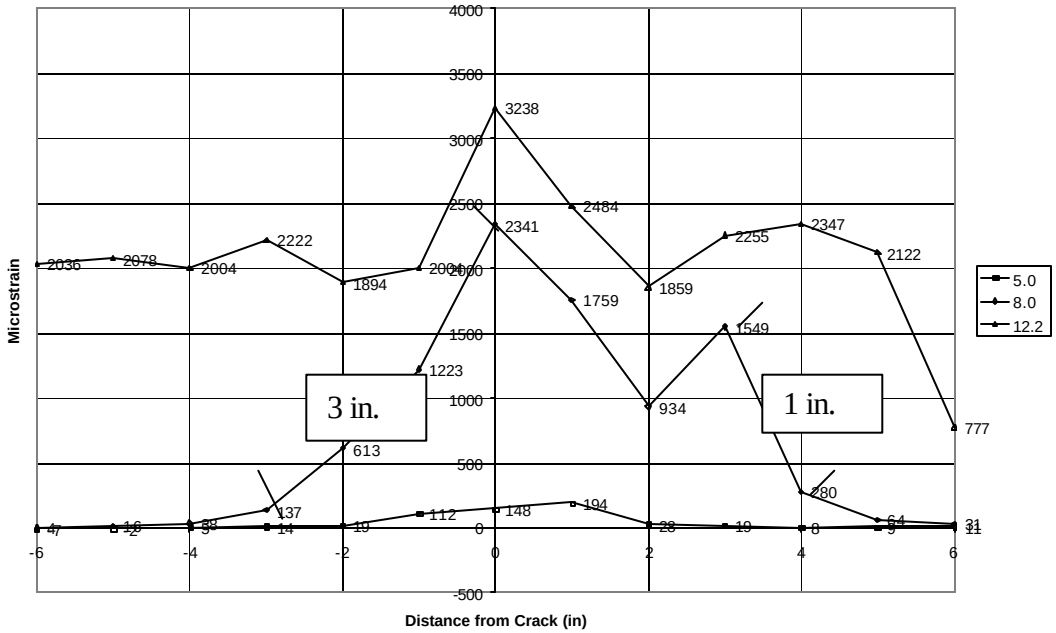

c) West center surface gages

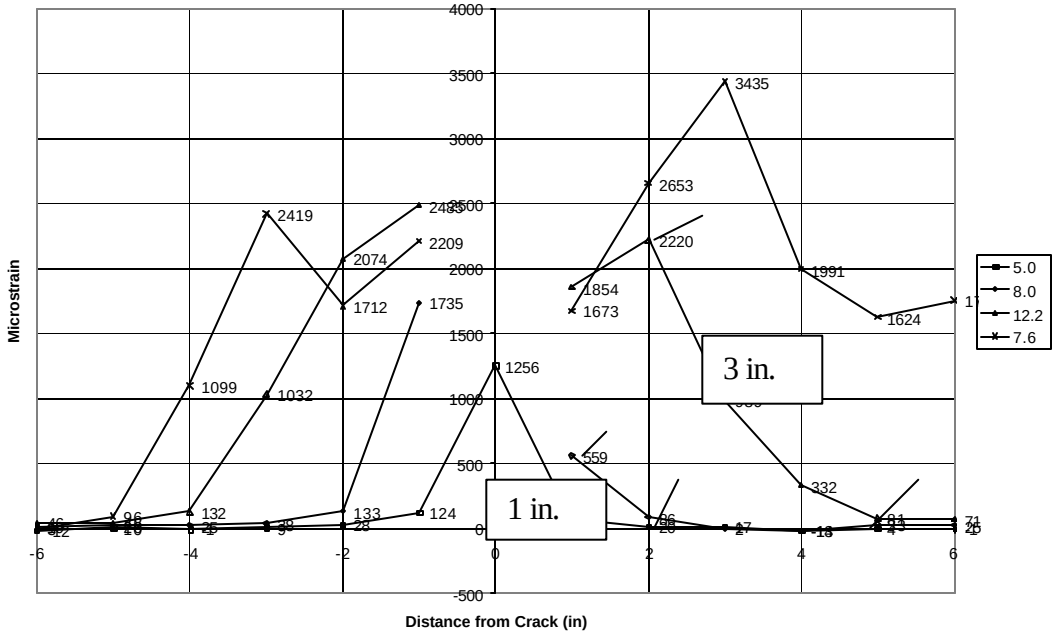

c) East center surface gages

Figure F-12 E12-45-3 Data Plots cont.

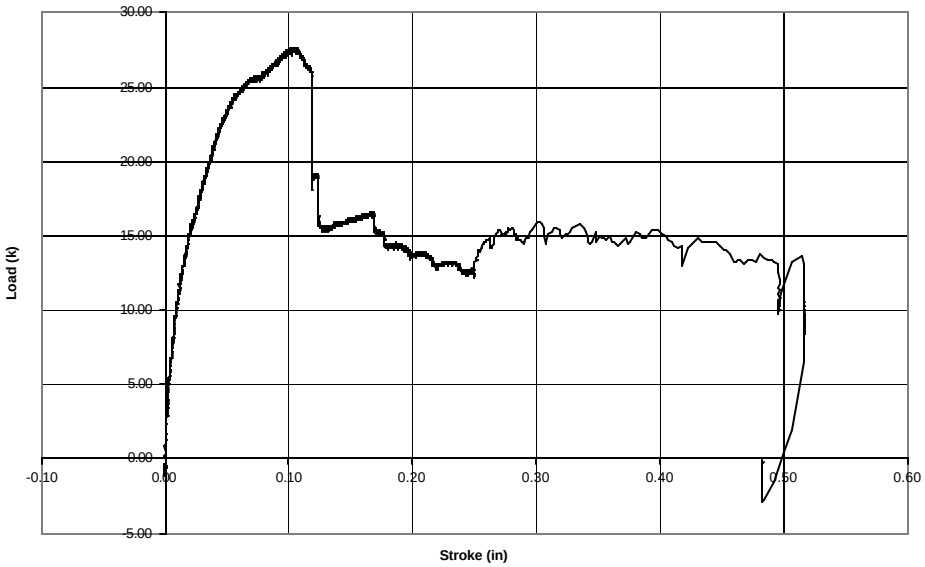

a) Load vs. stroke

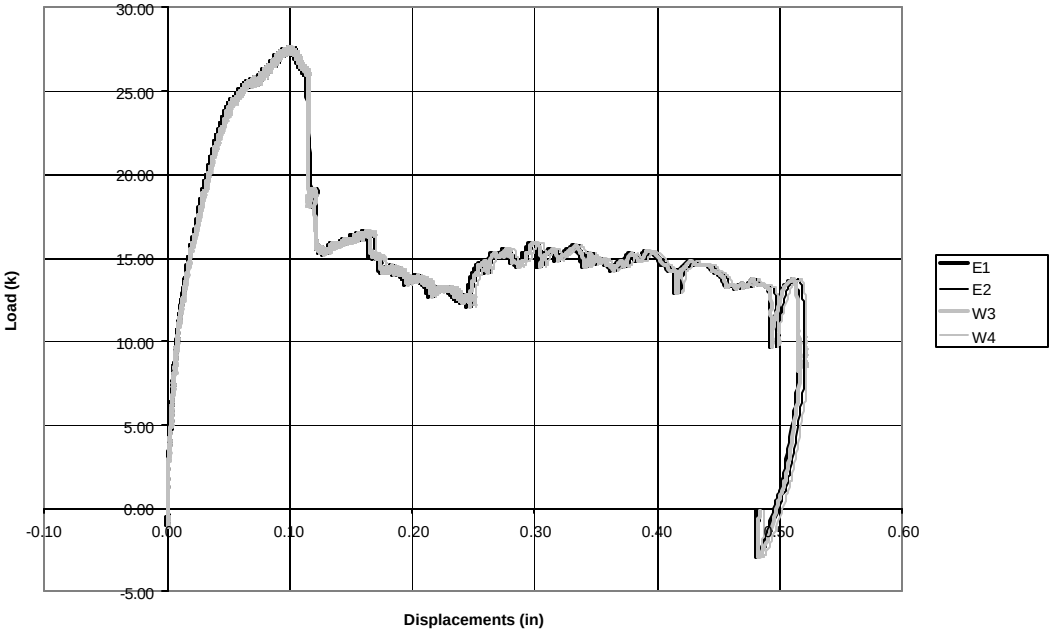

b) Load vs. LVDT Displacements

Figure F-13 NA13-90-2 Data Plots

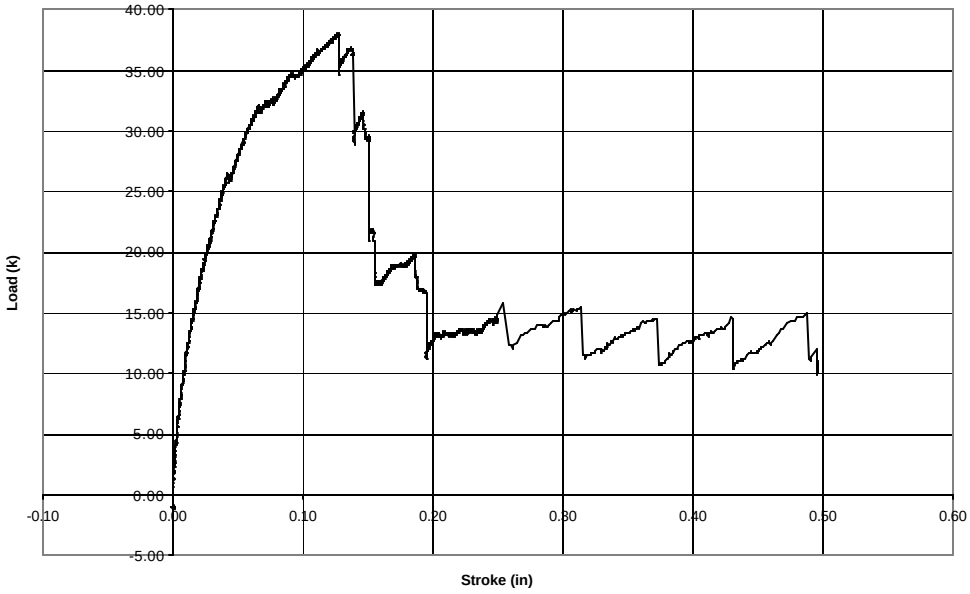

a) Load vs. stroke

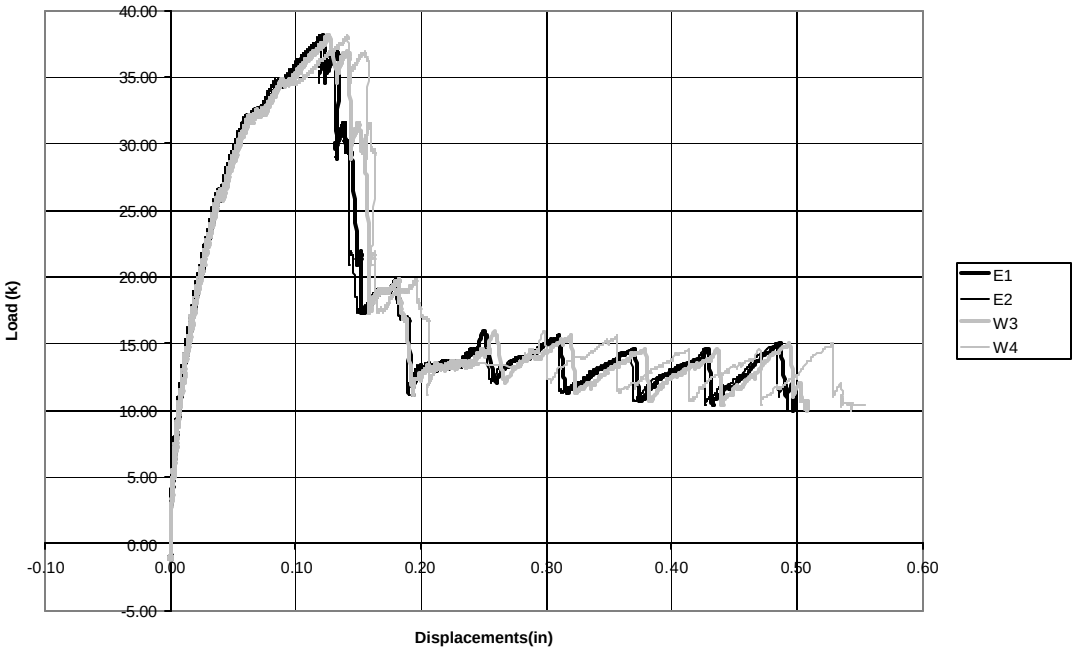

b) Load vs. LVDT Displacements

Figure F-14 NA14-90-2 Data Plots

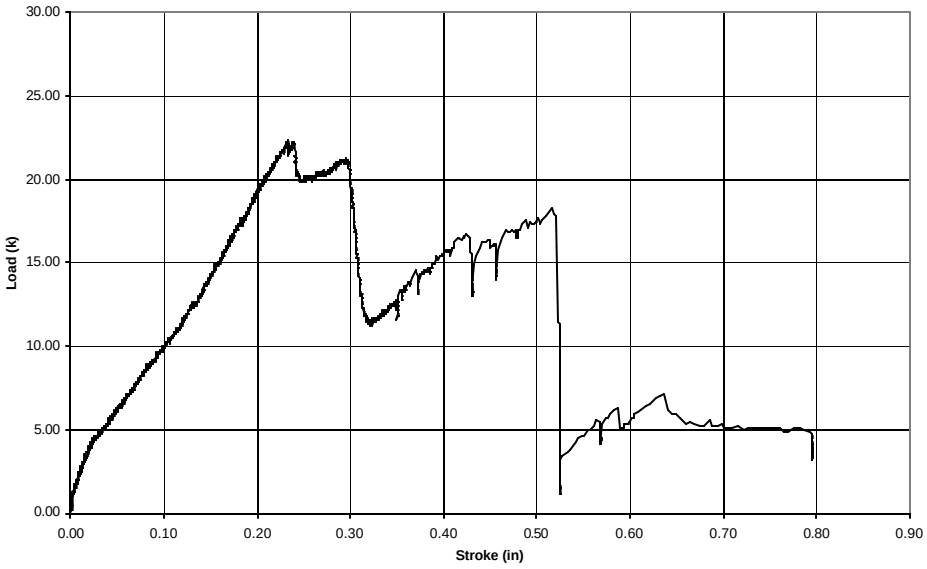

a) Load vs. stroke

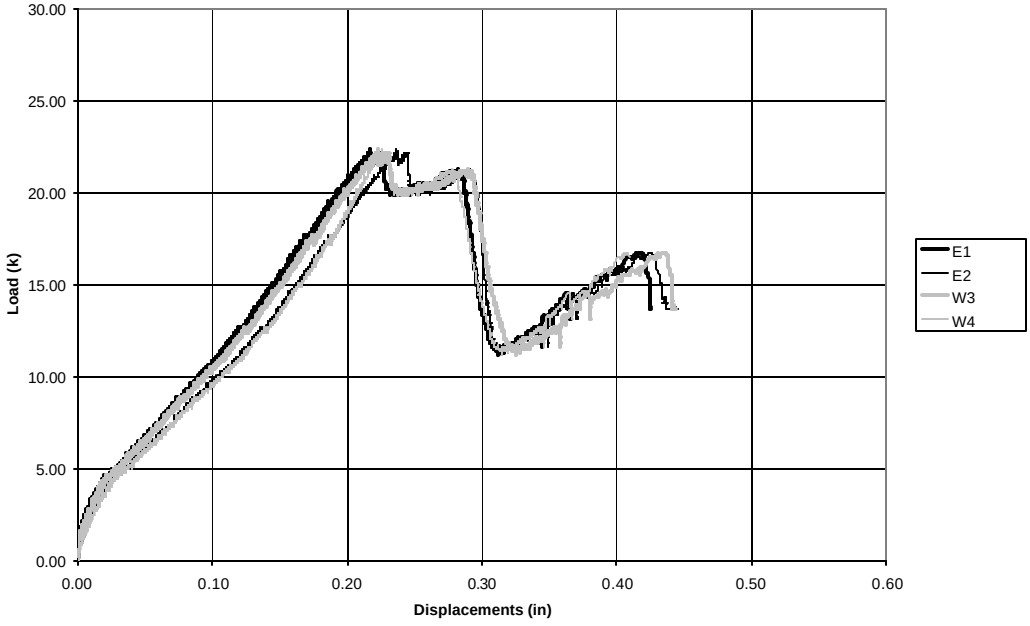

b) Load vs. LVDT Displacements

Figure F-15 NA15-45-2 Data Plots

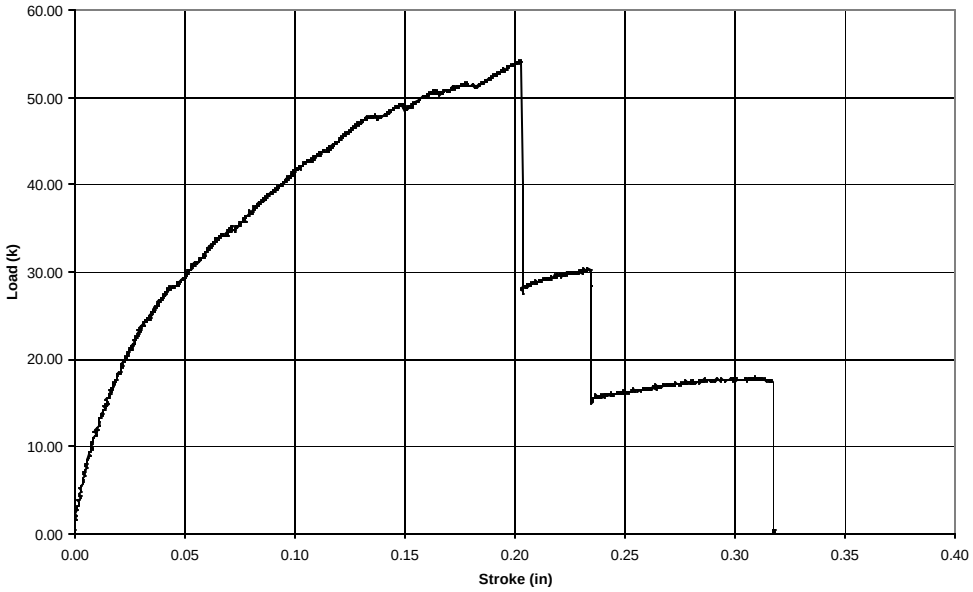

a) Load vs. stroke

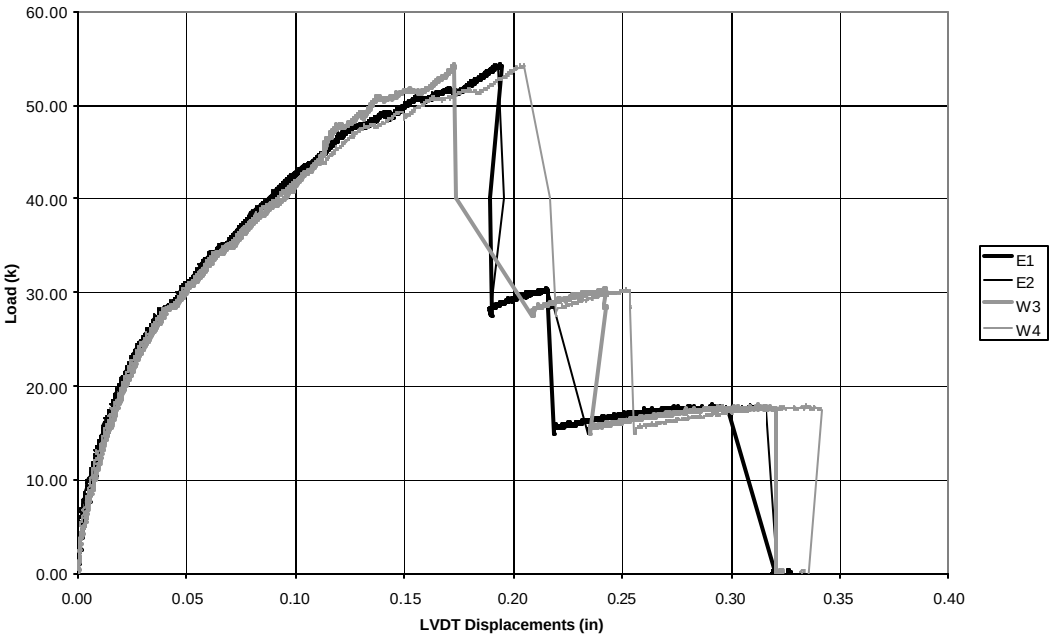

b) Load vs. LVDT Displacements

Figure F-16 NB16-90-2 Data Plots

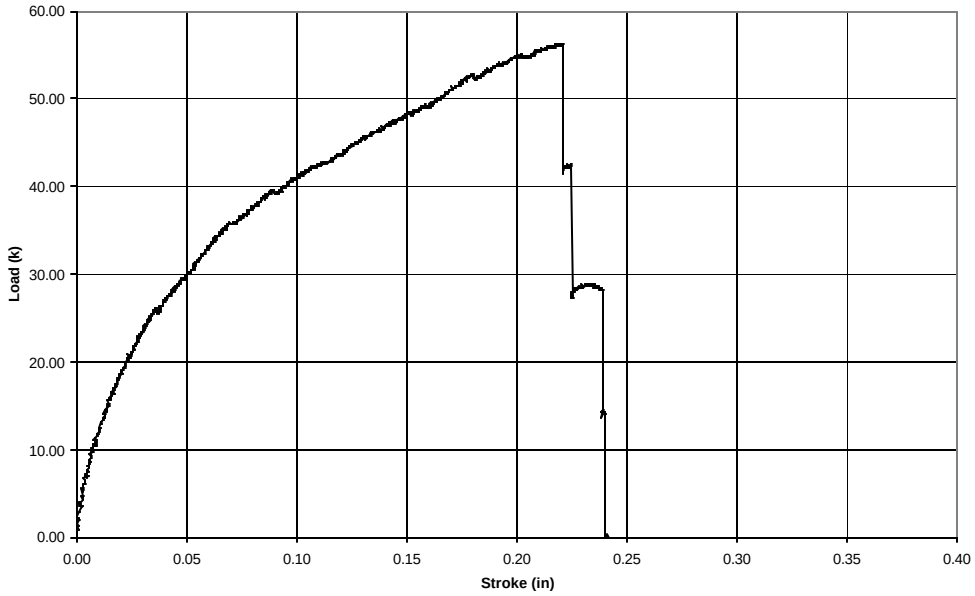

a) Load vs. stroke

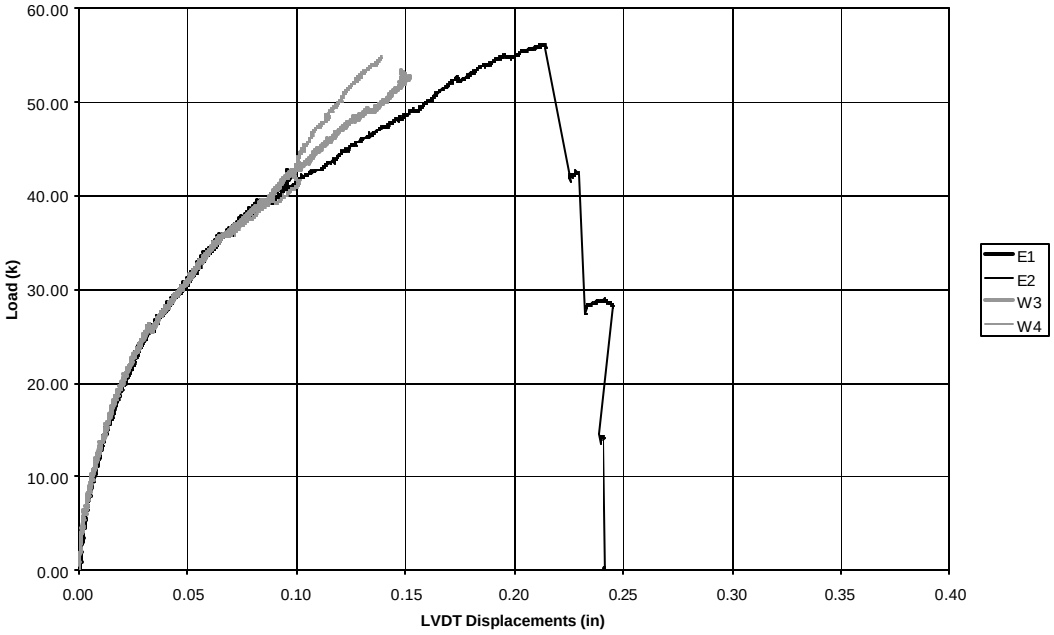

b) Load vs. LVDT Displacements

Figure F-17 NB17-90-2 Data Plots

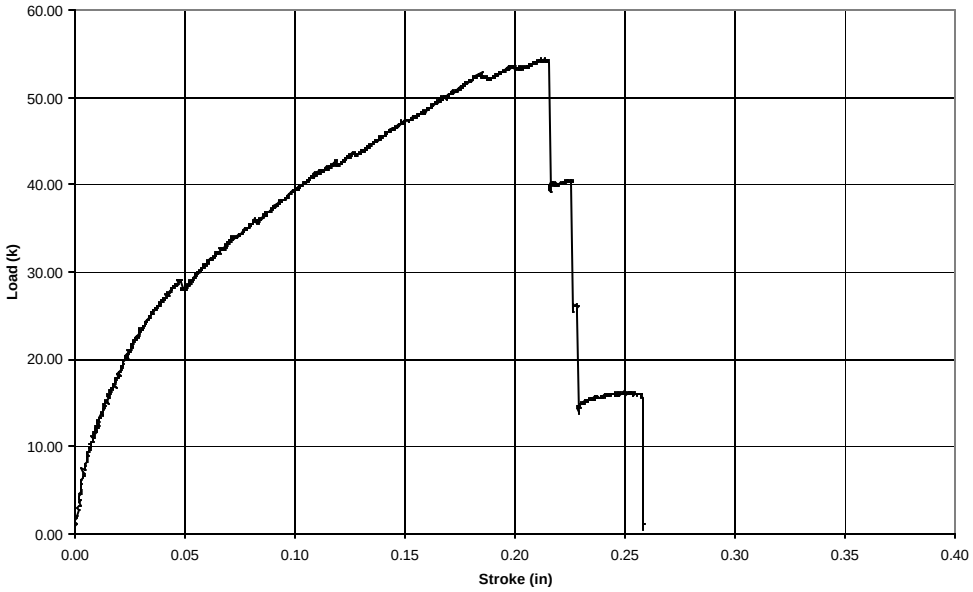

a) Load vs. stroke

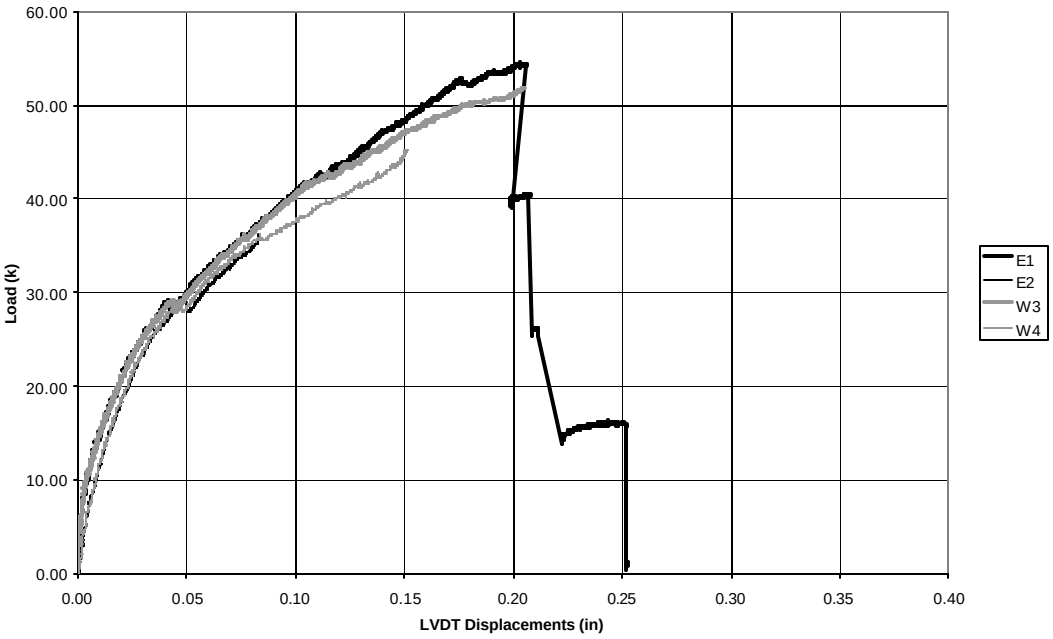

b) Load vs. LVDT Displacements

Figure F-18 NB18-90-2V Data Plots

Appendix G Bond Test Failure Surfaces

List of Tables

List of Figures

Photographs of the failure surfaces of the bond tests are shown in Figures G-1 through G-18. The numbering on the labels in the photographs of the bond test specimens does not match the captions because the numbering system was changed as shown in Table G-1.

Table G-1 Labeling Convention

Original Label	New Label
1	E1-90-1
2	E2-90-1
3	E3-90-1-U2
3R	E4-90-1-U2
4	E5-90-1-U1
4A	E6-90-1
5	E7-45-1
6	E8-90-2
7	E9-90-2
8	E10-90-3
9	E11-45-2
13	E12-45-3
10	NA13-90-2
11	NA14-90-2
12	NA15-45-2
16	NB16-90-2
17	NB17-90-2
18	NB18-90-2V

a) West Concrete b) West FRP

Figure G-1 Test E1-90-1 Failure Surfaces

c) East Concrete

d) East FRP

Figure G-1 Test E1-90-1 Failure Surfaces cont.

a) West Concrete

b) West FRP

Figure G-2 Test E2-90-1 Failure Surfaces

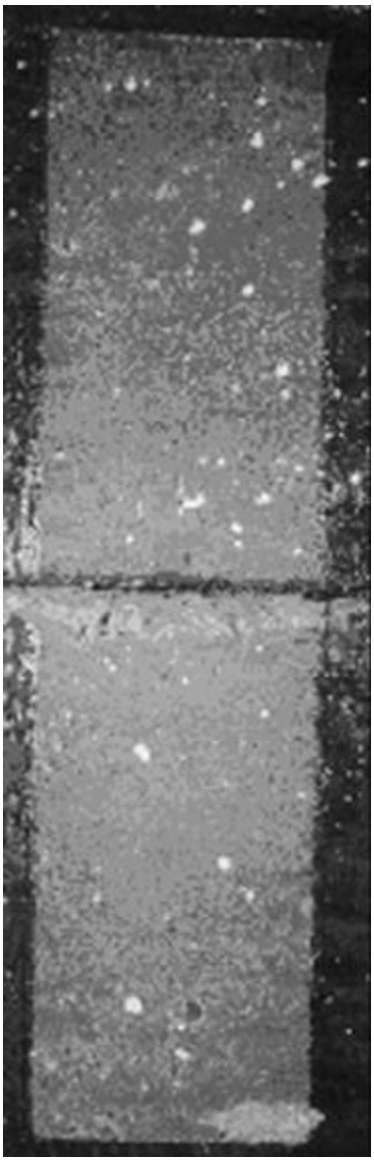

c) East Concrete

d) East FRP

Figure G-2 Test E2-90-1 Failure Surfaces cont.

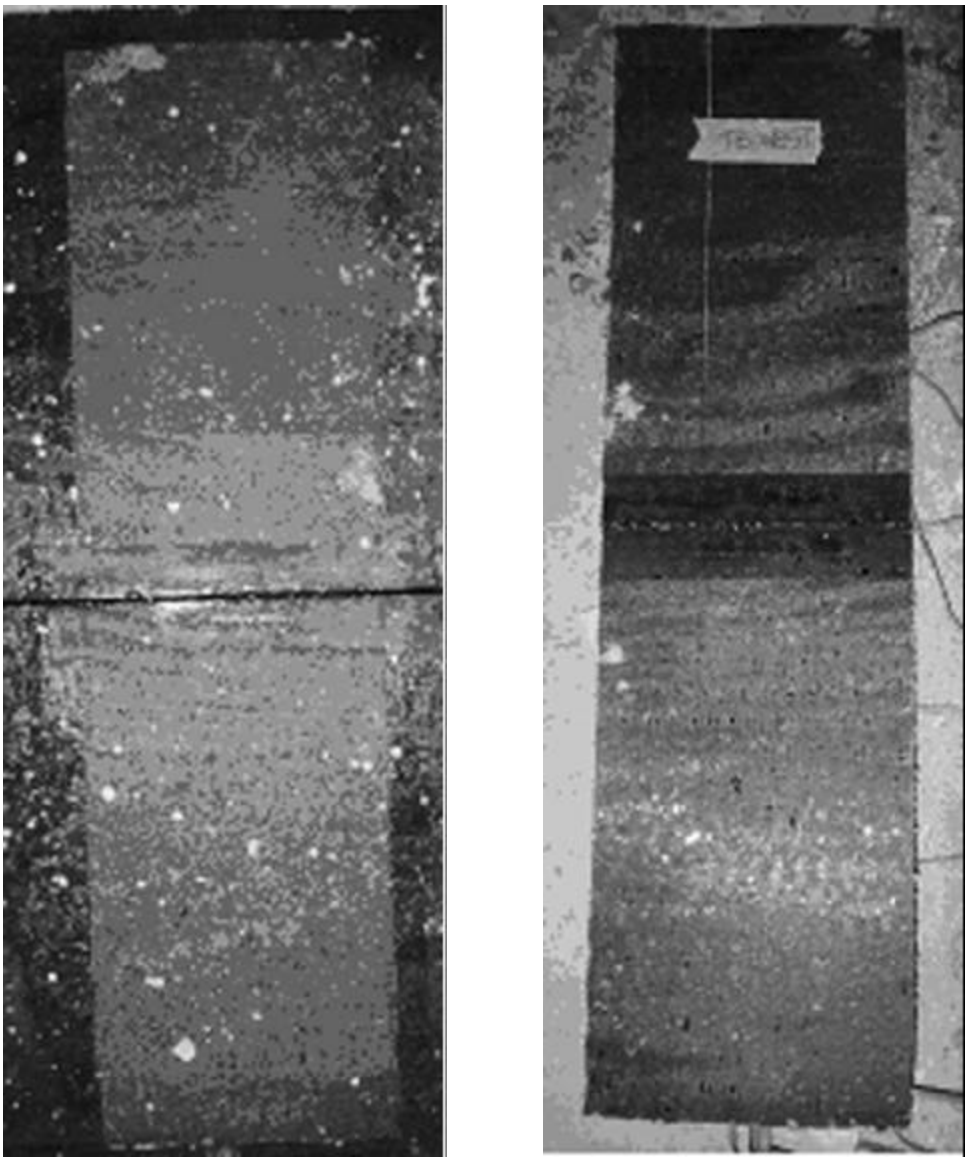

a) West Concrete b) West FRP

Figure G-3 Test E3-90-1-U2 Failure Surfaces

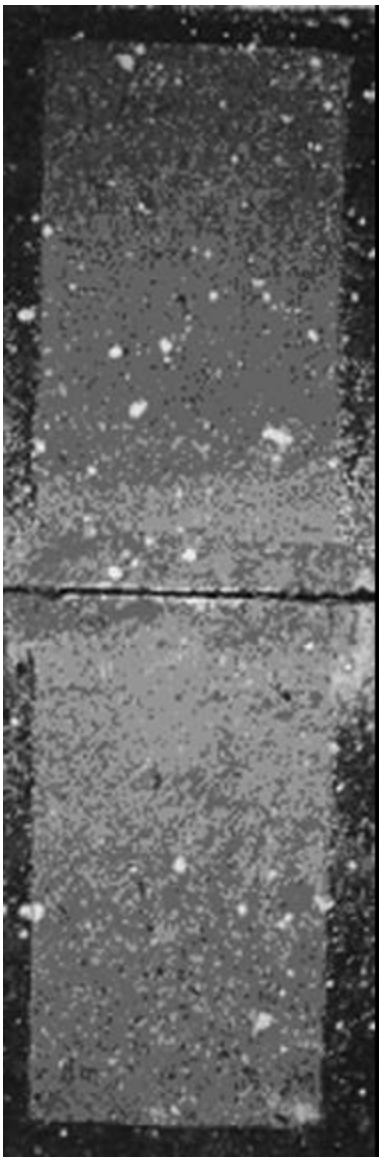

c) East Concrete

d) East FRP

Figure G-3 Test E3-90-1-U2 Failure Surfaces cont.

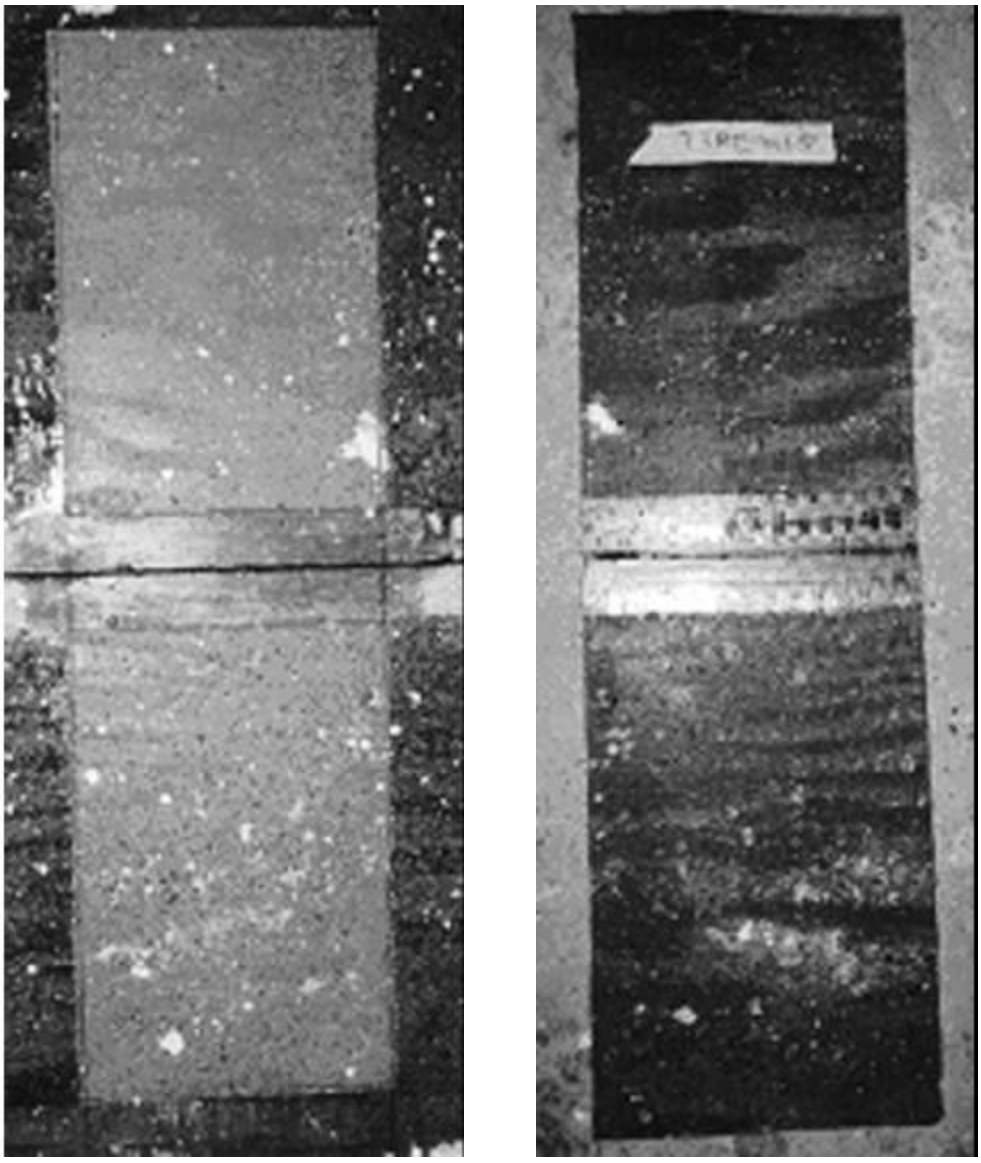

a) West Concrete b) West FRP

Figure G-4 Test E4-90-1-U2 Failure Surfaces

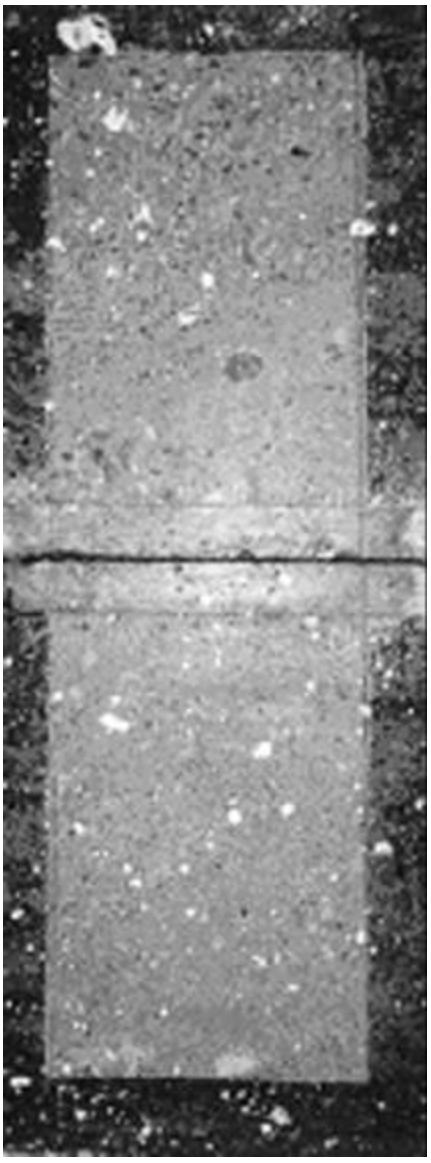

c) East Concrete d) East FRP

Figure G-4 Test E4-90-1-U2 Failure Surfaces cont.

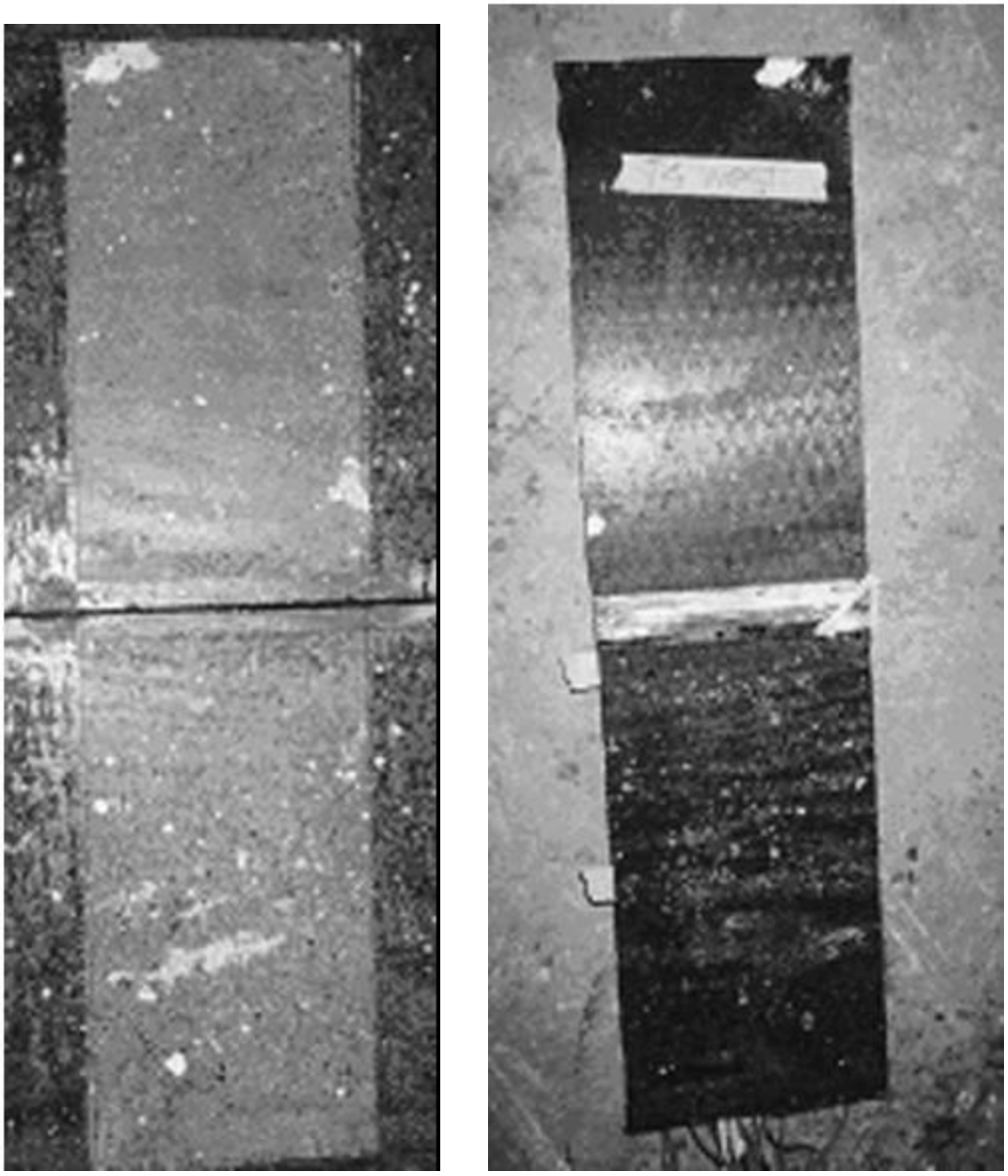

a) West Concrete b) West FRP

Figure G-5 Test E5-90-1-U1 Failure Surfaces

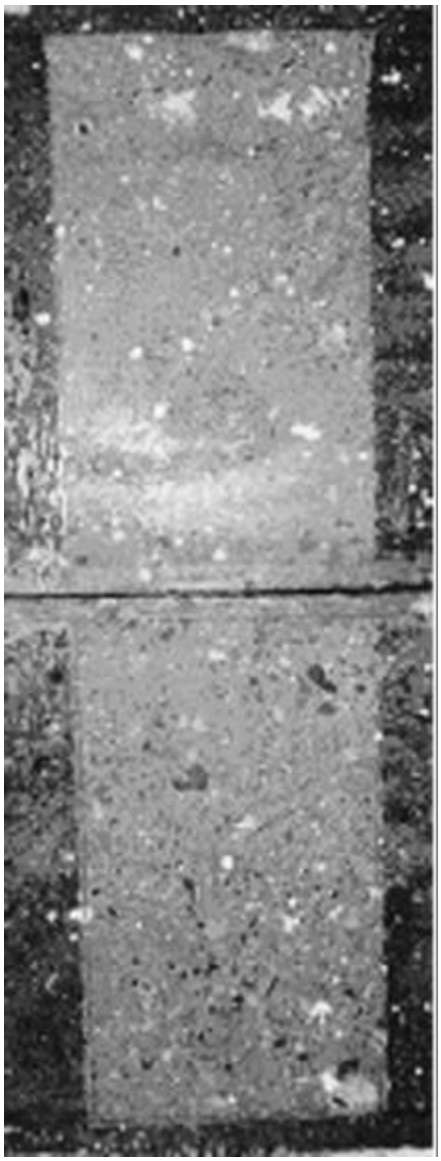

c) East Concrete

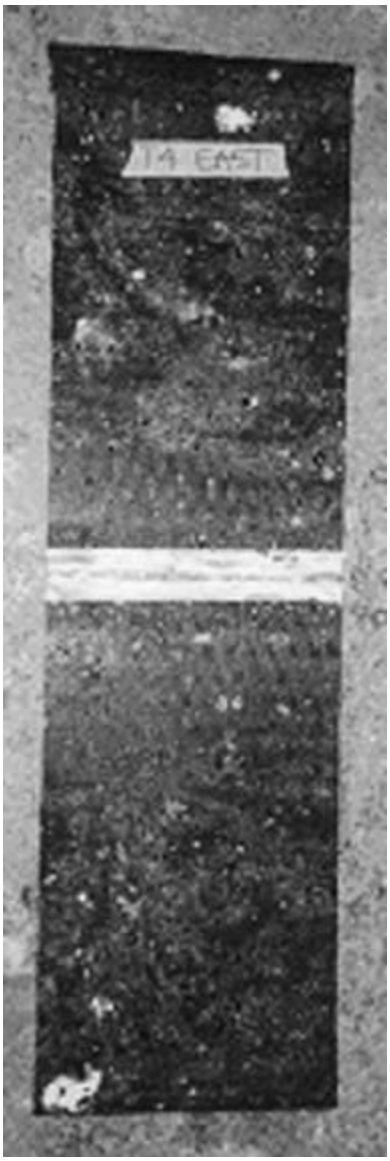

d) East FRP

Figure G-5 Test E5-90-1-U1 Failure Surfaces cont.

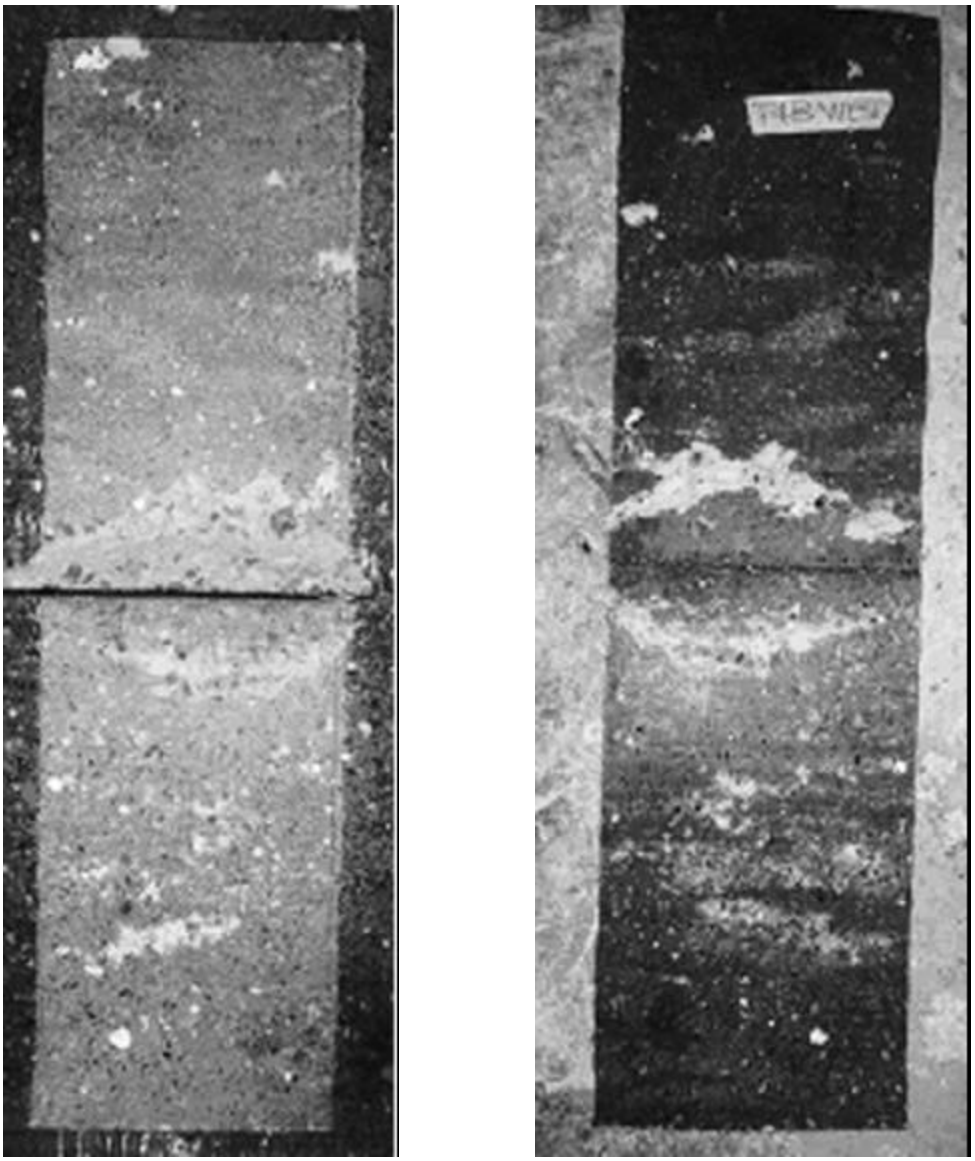

a) West Concrete b) West FRP

Figure G-6 Test E6-90-1 Failure Surfaces

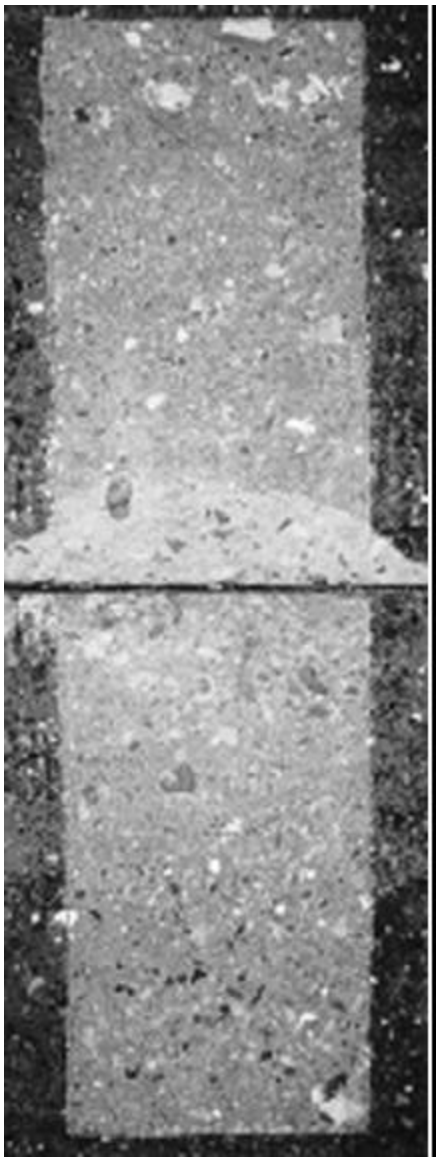

c) East Concrete

d) East FRP

Figure G-6 Test E6-90-1 Failure Surfaces cont.

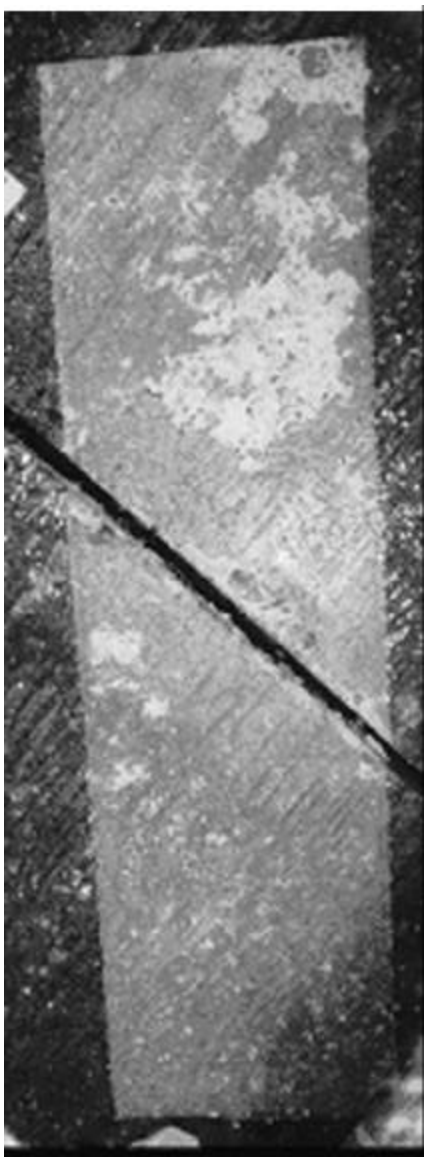

a) West Concrete

b) West FRP

Figure G-7 Test E7-45-1 Failure Surfaces

c) East Concrete

d) East FRP

Figure G-7 Test E7-45-1 Failure Surfaces cont.

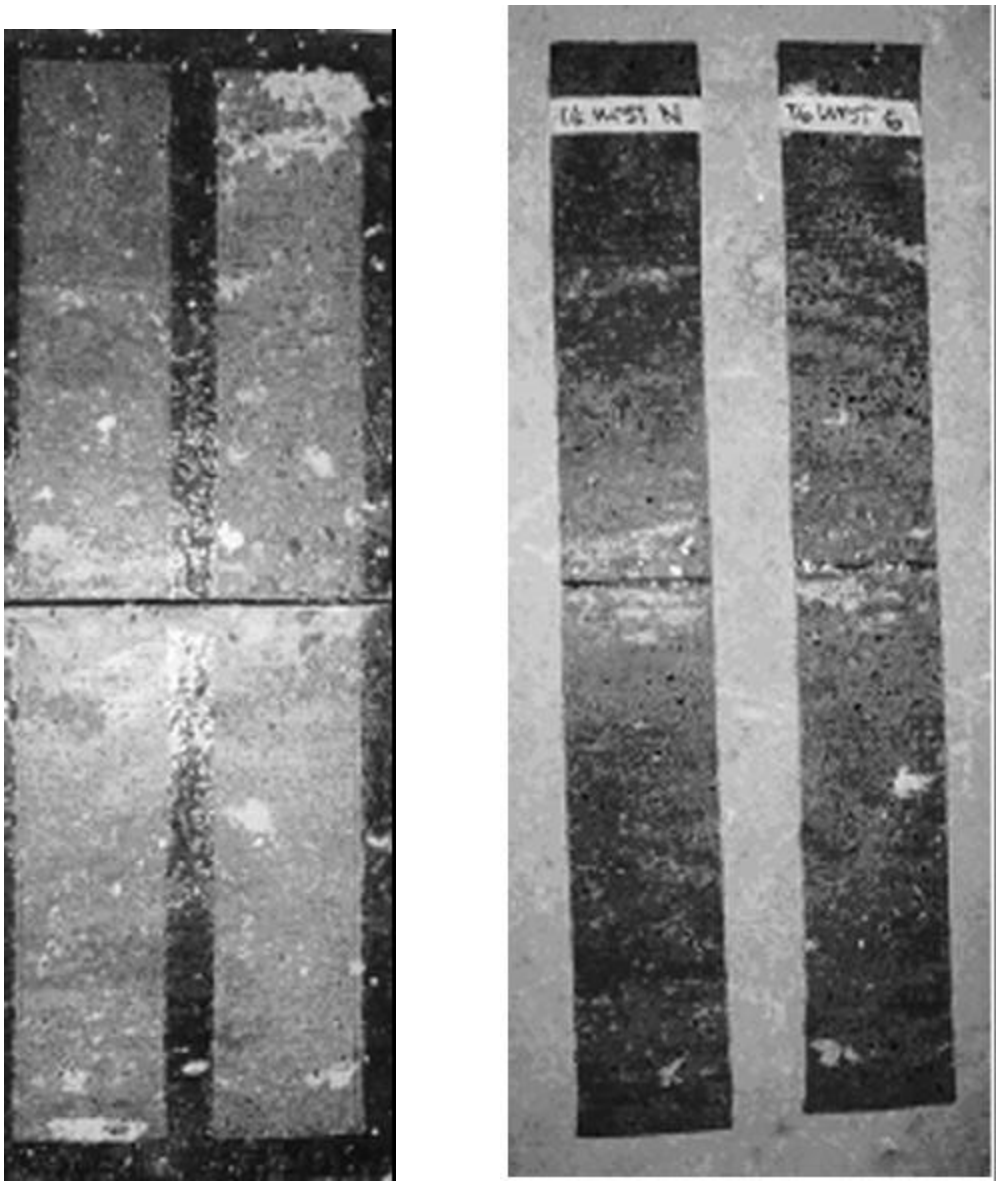

a) West Concrete b) West FRP

Figure G-8 Test E8-90-2 Failure Surfaces

c) East Concrete

d) East FRP

Figure G-8 Test E8-90-2 Failure Surfaces cont.

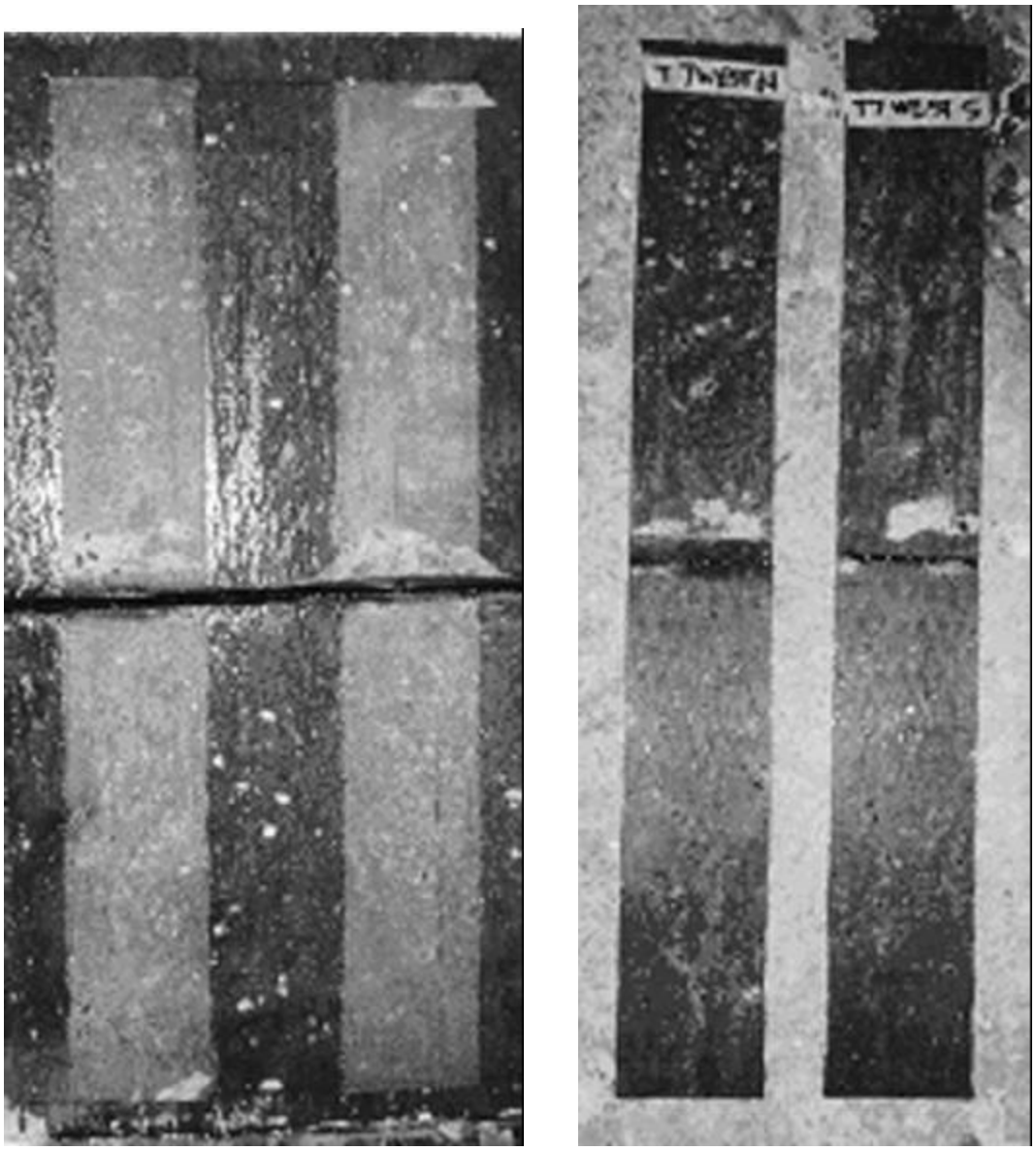

a) West Concrete b) West FRP

Figure G-9 Test E9-90-2 Failure Surfaces

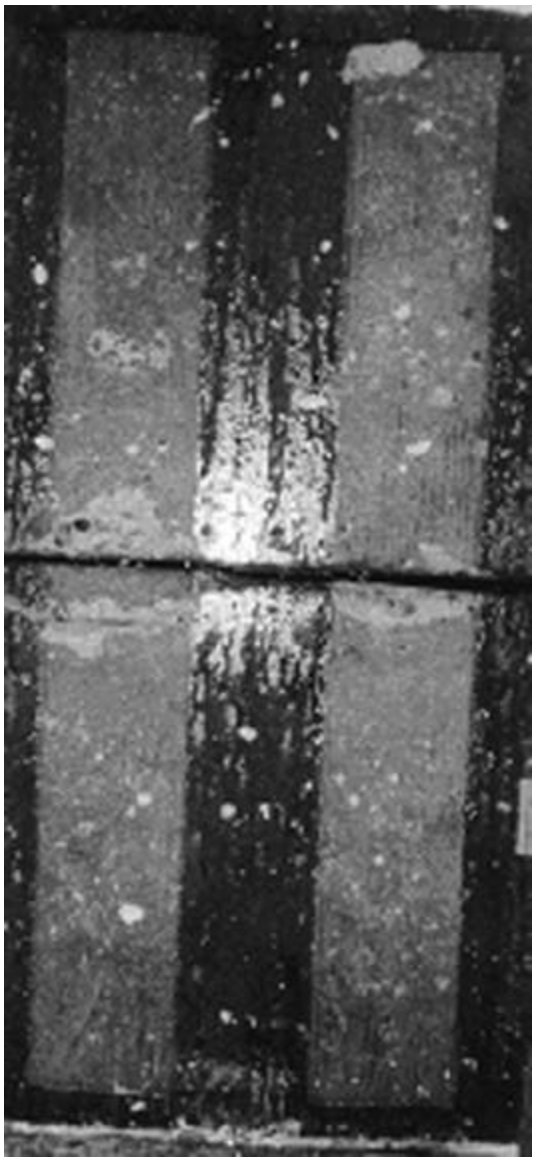

c) East Concrete

d) East FRP

Figure G-9 Test E9-90-2 Failure Surfaces cont.

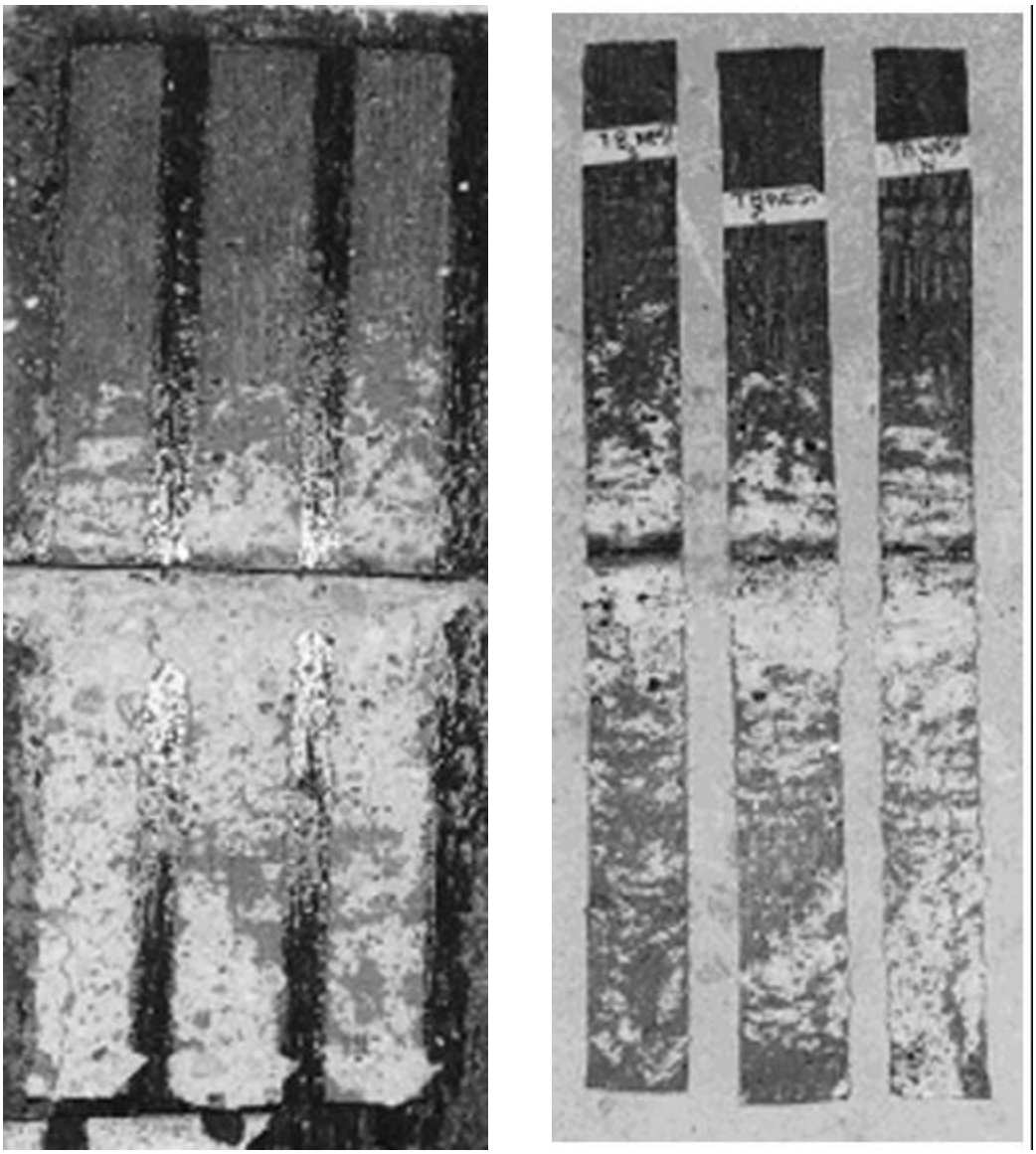

a) West Concrete b) West FRP

Figure G-10 Test E10-90-3 Failure Surfaces

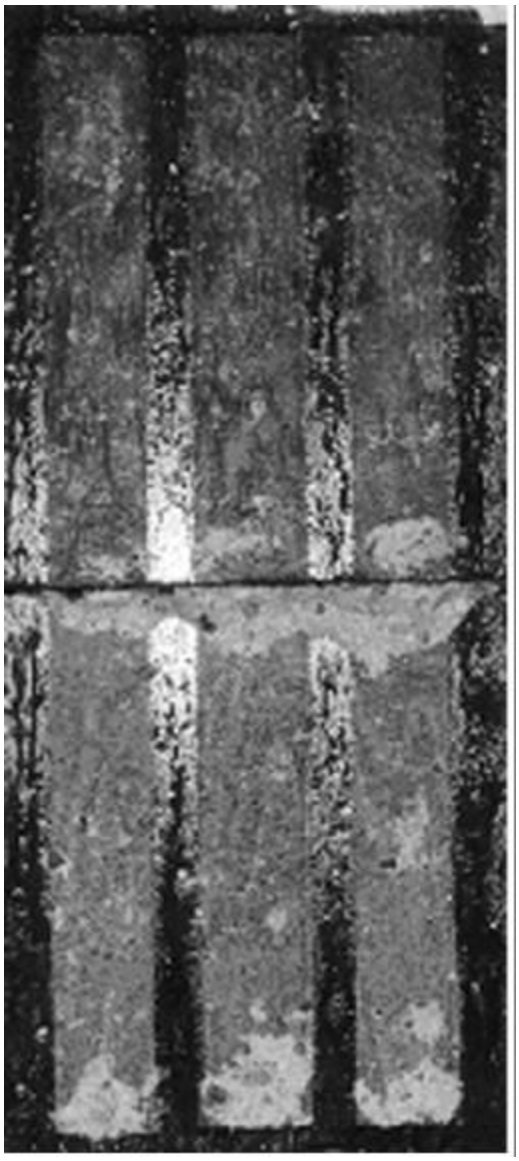

c) East Concrete

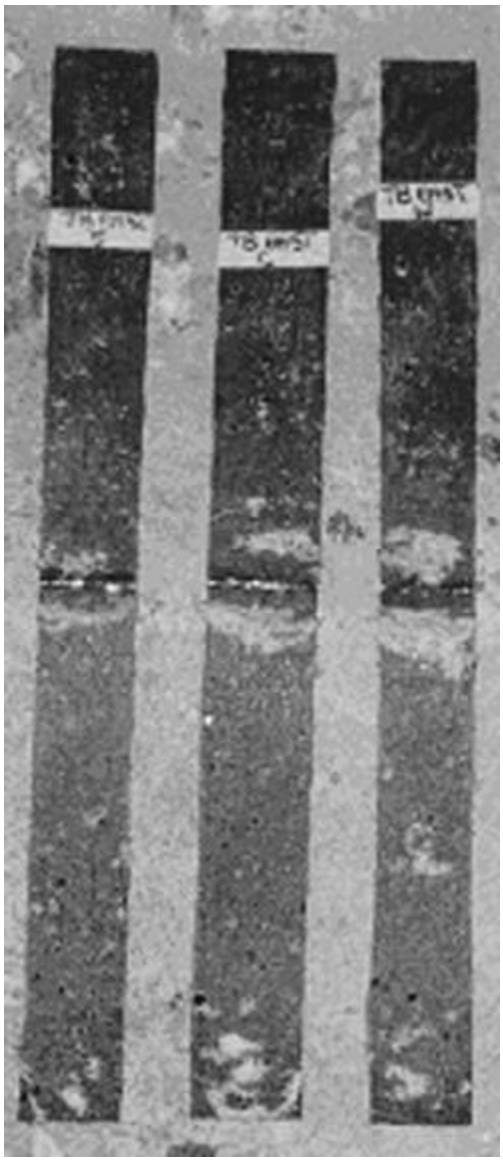

d) East FRP

Figure G-10 Test E10-90-3 Failure Surfaces cont.

a) West Concrete

b) West FRP

Figure G-11 Test E11-45-2 Failure Surfaces

c) East Concrete

d) East FRP

Figure G-11 Test E11-45-2 Failure Surfaces cont.

a) West Concrete

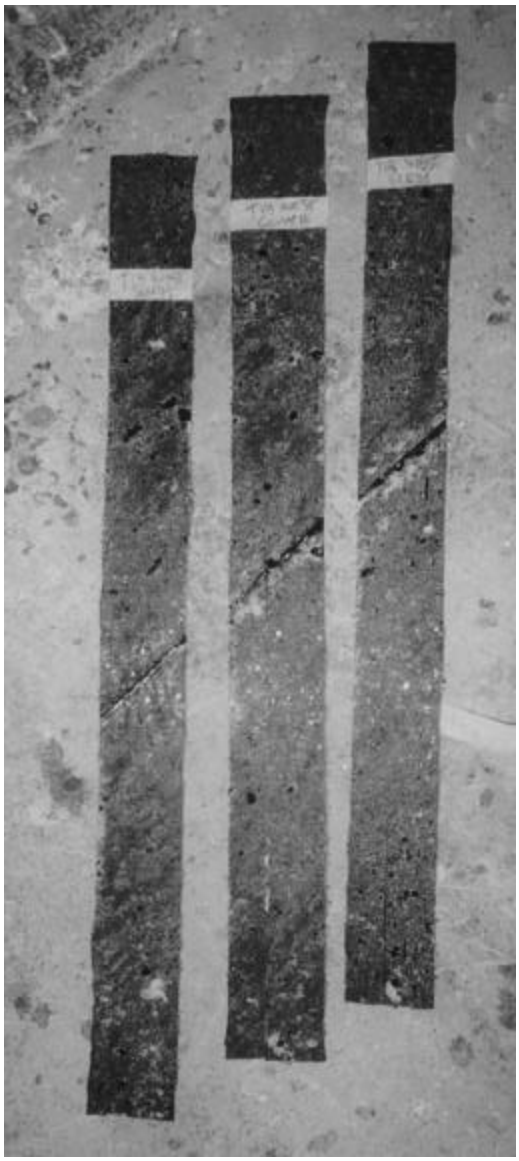

b) West FRP

Figure G-12 Test E12-45-3 Failure Surfaces

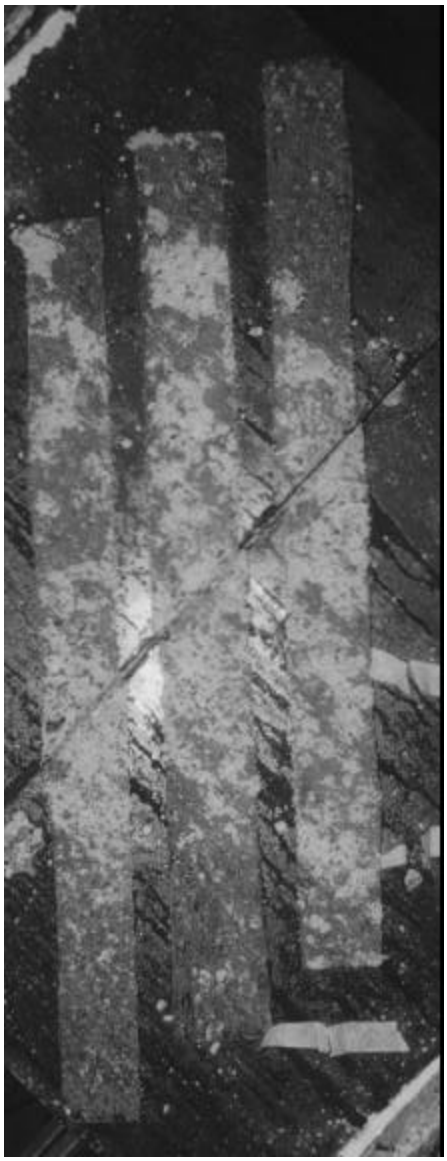

c) East Concrete

d) East FRP

Figure G-12 Test E12-45-3 Failure Surfaces cont.

a) West

b) East

Figure G-13 Test NA13-90-2 Failure Surfaces

a) West

b) East

Figure G-14 Test NA14-90-2 Failure Surfaces

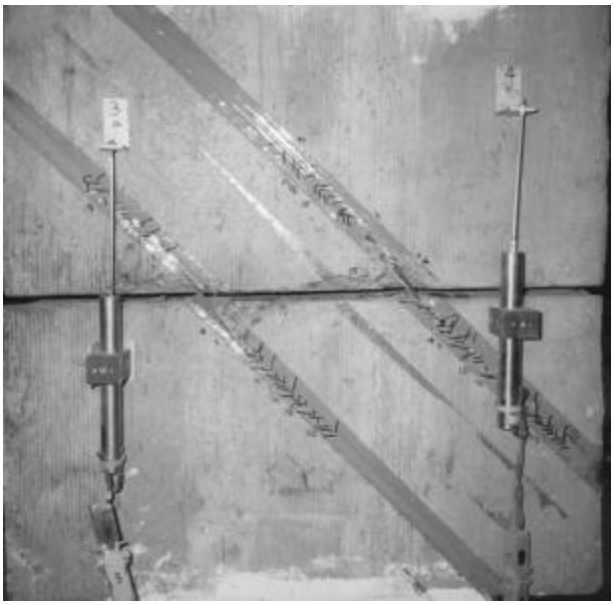

a) West

b) East

Figure G-15 Test NA15-45-2 Failure Surfaces

a) East

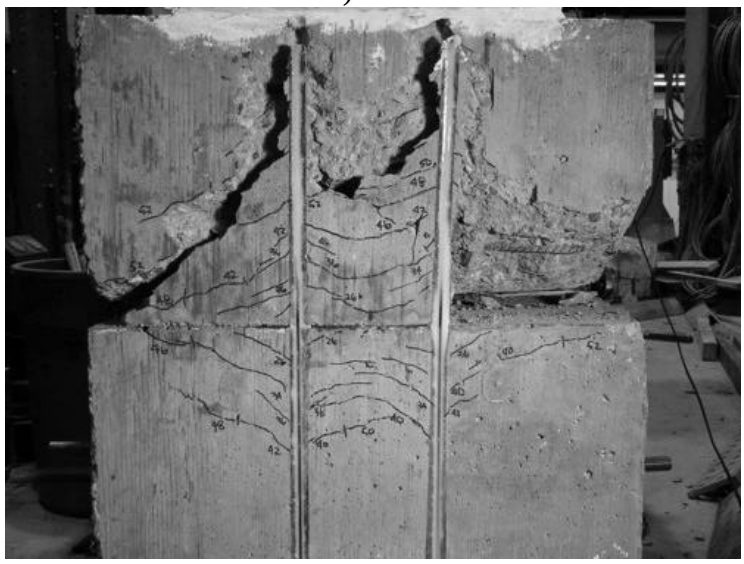

b) West

Figure G-16 Test NB16-90-2 Failure Surfaces

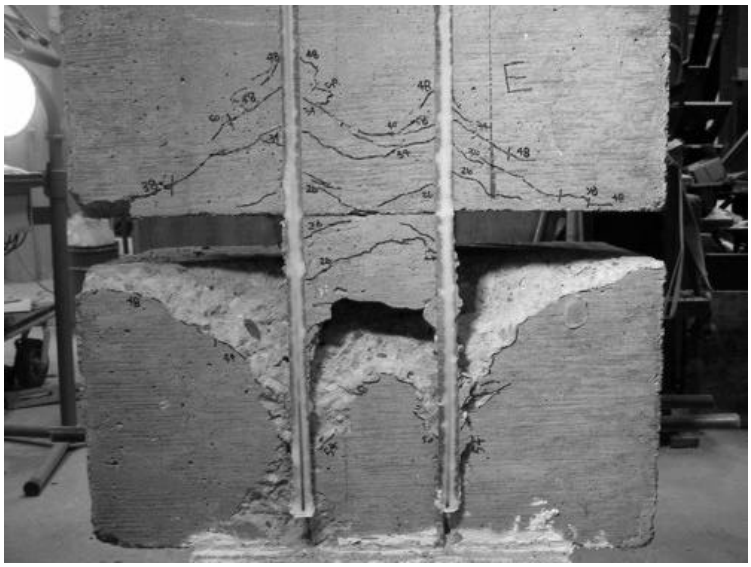

a) East

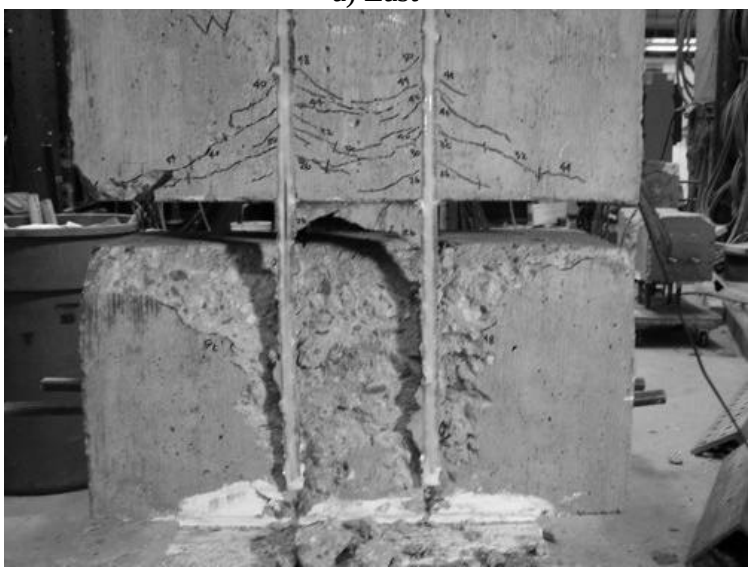

b) West

Figure G-17 Test NB17-90-2 Failure Surfaces

a) East

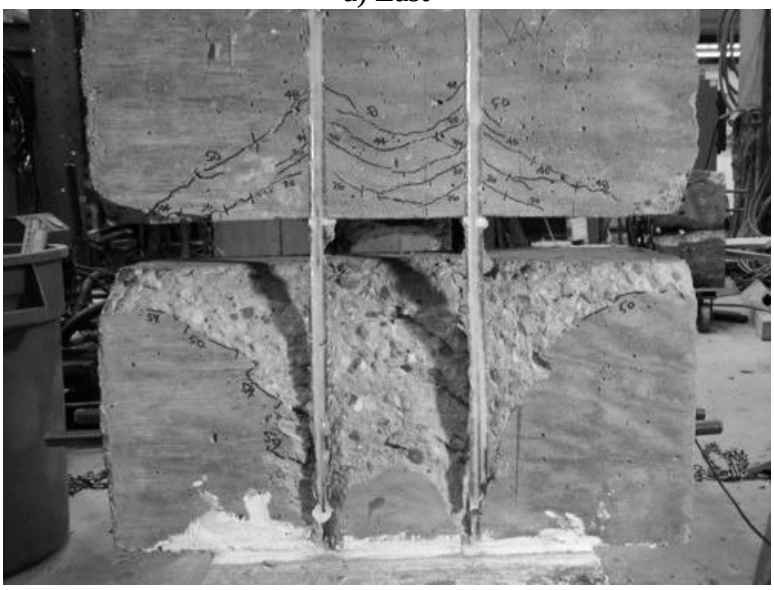

b) West

Figure G-18 Test NB18-90-2V Failure Surfaces

Appendix H Design Equations

H-1 Beam Design Equations

The beam test specimens were designed as simply supported beams. The design was based on ACI 318-99. The design of the beams is described below.

Beam dimensions: b = 12 in.
h = 32 in.
l = 192 in.

Assume: f_y = 60 ksi
f_c` = 6320 psi
aggregate size = ¾ in
cover = 2 in

Beam Design for Flexure

The minimum and maximum allowable reinforcement ratios were determined, and an area of steel was chosen.

$$\rho_{bal} = \frac{.85 f_c`}{f_y}\beta_1\left(\frac{87000}{87000 + f_y}\right) = \frac{.85 \cdot 6320}{60000}.85\left(\frac{87000}{87000 + 60000}\right) = .045$$

$$\rho_{max} = .75\rho_{bal} = .75 \cdot .045 = .034$$

$$?_{min} = \max\left(\frac{200}{f_y}, \frac{3\sqrt{f_c`}}{f_y}\right) = \max(.0033, .004) = .004$$

Try 5 #10 bars

A_s = 6.35 in^2

Bars were placed in 2 rows, with 3 bars in the bottom row and 2 bars in the top row.

$$d = 32 - 4 = 28 \text{ in}$$

$$b = 5 \cdot 1.27 + 2 \cdot .375 + 2 \cdot 2 = 11.1 \text{ in} < 12 \text{ in}$$

$$\rho = \frac{A_s}{bd} = \frac{6.35}{12 \cdot 28} = 0.019$$

The final reinforcement ratio was just under 2%. The beam width needed was less than 12 in. After determining the moment capacity of the beam, the load necessary to fail the beam in flexure was calculated.

$$M_n = A_s f_y\left(d - \frac{A_s f_y}{2 \cdot .85 f_c` b}\right) = 6.35 \cdot 60\left(28 - \frac{6.35 \cdot 60000}{2 \cdot .85 \cdot 6320 \cdot 12}\right) = 795 \text{ ft} \cdot \text{kips}$$

$$W = 0.15 \cdot 2 \cdot 1 \cdot 14 = 6 \text{ kips}$$

$$\frac{PL}{4} + \frac{WL}{8} = 795 \text{ ft} \cdot \text{kips}$$

$$\frac{P \cdot 14}{4} + \frac{6 \cdot 14}{8} = 795 \text{ ft} \cdot \text{kips}$$

$$P = 224 \text{ kips to fail in flexure}$$

The ratio of shear span to effective depth was calculated based on the unsupported length of the beam of 14 ft.

$$\frac{a}{d} = \frac{7 \cdot 12}{28} = 3$$

Beam Design for Shear

The design of the beam for shear was based on the short equation from ACI 318-02 for concrete strength.

$$V_c = 2\sqrt{f_c`}\, b_w d = 2\sqrt{6320} \cdot 12 \cdot 28 = 53.4 \text{ kips}$$

$$V_{s\min} = 50 b_w d = 50 \cdot 12 \cdot 28 = 16.8 \text{ kips}$$

$$s = \frac{A_v \cdot f_y \cdot d}{V_{s\min}}_{y} = .\frac{22 \cdot 60 \cdot 28}{16.8} = 22 \text{ in}$$

The minimum amount of steel shear reinforcement was calculated and the stirrup spacing required for minimum steel was 22 in. However, the maximum allowable stirrup spacing of d/2 corresponded to a stirrup spacing of 14 in. The maximum stirrup spacing controlled the design, so stirrups at 14 in. spacing were used for the MS span.

$V_s = 0$ for side with no stirrups

$$V_s = \frac{A_v \cdot f_y \cdot d}{s} = \frac{.22 \cdot 60 \cdot 28}{14} = 26.4 \text{ k}$$ for side with stirrups at maximum spacing

To ensure that the ends of the beam did not fail in shear because that was not a region of high moment, stirrups were placed at a spacing of 4 in. for the end regions of both spans

$$V_s = \frac{A_v \cdot f_y \cdot d}{s} = \frac{.22 \cdot 60 \cdot 28}{4} = 92.4 \text{ k}$$ for end regions

At the center of the beam on the side with no stirrups (NS side):

$$V_c = \frac{P}{2}$$

$$P = 2 \cdot V_c = 2 \cdot 53.4 = 107 \text{ k}$$

At the center of the beam on the side with minimum stirrups (MS side):

$$P = 2 \cdot V$$

$$V_n = V_s + V_c = 53.4 + 26.4 = 79.8 \text{ k}$$

$$P = 79.8 \cdot 2 = 160 \text{ k}$$

At end regions on both sides of the beam:

$$V_n = V_c + V_s = 53.4 + 92.4 = 145.8\,\text{k}$$

$$V_n = \frac{P}{2} + \frac{W}{2}$$

$$P = (V_n - \frac{6}{2}) \cdot 2 = (145.8 - 3) \cdot 2 = 286\,\text{k}$$

Summary for Beam Design

Shear strength of NS span:

P = 107 kips

Shear strength of MS span:

P = 160ips

Flexural strength of beam:

P = 224 kips

Shear strength of end regions of both spans:

P=286 kips

These capacities correspond to the point load applied by the actuator at the center of a simply supported beam. This beam design was performed using the concrete strength from the cylinders tested before the first test on beam B1. Using the concrete strength from the cylinders tested before testing of beam B2, the capacities are slightly higher.

For beam B2:

Shear strength of NS span:

P=111 kips

Shear strength of MS span:

P=164 kips

Flexural strength of beam:

P=226 kips

Shear strength of end spans:

P=290 kips

H-2 FRP Retrofit Design Equations

The retrofit scheme for the NSM FRP was intended to strengthen each span of the beam up to the flexural strength of the beam. The design of the retrofit was based on the proposed addition to ACI 440.2R related to strengthening with NSM FRP systems.

The shear contribution of the NSM FRP was added to the shear contributions of the steel and concrete. The equation for the shear contribution of the FRP depends on the dimensions of the NSM FRP (a_b and b_b are the cross-sectional dimensions of the tape), the bond stress τ_b, which can be conservatively taken as 1.0 ksi, and a total effective length of FRP. The total effective length of FRP is determined below for each span of the beam.

$$V_n = V_c + V_s + V_f$$
$$V_f = 2(a_b + b_b) \cdot t_b \cdot L_{tot}$$

For the strengthening of the NS span of the beam:

The overall depth of the beam was 32 in. Placing the NSM FRP tape at a 45 degree angle to the beam gave an overall length of 45 in. for one tape. The reduced effective length of the tape is given by l_{net} where l_b is the overall length of the tape, c_c is the concrete cover to the longitudinal bars, and α is the angle of the tape with respect to the longitudinal axis of the beam. The equations given here apply to inclined bars only.

$$l_{net} = l_b - \frac{2 \cdot c_c}{\sin \ a} = 45 - \frac{2 \cdot 2.5}{\sin \ 45} = 39 \text{ in}$$

The number of bars can be determined by choosing a bar spacing s_f. After trial and error, a spacing of 13 in. was chosen for the NS span of the beam to arrive at a strength close to the flexural strength of the beam.

$$N = \frac{2 \cdot l_{net}}{\sqrt{2} \cdot s_f} = \frac{2 \cdot 39}{\sqrt{2} \cdot 13} = 4 \text{ bars}$$

For each of the 4 bars, an effective length was determined that was equivalent to the length of the shorter segment of each bar that crossed an assumed shear crack. The effective lengths are then added to determine the total effective length L_{tot}.

$$k_a = \frac{\sqrt{2}}{2 \ \cos \ (a - 45)} = \frac{\sqrt{2}}{2 \ \cos \ (45 - 45)} = 0.707$$
$$L_i = k_a \cdot s_f \cdot i \quad where \ i = 1 \ldots \frac{N}{2}$$
$$L_i = l_{net} - k_a \cdot s_f \cdot i \quad where \ i = \frac{N}{2} + 1 \ldots N$$

$$L_1 = 0.707 \cdot 13 \cdot 1 = 9.2 \text{ in}$$
$$L_2 = 0.707 \cdot 13 \cdot 2 = 18.4 \text{ in}$$
$$L_3 = 39 - 0.707 \cdot 13 \cdot 3 = 11.4 \text{ in}$$
$$L_4 = 39 - 0.707 \cdot 13 \cdot 4 = 2.2 \text{ in}$$
$$L_{tot} = \sum_i L_i = 9.2 + 18.4 + 11.4 + 2.2 = 41.2 \text{ in}$$
$$V_f = 2(a_b + b_b) \cdot t_b \cdot L_{tot} = 2 \cdot (0.63 + 0.079) \cdot 1.0 \cdot 41.2 = 58.4 \text{ kips}$$
$$V_n = V_c + V_s + V_f = 58.4 + 53.4 = 111.8 \text{ kips}$$
$$P = 2 \cdot V_n = 2 \cdot 111.8 = 224 \text{ kips}$$

For strengthening of the MS span of the beam:

$$l_{net} = l_b - \frac{2 \cdot c_c}{\sin\ a} = 45 - \frac{2 \cdot 2.5}{\sin\ 45} = 39 \text{ in}$$

After trial and error, a spacing of 26 in. was chosen for the MS span of the beam to arrive at a strength close to the flexural strength of the beam.

$$N = \frac{2 \cdot l_{net}}{\sqrt{2} \cdot s_f} = \frac{2 \cdot 39}{\sqrt{2} \cdot 26} = 2 \text{ bars}$$

For each bar, an effective length was determined as for the NS span. The effective lengths were then added to determine the total effective length L_{tot}.

$$k_a = \frac{\sqrt{2}}{2\cos(a - 45)} = \frac{\sqrt{2}}{2\cos(45 - 45)} = 0.707$$

$$L_i = k_a \cdot s_f \cdot i \quad where\ i = 1 \ldots \frac{N}{2}$$

$$L_i = l_{net} - k_a \cdot s_f \cdot i \quad where\ i = \frac{N}{2} + 1 \ldots N$$

$$L_1 = 0.707 \cdot 26 \cdot 1 = 18.4 \text{ in}$$

$$L_2 = 39 - 0.707 \cdot 26 \cdot 2 = 2.2 \text{ in}$$

$$L_{tot} = \sum_i L_i = 18.4 + 2.2 = 20.6 \text{ in}$$

$$V_f = 2(a_b + b_b) \cdot t_b \cdot L_{tot} = 2 \cdot (0.63 + 0.079) \cdot 1.0 \cdot 20.6 = 29.2 \text{ kips}$$

$$V_n = V_c + V_s + V_f = 29.2 + 53.4 + 26.4 = 109 \text{ kips}$$

$$P = 2 \cdot V_n = 2 \cdot 109 = 218 \text{ kips}$$

These capacities have been calculated using the concrete strength from the cylinders tested before testing beam B1. For beam B2, the capacities are slightly higher.

Strength of NS span with NSM FRP retrofit:

P = 228 kips

Strength of MS span with NSM FRP retrofit:

P = 222 kips

Appendix I NSM FRP Repair Procedure for Beams

Near surface mounted (NSM) FRP can be used to repair shear cracks in beams. This repair method is advantageous for situations such as repairing bridges above roadways because heavy machinery is not required, which can reduce traffic interruptions. This repair method is particularly useful for strengthening beams in shear, because it can change the failure mode from a brittle shear failure to a more ductile flexural failure. The procedure for application of NSM FRP to a beam with shear cracks is described below. This application procedure assumes that the NSM FRP tape is applied at a 45 degree angle to the beam, and that 3M DP-460 NS is used as the adhesive. If desired, a crack injection epoxy can be used prior to FRP application to fill and seal large cracks. Safety glasses and gloves should be worn while applying FRP.

1. Measure the diagonal of the beam perpendicular to the shear crack and cut FRP tape to the length of the diagonal.
2. Wipe NSM tape with acetone to remove dust and grease from the surface. Set tape aside on a clean surface.
3. Mark a straight line at 45 degrees on the beam in the location where the FRP will be applied
4. Using a saw with a 0.25 in. wide blade, cut a 0.75 in. deep groove along the line. Figure G-1 shows a groove being cut.
5. Brush out debris from the inside of the groove.
6. Use high-pressure air to thoroughly clean all dust from the inside of the groove.
7. If a clean appearance is desired on the surface of the beam, apply masking tape to the surface of the beam along the entire length of the groove to prevent excess epoxy from marring the surface. Figure G-2 shows grooves with masking tape applied.
8. Insert adhesive cartridge into pneumatic gun.
9. Depress trigger to discard a small amount of epoxy until the two components are flowing equally.
10. Attach mixing nozzle.
11. Coat both sides of FRP tape with epoxy.
12. Fill groove approximately halfway with epoxy. Figure G-2 shows application of epoxy into a groove using a pneumatic gun.
13. Insert tape into the center of the groove and press down until epoxy seeps out equally on each side of the tape. Figure G-3 shows the application of NSM FRP tape into a groove.
14. Fill any remaining voids in the groove with epoxy.
15. Smooth surface and remove excess epoxy with a trowel.
16. Visually inspect tape to ensure that it is centered in the groove. Also inspect epoxy to ensure that there are no voids in the groove. If necessary, adjust the position of the tape or add additional epoxy. Use a trowel to smooth the surface.
17. Remove masking tape.
18. Use acetone or solvent to remove any epoxy from the pneumatic gun or other equipment as soon as possible.

19. Allow at least 24 hours for adhesive to cure.
20. Inspect the FRP installation after 24 hours to verify that the adhesive has fully cured. Adhesive should be solid to the touch in all locations. Adhesive should not be gooey or sticky.

In the long term, inspections can be made to verify that the FRP installation continues to be successful. The end of the groove should be visually inspected to ensure that there is no gap caused by slipping between the FRP tape and the epoxy. The edges of the groove where the epoxy meets the concrete should be visually inspected to ensure that there are no cracks along the interface between the concrete and the epoxy. Also, the concrete should be inspected near the shear cracks to ensure that it is not deteriorating. Deterioration and crumbling of the concrete near the shear crack, cracking of the epoxy, and cracking along the interface between the concrete and epoxy are possible signs that the FRP installation may be approaching failure.

Figure G-1 Cutting a Groove for NSM FRP

Figure G-2 Applying Epoxy

Figure G-3 Applying NSM FRP Tape into Groove